Queen Mary University of London

PhD Thesis

Thesis Submitted in Partial Fulfillment of the Requirements for the Degree of Doctor of Philosophy

Neutrophil Microvesicles Restrict the Phlogistic Activation of Macrophages

Author:
Hefin Ioan Rhys
MPharmacol,
University of Bath, 2013

Supervisors:
Prof. Mauro Perretti
Dr. Lucy Norling
Dr. Adrian Moore

October 29, 2017

Statement of originality

I, Hefin Ioan Rhys, confirm that the research included within this thesis is my own work or that where it has been carried out in collaboration with, or supported by others, that this is duly acknowledged below and my contribution indicated. Previously published material is also acknowledged below.

I attest that I have exercised reasonable care to ensure that the work is original, and does not to the best of my knowledge break any UK law, infringe any third party's copyright or other Intellectual Property Right, or contain any confidential material.

I accept that the College has the right to use plagiarism detection software to check the electronic version of the thesis. I confirm that this thesis has not been previously submitted for the award of a degree by this or any other university.

The copyright of this thesis rests with the author and no quotation from it or information derived from it may be published without his prior written consent.

Signature:

Date: October 29, 2017

Collaboration and publications:

- Headland, S. E. *et al.*, 2014[1]
- Leoni, G., *et al.*, 2015[2]
- Headland, S. E. *et al.*, 2015[3]
- Jones, H. R. *et al.*, 2016[4]
- Norling, L. V. *et al.*, 2016[5]
- Simeoli, R. *et al.*, Under review

Acknowledgements

I would like to thank my supervisors, Mauro, Lucy and Adrian for giving me the opportunity, support, and their expertise to complete my PhD. Thank you for giving me the freedom to pursue my own ideas, and for giving me opportunities to attend and present at conferences both at home and internationally.

I would also like to thank my Biopharmily for making my PhD fun and sociable, even when things were tough, especially Dianne whom I adopted as a tertiary supervisor while Lucy was on maternity leave (whether she agreed to it or not) and Sarah who mentored me in vesicle research and gossip.

Lastly, and most importantly, I would like to thank my husband, Zand, without whom I would have given up a long time ago. Thank you for encouraging me when motivation was low, and for comforting me when p values were high.

Abstract

Released in response to cellular activation, microvesicles are a major vector mechanism for the delivery of protein, nucleic acid and bioactive lipid payloads in local tissues and plasma. Large numbers of microvesicles (including those from neutrophils) are found within inflammatory sites, such as the rheumatoid synovium. Human neutrophil microvesicles promote tissue protection, and in some cases repair, by affecting function and phenotype of other inflammatory cells. Of these, tissue macrophages are central to the recovery of homeostasis after an inflammatory insult.

The data herein indicate that microvesicles released by activated neutrophils impede lipopolysaccharide and interferon gamma-induced "M1-like" polarisation of macrophages via phosphatidylserine (PtdSer) exposure, and induce annexin A1-dependent release of transforming growth factor beta (TGFβ). Macrophages treated with these vesicles stimulate the production of cartilage matrix from chondrocytes, and are unable to induce an inflammatory phenotype in fibroblasts. The efficacy of these vesicles is reproduced in two *in vivo* models of acute inflammation, zymosan-induced peritonits and K/BxN serum-transfer arthritis.

Finally, the possibility of using both autologous, and cell-line-derived microvesicles as pharmacodynamic tools is explored. Microvesicles generated from neutrophils from patients with rheumatoid arthritis are found to be protective, and can outcompete the pro-inflammatory effects of both platelet microvesicles, and those isolated from synovial fluid of patients with rheumatoid arthritis. By building on the observation that anxA1 on microvesicles stimulates TGFβ release in macrophages, a cell line was transfected to release anxA1^{+} microvesicles, and their effects compared to those of their wild type counterparts.

Contents

List of Figures

List of Tables

Acronyms

ºC	degrees Celcius
µM	micromolar
µg	microgram
µm	micrometer
AB	apoptotic body
ABC	ATP-binding cassette
ACPA	anti-citrullinated protein antibodies
anxA1	annexin A1
anxA5	annexin A5
APC	antigen-presenting cells
atm	atmospheres
ATP	adenosine triphosphate
AU	arbitrary units
BODIPY maleimide	boron-dipyrromethene maleimide
BSA	bovine serum albumin
bsd	blasticidin-S deaminase
CCD	charge-coupled device
CFSE	carboxyfluorescein succinimidyl ester
cP	centipoise
DAMP	damage-associated molecular pattern
DHA	docosahexaenoic acid
EDTA	ethylenediaminetetraacetic acid
FBS	foetal bovine serum
FITC	fluorescein isothiocyanate
FMO	fluorescence minus one
FSC	forward angle light scatter
G	gauge (needle size)
GDP	guanine diphosphate
GEF	guanine nucleotide exchange factors
GM-CSF	granulocyte-macrophage colony-stimulating factor
GTP	guanine triphosphate
HEPES	4-(2-hydroxyethyl)-1-piperazineethanesulfonic acid
HIV	human immunodeficiency virus
HUVEC	human umbilical vein endothelial cells

IC	immune complex
IFNγ	interferon gamma
IL	interleukin
LED	light-emitting diode
LPS	lipopolysaccharide
LTB_4	leukotriene B_4
M-CSF	macrophage-colony stimulating factor
MCP-1	monocyte chemoattractant protein 1
MHC	major histocompatibility complex
MHz	megahertz
min	minutes
miRNA	micro ribonucleic acid
mL	millilitre
mM	millimolar
MMP	matrix metalloproteinase
mRNA	messenger ribonucleic acid
MV	microvesicle
MV_{OA}	osteoarthritis synovial fluid-induced MV
MV_{Post}	transmigrated-neutrophil-derived MV
MV_{Pre}	pre-transmigrated-neutrophil-derived MV
MV_{RA}	rheumatoid arthritis synovial fluid-induced MV
$MV_{TNF\alpha}$	TNFα-induced MV
MVB	multivesicular body
NET	neutrophil extracellular traps
nm	nanometer
ORF	open reading frame
PAF	platelet-activating factor
PAMP	pathogen-associated molecular pattern
PBMC	peripheral blood monouclear cells
PBS	phosphate-buffered saline
PCR	polymerase chain reaction
PE	phycoerythrin
pg	picograms
PM	plasma membrane
PMT	photomultiplier tube
PPP	platelet-poor plasma
PRP	platelet-rich plasma
PtdCho	phosphatidylcholine

PtdEth	phosphatidylethanolamine
PtdSer	phosphatidylserine
RNS	reactive nitrogen species
ROCK	rho-associated protein kinases
ROS	reactive oxygen species
S	sedimentation coefficient
SSC	right angle light/side scatter
TBST	tris-buffered saline with tween
TEMED	N,N,N',N'-teteramethylethylenediamine
TGFβ	transforming growth factor β
TLR	toll-like receptors
TNFα	tumour necrosis factor α
TRPS	tunable resistive pulse sensing
U	enzyme unit
V	volt
VEGF	vascular endothelial growth factor

Chapter 1

Introduction

1.1 The observation of extracellular vesicles

In 1946, Chargaff and West noted that centrifuging platelet-poor plasma at high speed prolonged its clotting time[6]. The clotting factor, which was not depleted at 5,000×g but formed a pellet at 31,000×g, could restore the clotting time of depleted healthy and haemophiliac plasma in a concentration-dependent manner. The authors ascribed this activity to a thromboplastic lipoprotein of high molecular weight and postulated that the pelleted fraction may also contain "minute breakdown products of the blood corpuscles." The identity of the prothrombotic agent remained elusive until when, twenty-one years later, Wolf confirmed using electron microscopy that the pelleted fraction responsible for this prolonged clotting time consisted of particulate matter rich in phospholipids[7]. In refinement of Chargaff and West's hypothesis that the material was a product of circulating cells, Wolf suggested these particles were released from activated platelets and that their function was to potentiate the clotting process. Wolf termed these particles "platelet dust."

Following a separate line of research in 1954, Palay and Palade described the presence of vesicular structures in neurons, containing smaller vesicles, some of which appeared to be inward invaginations[8]. The same structures were identified in regenerating nerve fibres[9], epithelia[10], granulocytes and monocytes[11], and were termed multivesicular bodies by Sotelo and Porter in 1958[12]. Extracellular vesicles of the same size and morphology as those found within multivesicular bodies were detected in breast cancer biopsies[13] and virtually all sera[14]. Initially mistaken for viruses, these vesicles were termed virus-like particles, although Dalton asserted this nomenclature was unwarranted and preferred the term microvesicles[15]. While microvesicles and multivesicular bodies continued to be curiosities within electron micrographs, their biological relevance remained unknown[16–18].

The first report of a functional importance of extracellular vesicles came in 1981 when Trams *et al.* proposed they were non-soluble vectors for ectoenzymes, enzymes found on the extracellular leaflet of biological membranes[19]. Importantly, this study identified two main populations of what the authors termed "exosomes" released from glioma and neuroblastoma cell lines: small vesicles around 40nm in diameter,

and larger vesicles ranging from 500nm to 1,000nm. It was later demonstrated that prostasomes, vesicles released by prostate tissue, are formed by inward budding into the lumens of late endosomes, defining the origin of multivesicular bodies[20]. Considered a tissue-specific case of the exosome, prostasomes were externalised when multivesicular bodies fused with the plasma membrane, a process subsequently termed exocytosis.

While the first physiological roles for exosomes began to emerge (in protein recycling and shedding during reticulocyte maturation[21–23]), the problem remained that the larger vesicle population described by Trams *et al.* was too large to be derived from multivesicular bodies. Instead, Stein & Luzio proposed the term ectocytosis in 1991 to describe the direct budding of larger, right-side-out (where the outer leaflet of the cell remains the outer leaflet of the vesicle) membrane vesicles from the plasma membrane[24]; initially observed by Scott in 1978[25]. These plasma membrane-derived vesicles (whose release was $[Ca^{2+}]$ and temperature-dependent) were termed microparticles, and were presumed to represent the observed larger fraction of vesicles[26,27]. The term ectosome was proposed in 1999 to maintain consistency with the exosome terminology, but has fallen out of favour as the two are phonetically very similar. This nomenclature is still used (more commonly to describe neutrophil-derived vesicles), but "microvesicle" predominates, despite these vesicles being sub-micron in size.

Finally, distinct from exosomes and microvesicles in size, morphology and release mechanism, are vesicles first observed in 1965 being released from cells undergoing apoptosis[28]. These larger (1µm - 5µm) and irregularly shaped vesicles are considered a hallmark feature of programmed cell death and were named apoptotic bodies by the same group's seminal review in 1972[29]. Apoptotic bodies form from membrane blebs during cell death which fragment and undergo fission. Prior to apoptotic body formation, phosphatidylserine (PtdSer), a membrane phospholipid usually maintained asymmetrically on the cytosolic membrane leaflet, is exposed, contributing to plasma membrane instability and blebbing[30]. Outward expression of PtdSer is a property apoptotic bodies and microvesicles share, as the same process occurs prior to the formation of a *subset* of microvesicles also[31].

Together, exosomes, microvesicles and apoptotic bodies form the family of extracellular vesicles (Figure 1.1 and Table 1.1). Far from being functionless waste products (indeed, nature is rarely so wanton), this family have been directly implicated in a plethora of physiological and pathophysiological processes. While these structures have both distinct and overlapping functions, microvesicles are emerging as a remarkably pivotal vector of intercellular signalling in the context of inflammation. For example, monocytes, endothelial cells and platelets release microvesicles capa-

ble of promoting inflammatory and clotting responses[32–35]. Conversely, neutrophil microvesicles can promote tissue protection, and in some cases repair, by affecting function and phenotype of other inflammatory cells[36,37]. Of these, tissue macrophages are central to the recovery of homeostasis after an inflammatory insult and there is some evidence to suggest a re-programming of macrophages by neutrophil-derived microvesicles[37,38].

Table 1.1: Extracellular vesicles

Member	Size	Source	Release	PtdSer expression
Exosomes	~40nm - 200nm	MVB	Exocytosis	No
Microvesicles	~100nm - 600nm	PM	Ectocytosis	A subset
Apoptotic bodies	1µm - 5µm	PM	Membrane blebbing	Yes

MVB multivesicular body; **PM** plasma membrane

1.2 Microvesicle formation

The controlled release of microvesicles from the plasma membrane is a property shared by all eukaryotic cells[39]. Bacteria also shed outer membrane vesicles; similar nano-scale vesicles from which eukaryotic ectocytosis appears to be conserved[40]. Evolutionary persistence of these structures is indicative of their importance as a fundamental mechanism of cellular membrane dynamics and signalling. The process of ectocytosis itself is not fully annotated, but is governed by interactions between Ca^{2+}, Rho GTPases, plasma membrane asymmetry, and filamentous and cortical actin cytoskeletal architecture[41].

1.2.1 Ligand-induced Ca^{2+} flux

Initial work into the mechanism of ectocytosis took a top-down, functional approach, focussing on exogenous stimuli which induce microvesicle release rather than the molecular pathways involved. "Activating" stimuli like adenosine triphosphate (ATP), thrombin, and lipopolysaccharide (LPS) potently induce microvesicle release from all cells expressing their cognate receptors[32,42–44]. The common denominator between all ectocytosis-driving stimuli is their induction of a potent flux in intracellular Ca^{2+}. Blockade of Ca^{2+} mobilisation with the intracellular, bivalent cation chelator, BAPTA-AM, universally negates microvesicle release in both the steady state and in cells treated with these activating stimuli[1,45]. It would seem that any ligand which induces biologically significant Ca^{2+} movement into the cytosol, also induces ectocytosis; the two processes appear immutably linked. Therefore, any ligand-receptor interaction

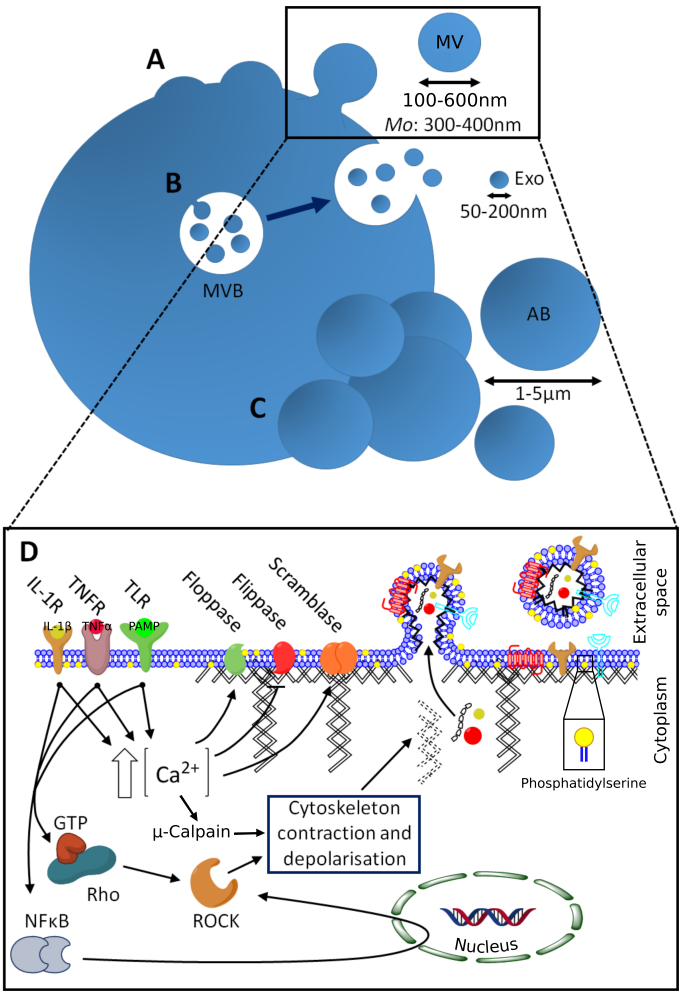

Figure 1.1: Formation and classification of extracellular vesicles. A Microvesicles (MV) are membrane vesicles that bud directly from the plasma membrane of all eukaryotic cells. Their diameter is in the range 100nm - 600nm, with a modal diameter around 300nm - 400nm. **B** Exosomes (Exo) are vesicles which bud inwards into late endosomes to form multivesicular bodies (MVB). During exocytosis, these bodies fuse with the plasma membrane and release their cargo of 50nm - 200nm diameter exosomes. **C** Apoptotic bodies (AB) are larger, irregularly shaped vesicles which are formed from large membrane blebs during apoptosis. **D** Activation of receptors coupled to Ca^{2+} signalling promotes PtdSer exposure on the outer leaflet by modulating flippase, floppase and scramblase activity. Ca^{2+}-activated µ-calpain (which can be inhibited by calpeptin) cleaves cortical actin and activation of rho-associated protein kinases (ROCK) by RhoA (and possibly NFκB) induces cytoskeletal contraction. Budding vesicles take membraneous proteins, and cytosolic components before a fission event releases the microvesicle into the extracellular space. GTP, guanine triphosphate; IL-1β, interleukin-1β; PAMP, pathogen-associated molecular pattern; ROCK, rho-associated protein kinases; TNFα, tumour necrosis factor α.

resulting in the opening of bivalent cationic ion channels, G_q-protein disassembly or membrane depolarisation, will prompt rapid dissemination of microvesicles from the cell. Microvesicle release can also be induced experimentally, independently of ligand-receptor interactions with Ca^{2+} ionophores, such as A23187[46]. This coupling to Ca^{2+} flux appears to explain the promiscuous and ubiquitous nature of ectocytosis in eukaryotic cells, and is the signal required by the downstream cellular machinery responsible for vesicle formation.

1.2.2 Rho GTPases

The Rho family of 23 small, membrane-bound GTPases (G proteins), such as Cdc42, Rac1 and RhoA, are master controllers of signalling that results in changes to the actin architecture[47]. In their inactive state, Rho family members bind guanine diphosphate (GDP) via a nucleotide binding domain. Activation of guanine nucleotide exchange factors (GEF) by upstream receptor signalling or Ca^{2+} and cyclic adenosine monophosphate signals allows them to bind to Rho enzymes and sterically hinder the interaction between GDP and the GTPase[48]. This allows dissociation of GDP and frees the nucleotide binding domain for an available guanine triphosphate (GTP) molecule (both molecules compete for binding, but the latter is ~10x more concentrated in the cytosol[49]). Once bound to GTP, classical Rho molecules bind to their respective effectors and propagate the signal. This signal is temporally regulated by the enzymes' intrinsic GTPase activity which dephosphorylates GTP back to GDP, returns the GTPase to its inactive state and is promoted by GTPase-activating proteins[50–52]. The functions of Rho family members are diverse and are required for cell division, migration, adhesion and membrane dynamics.

Of the best studied Rho proteins, RhoA activation is required during microvesicle formation[53]. When RhoA is GTP-bound, it interacts with and affects a conformational change in ROCK[54–56]. This conformational change increases the kinase activity of ROCK, which phosphorylates myosin light chain phosphatase and may phosphorylate myosin light chain directly[55]. The net effect of this is increased association of myosin light chain to the actin filaments and a subsequent increase in cytoskeletal contractility[57]. ROCK homologues I and II can also be directly activated by cleavage of their regulatory domain by caspases 3 and 2, respectively[53,57]. The particular ROCK which transposes a cellular signal into microvesicle release appears to depend on the nature of the signal. For example, thrombin-mediated activation of human endothelium results in ROCK II and not ROCK I-dependent microvesicle release[53]. On the contrary, ROCK I predominantly controls apoptosis-associated microvesicle release[57]. Activation of either ROCK homologue is a critical checkpoint during ectocytosis, and their inhibition with Y-27632 (a partially-selective small

molecule inhibitor) arrests microvesicle formation[57].

Just how ROCK-induced contraction of the actin cytoskeleton facilitates microvesicle release is still under debate. A predominant theory is that contraction needs to be secondary to depolymerisation of the cortical actin mesh proximal to the elected patch of membrane[58–60]. This is demonstrated by the inhibition and potentiation of microvesicle release by jasplakinolide (a peptide which promotes actin nucleation and polymerisation) and cytochalasin D (an alkaloid which prevents polymerisation of actin monomers), respectively[1]. This theoretical sequence of events would allow decoupling of actin from membrane components and its retraction into the cytosol, leaving a patch of unsupported membrane. The unanchored patch of membrane is then free to bow to entropy and form a membrane bleb in response to changes in membrane asymmetry (discussed below).

One issue with this theory is that ROCKs also activate LIM domain kinase which phosphorylates and inactivates cofilin[61]. Cofilin promotes depolymerisation of actin filaments, so its inhibition by ROCKs stabilises the cortical actin mesh[62]. Both RhoA and ROCK also activate PI(4)P 5-kinases, which promote actin filament assembly[63]. Cofilin and PI(4)P 5-kinase activity need to be overcome to allow detachment of actin from the membrane, a role fulfilled by Ca^{2+}-dependent calpain proteases (most likely µ-calpain)[64,65]. µ-calpain directly binds cytosolic Ca^{2+} in the µM range (whereas m-calpain is sensitive only at mM Ca^{2+} levels, hence their respective prefixes) and becomes catalytically active[66]. The activity of calpain enzymes does not appear selective for defined amino acid sequences but rather depends upon tertiary structure, and so they have a wide range of cellular targets, including notably, filamentous actin. Inhibition of calpains with the small molecule inhibitor calpeptin blocks the production of microvesicles from platelets and abrogates actin degradation[67]. The importance of calpains in membrane release during ectocytosis is perhaps demonstrated by calpeptin's blockade of microvesicle release despite concurrently activating Rho GTPases (including RhoA)[68]. While detachment and contraction are required to free membrane patches destined for blebbing, changes in membrane phospholipid asymmetry may drive the entropic formation of the bleb, as well as facilitate cytoskeleton detachment.

1.2.3 Membrane asymmetry

Eukaryotic lipid bilayers are given structure by a family of amphiphatic aminophospholipids, the glycerophospholipids[69]. This group of lipids consists of phosphatidylinositol, phosphatidic acid, phosphatidylcholine (PtdCho), phosphatidylethanolamine (PtdEth) and PtdSer. The bilayer of the plasma, golgi and mitochondrial membranes maintain an asymmetrical distribution of these lipids between membrane

leaflets[70]. The exception to this is in the endoplasmic reticulum, where most of the cell's membrane lipids are synthesised, which maintains equal proportions in each leaflet[71,72].

The functional consequences of a non-uniform distribution are related to the signalling capacity of bioactive lipids. By actively controlling exposure of certain lipid ligands to the extra and intracellular space, the cell can exert spatial and temporal control over signalling events. For example, the translocation of PtdSer (which is almost exclusively reserved to the inner plasma membrane leaflet) to the outer leaflet, promotes activation of the clotting cascade and provides a phagocytosis signal to myeloid cells[30,73]. Active membrane redistribution also allows the generation of lipid rafts and both inward and outward membrane blebs (including structures such as caveolae)[69]. Changes in membrane lipid distribution also alter the fluidity of regions of the bilayer, facilitating formation of pseudopodia and other membrane extrusions[74]. The simplest mechanism by which phospholipids translocate across membrane leaflets is spontaneously under equilibrium[69]. For small and/or negatively charged lipids like cholesterol and diacylglycerol, the "half life" for translocation is seconds, and their retention is controlled by the relative abundance of larger lipids with which they interact. For the large glycerophospholipids, the half life is hours to days, and so effective control of membrane position relies on transporters that transfer lipids to the opposing layer[71].

Eukaryotes and some prokaryotes express a family of P-type ATPases which actively pump cations across membrane against their electrochemical gradient[75]. The P type IV (P_4) ATPases catalyse unidirectional transport of phospholipids across lipid bilayers and therefore maintain asymmetry. This family of transporters largely transfers PtdSer, PtdEth and possibly PtdCho from the outer to the inner membrane leaflet (with particularly high selectivity for PtdSer). Lipid transporters which act in this direction only are collectively known as flippases[76]. Conversely, the ATP-binding cassette (ABC) transporters (specifically the ABCA subfamily) catalyse the ATP-dependent efflux of cholesterol and PtdSer to the outer membrane leaflet, and are known as floppases[77]. The actions of flippase and floppase transporters on PtdSer directly oppose each other, but the inward translocation is heavily favoured at equilibrium, and so PtdSer is actively retained in the cytosolic leaflet.

Changes in intracellular Ca^{2+} rebalance lipid equilibrium by inhibiting flippase activity, and enhancing floppase and scramblase activity. Scramblase enzymes are Ca^{2+}-dependent but ATP-independent enzymes which allow the bidirectional movement of lipids across both membrane leaflets[78]. As the process is passive, activation of scramblases allows Le Châtelier's principle (that a system in equilibrium adjusts itself to counteract the effect of an applied change) to take precedence, where

membrane distribution becomes more equal. The net effect of decreased flippase and increased floppase and scramblase activity is significant exposure of PtdSer on the cell surface.

A key scramblase which appears important in PtdSer exposure is TMEM16F, a Ca^{2+}-activated Cl^- channel[79]. A loss of function mutation in TMEM16F has been linked to Scott syndrome, a bleeding disorder due to impaired scramblase activity and thus, reduced microvesicle release in platelets[80]. Mice in which the TMEM16F gene has been knocked out exhibit reduced PtdSer exposure on activated platelets and subsequent defects in coagulation and haemostasis similar to those in Scott syndrome[78]. Exposure of murine TMEM16F$^{-/-}$ platelets to high concentrations of the Ca^{2+} ionophore A23187, or human Scott syndrome platelets to three hour stimulation with proapoptotic agonist ABT737, is still able to induce PtdSer exposure, suggesting a role of TMEM16F-dependent and independent PtdSer exposure on activation and apoptosis, at least in platelets[78,81]. While it seems TMEM16F is the most important scramblase involved in rapid PtdSer exposure, other scramblases may therefore play a role.

As many cytosolic membrane lipids act as anchors for the cytoskeleton, this redistribution severs those connections, freeing the patch of membrane to change shape (which is facilitated by the change in ratio of membrane pliability between the leaflets).

The timely convergence of all these mechanics allows the formation of a membrane bleb which takes a passive sample of the cell's plasma membrane and cytosolic constituents, as well as being actively enriched in others[82]. Due to the extremely rapid release of microvesicles upon stimulation, it seems reasonable to assume this enrichment occurs at susceptible membrane patches (or lipid rafts) prior to vesiculation.

Traditionally, most literature has defined microvesicles as being PtdSer$^+$. An issue with this definition, however, and the biogenesis pathway so far described, is that not all microvesicles are positive for PtdSer, and in fact the majority of microvesicles in plasma are PtdSer$^-$[83,84]. There may be two explanations for this: firstly, that all microvesicles do express PtdSer on release, but either lose expression or the expression is masked by the many PtdSer-binding proteins present in plasma, or secondly that PtdSer$^-$ microvesicles exist and there is therefore a biogenesis pathway which is independent of the lipid's exposure. The former explanation seems unlikely as gold labelling of annexin A5 (anxA5) in cryo transmission electron micrographs produced by the Brisson group shows a clear distinction between microvesicles which express PtdSer and those which are completely negative[83].

Whether PtdSer exposure is involved or not, once an outward bleb has formed,

a fission event must occur at the neck of the bleb to release the microvesicle into the extracellular space. Although this fission event has not been delineated in the context of ectocytosis, it is likely similar to dynamin-mediated fission observed in endocytosis[85].

1.3 Isolation of microvesicles

The isolation of microvesicles from biological fluids and cell culture medium requires the removal of cells and objects in a similar size range as microvesicles, such as platelets, apoptotic bodies and exosomes, and should have minimal protein contamination. The most common technique to isolate microvesicles both historically and currently is differential centrifugation, although commercially available isolation kits are now in use (discussed below).

Differential centrifugation involves applying centrifugal fields to homogeneous mixtures of particles at sequentially higher relative centrifugal forces to speed up particle sedimentation. The larger and denser a near-spherical particle is (with respect to the fluid in which it is suspended), the faster it will sediment. Therefore generally speaking, larger objects sediment and form pellets faster than smaller objects in the same suspension. Thus the basis of differential centrifugation in microvesicle isolation is to pellet cells during low-force centrifugation, collect the cell-free supernatant (within which any smaller particles are still mainly present) and apply a greater centrifugal force to pellet platelets and apoptotic bodies, resulting in a suspension highly enriched in microvesicles and exosomes. As microvesicles are generally larger than exosomes, the next step is to pellet the microvesicles while leaving the majority of exosomes in suspension.

While this process is easy, cheap and the most widely used method for the isolation of both microvesicles and exosomes, it has two main problems associated with it. Firstly, due to small overlaps in size distribution, microvesicle preparations will typically contain contaminating platelets and/or apoptotic bodies (depending on the source) and exosomes. As such, it is virtually impossible to generate a pure population of microvesicles; thus preparations should be referred to as microvesicle-enriched. The second and most difficult to control for problem is the breadth of centrifugation forces and times reported in the literature for each step of the centrifugation process. There is currently no consensus on the most appropriate parameters to use with most laboratories using their own protocols. Parameters reported for pelleting cells range from $600\times g$ for 10 min[86] to $4{,}000\times g$ for 20 min (twice)[87], for platelets and apoptotic bodies range from $1500\times g$ for 20 min to $13{,}000\times g$ for 2.3 min[88] and for microvesicles range from $10{,}000\times g$ for 30 min[89] to $100{,}000\times g$ for 90 min[90]. This variation in

isolation also explains variations in reported vesicle size distributions[91–93].

Even if a standard relative centrifugal force and centrifugation time were agreed between researchers, these parameters are not enough to standardise pelleting time without controlling for different k factors between centrifuges. The k factor (or clearing factor) parameter is intrinsic to a particular centrifuge and rotor combination and represents the relative efficiency of that combination at pelleting particulate matter. The k factor can be used to estimate the sedimentation time for a particle in suspension with a known sedimentation coefficient[94,95]:

$$t = \frac{k}{s} \tag{1.1}$$

where t is the time in hours it takes for the particle to sediment and s is the particle's sedimentation coefficient. k for a particular centrifuge setup depends on the minimum and maximum rotor radius, the angular velocity (which can be calculated from the maximum revolutions per minute for convenience) and can be given as[94,95]:

$$k = \frac{2.53{\times}10^5 \cdot \ln(\mathrm{r_{max}}/\mathrm{r_{min}})}{(\mathrm{RPM_{max}}/1000)^2} \tag{1.2}$$

where $\mathrm{r_{max}}$ and $\mathrm{r_{min}}$ are the maximum and minimum rotor radii, respectively. As such, as k increases, so does the time required for a particular particle to sediment. This equation gives k_{max} for the centrifuge setup; for runs which use lower than maximum speeds, the k_{adjusted} is calculated[94,95]:

$$k_{\mathrm{adjusted}} = k \cdot \left(\frac{\mathrm{RPM_{max}}}{\mathrm{RPM_{actual}}}\right)^2 \tag{1.3}$$

The sedimentation coefficient, s, is a property of the particle in suspension which depends only on its mass, radius, and the viscosity of the medium through which it is travelling, given by[94,95]:

$$s = \frac{m}{6\pi\eta r_0} \tag{1.4}$$

where m is the mass of the particle, η is the viscosity of the fluid and r_0 is the particle radius. Combining these equations yields a single model to estimate the pelleting time of microvesicles (or any near-spherical particle) in suspension:

$$t = \left(\frac{2.53{\times}10^5 \cdot \ln(\mathrm{r_{max}}/\mathrm{r_{min}})}{(\mathrm{RPM}/1000)^2}\right) \cdot \left(\frac{\mathrm{RPM_{max}}}{\mathrm{RPM_{actual}}}\right)^2 / \frac{m}{6\pi\eta r_0} \tag{1.5}$$

Using this model, Figure 1.2 shows the estimated sedimentation time for a microvesicle with 150nm radius and 0.24pg mass[96] in different fluids at 20°C and 4°C, at a range of k factor setups. Figure 1.3 illustrates the change in fluid viscosity as a function

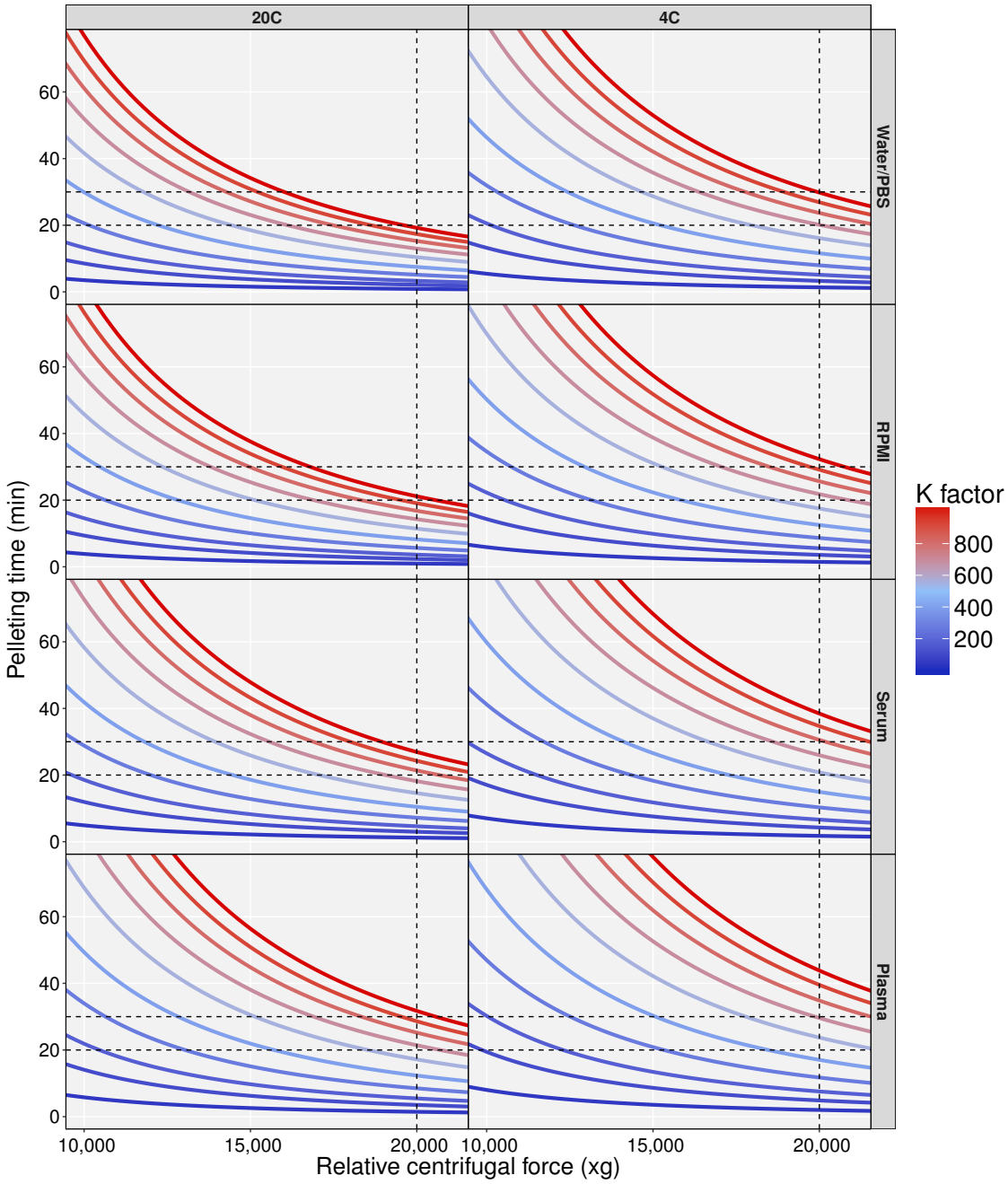

Figure 1.2: Hypothetical pelleting times of microvesicles. Hypothetical curves generated using Equation 1.5, displaying pelleting time for microvesicles of radius 150nm and mass 0.24pg with increasing centrifugal force. Panels indicate pelleting times in different fluids at 20°C and 4°C at a range of centrifuge k factors. Dotted lines highlight the range of k factors for which the particles pellet between 20 and 30 minutes at 20,000×g.

of temperature (at 1 atm) for these fluids with the corresponding sedimentation coefficients and sedimentation times of microvesicles under these conditions (assuming 150nm radius and 0.24pg vesicle mass).

It is important to note, however, that this model makes several assumptions. Firstly that the particles are perfectly spherical and remain so in the centrifugal field, that the particles do not come into contact with the walls of the tube or each other, that the fluid viscosity is constant along the path of the vesicle and that the speed of the rotor is immediately that which is specified. As most of these assumptions are not viable and as the mass of an individual particle is very difficult to measure (only a single paper has attempted such measurement[96]), this model serves as an approximation only. What this model does solidly allow, however, is the comparison of *relative* pelleting times between centrifuge setups with different k factors.

As the field of vesicle research has expanded, a number of commercially available kits for isolating *exosomes* from samples have been released which can be used to separate them from microvesicle preparations. These antibody-based kits still require larger contaminants to be removed by differential centrifugation first, and include products such as ExoQuick™ (System Biosciences, USA), ExoCap™ (MBL, USA), Total Exosome Isolation Reagent (Thermo Fisher, USA), Exo-spin™ (Cell Guidance Systems, UK) and PureExo® (101Bio, USA). While used by some labs due to their applicability to small volumes (where centrifugation would result in excessive sample loss), a handful of papers comparing one or more of these kits to differential and/or sucrose-gradient centrifugation have typically found that while they may improve yield, they may form vesicle aggregates and may co-precipitate non-exosome associated proteins[97–99].

Finally, sucrose density gradient centrifugation has been successfully used to isolate highly enriched microvesicle populations[100], but requires centrifugation times in excess of 15 hours, and depending on the downstream application, the microvesicle fraction may have to be centrifuged again in buffered-saline to remove the sucrose buffer (causing excessive vesicle loss).

1.4 Detection, enumeration and phenotyping of microvesicles

1.4.1 Electron microscopy

Due to their small size, it is nearly impossible to visualize, size and quantify microvesicles using conventional light and fluorescent microscopy techniques. The gold standard in accurate small particle visualisation and sizing is cryo transmission

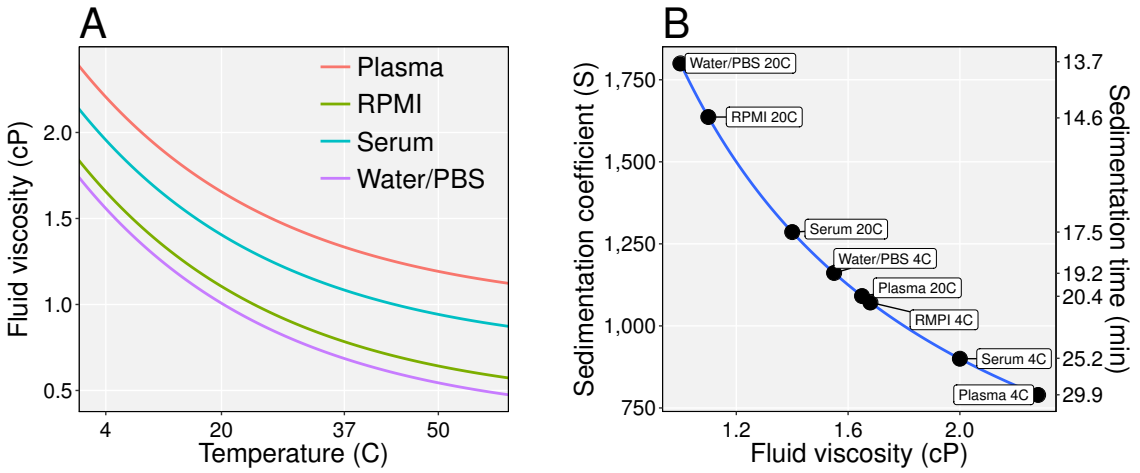

Figure 1.3: The importance of fluid viscosity on particle pelleting time. A Changes in viscosity of human plasma, serum, RPMI medium and water/phosphate-buffered saline (PBS) at different temperatures. **B** Differences in sedimentation coefficient and sedimentation time of 150nm radius, 0.24pg mass microvesicles in fluids of decreasing viscosity. Labels indicate individual conditions.

electron microscopy which, when combined with immunogold labelling, can be used to probe for up to two markers simultaneously on the vesicles.

While scanning electron microscopy can generate high detail images of the 3 dimensional structure of small objects and can also be combined with immunogold labelling, the non-aerial topography data it generates makes it hard to measure the dimensions of vesicles. Standard transmission electron microscopy generates images of planar electron density and allows the dimensions of a field of vesicles (and their purity) to be measured. Sample processing for standard transmission electron microscopy can be harsh on biological structures and may introduce artefacts. For example, a once considered hallmark of exosomes, that they exhibit a "cup" shape when imaged by electron microscopy[101], is due only to the dehydration step involved in sample processing[102]. In fact, exosomes and microvesicles are spherical, as demonstrated by cryo transmission electron microscopy which involves as little sample manipulation as possible[102]. The sample is snap frozen in liquid ethane and imaged, such that the specimens are unfixed and can be imaged in their native structure.

The main caveats with these techniques, however, is that they are low throughput, highly technical, and don't allow estimation of vesicle concentration[103]. In response to this poor scalability, a staple method of particle measurement in the microvesicle field has become flow cytometry.

1.4.2 Flow cytometry

Flow cytometry has revolutionised multiparameter characterisation of cells at extremely high throughput. It allows quantitative assessment of relative and absolute object numbers per unit volume within and between samples, and semi-quantitative assessment of changes in cell phenotype, viability and cell cycle, Ca^{2+} flux and more. Flow cytometry is commonly used to discriminate between distinct cell populations by their relative size by measuring the forward angle light scatter (FSC), and their relative granularity by measuring right angle light/side scatter (SSC). When samples are combined with bead standards of known concentrations, absolute concentrations of different cell populations can be reported. For these reasons, flow cytometry has become a common method of identifying and phenotyping microvesicles (by their cell of origin and/or contents). Traditionally, however, published flow cytometry data on microvesicles has been plagued by uncritical use of instruments, and poorly controlled experiments, making the interpretation and reliability of much of the published experiments difficult. While flow cytometry can be the most powerful method of analysing vesicles, there are many challenges and limitations which must be acknowledged and mitigated by the researcher.

1.4.2.1 Differences in refractive index

The most commonly used method of microvesicle identification in aqueous samples is by their size. In cytometry, by including beads of known sizes (typically in the range of 100nm to 1,000nm in diameter), the microvesicle population can in theory be identified by its position in the FSC and SSC plot, relative to the size beads. There are, however, significant problems with this strategy. Firstly, while the FSC parameter is often thought of as a direct measurement of object size, it is not. Generally speaking, the greater the diameter of an object passing through the scatter laser, the greater its FSC will be, relative to other objects of the same refractive index. The issue with using beads to size (and identify by size) microvesicles is that polystyrene and latex beads possess refractive indices of ~1.61 compared to ~1.38 for microvesicles[104–106]. This is compounded by the fact that refractive index varies considerably within a single population of vesicles, largely dependent on diameter, and between vesicles from different sources[106]. Therefore one cannot simply construct a standard curve of bead sizes and interpolate microvesicle size from their FSC[107]. This difference in refractive index can also convince researchers to exclude much of the microvesicle population, which may fall below the 100nm or above the 1,000nm bead populations on the FSC and SSC plot.

Synthetic liposomes of known sizes and refractive indices more similar to those of

biological vesicles have been shown to be superior calibrators than beads, but these must be generated freshly for each experiment and are not commercially available[108]. Additionally, the size and coefficient of variance of the size will depend upon and vary with each generation, and the liposomes must themselves be sized using a technique able to resolve small particle size accurately.

1.4.2.2 Vesicles scatter very little light

The most common way of triggering events when analysing cells on a flow cytometer, such that the pulse data is recorded and integrated for a particular event, is by setting a threshold on the FSC detector. For particles as large as cells, this is more than sufficient to detect each object as it passes through the flow cell, as the amount of light they scatter in the forward direction is considerable. Cells scatter so much light in the forward direction that, in many instruments, a photodiode is used as its detector rather than the more sensitive photomultiplier tube (PMT) generally used for other parameters, and this is preceded by a neutral density filter to prevent the detector from saturating easily.

The light scatter produced and detected by a particle depends on the ratio between the particle diameter and the wavelength of light it is interrogated with, the refractive index of the particle, the angle of light detection, and the intensity of the laser. This creates problems when trying to detect the scattered light of microvesicles, whose diameter is around or even smaller than the wavelength of the scatter laser (most commonly a 488nm).

The phase function of scattered light (the probability density that photons of light will be scattered in any direction in a sphere) for particles of varying diameters from lasers of different wavelengths is simulated in Figure 1.4. Note that while the shape of the phase function of submicron particles can be seen when logarithmic, the scatter becomes negligible when plotted in linear coordinates. Note also that as the ratio of particle diameter to wavelength approaches zero, the phase function approximates Rayleigh scattering, where light is scattered equally in all directions, and that for cell-sized particles, the phase function exhibits Mie scattering, where light is predominantly scattered in the forward direction[109]. Finally, these simulations demonstrate that forward scatter is inversely proportional to laser wavelength. As such, when the cytometer is set up to trigger on FSC, the majority of microvesicles do not scatter enough light to be detected above the optical and electronic noise. The ability to resolve small particle populations by their FSC is also variable between cytometer models and even between machines of the same model because it is the most alignment-critical parameter (and thus most susceptible to variation). SSC has been used as a trigger as it is typically detected with a PMT and is not preceded

by a neutral density filter, allowing for more sensitivity, but many of the smaller vesicles still will not scatter enough light to be detected above the noise.

Alternatively, the wavelength of the scatter laser can be reduced to decrease the ratio between it and the particle diameter and increase the amount of scattered light. Nevertheless, even when using violet or even ultraviolet lasers (typically 405nm and 355nm, respectively) for the scatter parameters, the majority of the microvesicle population has a diameter smaller than this, and will scatter very little light.

Additionally, next generation flow cytometers are available which have much lower limits of detection. These include the Apogee Micro and Micro-Plus (Apogee Flow Systems, UK) small particle cytometers which are shown to have detection limits of ~200nm and <100nm, respectively, especially when used in conjunction with silica sizing beads (whose refractive index is more comparable to phospholipid particles)[110].

1.4.2.3 Separating weak signals from noise

Even in the absence of light, photodiode and PMT detectors produce a "dark current" as background output. If a photon of light collides with either form of detector, electrons are released to produce current. When the light received is being scattered or released from particles in the flow stream of a cytometer, the number of photons results in a peak of current output, where the current increases as the particle enters the interrogation point, and declines again as it leaves, returning to dark current output. As both optical and electronic noise can cause small fluctuations in the dark current, what constitutes a peak generated by an object of interest must be defined by setting a threshold current or "trigger". If the output current of a detector reaches this threshold, an event is "triggered", and the electronics of the cytometer can measure the width, height and area of the peak which are saved as data.

The voltage gain of the detector (which indirectly controls the number of electrons produced in response to one photon) correlates with the noise of the dark current. For example, if some optical disturbance in the flow cell, such as a bubble, causes photons to be scattered onto the detector, the current generated during this event would be larger if a high gain is applied to the detector, compared to if a low gain were applied. This can become a problem when the signals from objects of interest are very small, as increasing the detector gain will not only increase the current generated by these objects, but also of fluctuations in the dark current.

When the detector voltage gain is high and the threshold is low on a scatter parameter set as the instrument trigger, a large amount of optical and electronic noise (although the former is far more consequential) masks much of the vesicle population and raises the lower limit of detection. Sources of optical noise can be

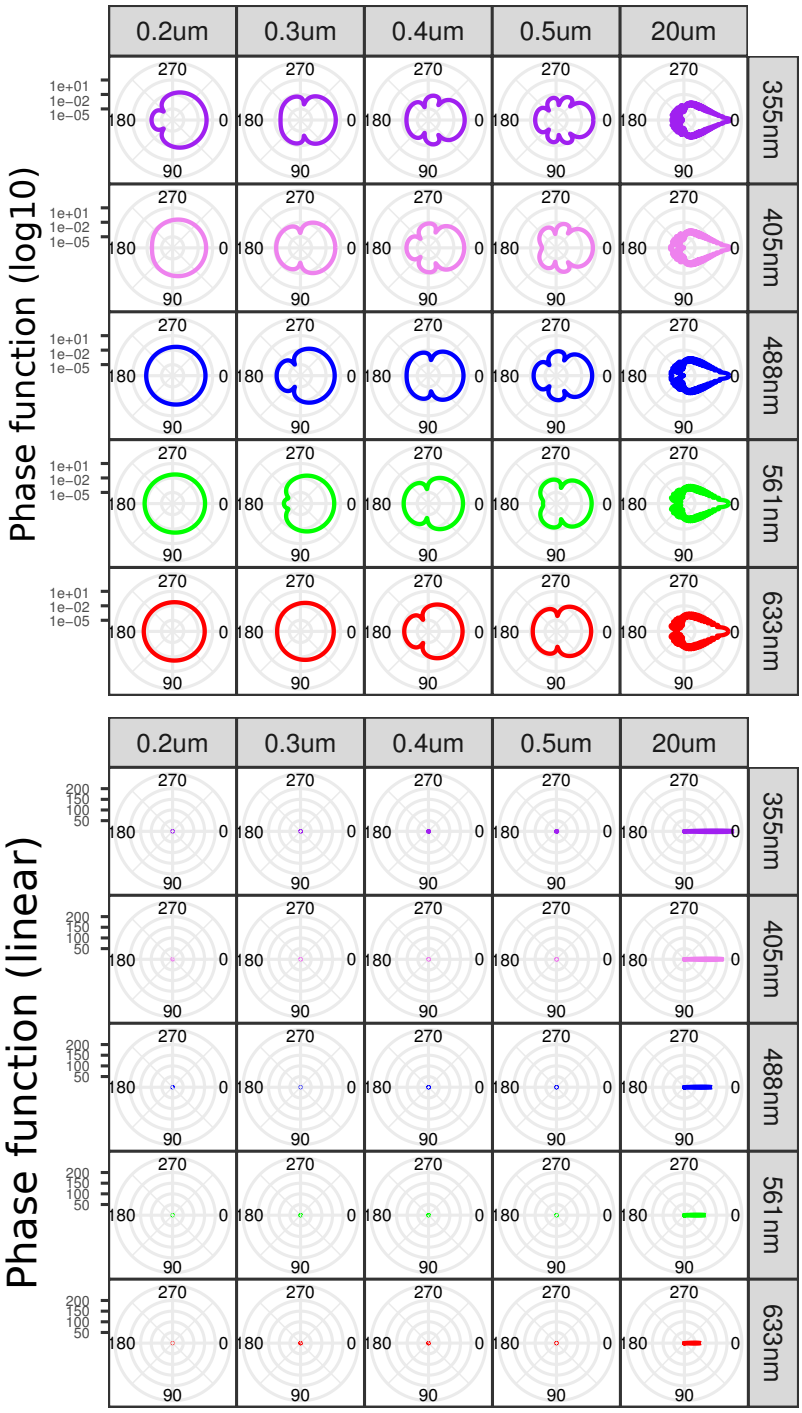

Figure 1.4: Particle light scattering profiles. The shape of scattered light from particles depends on their size (columns) and the wavelength of light (rows). The polar axes denote angle of light scatter from the angle of incidence (for example, in the flow cell of a flow cytometer), the y axis denotes the phase function of scatter (the probability density of photons being scattered in that direction; $\log_{10}$ in the top panel, linear in the bottom). Each facet shows the simulated phase function of scattered light from a particle of a specific diameter, at a specific laser wavelength.

split into those intrinsic to the sample, and those intrinsic to the cytometer.

Air bubbles in the sheath fluid can refract enough light to create scatter signals of a similar intensity to those from vesicles, as can any salt aggregates or microbial contamination. As such, degassing and filtering the sheath fluid prior to use can remove these contaminants, as can running a detergent or bleach through the sample line prior to acquisition or even widening the obscuration bar which blocks the scatter laser in the line of incidence (if triggering on FSC). More drastic instrument modifications to reduce noise include optimising the detection geometry, replacing the FSC photodiode with a more sensitive PMT or, less drastically, switching the trigger channel to one which employs a PMT (SSC for example)[111]. These optimisations, however, become difficult when the cytometer is used by many researchers for many applications; not to mention the increased risk of noise events in this situation. Noise intrinsic to the sample can be from air bubbles, salt and protein aggregates (including from antibody conjugates), membrane fragments and any other objects of a similar size to vesicles.

In the last five years the main change in approach to tackle issues of low scatter detection and high noise has been to switch from using scatter-based triggering, to using fluorescence-based triggering instead. This involves running vesicles, all of which have been fluorescently labelled with a fluorescent protein or dye, and using a fluorescence channel as the trigger instead. The value of this approach is that the fluorescence signal depends on the number of photons released from fluorophores associated with the vesicle, and is therefore only indirectly related to vesicle diameter. Although smaller vesicles will carry/contain fewer fluorophore molecules, if the fluorophore is sufficiently bright, the signal will generally be considerably larger than those in the scatter channels, and as such, a much greater proportion of the population can be detected.

1.4.2.4 Avoiding coincidence

An often overlooked hurdle when analysing vesicles by flow cytometry is that due to their small size, several microvesicles can pass through the interrogation point of the laser at once, being recorded as a single, coincidence event. The major challenge in detecting and excluding such events, which may give false positive results when phenotyping or counting, is that traditional doublet discrimination techniques used for cells do not work for microvesicles. This is due in part to microvesicles having a much greater range of relative sizes than cells, where a vesicle 400nm in diameter may have a scatter profile similar to two vesicles each 200nm in diameter (and therefore the two events cannot be discriminated from each other) and also that the closer a signal is to the instrument's lower limit of detection, the greater stochastic error

associated with the signal.

The only way to mitigate the contribution of coincidence events is to serially dilute the vesicle sample and run each dilution. When the drop in threshold rate of the cytometer becomes linear with sample dilution, the researcher can be confident that the majority of the events recorded are single vesicles. The result is that any one experiment may require three or more times the number of acquisitions as original experimental samples.

1.4.2.5 Low antigen density

Perhaps the most challenging limitation of analysing vesicles by flow cytometry (and indeed all analysis techniques) is that the total copy number of antigens of interest per vesicle is very low, particularly in weakly expressed antigens.

A hypothetical relationship between vesicle size, antigen density and total antigen copy number is modelled in Figure 1.5, using 5,000, 40,000 and 80,000 copies per platelet as examples of low, medium and high antigen density, respectively. If a platelet is assumed to have a 5µm^2 surface area[112], then the product of the antigen densities for these copy numbers and the surface area of a vesicle (calculated as $\pi \times diameter^2$) gives an estimate of the copy number for that vesicle. This relationship assumes that the vesicle is perfectly spherical, that antigen density is uniform across the membrane, and is only applicable to surface antigens (though vesicle volume could in theory be substituted in the case of luminal antigens). Nevertheless, this relationship predicts that for vesicles smaller than ~250nm, weakly expressed antigens are very difficult to detect above background. A major implication of this is that the true proportions of vesicle subsets in a population can be difficult or impossible to ascertain, and that a vesicle preparation may be declared devoid of a particular antigen when it is in fact weakly expressed.

This challenge can be mitigated in several ways, each of which aims to maximise the signal to noise ratio of the fluorescence measurements. Firstly, fluorophores which are as bright as possible (given as the product of the extinction coefficient and the quantum yield) should be used and at concentrations titrated to maximise the signal to noise ratio. The quantum yield (or efficiency) is the ratio of emitted photons per absorbed photons, and the extinction coefficient is the amount of light of a particular wavelength a compound absorbs (therefore fluorophores which absorb more photons at a particular wavelength and emit a greater proportion of them will be brighter).

The PMT gain voltages should be set so that a negative population is sufficiently separated from noise, and the fluorophore panel should be designed such as to minimise the amount of fluorescence compensation required. Finally, weak antigenic

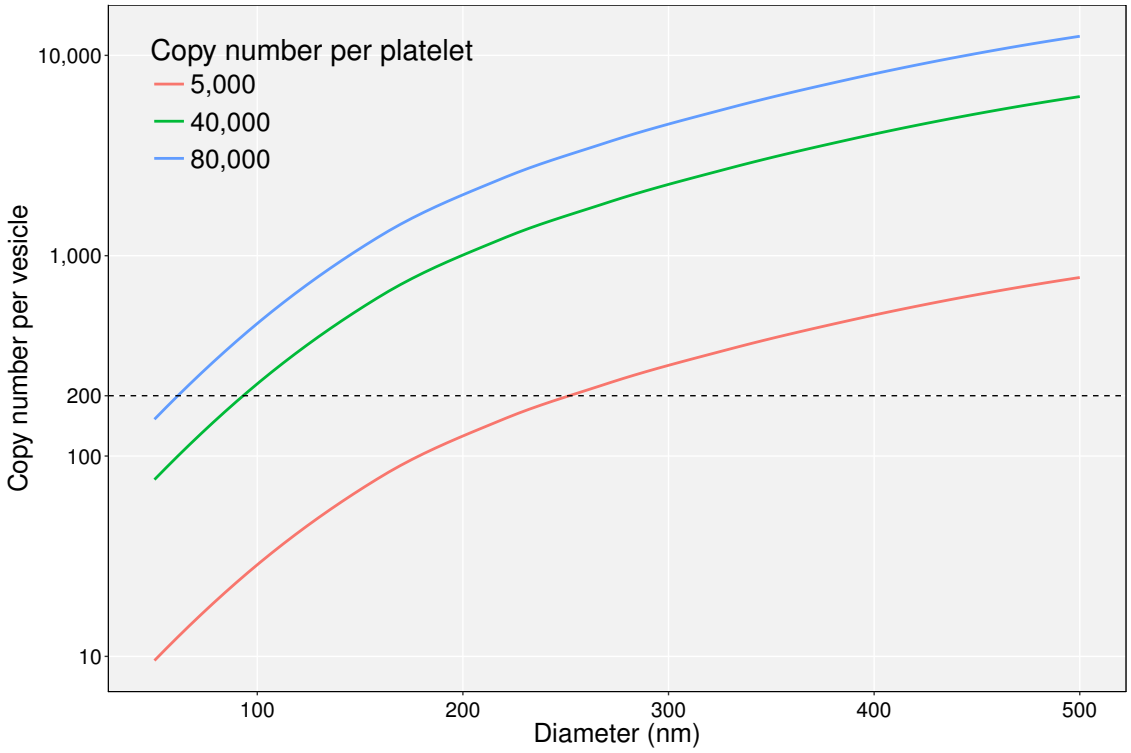

Figure 1.5: Relationship between the total copy number for a particular surface antigen and vesicle diameter. The three coloured lines represent the relationship for antigen densities equivalent to 5,000, 40,000 and 80,000 antigens per platelet with a 5μm^2 surface area. The dotted line represents the lower limit of detection of the molecular equivalent of soluble fluorescein molecules for many modern flow cytometers. Each relationship assumes the vesicle is perfectly spherical, and that the antigen is uniformly distributed across the membrane.

signals can be amplified by probing for the antigen with an unconjugated primary antibody, followed by a secondary antibody-fluorophore conjugate. The benefit of this approach is that more than one secondary antibody may bind to one primary antibody, thus increasing the number of fluorophore molecules per antigen. The major drawbacks of this technique are that it requires more time and more controls to ensure any signals seen are not a result of non-specific binding.

1.4.3 Nanoparticle tracking analysis

Nanoparticle tracking analysis is a technique that allows the size of individual small particles and their concentration within solution to be quantified in high throughput, where sample recovery is possible. The technique estimates particle size based on their Brownian motion in solution i.e. smaller particles resonate at a higher frequency than larger particles. Individual particles are imaged and tracked over time by a video camera which detects the light they scatter from a laser which illuminates the chamber.

While fluorescent probes aren't necessary for sizing and enumeration, they can be included so that target particle populations can be identified and interrogated (e.g. $PtdSer^+$ vs. $PtdSer^-$ microvesicles) as the instruments can be fitted with an excitation laser and fluorescence bandpass filters[91]. To circumvent the problem of rapid photobleaching while fluorescently-labelled vesicles are being excited, this technique is commonly performed under flow conditions, so that the time an individual vesicle remains within the laser beam is minimal. Nevertheless, nanoparticle tracking analysis has, as yet, poor fluorescence sensitivity compared to flow cytometry.

1.4.4 Tunable resistive pulse sensing

Another technique which is both sensitive and high throughput in quantifying vesicle size is tunable resistive pulse sensing (TRPS). TRPS measures the current through a nano-sized pore whose diameter can be dynamically changed (i.e. tuned) to allow particles of varying sizes to pass through it. Particles on one side of the pore are driven through it by a combination of pressure and voltage, and the impedance of the pore is measured at 0.5MHz. As a single particle passes through the pore, it increases the impedance (i.e. decreases the current passing through the pore), the magnitude of which is directly proportional to particle volume, which is used to measure particle radius. The duration of the impedance can be used to calculate each particle's ζ-potential, the potential difference between the surface of a particle and the charge of its medium, and the frequency of impedances can be used to calculate the concentration of particles in the medium[113].

While TRPS has a similarly low size limit of detection as nanoparticle tracking analysis and can estimate particle concentration, it is arguably less flexible in phenotyping particles as there is no capability to measure fluorescence. Instead, binding of aptamer probes to target molecules on microvesicles can be quantified by measuring changes in ζ-potential. Aptamers are small peptide or oligonucleotide molecules which are screened for their affinity to molecular targets of interest, however, they are not as widely commercially available as antibody probes[114].

1.4.5 Imaging cytometry

While nanoparticle tracking analysis and next generation flow cytometry provide useful techniques for small particle analysis, one of the most powerful but underused technologies is the ImageStream platform. Pioneered by Amnis, the Flowsight, $ImageStream^X$ and $ImageStream^X$ Mk II are cytometers which take brightfield, darkfield and fluorescent images of each object that passes through the flow cell. The major implication of this is that the researcher can interrogate ambiguous

populations by directly viewing the images associated with each event. In other words, the user can see individual microvesicles and differentiate them from noise and artefacts.

Not only do these systems allow visual inspection of microvesicles, they also boast extremely minimal noise and therefore have lower limits of fluorescence detection, allowing resolution of fluorescent objects as small as 20nm in diameter[1]. This is due, in part, to their time delay integration mode of object imaging, which allows a single particle to be imaged for orders of magnitude longer than in standard cytometers. It must be noted, however, that while these instruments can resolve very small fluorescent objects, as all object measurements are made directly from their images, objects smaller than the wavelength of visible light (~400nm) cannot be resolved using brightfield detection alone. Their resolution of particle SSC is similarly poor compared to standard cytometers and so still rely on fluorescence triggering to resolve as much of the microvesicle population as possible.

Usefully, ImageStream cytometers utilise syringe-driven sample injection, and therefore accurately aspirate and measure the volume of sample injected into the flow cell. This means the number of objects per mL of sample can be reported with a reasonably high degree of accuracy without the need for counting beads. The implication of this is that the density of microvesicle preparations can be adjusted and standardised prior to their experimental use.

Additionally, the ImageStream technology has an extraordinary number of parameters that can be used to characterise populations. These include up to 9 fluorescent channel parameters (the images of which can be overlaid with each other and the brightfield image), morphology measurements, such as circularity, aspect ratio and symmetry, SSC and many more. Although the instruments do not have a FSC parameter, object area and/or diameter can be used to estimate relative size. Using these parameters, it was shown that the technology allows linear separation of size beads and microvesicle into discrete, resolved populations (Figure 3.1).

The main drawback of the ImageStream platform, however, is that because data on each object is collected via a charge-coupled device (CCD) rather than a PMT, the instrument has a smaller dynamic range for separating fluorescence signals than most modern flow cytometers.

1.5 Physiological and pathophysiological roles of microvesicles

1.5.1 Microvesicles as signalling vectors

The promiscuous nature of microvesicle release raises the question of how the functions of such ubiquitous structures can be controlled and fine-tuned. The protein, lipid and nucleic acid content of microvesicles depends on the cell type from which they bud, and also on the phenotype of that cell. For example, macrophages whose phenotype has been polarised *in vitro* release microvesicles containing the mRNA of genes associated with that phenotype[115]. Horizontal transfer of these mRNA transcripts within microvesicles resulted in their translation into protein in receptive macrophages, conditioning their phenotype to that of the donor cells. After performing transcriptomics on both the donor cells and their offspring microvesicles, the authors noted that while the expression of many transcripts was comparable between the two, some were enriched in the microvesicle fraction. This supports the view that microvesicles take both a passive sample of the cell's state, and are also selectively packaged. While mechanisms of protein and lipid trafficking to the membrane have been described[116–118], how mRNA is stably packaged into these vesicles is unknown.

Another question raised by this mode of nucleic acid transfer is how the luminal contents of the microvesicle are safely conveyed into the cytosol of the target cell. The uptake mechanisms of microvesicles by different cell types is a much debated issue. Several papers ascribe their internalisation by most cell types to be via endocytosis and not phagocytosis (a process usually associated with larger objects)[119], while others suggest that vesicle uptake by macrophages and dendritic cells is phagocytic and pinocytic, but not endocytic[120]. Either way, both pathways result in the formation of lysosomes or, in the case of endocytosis, recycling to the plasma membrane[121]. While the latter mechanism may explain the transfer of membrane proteins, how bioactive lipids, mRNA and miRNA species escape lysosomal degradation is not described. While passive fusion of the microvesicle and cell membranes has been proposed, the protein-rich plasma membrane does not readily permit this form of assimilation[122]. Nevertheless, microvesicles and exosomes represent the only mechanisms of long distance RNA transfer, as they are stable in plasma whereas RNA itself is not[123].

Not only do microvesicles transfer bioactive molecules to other cells, they participate in juxtacrine signalling by coming into direct contact with their target cells. Ligands expressed on the surface of the microvesicle can bind their cognate receptors and elicit a response independent of their uptake. In this situation, microvesicle internalisation may serve as a signal termination mechanism. Circulating microvesicles

can also interact with plasma proteins, both sequestering and reducing bioavailability of some, and modulating the function of others. For example, microvesicle-exposed PtdSer activates the clotting cascade by allosterically modulating factors X(a) and V(a), enhancing prothrombinase activity[43]. Indeed, for their surface area, microvesicles are considerably more potent at inducing platelet aggregation than platelets themselves, and are the main mechanism for the rapid induction of haemostasis. This is supported by data from patients diagnosed with Scott syndrome, whose impaired microvesicle release manifests most obviously as a severely diminished clotting response[124].

The most deeply studied population of microvesicles is platelet-derived. This is due to their abundance in plasma (second only to erythrocyte-derived microvesicles[1]), the fact they were the first population observed by Chargaff and West[6], and perhaps because their physiological (and pathophysiological) importance is so immediately apparent. However, all cell types release these nanostructures into their respective biological compartments and it stands to reason that all microvesicles, from every cell type, in every tissue and microenvironment within the body elicit functions that contribute in some way to health and possibly disease. While much progress has been made in the role of these vesicles in oncology, cardiovascular, respiratory and neurological health[39], the role of microvesicles in inflammation and immunology will be discussed below.

1.5.2 Microvesicles in adaptive immunity

One of the most exquisite mechanisms in adaptive immunity is the processing and presentation of exogenous antigens on the surface of antigen-presenting cells (APC), such as dendritic cells and macrophages. In the classical model of lymphocyte cell activation, an APC must provide two activation signals: a major histocompatibility complex (MHC)-mounted non-self antigen (which binds the T or B cell receptor), and co-stimulatory molecule expression (CD80 and CD86 which activate CD28 expressed on the lymphocyte)[125]. While much of this process is mediated by direct phagocytosis and processing of pathogens by APCs and the formation of a cell-cell immune synapse, both antigen acquisition and presentation can be mediated by vesicles. Vaccination of healthy mice with cell-free tumour-derived microvesicles results in dendritic cells which are positive for tumour antigens, and able to induce an antigen-specific adaptive response[126]. This supports a role of microvesicles in long distance cross-presentation and acquisition of pathogenic antigens.

Once positive for an exogenous antigen, APCs (even weaker APCs like B cells) activated by danger or pathogen-associated molecular pattern (PAMP)s, such as LPS, release microvesicles and exosomes carrying the antigen on their surface[101,127].

In theory, provided these vesicles meet the same requirements as immunogenic APCs (i.e. express high density MHC-mounted antigen and CD80/CD86), then they will be able to induce lymphocyte activation in the absence of their donor APCs. There is also evidence of vesicular antigen presentation which is independent of MHC expression, although the role and importance of this mechanism *in vivo* is not clear[128].

Activated T cell-derived microvesicles express Fas ligand which induces NFκB translocation in vascular endothelium and smooth muscle, upregulating nitric oxide synthase and cyclooxygenase-2[129,130]. $CD4^+$ microvesicles can activate B cells similarly to APC vesicles, and $CD8^+$ microvesicles may contribute to the killing of infected cells[131].

In addition to their physiological effects, inappropriate or modulated microvesicle release and signalling can amplify disease processes. For example, ectocytosis can be hijacked during viral infections. In the case of HIV, infected T cells release virus-laden microvesicles which provide a protective vector for viral dissemination[132]. HIV^+ microvesicles in plasma also suppress dendritic cell activation by binding to CD44[133]. Insufficient dendritic cell activation is a major hurdle in the development of a HIV vaccine and so this represents a targetable mechanism.

1.5.3 Microvesicles in innate immunity

The cells that constitute the innate arm of our immune system are the sensors and first responders to inflammatory stimuli like infection and damage. Tissue resident macrophages, dendritic cells and mast cells express pattern recognition receptors, such as toll-like receptors (TLR) and Nod-like receptors, to detect bacterial, viral and fungal molecular patterns. Engagement of TLR4 by LPS in monocytes, macrophages or dendritic cells induces the transcription of pro-interleukin (IL)-1β[134]. Engagement of the purinergic ligand-gated ion channel $P2X_7$ by ATP (which is released from cells undergoing necrosis and acts as a damage-associated molecular pattern (DAMP) when extracellular) induces inflammasome activation and the subsequent cleavage and release of bioactive IL-1β[135]. Unusually, however, IL-1β belongs to a class of proteins which lack an N terminal signal peptide which targets them to biological membranes and, as such, cannot be secreted from the cell via the classical secretory pathway[136]. A number of "leaderless" proteins have been identified including thioredoxin, macrophage migration inhibitory factor, galectins 1 and 3, fibroblast growth factors 1 and 2, IL-1α, IL-1β, IL-18 and annexin A1 (anxA1), all of which are readily secreted[137]. How these leaderless proteins were released from the cell remained a mystery until IL-1β was found to cofractionate with endosomes and lysosomes in monocyte preparations, suggesting it was released via a vesicular

pathway[138]. In 2001, MacKenzie *et al.* demonstrated the rapid release of IL-1β$^+$ microvesicles upon inflammasome activation in LPS-primed monocytes[32], and this has since been shown to depend on other vesicular pathways as well[139]. The presence of a number of leaderless proteins has since been confirmed within both exosomes and microvesicles, suggesting vesicular export as a common secretory pathway for these proteins[140,141].

The uncoupling of IL-1β synthesis by mononuclear phagocytes from its release is a biological safeguard against inappropriate inflammation. By limiting IL-1β release to vesicles, an initial PAMP signal is usually insufficient to induce its secretion[142]. Instead, primed cells must receive a temporally distinct second signal which induces microvesicle release (such as ATP generated during tissue damage).

IL-1β$^+$ microvesicles stimulate other tissue resident macrophages and dendritic cells to release pro-inflammatory cytokines, such as IL-6 and tumour necrosis factor α (TNFα) and chemokines, such as CCL2, CCL5, CCL22 and CXCL8, to activate the local endothelium and create chemotactic gradients for neutrophils, monocytes and lymphocytes[143]. Engagement of the IL-1 receptor on endothelial cells by these microvesicles induces the release of IL-6, IL-8, GM-CSF and PAF, and expression of P-selectin within minutes, E-selectin within ~4 hours and ICAM-1 and VCAM-1 within ~6 hours[144]. Endothelial cells can also be activated by platelet-derived microvesicles containing IL-1β[35].

Changes to vascular adhesion allow circulating leucocytes to tether and roll across the activated endothelium and eventually extravasate into the tissue. Typically, neutrophils are the first circulating cell type which capture and become activated, upregulating their expression of CD11b and shedding L-selectin[145]. Activated neutrophils on the endothelium release microvesicles enriched in complexed CD11b/CD18, and P-selectin glycoprotein ligand-1 which activate GPIba and P-selectin, respectively on platelets, activating them to promote thrombus formation and further endothelial cell activation[82].

Despite their capacity to propagate inflammation and induce damage, activated neutrophils release large numbers of microvesicles that are enriched in the potent anti-inflammatory and pro-resolving protein anxA1[36]. These anxA1$^+$ neutrophil microvesicles disrupt the interaction between endothelial cells and neutrophils both *in vitro* and *in vivo* by ligating anxA1's cognate receptor ALX/FPR2. The final step during neutrophil paracellular transmigration is the elongation of a uropod which fills the space through which the neutrophil is transmigrating[146]. The intravital microscopy experiments performed in this paper show that when transmigrating neutrophils finally retract this uropod, they often leave a microvesicle-like vesicle behind on the luminal side of the vessel wall. Although the purpose of these vesicles

and their similarity to ectocytic microvesicles is not fully known, they may restrict further leucocyte transmigration through anxA1 and by sterically plugging loose endothelial cell junctions.

Endothelium-activated monocytes release tissue factor$^+$ microvesicles which promote thrombus formation and haemostasis[147]. During monocyte transendothelial migration, monocyte-derived CCR5 is transferred via microvesicles to endothelial cells[148]. As CCR5 is one of the main receptors used by HIV for internalisation, this process was shown to make inflamed endothelium more susceptible to infection.

In the case of infectious disease, neutrophils stimulated with opsonised bacteria release microvesicles which are highly bacteriostatic compared to microvesicles generated spontaneously or with phorbol myristate acetate[149]. Microvesicles from opsonised *Staphylococcus aureus*-stimulated neutrophils contain functional myeloperoxidase and lactoferrin which may explain some of their antibacterial effect, although blockade of microvesicle CD18 (β2 integrin) reverted the inhibition of bacterial growth. The authors observed that these microvesicles formed Ca^{2+}-dependent, vesicle-bacteria aggregates via CD18 which prevented growth of *Staphylococcus aureus* and *Escherichia coli* (but not *Proteus mirabilis*) and made them available for phagocytosis by myeloid cells (regardless of whether they were opsonised). This either suggests that neutrophils release microvesicles relatively responsive to the pathogen that stimulated them, or simply that *Proteus mirabilis* was resistant to their effects in this system. In the same publication, the presence of these microvesicle-bacteria aggregates was confirmed in patients with bacteraemia whereas they were absent in healthy controls. These microvesicles therefore represent a novel bactericidal mechanism in neutrophils. Whether other leucocytes, such as natural killer cells, monocytes and macrophages, can generate pathogen-responsive microvesicles has not been investigated.

In the inflammatory microenvironment, there is some evidence that neutrophil microvesicles can modulate macrophage phenotype and dendritic cell activation. Human monocyte-derived macrophages treated with microvesicles isolated from TNFα-stimulated neutrophils expressed lower levels of IL-1β, IL-6, IL-8, IL-10, IL-12p70 and TNFα in response to zymosan and LPS, suggesting a lower extent of activation[37]. Macrophages treated with these microvesicles released TGFβ regardless of zymosan or LPS which, along with PtdSer, appeared responsible for many of the phenotypic effects seen. In similar experiments by the same group, monocyte-derived dendritic cells matured more slowly in response to LPS when treated with neutrophil microvesicles and expressed lower levels of CD86 and MHCII[150]. Macrophages stimulated with neutrophil microvesicles also exhibit a greater efferocytic capacity[151]. Dendritic cells stimulated with neutrophil microvesicles during maturation were

also less phagocytic of zymosan particles and less able to induce allogenic T cell proliferation. As with macrophages, microvesicle treatment induced TGFβ release from dendritic cells regardless of other treatments, and some of these effects were dependent on PtdSer. Microvesicle modulation of inflammatory cytokine and surface protein expression was found to be mediated by the interaction between PtdSer on the microvesicle, and the receptor tyrosine kinase Mer (most likely via the Protein S and/or Gas6 scaffold proteins). Release of TGFβ was shown to be independent of PtdSer, however[150]. The activation of platelets by pre-transmigrated neutrophil microvesicles may explain their apparent shift between inducing and inhibiting inflammation pre and post transmigration, respectively.

1.6 The resolution of inflammation

The functions served by inflammation are purely protective and have evolved in response to selection pressure from pathogenic infection and tissue damage. Shortly after detection of a noxious stimulus, local vascular permeability increases and innate leucocytes infiltrate the affected site which typically becomes reddened, swollen, hot, painful and may lose function. During the course of physiological inflammation, the cellular infiltrate contains and removes the injurious stimulus before repairing the damaged tissue, leaving the site and restoring it to its homeostatic condition. The process of restoring inflamed tissue to its normal state is called the *resolution* of inflammation, a term whose first documented usage was in 1838[152].

A deprecated view of the transition between inflammation and resolution was that removal of the initial stimulus leads to a transient decline in inflammatory signalling, and passive deactivation of the infiltrated cells. A wealth of evidence opposes this view, favouring the active resolution hypothesis which states that for inflammation to resolve itself, a network of active cellular and signalling events must occur to restore tissue homeostasis[153]. The majority of inflammatory events resolve themselves appropriately. The situation where resolution is impaired or delayed is termed chronic inflammation and can ensue as a result of excessive pro-inflammatory and/or insufficient pro-resolution signals[153]. It is important to note here that the terms anti-inflammatory and pro-resolving are not synonymous. Anti-inflammatory signals directly counter inflammatory signals (IL-1 receptor antagonist for example). Pro-resolution signals may do this, but also initiate active processes which result in tissue homeostasis. Our understanding of these processes is reviewed below.

1.6.1 Lipid class switching

The resolution of inflammation is programmed by early inflammatory events. When granulocytes extravasate and become activated, they promote transient lipid class switching of arachidonic acid products from the classical prostaglandins and leukotrienes to pro-resolving lipoxins[154]. Lipid class switching also involves the conversion of the ω-3 polyunsaturated fatty acids, eicosapentaenoic acid and docosahexaenoic acid (DHA) into E series resolvins, and protectins, maresins and D series resolvins, respectively[155]. These pro-resolving lipid mediators collectively reduce vascular permeability, inhibit further neutrophil transmigration, promote recruitment of non-phlogistic monocytes, induce neutrophil apoptosis and promote their efferocytosis by macrophages[156–160].

1.6.2 Apoptosis and efferocytosis

Neutrophil apoptosis at the site of inflammation is considered one of the fundamental checkpoints in inflammation resolution. Transmigrated neutrophils typically live 1 to 2 days before undergoing constitutive or induced (by macrophage-derived Fas ligand for example) apoptosis[161,162]. As opposed to necrosis which releases cytosolic DAMPs and is pro-inflammatory, apoptosing neutrophils expose PtdSer on their surface, which signals them for efferocytosis (in the presence of adaptor proteins, such as protein S or Gas6)[163]. Efferocytosis and contact with neutrophil apoptotic bodies decreases expression of TNFα , IL-12, IL-1β and IL-6, and increases expression of IL-10 and TGFβ in macrophages[151]. This switching of macrophage phenotype also promotes their production of lipoxins, DHA products and E series resolvins while decreasing their production of classical eicosanoids[164]. IL-10 and TGFβ further alter macrophage phenotype, enhancing efferocytosis and conditioning them into a "wound healing" phenotype which promotes matrix deposition, tissue remodelling and repair[165]. Adenosine released from apoptotic and necrotic neutrophils also induces macrophage vascular endothelial growth factor (VEGF) production which is important for endothelial and epithelial repair[166].

1.6.3 AnxA1

Neutrophils, monocytes and macrophages store large amounts of the pro-resolving protein anxA1[167]. In neutrophils, the majority of anxA1 is stored in the tertiary (gelatinase) granules which fuse rapidly with the membrane upon attachment to the endothelium[168]. AnxA1 is also found in the cytosol, where it rapidly localises the cytosolic leaflet of the plasma membrane at high intracellular Ca^{2+} concentrations and binds PtdSer[169–171]. Surface expression of anxA1 facilitates juxtacrine signalling

from neutrophils to other myeloid cells and endothelium which express ALX/FPR2, while release of anxA1$^+$ microvesicles allows for paracrine signalling. In addition to inhibiting neutrophil recruitment to the inflamed site, anxA1 promotes neutrophil apoptosis, the efferocytic capacity of macrophages (as well as regulating their TNFα and IL-6 production) and downregulates the degranulation of mast cells[172].

1.6.4 TAM receptors

Tyro3, Axl and MerTK form the TAM family of receptor tyrosine kinases. This receptor family binds to PtdSer via the adaptor proteins Gas6 and Protein S, and promotes the clearance of apoptotic moieties and regulation of the activation of innate leucocytes[173]. All three members are expressed by macrophages, dendritic cells, NK cells and platelets, with MerTK expression being absent in monocytes before transmigration[174], Tyro3 also being expressed in neuronal tissue[175], and Axl being expressed ubiquitously, but most highly in endothelium[176].

Of the family, MerTK is the best characterised member, especially with regard to macrophage function. Activation of MerTK in macrophages by PtdSer-Gas6/Protein S conjugates induces signalling through two distinct pathways. The first is PI3 kinase-linked and results in rac-mediated cytoskeletal rearrangement and the formation of a phagosome[177]. The result of this is efferocytosis of apoptotic bodies and cells, particularly neutrophils, by macrophages. The second pathway involves the MerTK dimer complexing with the type I IFN receptor dimer[173]. This results in phosphorylation and nuclear translocation of the STAT1 transcription factor, which drives expression of SOCS1 and SOCS3 which suppress TLR and inflammatory cytokine signalling. Activation of this pathway induces a wound-healing phenotype in macrophages[164].

The importance of MerTK in clearing self antigens and promoting resolution is exemplified in data showing an accumulation of apoptotic cells and increased infarct size post myocardial infarction in mice[178]. Similarly, in a model of pulmonary fibrosis, mice deficient in MerTK experienced more severe lung damage in response to bleomycin[179]. Indeed, loss of any one of the TAM family members in single, double, or even triple knockout mice, results in impaired clearance of dead cells, and supra-physiological inflammation[180,181].

While Gas6 and Protein S are required for signalling, there are no data suggesting this is limiting for PtdSer to achieve efficacy. This is likely attributable to their autocrine secretion from TAM-expressing cells[182].

The final stage of resolution is the intravasation of macrophages into the lymphatics where they travel to draining lymph nodes and restore the number of resident leucocytes to pre-inflammation numbers[183].

1.7 Diversity of the mononuclear phagocyte system

1.7.1 Monocytes and tissue macrophages

Dendritic cells, monocytes, monocyte-derived macrophages and tissue-resident macrophages form the mononuclear phagocyte system (deprecated: reticuloendothelial system where fibroblasts and endothelial cells were included in the same classification). Under homeostatic conditions, tissue resident macrophages, which are present in most tissues, such as alveolar macrophages, Kupffer cells, histiocytes, Langerhans cells, microglia and osteoclasts, perform janitorial functions, such as the removal of cellular and exogenous debris, erythrocyte recycling and iron homeostasis[184]. In the context of inflammation and infection these tissue macrophages, along with resident dendritic cells, are the first sensors of injurious stimuli, responding to PAMPs and DAMPs, and recruiting the initial wave of blood leucocytes[185]. While tissue macrophage pools were previously thought to be maintained by circulating monocytes, a series of papers suggest this is largely not the case and that these cells are derived from the yolk sac and proliferate locally[185–188]. On the other hand, there is evidence of exceptions to this, such as Langerhans cells in the skin, splenic macrophages and some tissues following severe inflammation where local proliferation is supplemented by monocyte infiltration[189,190].

The most prevalent population of circulating monocytes are $CD14^{high}$, $CD16^{-}$, $CCR2^{+}$, CX_3CR1^{low} and termed "classical monocytes"[191]. Upon detection of inflammation, these cells extravasate into the tissue, promoting inflammation and pathogen-killing before differentiating into macrophages or dendritic cells to serve higher functions. In 1989, a second population of circulating monocytes was discovered in humans found to be $CD16^{+}$ and represented ~10% of circulating monocytes[192]. These "non-classical monocytes" are smaller than classical monocytes, are found to preferentially crawl along the apical face of the endothelium and are $CD14^{low}$, $CD16^{high}$, $CCR2^{-}$, CX_3CR1^{high} (see Table 1.2 for a summary of the most commonly used markers)[193]. Non-classical monocytes are considered to be patrolling cells that monitor the integrity of the endothelium, inducing the recruitment of neutrophils to sites of endothelial damage[190]. These cells are sometimes referred to as "non-phlogistic" monocytes owing to their perceived inability to contribute significantly to tissue inflammation, although in some circumstances this is a misnomer[194]. Indeed the mouse orthologue of the non-classical monocyte (the $Ly6C^{-}$monocyte) has been shown to be required for the development of a model of autoantigen-induced arthritis whereas classical cells ($Ly6C^{+}$) were not[195]. In this model $Ly6C^{-}$ monocytes matured

into inflammatory macrophages to drive the disease, and then transitioned to a pro-resolving macrophage phenotype required for the disease model to spontaneously resolve.

A third population of circulating monocytes are described as "intermediate" as they form a continuous bridge between classical and non-classical cells for all the major phenotypic markers used to separate the two[196]. The general consensus is that these cells represent classical monocytes transitioning into a non-classical phenotype, although it remains possible that these cells may have distinct functions from the two canonical populations.

Table 1.2: Monocyte subsets in human and mouse

Antigen		Monocyte Subset		
		Classical	Intermediate	Non-classical
Human	CD14	++	+	+
	CD16	-	+	++
Mouse	Ly6C	++	+	-
Both	CCR2	++	+	-
	CX_3CR1	+	++	+++
	CD64	++	+	-

- not expressed; +/++/+++ relative expression within row

1.7.2 Macrophage plasticity

Macrophages are renowned for exhibiting remarkable plasticity and generate a wide spectrum of responses to a wide spectrum of stimuli. Initially described by Élie Metchnikoff in 1882 (who was awarded the Nobel prize with Paul Ehrlich 26 years later), macrophages were the first described professional phagocytes ("macrophage" translating roughly as big eater)[197].

Their sensitivity to pg/mL levels of LPS and the pro-inflammatory T_h1 cytokine interferon gamma (IFNγ) earned them credence as pro-inflammatory, pathogen-killing cells[198,199]. In response to these stimuli *in vitro* (in isolation or in combination), macrophages undergo oxidative burst, generating reactive oxygen species (ROS) and reactive nitrogen species (RNS) such as superoxide, hydrogen peroxide and peroxynitrite. They also shift to favour macropinocytosis over phagocytosis, release pro-inflammatory cytokines, such as TNFα, IL-6, IL-1β, IL-12p70, IL-23 and type I interferon, and upregulate proteins involved in antigen presentation, such as CD86 and MHCII[200]. In 1992, however, Stein *et al.* from Siamon Gordon's group

demonstrated that the T_h2 cytokine IL-4 (and the related IL-13) potently induces a distinct macrophage phenotype[201] which promotes T_h2 immunity and is evolutionarily conserved for the killing of helminth and fungal infections[202,203]. With the view that these were discrete and mutually exclusive macrophage phenotypes, they were named classically activated and alternatively activated, or M1 and M2 macrophages, respectively to conform to the T_h1 and T_h2 nomenclature. M2 macrophages express higher levels of scavenger receptors (such as the CD206 mannose receptor and the CD163 haemoglobin-haptoglobin receptor), arginase, IL-10 and the IL-1 decoy receptor[204]. While initially described as anti-inflammatory, IL-4-polarised macrophages are more correctly thought of as anti-inflammatory *only* in the context of T_h1-driven inflammation, but themselves promote a type 2 response.

The understanding that macrophages could exhibit such disparate phenotypes to regulate as well as promote inflammation led to the observation that the anti-inflammatory cytokine IL-10 invokes a macrophage phenotype that is regulatory (for both T_h1 and T_h2-driven inflammation), and promotes matrix deposition and tissue remodelling[205]. These "wound healing" macrophages secrete their own IL-10, TGFβ and deposit matrix components, such as versican and pentraxin 3, and α antitrypsin, to promote anabolism[206]. A highly similar phenotype is induced by TGFβ. A third seemingly distinct macrophage phenotype was identified in response to co-exposure to immune complexes and TLR activation[207]. These cells seem *in vitro* to share properties of both M1 and IL-4/IL-13-stimulated macrophages, at the same time releasing large quantities of IL-10, TNFα, IL-1β, IL-6 and expressing MHCII and CD86. The role of these cells is not fully understood but are suggested to be anti-parasitic and to contribute to the pathogenesis of rheumatoid arthritis (and likely any inflammatory disease involving immune complex deposition)[208]. In an attempt to reconcile these other alternatively activated macrophage phenotypes with the M1/M2 paradigm, IL-4/IL-13, immune complex and TLR ligand, and IL-10-induced macrophage phenotypes have been named M2a, M2b and M2c, respectively[209]. The most recent addition to the M2 family (predictably named M2d) is the result of exposing M1 macrophages to adenosine which results in an IL-10 and VEGF-releasing phenotype[166]. The physiological purpose of this population is likely to aid resolution and wound healing by promoting angiogenesis in response to adenosine, made extracellular by necrosis and tissue damage. Indeed, this is one of many pro-resolving functions of adenosine[210].

In recent years, the M1/M2 convention has been heavily criticised as unrepresentative of true macrophage biology[209]. Macrophages in complex *in vivo* environments rarely exhibit the characteristics of a single *in vitro* phenotype, often displaying mixed distributions of M1 and M2 markers. The discreteness of such populations

has also been refuted; where such an M1/M2 dichotomy exists in the tissue, it exists solely as a continuum and not as discrete populations.

The overenthusiastic compartmentalisation of different macrophage phenotypes is further exemplified by the work done on macrophages within atherosclerotic plaques. Exposure of macrophages to CXCL4 promotes a phenotype termed M4, the *in vivo* analogue of which appears more prone to foam cell formation and plaque instability[211]. Uptake of a large number of oxidised phospholipids induces a phenotype referred to as M_{ox} which expresses sulfiredoxin-1, thioredoxin reductase and haem oxygenase-1 and provides plaque-protective antioxidant functions and also immunoregulation by the carbon monoxide they produce[212]. Finally, a distinct population of macrophages appears to cluster proximal to the vasa vasorum in plaques which express IL-10, carbon monoxide and high levels of the haemoglobin-haptoglobin complex receptor CD163[213]. This population is induced by the haem-hapt complex and is referred to as M_{haem} (see Table 1.3 for a more comprehensive summary of reported phenotypes).

Many research groups are moving away from the M1/M2 nomenclature now that its relevance to physiology has been brought into question. What seems apparent is that the macrophage is a remarkably dynamic cell type, the phenotype for which is a complex function of multiple stimuli, tissue, and disease context. Nevertheless, in *in vitro* models of mono-stimulation, these phenotypes are stable and can be thought of to represent extremes of several, multidimensional activation spectra, and act as useful models in studying modulators of these phenotypes. The generalisation of these phenotypes to physiology, however, should be done with extreme caution, although the terms “M1-like” and “M2-like” are useful in describing *relative* changes in phenotype only.

1.8 Rheumatoid arthritis

Rheumatoid arthritis is a systemic, chronic inflammatory condition whose prime manifestation is symmetrical inflammation and destruction of cartilagenous joints. The stereotypical form of the disease involves inflammation of the synovial membrane of the metacarpophalangeal and interphalangeal joints of the hand, but over time can progress into polyarthritis where joints of the feet, spine, shoulder and knee are affected, as well as inflammation of the skin, kidneys, blood vessels, eyes, and fibrosis of the lung.

The ætiology of rheumatoid arthritis is poorly annotated. While the molecular basis for the timing of onset is obscure, environmental, genetic and epigenetic factors are proposed to trigger loss of self tolerance[214]. The reason for the initial loss of tolerance is not understood, but smoking represents the strongest associated

environmental factor (with reported odds ratios of 1.8 to 1.3), the effects of which synergise with expression of the HLA-DRB1 shared epitope and PTPN22 R620W polymorphisms (individual odds ratios of 5.6 to 11.3 and 1.6 to 2.8, respectively)[215]. Half of the risk of developing rheumatoid arthritis is associated with these and other polymorphisms, which modulate lymphocyte activation, and although tissue damage or infection are suggested to act as triggers for the manifestation of these polymorphisms, no credible link between either has been demonstrated. Detection and use of rheumatoid factor and more recently anti-citrullinated protein antibodies (ACPA) as biomarkers for rheumatoid arthritis led to the realisation that proteins in patient joints were highly citrullinated[216]. Whether this inappropriate post-translational citrullination is triggered by an environmental stimulus is not known, but the presence of citrullinated-protein specific lymphocytes producing antibodies in secondary lymphoid organs suggest this is at least a terminal trigger for the loss of tolerance[217]. The deposition of these antibodies as immune complexes on the cartilage surface induces activation of synovial macrophages and dendritic cells which recruit monocytes and neutrophils into the synovial membrane (and fluid)[218,219]. Inflammation and excessive proliferation induce swelling and hyperplasia of the synovial membrane, forming a pannus which causes pain and loss of function of the joints affected. Recruitment of lymphocytes completes an inflammatory feedback loop between innate and adaptive cells, the long term effect of which is cartilage degradation, bone erosion and patient disability. While the roles of T and B cells are important to the progression of rheumatoid arthritis, only the contributions of neutrophils, monocytes and macrophages will be discussed here.

1.8.1 Neutrophils in RA

Recognition of immune complexes by Fcγ receptors on granulocyte-macrophage colony-stimulating factor (GM-CSF)-primed neutrophils induces respiratory burst and full degranulation[220]. In the pannus and synovial fluid, this increase in ROS and cytotoxic enzymes, such as myeloperoxidase, promotes a cytotoxic and catabolic environment, overcoming protective antioxidant and antiprotease mechanisms and facilitating cartilage erosion. Granule proteins may inhibit chondrocyte proliferation and potentiate synoviocyte proliferation[221]. Transmigrating neutrophils also release IL-8 and leukotriene B_4 (LTB_4) which potently recruit subsequent waves of neutrophil extravasation and MHCII-induced T cell activation[222,223]. The life of a neutrophil in circulation is ~24 hours, but activation cues in an inflamed microenvironment can extend this time to several days[224]. The timely induction of neutrophil apoptosis is a critical checkpoint required for the resolution of inflammation, but its dysregulation and prolonged neutrophil lifespan in rheumatic synovia results in perpetual inflam-

mation, neutrophil necrosis and NETosis[225]. NETosis is a form of programmed cell death where neutrophils extrude their DNA into the extracellular space as structures called neutrophil extracellular traps (NET)[226]. NET are complex structures of chromatin, citrullinated histones and granule proteins released in response to prolonged activation that immobilise and opsonise pathogens. Both circulating and synovial fluid neutrophils from rheumatoid arthritis patients undergo NETosis more readily than healthy neutrophils, and are thus thought to contribute to the loss of tolerance to and processing of auto-antigens[214].

At the cartilage-pannus junction, immune complex-primed neutrophils attempt to phagocytose the cartilage face. Unable to internalise the large surface, neutrophils secrete lysosomes onto the cartilage face, degrading it in a process termed "frustrated phagocytosis"[227]. Secretion of receptor activator of nuclear kappa-B ligand by activated neutrophils promotes intra-articular osteoclastogenesis of macrophages - which subsequently erode the bone and contribute to loss of function[228].

1.8.2 Monocytes and macrophages in RA

While synovial tissue macrophages, monocytes and monocyte-derived macrophages do not appear causative to rheumatoid arthritis, the relative success of treatments with macrophage-modulating efficacy demonstrates their core importance to disease progression. At the earliest stages of the disease, tissue macrophages recruit $CCR2^{-}$ monocytes into the synovium which in mouse models, are required for the initiation of clinical arthritis[195]. This is striking for two reasons: firstly, that it is the monocyte and not the archetypal neutrophil as the front-line of recruitment, and secondly that the so-called non-phlogistic monocyte is required for disease progression and not the inflammatory monocyte. Recruited monocytes then differentiated into macrophages resembling an M1-like phenotype, promoting inflammation and worsening clinical score, before transitioning into a more M2-like, pro-resolution phenotype which promoted spontaneous resolution. Whether these processes are analogous in the human is not clear, but an important critique of this model is that unlike the clinical situation, it fully resolves.

Another contradiction to the traditional view that alternatively activated macrophages are anti-inflammatory is the observation that M2 macrophages exposed to immune complexes and TLR ligands, such as LPS and Pam3CSK4 (TLR4 and TLR1/2, respectively), secrete high levels of TNFα, IL-1β and IL-6 and may promote synovial inflammation[208]. Indeed monocytes and macrophages are the main source of intra-articular TNFα and IL-1β, the latter of which is released in response to inflammasome activation, and induces activation of the endothelium and chondrocyte apoptosis[229]. Juxtacrine contact between macrophages and synovial fibroblasts

induces IL-6 (mainly from the fibroblasts), IL-8 and GM-CSF[230].

Monocytes and macrophages release matrix metalloproteinase (MMP)s, most prominently MMP 9 and 12, in response to TNFα, IL-1β and prostaglandin E2 which degrade the local matrix and cartilage[231]. Similarly to neutrophils, macrophages can also undergo frustrated phagocytosis, but also osteoclastogenesis to create an overwhelmingly catabolic environment[232].

In light of the contributions of synovial monocytes/macrophages to rheumatoid arthritis, it is not surprising that therapies modulating these cells (at least indirectly) have met with moderate success in the clinic. In the biologic family of anti-rheumatic drugs, etanercept, infliximab, adalimumab and certolizumab neutralise soluble TNFα (much of which is monocyte/macrophage-derived) and induce reverse transmembrane TNFα signalling in monocytes, inducing their apoptosis[233]. Abatacept, licensed for the treatment of rheumatoid arthritis in the US, is an Fc-CTLA-4 chimera which prevents CD80/CD86-mediated activation of T lymphocytes by macrophages and dendritic cells, and impairs macrophage TNFα release[234]. The contribution to rheumatoid arthritis pathology by monocytes/macrophages is therefore non-redundant and represents a targetable aspect of the disease. Despite this, no treatment currently offers permanent remission, and sub groups of patients remain refractory to TNFα blockade[235]. While these therapies are anti-inflammatory, they do not necessarily promote resolution of synovial inflammation or restore immune tolerance. New approaches are therefore needed to drive active resolution in the local environment. As such, the present project aims to explore and delineate the effects of neutrophil-derived microvesicles on the phenotype and function of macrophages in the context of rheumatoid arthritis.

Table 1.3: *In vitro* human macrophage subsets

	Macrophage Subset							
	M1	M2a	M2b	M2c	M2d	M4	M_{ox}	M_{haem}
Induced by	LPS & IFNγ	IL-4/IL-13	IC and TLR ligands	IL-10	Adenosine	CXCL4	ox-Phospholipids	Haem-hapt
Cytokines	IL-12p70^{high} IL-10^{low} IL-23 IL-1β IL-6 Type I Interferon	IL-12p70^{low} IL-10^{high} IL-1RA Decoy IL-1R	IL-10 TNFα IL-1β IL-6	IL-10 TGFβ	IL-10	TNFα	?	IL-10
Surface proteins	CD86 MHCII CD80 FcγI/II/III	CD206 CD163 CD200R	CD86 MHCII	CD206 SLAM	?	CD86 CD206	?	CD163
Chemokines	CXCL8-11 CXCL15-16 CCL2-5	CCL16-18 CCL22 CCL24	CCL1	CCL16 CCL18 CXCL13	?	CCL18 CCL20	?	?
Intracellular proteins	iNOS	Arginase	?	?	?	?	HO-1 SD-1 TR reductase	HO-1
Soluble effectors	ROS/RNS	Polyamines	?	Versican PTX3 α antitrypsin	VEGF	?	CO	CO

IC immune complex; **TLR** toll-like receptor; **SLAM** signalling lymphocyte activation molecule; **iNOS** inducible nitric oxide synthase; **HO-1** haem oxygenase-1; **SD-1** sulfiredoxin-1; **TR reductase** thioredoxin reductase; **ROS** reactive oxygen species; **RNS** reactive nitrogen species; **VEGF** vascular endothelial growth factor; **CO** carbon monoxide; **PTX3** pentraxin 3

1.9 Project aims

1. The present project aims to optimise and characterise the production of microvesicles from primary human neutrophils, including:
    - measurement of their concentration
    - measurement of their phenotype
    - their stability over time under different storage conditions
2. Once protocols to produce and store microvesicles have been optimised, the project aims to determine if neutrophil-derived microvesicles alter classical macrophage activation, using a panel of phenotypic markers
3. If efficacy is observed, the project aims to identify the mechanisms responsible
4. The project will identify whether microvesicles from neutrophils given different stimuli elicit similar effects
5. The project will identify if the effects observed are specific to microvesicles and not exosomes
6. Following this, the project will examine whether any changes in macrophage phenotype or activation induced by neutrophil microvesicles, have functional consequences on cell function. Specifically, the project will test whether vesicles alter the interaction between macrophages and:
    - chondrocytes
    - fibroblast-like synoviocytes

    These functional studies have been chosen as soluble factors released by macrophages are able to modulate chondrocyte survival and cartilage deposition, and the close proximity of both resident and infiltrating macrophages to synovial fibroblasts in the pannus, facilitates intimate control of phenotype between these cell types[236]
7. If the *in vitro* data supporting the above hypotheses are robust, the hypotheses will be tested in two *in vivo* models of compartmentalised inflammation:
    - zymosan-induced peritonitis
    - K/BxN serum-transfer arthritis
8. Finally, to answer more experimental hypotheses, the project will aim to test *in vitro*, the validity of microvesicles as therapeutics. This will test the hypotheses that:

- autologous vesicles from rheumatoid arthritis patients, and
- vesicles generated using engineered cell lines

have similar effects as those seen from healthy neutrophil vesicles. Generation of the cell line will require:

- identifying a protein determinant of microvesicle activity
- achieving stable transfection of the cells with the protein
- confirming presence of the protein in secreted microvesicles

Chapter 2

Materials and Methods

2.1 Running sizing beads on flow cytometers

Fluorescent 0.02µm FluoSpheres (F-8782), 0.1µm (L1528-1ML), 0.5µm (L1403-1ML) and 1µm (L1278-1ML) latex calibration beads (Sigma-Aldrich) were diluted 1:15,000 in double sterile-filtered (0.22µm; SLGP033RS, Millipore) phosphate-buffered saline (PBS) after 5 minute sonication and vortexing to disperse aggregates. Individual beads were acquired on the ImageStream and the LSRFortessa with all lasers turned on, slow flow rate and 60x magnification (ImageStream only) using fluorescence triggering on the beads' brightest channel (the phycoerythrin channel).

2.2 Isolation of whole blood components

A graphical representation of this procedure is shown in Figure 2.1. All volunteers gave written, informed consent to blood collection and the procedure was approved by the East London & The City Local Research Ethics Committee (Rec Ref. 05/Q0603/34 ELCHA, London, United Kingdom) for healthy controls and The East London & The City Research Ethics Committee (Rec Ref. 07/Q0605/29) for arthritis patients, in accordance with the World Health Organization guidelines on drawing blood. Whole blood was drawn from healthy volunteers using a 21G (or 19G if platelets were used) butterfly needle with tourniquet applied and anticoagulated with 0.32% w/v (final, in water) sodium citrate. All blood cells are from healthy controls unless indicated otherwise in figure legends.

2.2.1 Collection of plasma

Platelet-rich and platelet-poor plasma were generated by centrifuging whole blood at 130×g for 20 minutes to separate plasma and cells, then the platelet-rich plasma recovered and, if needed, platelets depleted by a second centrifugation at 13,000×g for 2 minutes.

2.2.2 Removal of erythrocytes

For every 30mL of whole blood, erythrocytes were depleted by sequentially layering 10mL of PBS then 8mL of 6% w/v dextran (high molecular weight, 31392-250G, Sigma-Aldrich, in PBS) onto the blood after removal of plasma as above. The blood was gently inverted to mix the PBS and dextran, and left to sediment at room temperature for 15 minutes.

2.2.3 Separation of neutrophils and PBMC

After dextran sedimentation of erythrocytes, the leucocyte-rich fraction from every 30mL of whole blood was carefully layered over 10mL Histopaque 1077 (10771, Sigma-Aldrich) in a fresh 50mL tube and centrifuged for 30 minutes at room temperature at $450\times g$ to separate granulocytes from peripheral blood monouclear cells (PBMC).

Remaining plasma was aspirated, the PBMC were carefully collected with a Pasteur pipette and transferred into a new 50mL tube. Remaining supernatant was aspirated and the residual erythrocytes were lysed through hypotonic shock with 9 mL of ice-cold, ultra pure distilled water. Isotonicity was quickly restored by adding 1mL of 10x Hanks Balanced Salt solution (H4641, Sigma-Aldrich). Both granulocyte and PBMC fractions were made up to 50mL with PBS and pelleted at $300\times g$ for 10 minutes at room temperature. The supernatant of both fractions was aspirated, the granulocyte pellet was resuspended in phenol red-free RPMI (11835-063, Gibco) and their concentration adjusted as needed, and the PBMC fraction was resuspended in 50mL of PBS and centrifuged at $120\times g$ for 20 minutes to further remove platelets.

2.3 Generating monocyte-derived macrophages

The PBMC pellet generated in Section 2.2.3 was resuspended in RPMI (R8758, Sigma-Aldrich) with 100U penicillin and 100µg/mL streptomycin (P4333, Sigma-Aldrich) without serum at 1.8×10^6/mL and 500µL was seeded per well of a 24-well suspension culture plate. Suspension plates were used to allow subsequent detachment of otherwise extremely adherent macrophages. After incubation at 37°C for 1 hour, PBMC were washed vigorously 3 times with PBS to deplete lymphocytes and covered with RPMI with 100U penicillin and 100µg/mL streptomycin, 10% v/v heat inactivated foetal bovine serum (FBS; 10500, Life Technologies, lot 08Q1150K) and 50ng/mL macrophage-colony stimulating factor (M-CSF; 300-25, PeproTech; referred to as "complete medium"). Cells were cultured at 37°C with 5% CO_2 and their medium was replaced on day 5. At day 7, macrophages were washed twice with PBS and used as needed.

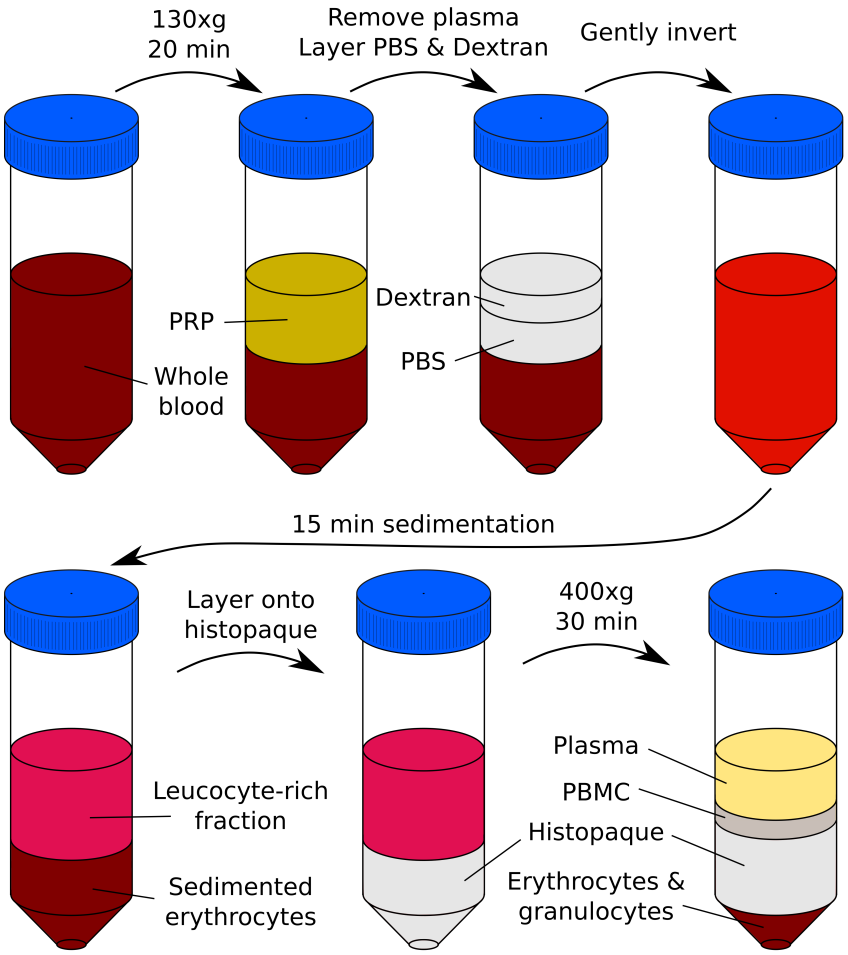

Figure 2.1: Isolation of blood components. The procedure is shown for each 30mL of blood to isolate platelet-rich plasma (PRP), peripheral blood mononuclear cells (PBMC) and a fraction containing neutrophils and erythrocytes, the latter of which are subsequently removed by hypotonic lysis.

2.4 Microvesicle generation and storage

2.4.1 Inflammatory agonists

For fixed-time microvesicle generation, 2×10^7 neutrophils/mL were stimulated with 50ng/mL TNFα (T0157-10UG, Sigma-Aldrich), 50ng/mL IL-8 (200-08, Peprotech), 10nM LTB_4 (20110, Cayman Chemical), 1µg/mL zymosan (Z4250, Sigma-Aldrich), 10ng/mL *E. coli* (EC1-5G, Sigma-Aldrich) or vehicle (PBS) for 20 minutes at 37°C before placing on ice to arrest microvesicle production. Cell suspensions were then either processed for ImageStream analysis or their neutrophils and large contaminants (such as platelets) were pelleted by centrifugation at 4,400×g for 15 minutes at 4°C followed by a second centrifugation at 13,000×g at 4°C for 2 minutes to remove residual contaminants (such as smaller platelets, zymosan particles and *E. coli*). Samples were resuspended in phenol-red free RPMI before proceeding to processing

for ImageStream analysis. Microvesicles generated this way by TNFα are referred to as $MV_{TNF\alpha}$.

For real-time microvesicle generation, freshly isolated neutrophils were resuspended at 1×10^6/mL in phenol red-free RPMI and labelled with boron-dipyrromethene maleimide (BODIPY maleimide), which has similar excitation and emission spectra to fluorescein isothiocyanate (FITC), at 2.5 µM, 2 minutes prior to sample acquisition, then the sample loader lowered. 50ng/mL TNFα or equal volume of vehicle (PBS) was added immediately prior to loading the sample. Acquisition of events was started as soon as the flow rate had equilibrated, and the events appearing in the microvesicle population gate collected for 45 minutes (488nm and 785nm lasers switched on).

2.4.2 Pre and post neutrophil transmigration

To optimise the generation of transmigrated-neutrophil-derived MV (MV_{Post}) and pre-transmigrated-neutrophil-derived MV (MV_{Pre}), cultures of human umbilical vein endothelial cells (HUVEC) were generated from healthy human umbilical cords. HUVEC were generated by cannulating the umbilical vein with a 21G butterfly needle and flushing it twice with 30mL of PBS in a syringe. The PBS was expelled by flushing the vein through with air, and replacing it with 0.2% w/v collagenase D (in RPMI, 103586, Roche) until full. The non-cannulated end of the cord was clamped with a haemostat, and more collagenase was pushed into the vein until no more could be added. The cannulated end of the cord was clamped with a haemostat and the entire cord was incubated at 37°C for 15 minutes. The non-cannulated end of the cord was unclamped and the cell suspension was collected into a 50mL tube containing 10mL of RPMI + 20% v/v human serum (H4522, Sigma-Aldrich). Cells were pelleted at $300\times g$ for 10 minutes, resuspended in 12mL of RPMI + 20% human serum and seeded into a T75 flask, precoated with 5% w/v bovine gelatin (G9391-500G, Sigma-Aldrich). Cells were washed with PBS 24 hours later, and split 1 in 3 when ~80% conlfuent. HUVEC were seeded at P2 onto 6-well 3µm-pore transwell inserts (a single T75 flask at ~80% confluency per 6 wells; 353091, Scientific Laboratory Supplies), pre-coated for 24 hours with 5% w/v bovine gelatin with 10ng/mL fibronectin (341635, Calbiochem) for 2 hours and then washed with PBS and transferred into fresh plates. After 48 hours, transwells were inspected to ensure 100% confluency and stimulated with 50ng/mL TNFα (under the transwell). 4 hours later, transwells were washed twice (above and below) with PBS and 3×10^6 isolated human neutrophils in 1mL were seeded per well in serum-free RPMI or RPMI with 10% v/v extracellular vesicle-free FBS (generated by centrifuging whole FBS at $100{,}000\times g$ for 1 hour at 4°C and double filtering through 0.22µm filters), in the

presence of 50ng/mL IL-8 (200-08, PeptroTech) or vehicle alone (PBS). 1mL of matched-condition RPMI was added to the bottom of each well and plates incubated for 90 minutes at 37°C. Transwells were removed to stop transmigration and the suspensions above and below the transwell were collected and both the number of neutrophils and microvesicles were collected.

2.4.3 From synovial fluid

Cell-free synovial fluid from 3 rheumatoid arthritis (aM011-fl-RA, Cambridge Bioscience) and 3 osteoarthritis patients (aM011-fl-OA, Cambridge Bioscience) was thawed at 37°C and treated with 40U/mL hyaluronidase with a sterile magnetic stirrer at 37°C until viscosity was comparable to water (between 40 and 75 minutes). Samples were centrifuged at 13,000×g for 2 minutes and the supernatant at 20,000×g for 30 minutes to pellet platelets/apoptotic bodies and then microvesicles (which were resuspended in RPMI and stored at -80°C). Microvesicle-free synovial fluid was aliquotted and stored at -80°C until use.

To generate rheumatoid arthritis synovial fluid-induced MV (MV_{RA}) and osteoarthritis synovial fluid-induced MV (MV_{OA}), 2×10^7/mL human neutrophils were treated with rheumatoid and osteoarthritis synovial fluid, respectively (1 in 10 for comparison to TNFα and transmigration, 1 in 100 for all other assays). After 20 minutes at 37°C, samples were placed on ice to arrest microvesicle production, which were isolated as in Section 2.4.1.

2.4.4 Storage

For storage longer than 24 hours, microvesicles were frozen slowly in a Mr. Frosty unit (5100-0036, Thermo Scientific) at -1°C/minute to -80°C. All frozen microvesicle samples were thawed quickly in a 37°C water bath. The same was performed for the comparison of storage temperatures of between 37°C and -80°C.

For comparison between relative yield of microvesicle recovery between standard microfuge tubes, and those made from a hydrophilic polypropylene polymer with low protein binding (LoBind; Z666513, Sigma-Aldrich), $MV_{TNF\alpha}$ were generated and separated from cells as in Section 2.4.1. Each sample of vesicle suspension was then split in equal volume between a standard polypropylene microfuge tube, and a LoBind microfuge tube, labelled with 50µM BODIPY maleimide FL, and centrifuged at 20,000×g for 30 minutes at 4°C to pellet the vesicles. After aspiration of the supernatant, pellets were resuspended in 30µL of PBS each, and acquired on the ImageStream using the 488nm laser.

2.5 Tsg101 western blot

Isolated human neutrophils (3×10^7) were stimulated with 50ng/mL TNFα for 20 minutes at 37°C before cells and platelets/apoptotic bodies were removed as previously described. The supernatant was split equally between tubes which were centrifuged at 20,000×g for 30 minutes or 100,000×g for 1 hour at 4°C (in rotors with k_{adjusted} factors of 692.39 and 406.43, respectively). Pellets were resuspended in lysis buffer (89900, Life Technologies) with protease inhibitor (1 tablet/50mL; 88266, Life Technologies).

A confluent T25 flask of C28/I2 cells was also lysed to provide a positive control. Total protein content in each sample was quantified using a BCA kit (23227, Life Technologies) as per manufacturer's instructions. 30µg of protein from each sample was boiled for 5 minutes at 100°C in 1x Laemmli buffer containing 2% w/v sodium dodecyl sulphate (436143, Sigma-Aldrich), 10% v/v glycerol (G5516, Sigma-Aldrich), 5% v/v 2-mercaptoethanol (M6250, Sigma-Aldrich), 0.002% w/v bromophenol blue (114391, Sigma-Aldrich), 0.0625M Tris HCL (T3253, Sigma-Aldrich), before loading into a 10% w/v sodium dodecyl sulphate polyacrylamide gel, including a molecular weight ladder (26623, Life Technologies).

The 10% resolving gel was prepared by combining 3.3mL of ProtoFLOWGel (H16996, Scientific Laboratory Supplies), 2.5mL of 4% w/v Resolving gel buffer (EC-892, Scientific Laboratory Supplies), 4.1mL of deionised water, 100µL of 10% w/v ammonium persulphate (A3678, Sigma-Aldrich) and 10µL of N,N,N',N'-teteramethylethylenediamine (TEMED; T9281, Sigma-Aldrich). The stacking gel was poured between glass plates and 500µL of isopropanol (I9516, Sigma-Aldrich) was added to force the gel to set evenly. The resolving gel was prepared by combining 650µL of ProtoFLOWGel, 1.25mL of Stacking gel buffer (EC-893, Scientific Laboratory Supplies), 3.05mL of deionised water, 50µL of 10% w/v ammonium persulphate, and 5µL of TEMED. The stacking gel was layered onto the resolving gel, the comb was inserted, and the gel was left to solidify for 20 minutes. The gel was run at 120V until the buffer front reached the end of the gel, and the protein bands were transferred overnight at 50V onto a methanol-activated polyvinyldene fluoride membrane (IPVH00010, Immobilon) at 4°C.

The membrane was blocked in 5% w/v milk (in TBST buffer: 50mM Tris, 150mM NaCl, 0.1 % v/v Tween 20) for 1 hour at room temperature while shaking. The milk was replaced with a polyclonal rabbit anti-Tsg101 antibody (1 in 250 in 5% w/v milk; HPA006161, Atlas Antibodies, in TBST buffer) for an hour, before washing 3 times and replacing the antibody with a polyclonal horseradish peroxidase-conjugated goat anti-rabbit antibody (1 in 2,000; P0448, Dako, in 5% w/v milk in TBST).

After an hour incubation, the membrane was washed 3 times and replaced with a monoclonal mouse anti β-actin antibody (1 in 2,000; A5441, Sigma-Aldrich, in 5% w/v milk in TBST). Finally, after an hour incubation, the membrane was washed 3 times, incubated for an hour with a polyclonal horseradish peroxidase-conjugated goat anti-mouse antibody (1 in 5,000; P0447, Sigma-Aldrich, in 5% w/v milk in TBST), before being washed 3 times more. Luminata forte substrate (WBLUF0500, Millipore) was added to cover the membrane which was imaged using a FluorChem R digital imager.

2.6 Fluorescent microvesicle labelling

Microvesicle labels BODIPY maleimide FL or Texas Red (B10250 and D6116, respectively, Thermo Fisher), carboxyfluorescein succinimidyl ester (CFSE; C34554, Molecular Probes) and PKH (MINI67, Sigma-Aldrich) were used at concentrations indicated and incubated with microvesicles for 20 minutes at room temperature (5 min for PKH). To wash away unbound dye, 1mL of sterile, double-filtered (0.22µm) PBS was added to each sample, which were then centrifuged at 20,000×g for 30 minutes to remove excess dye. It is important to remove excess generic vesicle dye, as this significantly compromises the signal-to noise ratio and the detection of smaller vesicles. Vesicles were then resuspended in the buffer and volume specified in figure legends.

For identification of microvesicles in biological fluids, whole blood (diluted 1 in 10 with phenol red-free RPMI), platelet-rich plasma, platelet-poor plasma and isolated neutrophils were stained with 50µM BODIPY maleimide FL or Texas Red.

For detection of outward PtdSer expression, vesicle preparations were resuspended in 1x anxA5-binding buffer (51-66121E, BD Pharmingen) with 10µg/mL FITC-conjugated anxA5 (640905, Biolegend), incubated at room temperature for 15 minutes in the dark, and acquired on the ImageStream using the 488nm laser.

2.7 Antibody labelling for cytometry

2.7.1 Cells

Antibody labelling of human cells was performed in 96-well, U-bottom plates after blocking Fc receptors by resuspending the cells in 100µL of FACS buffer (PBS + 0.02% w/v bovine serum albumin (BSA)) containing 160µg/mL human IgG (G4386, Sigma-Aldrich) and incubating them at 4°C for 15 minutes. 100µL of FACS buffer was added to each well and cells were washed three times by centrifuging the plate

at 300×g for 30 seconds, discarding the supernatant and resuspending in 200µL of FACS buffer. Cell pellets were then resuspended in 50µL FACS buffer containing antibodies raised against targets of interest, or appropriate staining controls, and incubated at room temperature in the dark for 30 minutes. Concentrations and details of antibodies used to label human neutrophils and macrophages are shown in Table 2.1. Note that the antibody raised against "HLA-DR, DP & DQ" is a monoclonal antibody which binds to all three major human MHC class II proteins (DR, DP and DQ).

150µL of FACS buffer was added to each well and cells were washed three times by centrifuging the plate at 300×g for 30 seconds, discarding the supernatant and resuspending in 200µL of FACS buffer. Cell pellets were resuspended in 100µL of 1% v/v formaldehyde and incubated at 4°C for 15 minutes to fix them. 100µL of FACS buffer was added to each well and cells were washed twice by centrifuging the plate at 300×g for 30 seconds, discarding the supernatant and resuspending in 200µL of FACS buffer. Fixed cells were resuspended in between 200µL and 500µL of FACS buffer (depending on cell numer) and acquired on either an LSRFortessa, FACSCanto II or ImageStream^{x} MkII.

Antibody labelling of mouse cells was performed as above, but instead of blocking with human IgG, Fc receptors were blocked with cell-free supernatant from 2.4G2 hybridoma cells containing anti CD16/32 IgG (produced in-house and kindly given by Dr. Oliver Haworth). Details of mouse antibodies can be found in Table 2.2.

Biological negative populations were used to gate cells positive for CD45, CD11b, CD66b and CD90, and a fluorescence minus one (FMO) control was used to gate cells positive for F4/80. Isotype-matched control antibodies were used for all antigens whose expression was of interest, to validate the effectiveness of Fc-mediated and non-specific antibody binding (but were never used as gating controls).

2.7.2 Microvesicles

For identifying circulating populations of microvesicles, platelet-poor plasma was generated from 5mL of blood from each healthy donors (as described in Section 2.2). 150µL of undiluted plasma was stained with 50µM BODIPY maleimide (Texas Red) and washed as per Section 2.6, and split equally between three tubes. One tube was stained with antibodies against CD41, CD45 and CD146, another with antibodies against CD14, CD66b and CD3, and the last one with an anti-CD235 antibody (see Table 2.3 for antibody details). All staining was performed at room temperature in the dark for 30 minutes with antibodies resuspended in 0.22µm-filtered FACS buffer. Remaining plasma was used for appropriate isotype and staining controls. Stained

plasma was then acquired on the ImageStream (unwashed) with all lasers turned on and at full power.

For comparing plasma microvesicle populations between healthy and rheumatoid arthritis patients, 500µL of platelet-free plasma (generated as per Section 2.2) from healthy donors and rheumatoid arthritis patients was stained with 50µM BODIPY maleimide and split between 3 tubes. Each tube was stained with antibodies against anxA1, then either with antibodies against CD66b, CD14 or CD41, and acquired on the ImageStream. FMO controls were used to gate on all antigens labelled on microvesicles.

2.7.3 AnxA1

AnxA1 staining on cells or microvesicles was carried out as above using a monoclonal antibody produced in-house (clone 1B, 10µg/mL, mIgG1), followed by an additional staining step after washing, with a secondary goat anti-mouse IgG F(ab')2-FITC (2µg/mL; M35001, Caltag Lab.), both for 30 minutes at 4°C. Where anxA1 was being probed for, FACS buffer was supplemented with 3mM CaCl to prevent anxA1 dissociating from PtdSer. Where anxA1 staining was done in tandem with other antibodies, anxA1 staining was performed first followed by a wash step, at which point remaining antibody labels were added.

2.7.4 Compensation beads

Correct compensation of polychromatic cytometry data requires that compensation samples meet three criteria: they must be at least as bright as any sample the compensation matrix will be applied to, the fluorophore must be the same (and handled the same) as those used in any sample the compensation matrix will be applied to, and the autofluorescence of the positive and negative populations must be equivalent. Cells are commonly used to generate single colour compensation controls, most often successfully, but often do not satisfy the first criterion, do not provide clear positive and negative populations, and may require reserving otherwise sparse cells for the purpose. For rare antigens, it may be difficult to determine a positive population of cells without acquiring large numbers of events.

To circumvent these caveats, all compensation for antibody conjugates was performed using OneComp eBeads (01-1111, Invitrogen) which are a suspension of two bead populations: positive beads, which bind mouse, rat and hamster antibodies, and negative beads which do not bind antibody. The positive beads can bind enough antibody to achieve a larger separation between positive and negative peaks than

generally seen with cells at appropriate PMT voltages, and their use negates the need for reserving cells purely for compensation.

To prepare the beads, the antibodies used in each experiment (from the same lot) were diluted in 100µL of FACS buffer to the concentration used in the experiment for cells, or 1/4 this for microvesicles, and added to 20µL of bead suspension. Antibody-bead suspensions were incubated in the dark at room temperature for 30 minutes before adding 1.5mL of FACS buffer and centrifuging a $500\times g$ for 5 minutes. The supernatant was aspirated and the bead pellet was resuspended in 300µL of FACS buffer and acquired on the instrument (used for both standard and imaging cytometers). To generate compensation values for non-antibody fluorophores (BODIPY maleimide or anxA5 for example), vesicles/cells were used instead.

2.7.5 Intracellular staining

Where total antigen expression was of interest (plasma membrane and intracellular), cells were fixed and permeabilised prior to Fc receptor blockade by resuspending them in 100µL of IC Fixation Buffer (00-8222, Invitrogen) and incubating at 4°C for 15 minutes (in a U-bottom 96-well plate). Cells were centrifuged at $300\times g$ for 30 seconds to pellet cells, the supernatant was discarded and the pellet was resuspended in 100µL Permeabilization Buffer (00-8333, Invitrogen). After incubation at 4°C for 15 minutes, cells were washed, Fc receptor blocked and antibody stained as per Section 2.7.1.

2.8 Analysing microvesicles by ImageStream

Microvesicles were acquired on the ImageStream in volumes of between 30µL and 50 µL at slow flow rate, 60x magnification with any excitation lasers required for the fluorophores being used and the 785nm (scatter) laser, turned on and at full power. The "Remove beads" setting was turned off upon loading each sample, and sample acquisition was started only once the flow rate had stabilised. Microvesicle-free samples (processed and "stained" as through they contained vesicles) were run as controls to ensure there was no contribution to the vesicle gate from particulate matter present in staining reagents. A storage gate was set to all events, and the stopping gate was set to the vesicle population which is characterised by low SSC and low to mid fluorescence of the generic label. At least 10,000 objects in the vesicle gate, and at least 2 seconds of acquisition were acquired per sample to ensure stability of fluorescence and concentration estimates. A schematic of the optical path and main features of the ImageStream platform is shown in Figure 2.2.

To determine the concentrations of microvesicle populations, IDEAS software was used. A scatter plot showing Channel 02 fluorescence intensity plotted against scattering intensity of Channel 12 was generated and a microvesicle gate re-applied and inspected visually to exclude inappropriate events. The gate was adjusted where necessary and sub-gated to identify lineage-specific populations. The objects/mL statistic was applied to each population (and total microvesicles).

Unlike traditional flow cytometers, the ImageStream does not give the option of an explicit trigger channel and instead triggers on any channel in which a signal above background is sufficient. As such, vesicles were detected using fluorescence triggering when using a generic fluorescent label, without the need to alter instrument configuration.

Fluorescence channels are more sensitive at triggering on microvesicles than the brightfield as significant haloing contributes to the sample fluorescence, augmenting the signal to noise ratio. Microvesicles smaller than the minimum wavelength of visible light (~400nm) cannot be seen in a brightfield image.

Table 2.1: Human neutrophil and macrophage antibodies

Antigen	Clone	Concentration used (µg/mL)	Conjugate	Isotype	Cat#, source
CD66b	G10F5	0.25	PE	mIgM, 401611, Biolegend	305105, Biolegend
CD62L	DREG-56	1.0	PE/Cy5	mIgG1, 400115, Biolegend	304808, Biolegend
CD11b	ICRF44	10.0	PB	mIgG1, 400131, Biolegend	301316, Biolegend
$HLA_{DR/DP/DQ}$	Tü39	1.25	FITC	mIgG2a, 555573, BD Biosciences	555558, BD Biosciences
CD86	IT2.2	1.00	PE	mIgG2b, 400311, Biolegend	305405, Biolegend
CD206	15-2	4.00	APC	mIgG1, 400119, Biolegend	321109, Biolegend

APC allophycocyanin; **FITC** fluorescein isothiocyanate; **mIg** murine immunoglobulin; **PB** Pacific Blue; **PE** phycoerythrin; **PE/Cy5** phycoerythrin cyanine 5

Table 2.2: Mouse antibodies

Antigen	Clone	Concentration used (µg/mL)	Conjugate	Isotype	Cat#, source
F4/80	BM8	2	BV650	rIgG2a	123149, Biolegend
CD86	GL-1	2	BV421	rIgG2a, 400535, Biolegend	105031, Biolegend
MHCII	M5/114.15.2	5	AF700	rIgG2b, 400628, Biolegend	107622, Biolegend
CD206	C 068C2	2	APC	rIgG2a, 400511, Biolegend	141708, Biolegend
CD90	778053	2	AF488	rIgG2a	FAB7335G, RnD Systems
CD106	429	2	PE/Cy7	rIgG2a, 105719, Biolegend	105720, Biolegend
CD55	583905	2	PE	rIgG2a, IC006P, RnD Systems	FAB5376P, RnD Systems
CD45	30-F11	1	PerCP	rIgG2b	103130, Biolegend
CD11b	M1/70	0.125	BV785	rIgG2b	101243, Biolegend

AF Alexa Fluor; **APC** allophycocyanin; **BV** Brilliant Violet; **PE** phycoerythrin; **PE/Cy7** phycoerythrin cyanine 7; **PerCP** peridinin chlorophyll; **rIgG** rat γ immunoglobulin

Table 2.3: Plasma microvesicle antibodies

Antigen	Clone	Concentration used (µg/mL)	Conjugate	Isotype	Cat#, source
CD235	HIR2	0.25	FITC	mIgG2b, 11-4732-41, eBioscience	11-9987-80, eBioscience
CD41	HIP8	0.25	FITC	mIgG1, 400107, Biolegend)	303703, Biolegend
CD45	HI30	0.5	PerCP/Cy5.5	mIgG1, 45-4714-80, eBioscience	45-0459-42, eBioscience
CD146	SHM-57	0.5	APC	mIgG2a, 400221, Biolegend	342011, Biolegend
CD14	HCD14	2.0	PE/Cy7	mIgG1, 400125, Biolegend	325617, Biolegend
CD66b	80H3	2.0	FITC	mIgG1, 400107, Biolegend	MCA216F, AbD Serotec
CD3	UCHT1	0.5	APC	mIgG1, 400119, Biolegend	300411, Biolegend

APC allophycocyanin; **FITC** fluorescein isothiocyanate;
mIg murine immunoglobulin; **PB** Pacific Blue; **PE** phycoerythrin;
PE/Cy phycoerythrin cyanine; **PerCP/Cy** peridinin chlorophyll cyanine

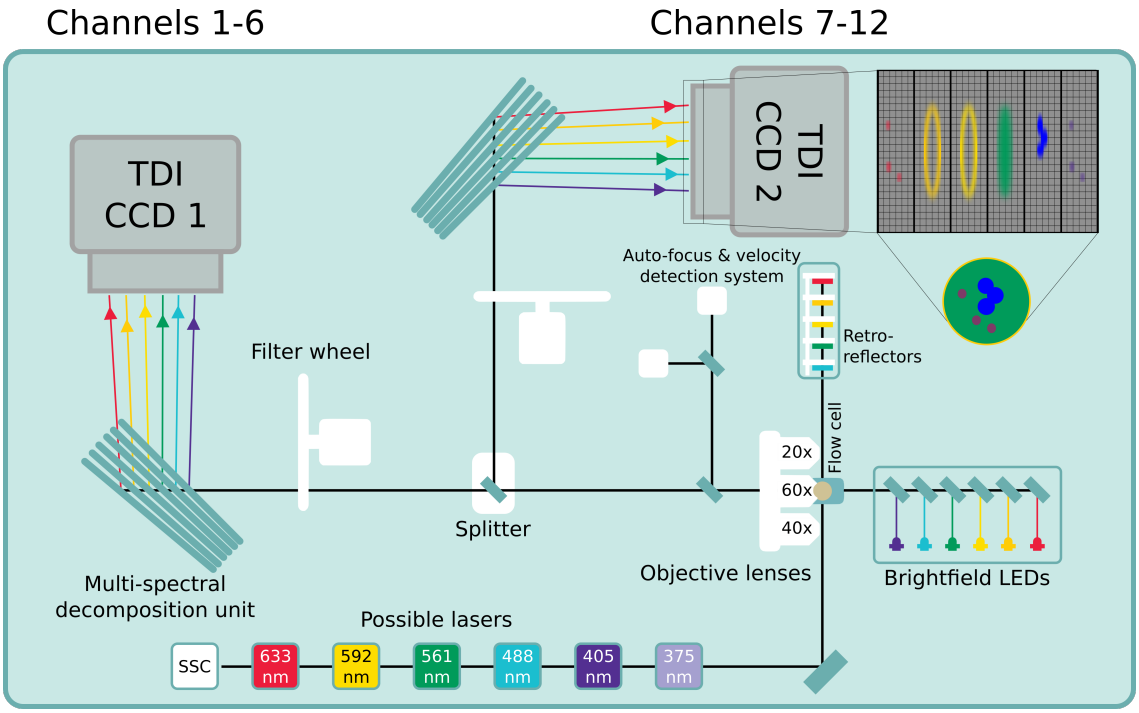

Figure 2.2: Schematic of the ImageStream Optics. Aerial schematic of the optics of the ImageStream^x MkII, where the sample flow is perpendicular to the page. Each laser is facing upwards and is reflected into the optical path by a dichroic mirror. A series of light-emitting diode (LED)s combine to produce white light illumination for brightfield images. Retro-reflectors reverse the optical path of laser light to ensure maximal excitation of objects in the flow cell. The auto-focus and velocity detection system monitors images of speed beads to make real-time corrections to the focus (distance between the objective lens and the flow cell) and to monitor flow speed. The multi-spectral decomposition units are each a series of band-pass dichroic mirrors, each of which is set at a shallower angle than the last, such that different band-passes of light are reflected onto one of six different regions of the time delay integration charge-coupled device (TDI CCD). The layout of a TDI CCD chip is shown top right, with channel images deconvoluted into an example cell. Image adapted from the ImageStream System Software User's Manual.

2.9 Blocking external PtdSer on microvesicles

PtdSer exposed on the outer membrane leaflet of microvesicles (generated as per Section 2.4.1) was blocked by resuspending a sufficient number of vesicles for the experiment in 1x anxA5-binding buffer containing 50µg/mL anxA5 (PK-CA577-1005-100 , PromoKine). Control vesicles for these experiments were resuspended in 1x anxA5-binding buffer without anxA5. Control and anxA5-blocked microvesicles were incubated at 4°C for 30 minutes before adding them to macrophage cultures as per the experiment design. To control for any direct effects of soluble anxA5 on macrophage phenotype, an additional control treatment was included which consisted of 1x anxA5-binding buffer with 50µg/mL anxA5, but no vesicles (incubated under

the same conditions).

2.10 Stimulation of monocyte-derived macrophages

2.10.1 Classical and alternative activation

Classical or pro-inflammatory activation of macrophages was achieved by treating naïve monocyte-derived macrophages on day 7 of differentiation (generated as per Section 2.3) with 10ng/mL LPS from *E. Coli* 0111:B4 (L2630, Sigma-Aldrich) and 20ng/mL IFNγ (300-02, PeproTech) for 24 hours at 37°C. These concentrations were chosen as they induce sub-maximal macrophage activation.

Alternative activation of macrophages was achieved by treating naïve monocyte-derived macrophages on day 7 of differentiation with 20ng/mL IL-4 for 24 hours at 37°C. For the IL-4 titration experiment, between 5 and 20ng/mL IL-4 was used instead.

Naïve, control macrophages used in experiments were monocyte-derived macrophages on day 7 of differentiation, cultured in medium alone for 24 hours at 37°C.

2.10.2 Stimulation with vesicles

Microvesicle populations generated as per Section 2.4, were pooled between at least 3 donors and used to stimulate macrophages for 24 hours at 37°C at the same time as activating stimuli described in Section 2.10.1, as well as any other treatments described in figure legends. For each experiment, the number of vesicles used is described in the figure legend, as is the number of donors whose vesicles were pooled (the same preparation of vesicles was used within each experiment).

2.10.3 Nanoparticle tracking analysis

The chamber was flushed with double 0.22µm filtered, deionised water until clean, and then 0.5mL of PBS was flushed through (filtered as above) and the absence of particulate matter was confirmed. 400µL of microvesicle sample was loaded into a 1mL syringe and flushed through until vesicles were visible using the camera. The focus and camera gain settings were optimised, and the sample was injected into the flow cell at speed 50, before acquiring 3, 60-second recordings. Filtered PBS was flushed through the system between samples until no particles could be seen. Data plotted for each sample is the mean of the three technical replicates. The analysis

was performed using an NS300 analyser, using a 488nm laser, high sensitivity camera, and syringe pump.

2.11 Cytometric bead array

Once experimental treatments had concluded, supernatants were collected, centrifuged at 300×g for 5 minutes to remove non-adherent cells, and split equally between two microfuge tubes. One tube per sample was used to assay the concentration of IL-10 (558274, BD Biosciences), and IL-12 p70 (558283, BD Biosciences) by cytometric bead array, the other was acidified for 10 minutes at room temperature with 1N HCl to release latent TGFβ, and then neutralised with 1.2N NaOH containing 0.5M 4-(2-hydroxyethyl)-1-piperazineethanesulfonic acid (HEPES). This was because the TGFβ kit could only be run in isolation (560429, BD Biosciences).

After collection of the supernatant, cells were covered with PBS with 1mM ATP (A2383, Sigma-Aldrich) for 30 minutes to induce IL-1β release. This was made cell free as above and the IL-1β was then quantified using a cytometric bead array following the procedure below (558279, BD Biosciences).

The cytometric bead array assay (558264, BD Biosciences) was used to quantitatively measure the concentrations of these analytes, following manufacturers instructions. The principle of this procedure is that the supernatant is incubated at room temperature with beads coated with antibodies against the different antigens of interest simultaneously. After 1 hour, PE-conjugated detection antibodies raised against each antigen of interest are added and samples are incubated for a further 2 hours at room temperature. The beads were washed to remove unbound detection antibody by centrifuging at 500×g for 5 minutes and resuspending in 300µL of Wash Buffer. Beads which bind to different antigens have discrete APC and APC-Cy7 fluorescence values and so can be resolved from each other on a flow cytometer. Protein standards for each analyte are incubated with beads alongside experimental samples to construct a standard curve of PE fluorescence from which the concentration of unknowns could be interpolated. Beads from the IL-1β kit were combined with the beads from the IL-12 p70 and IL-10 kits prior to acquisition.

2.12 Detachment of macrophages

After removal of supernatant, macrophages were detached by washing once with PBS and replacing with Accutase (A6964, Sigma-Aldrich) with 0.5% w/v ethylenediaminetetraacetic acid (EDTA). After 20 minutes at 37°C, the plate was placed at 4°C for 30 seconds, and then each well was gently agitated with the rubber stopper of

a 1mL syringe before flushing and collecting the cell suspension with a 1mL pipette into microfuge tubes. Cells were centrifuged at 300×g for 5 minutes and, after aspiration of the supernatant, were processed as required by the experiment.

2.13 Microvesicle internalisation assays

2.13.1 Comparing fluorescent labels

To compare the suitability of microvesicle dyes as indicators of internalisation by macrophages, $MV_{TNF\alpha}$ were generated from 2×10^7 neutrophils from 3 donors, pooled, and stained with 5µM CFSE, 50µM BODIPY maleimide or 50µM PKH as per Section 2.6 (including wash). 5×10^6/mL of each stained microvesicle population was seeded onto monocyte-derived macrophages generated as per Section 2.3 and incubated for 90 minutes at 37°C. Cells were washed twice with PBS and coated with trypsin with 0.05% w/v EDTA (25300-062, Life Technologies) until the cells started to detach, where they were flushed and collected in complete medium with a 1mL pipette. Macrophages were centrifuged at 300×g for 5 minutes, resuspended in 1% v/v formaldehyde fixative (P/0840/53, Fisher Scientific) and acquired on the ImageStream at 40x magnification with the 488nm laser turned on. A 75% "Threshold" mask was applied to the Channel 02 images (setting the threshold higher than the macrophages' natural green fluorescence) to facilitate counting the number of microvesicles per cell and to quantify the intensity of the fluorescent spots.

2.13.2 Blocking the PtdSer-Mer interaction

To assess the importance of PtdSer on microvesicle internalisation by macrophages, $MV_{TNF\alpha}$ microvesicles pooled from 3 donors were stained with 5µM CFSE as above and seeded onto monocyte-derived macrophages at 5×10^6/mL after 15 minutes of either PtdSer blockade, or vehicle control (as per Section 2.9). Treatments were staggered such that macrophages treated for 5, 30, 60 and 90 minutes were all processed at the same time as in Section 2.13.1 above. A separate experiment was conducted as above, where macrophages were treated with a Mer receptor inhibitor, UNC-569 (445835-10MG, Millipore) at 10nM or vehicle (0.1% v/v dimethyl sulfoxide) for 15 minutes prior to addition of untreated $MV_{TNF\alpha}$.

2.14 The C28/I2 micromass culture system

C28/I2 pro-chondrocyte cells were cultured in monolayer in DMEM (D5796, Sigma-Aldrich) diluted 1:1 with Ham's F12 (N4888, Sigma-Aldrich) with 10% v/v non-heat

inactivated FBS (10270-106, Invitrogen, lot 41A0940K) and 100U penicillin and 100µg/mL streptomycin ("Complete C28/I2 medium").

To generate 3D micromass constructs, monolayers were detached with trypsin with 0.05% w/v EDTA and centrifuged at 300×g for 5 minutes. Cells were resuspended in complete C28/I2 medium at 2.5×10^7/mL and 20µL of suspension was seeded per 48-well cell culture plate as a spot in the centre, using a positive displacement pipette. The outer wells were filled with PBS to maintain humidity, the plate was incubated at 37°C for 2 hours, and 500µL of complete C28/I2 medium was carefully added to each micromass. After 24 hours at 37°C, the medium was aspirated and replaced with serum-free, phenol red-free DMEM/F12 (21041-025, Invitrogen) supplemented with insulin (10µg/mL), transferrin (5.5µg/mL), selenium (6.7ng/mL) solution (41400-045, Life Technologies), penicillin and streptomycin as above, to induce chondrocytogenesis. After 24 hours at 37°C, micromasses were washed once with PBS and covered with treatments for a further 24 hours at 37°C.

To quantify glycosaminoglycan production, the medium was aspirated, micromasses were washed once with PBS and fixed in 100µL of 4% v/v glutaraldehyde (G-6257, Sigma-Aldrich) for 15 minutes at room temperature. Micromasses were rinsed once with 200µL of 0.1N HCl (to acidify) which was aspirated and replaced with 100µL of Alcian blue 8GS (which stains glycosaminoglycans at low pH; A-5269, Sigma-Aldrich) and left on a rocker at room temperature overnight. Alcian blue was aspirated and the micromasses washed once with 0.1N HCl and once with PBS before adding 100µL of 6M guanidine HCl (50950-250G, Sigma-Aldrich). Plates were left on the rocker overnight to extract the glycan-bound Alcian blue which was quantified by constructing a standard curve and measuring absorbance of 630nm light. To control for the variable number of cells in each micromass contributing to glycan deposition, supernatant DNA concentration was quantified by staining with 1x SYBR Green (S7563, Invitrogen), constructing standard curves of genomic DNA and quantifying fluorescence at 535nm (excitation at 485nm). Data are expressed as the µg of Alcian blue per ng of DNA per mL of supernatant.

2.15 Macrophage-conditioned medium

To generate single treatment conditioned-medium, macrophages were treated with complete medium alone, 50ng/mL IFNγ, 50ng/mL IL-4, rheumatoid arthritis synovial fluid or osteoarthritis synovial fluid (both pooled from 3 donors, diluted 1 in 100) for 24 hours at 37°C. Supernatants were centrifuged at 300×g for 5 minutes to remove cells. To control for the effects of these stimuli residual in the conditioned media, each condition had a mirrored "cell-free" conditioned-media condition, where

wells of medium alone were treated with the above stimuli. Comparing the cell-conditioned and cell-free-conditioned media allowed controlling for the effect of the exogenously-added mediators on chondrocyte function.

To test the effect of anxA1 blockade on macrophage conditioned-medium, macrophages were treated with vehicle (PBS) or 3×10^6/mL $MV_{TNF\alpha}$, MV_{RA} or MV_{OA} in the presence of 10µg/mL neutralising anxA1 antibody (clone 1B) or 10µg/mL control mIgG1 for 24 hours at 37°C. Supernatants were centrifuged at $300\times g$ to remove cells.

To test the effect of both TGFβ depletion and anxA1 blockade on macrophage conditioned-medium, macrophages were treated with vehicle (PBS) or 3×10^6/mL $MV_{TNF\alpha}$, in the presence of 10µg/mL 1B anxA1-neutralising antibody or 10µg/mL mIgG1, and then incubated for 2 hours with 1 in 100 beads coated with either an anti-TGFβ antibody (560429, BD Bioscience) or a control antibody (558279, BD Bioscience) at 4°C. Supernatants were centrifuged at $300\times g$ to remove cells.

For all experiments, supernatants were then centrifuged at $13{,}000\times g$ for 2 minutes to remove platelets/apoptotic bodies and at $20{,}000\times g$ for 30 minutes to remove microvesicles and beads. Microvesicles were removed as previous work from this lab has shown direct effects of microvesicles on chondrocytes[3]. Supernatants were then used as described.

2.16 Treatment of primary synovial fibroblasts

Primary synovial fibroblasts from osteoarthritis patients undergoing arthroscopy were a gift from Dr. Trinidad Montero-Melendez (William Harvey Research Institute). Cells were seeded at low passage numbers (<P10) onto glass coverslips in 24-well plates and allowed to adhere for 24 hours in RPMI medium with 10% v/v non heat-inactivated FBS, 2mM L-glutamine, 100U/mL penicillin, 100µg/mL streptomycin, 1mM sodium pyruvate (S 8636, Sigma-Aldrich) and 1x MEM non-essential amino acid solution (M 7145, Sigma-Aldrich).

To establish an inflammatory phenotype in synovial fibroblasts, cells were cultured with 1% v/v (in PBS) rheumatoid arthritis patient synovial fluid generated as in Section 2.4.3, or vehicle (PBS) for between 0 and 72 hours. Treatments were staggered such that all cells were processed for staining together.

For all experiments, 1x golgi block (4980-03, eBioscience) was added to the existing culture medium of fibroblasts to facilitate cytoplasmic accumulation of cytokines, 6 hours prior to fixation. Fibroblasts were fixed by aspirating the supernatant, washing the cells once with PBS, and fixing with 1% v/v formaldehyde for 15 minutes at room temperature. After removal of fixative, cells were washed twice with PBS

Table 2.4: Immunofluorescence antibodies

Antigen	Clone	Host species	Concentration used (µg/mL)	Cat#, source
CD55 (DAF)	28	Mouse	10	ABIN1995655, antibodies-online
CD21 (C3dR)	Bu32	Mouse	15	354902, Biolegend
CD106 (VCAM-1)	STA	Mouse	5	305802, Biolegend
MCP-1	2D8	Mouse	10	MA5-17040, ThermoFisher
TNFα	28401	Mouse	15	MA5-23720, ThermoFisher
IL-6	MP5-20F3	Rat	5	MA1-22531, ThermoFisher
Mouse IgG	/	Goat	4	F-11021, ThermoFisher
Rat IgG	/	Donkey	4	A-21208, ThermoFisher

with 0.02% w/v BSA (staining buffer) and permeabilised by covering with 0.1% v/v triton X-100 (X100-100ML, Sigma-Aldrich) in staining buffer for 15 minutes at room temperature. After removal of triton X-100, cells were washed twice with staining buffer and covered in the appropriate primary antibody or negative control in staining buffer (one antigen per coverslip). After 30 minutes at 4°C, primary antibody solutions were aspirated, cells washed twice in staining buffer, and covered in appropriate secondary antibody. See Table 2.4 for details of all primary and secondary antibodies.

2.17 Macrophage-fibroblast co-culture system

To model the close interaction between macrophages and fibroblasts in the synovial membrane, but still allow independent observation of fibroblast phenotype, monocyte-derived macrophages were differentiated as in Section 2.2, on 6-well 3µm-pore transwell inserts (353091, Scientific Laboratory Supplies). Following 24 hour treatment of day 7 macrophages with medium alone, 20ng/mL IFNγ & 10ng/mL LPS, 50ng/mL IL-4, 3×10^6 $MV_{TNF\alpha}$/mL or combinations thereof, transwells were washed twice with PBS, placed into a 6-well plate containing glass coverslips of

synovial fibroblasts, such that the transwell membrane was in contact with both fibroblasts and macrophages. The wells were incubated for a further 24 hours in complete macrophage medium at 37°C, from which point fibroblasts were treated as in Section 2.16 (including addition of golgi block 6 hours prior to fixation).

2.18 Culture of HL60, NB4 and HEK293 cells

HL60 (CCL-240, ATCC) and NB4 (ACC 207, DSMZ) cell lines are two, promyelocytic, suspension cell lines derived from separate patients with acute promyelocytic leukaemia. These cells have been used as surrogates for the study of certain processes in monocytes and neutrophils, as they can be induced to differentiate into models of these cell types experimentally[237,238]. Both HL60 and NB4 cells were cultured in RPMI with 10% v/v FBS and 2mM L-glutamine between passages 10 and 35 from origin. Both lines were maintained at between 0.25×10^5 and 2×10^5 cells/mL.

HEK293 human embryonic kidney cells (CRL-1573, ATCC) were used as a backup transfection system in the event that neither HL60 or NB4 cells could be transfected. HEK293 cells were cultured in DMEM with 10% v/v FBS and 2mM L-glutamine between passages 64 and 75 from origin. Cells were maintained at between 30% and 80% confluency. All cells were cultured at 37°C, with 5% v/v CO_2 in humidified incubators.

2.19 Alamar blue viability assay

Alamar blue viability dye (DAL1025, Thermo Fisher) was used to optimise blasticidin (R21001, Thermo Fisher) selection conditions for HL60, NB4 and HEK293 cell lines. Alamar blue is a reagent which is reduced by metabolically-active cells to the yellow/green-excitable fluorophore resorufin, and can be used to compare relative viability of cell colonies.

2.19.1 Cell number titration

Initially, the optimal number of cells per reaction was determined by serially diluting each cell line into a 96-well plate, from 0 to 7.5×10^4 cells/well, and staining for 1 hour with 10% v/v alamar blue at room temperature. The plate was then run on a NOVOstar fluorescence plate reader with excitation at 560nm and emission read at 590nm, including a blank, alamar blue-only control. The background fluorescence reading for the blank sample was subtracted from each experimental sample.

2.19.2 Blasticidin titration

To determine the kinetics of blasticidin-induced cell death, HL60, NB4 and HEK293 cells cultured under conditions described above, in their respective growth medium alone, or with between 5 and 20µg/mL of blasticidin. Every other day for 12 days from 24 hours after seeding, cells from each line in medium alone were counted using a haemocytometer. 3×10^4 of these cells and an equal volume of cell suspensions treated with blasticidin were transferred into a 96-well plate, stained with alamar blue for 1 hour and read as above.

2.20 Comparing activity of microvesicles and exosomes on macrophages

$MV_{TNF\alpha}$ were generated and pooled from 3 donors (2×10^7 human neutrophils from each, as per Section 2.4.1). The microvesicle pellet was retained and the supernatant further centrifuged at 100,000×g for 1 hour at 4°C. Both pellets were resuspended in 100µL of RPMI and, along with the supernatant, were kept. Human monocyte-derived macrophages were treated with medium alone, or 20ng/mL IFNγ & 10ng/mL LPS for 24 hours, with the entire 20,000×g pellet, 100,000×g pellet, or supernatant. Macrophages were detached, stained with antibodies against HLA-DR, DP & DQ, CD86 and CD206, and analysed on a flow cytometer.

2.21 Zymosan-induced peritonitis model

A model of sterile, acute peritoneal inflammation can be induced in mice by injecting zymosan A (Z4250, Sigma-Aldrich) intraperitoneally. This simple model provides a convenient compartment in which potential modulators of inflammation can be injected. Ten-week-old C57BL/6 mice (Charles River, UK) were injected intraperitoneally with 0.5mL of 2mg/mL zymosan using a 29G needle. After 24 hours, mice were randomised and injected with 500µL PBS alone, or containing a range of $MV_{TNF\alpha}$ doses, pooled from equal numbers of vesicles from 5 human donors, as indicated in each figure legend. Which mouse received which treatment was blinded from its administration until the conclusion of the analysis.

After a further 24 hours, at the peak of macrophage presence in the peritoneum, mice were euthanised with a rising concentration of CO_2, and the skin above the peritoneum washed with 70% v/v ethanol and removed. The peritoneal cavity was lavaged by injecting it with 5mL of air, followed by 5mL of ice-cold PBS with 2mM EDTA using a 25G needle. The mouse was agitated to detach as many cells as

possible, and the lavage fluid collected with a 19G needle, avoiding blood vessels and viscera.

The lavage fluid was centrifuged at 300×g for 5 minutes at 4°C to pellet cells which were then processed and stained for F4/80, MHCII, CD86 and CD206 by flow cytometry as per Section 2.7. The supernatant from the two group peritonitis experiment was sent to Labospace to quantify the concentrations of TGFβ, IL-1β, monocyte chemoattractant protein 1 (MCP-1), KC, IL-6 and TNFα by Luminex.

2.22 K/BxN model of autoantigen-induced arthritis

2.22.1 Serum transfer and ankle injection

The K/BxN serum-transfer model allows the induction of a neutrophil-driven, acute arthritis in mice by injecting naïve mice with serum from transgenic mice expressing the KRN T cell receptor transgene and I-Ag7 MHCII variant[239]. These mice express autoantibodies against the ubiquitously expressed glucose-6-phosphate isomerase, which accumulate and form immune complexes in joints. The result is the systemic and symmetrical manifestation of joint inflammation only 2 to 4 days after injection.

K/BxN arthritis was induced by injecting 8-week-old C57BL/6 mice intraperitoneally with 200µL of K/BxN mouse serum from a single batch, diluted 1 in 2 with PBS, produced and kindly given by Dr. Dianne Lukes (William Harvey Research Institute) who bred KRN mice with NOD mice, and collected the serum from the offspring at 10 weeks of age. This injection was repeated again 48 hours later. 24 hours later, mice were anaesthetised with 3% v/v isofluorane, and injected intra-articularly into the synovial space of each ankle. Each mouse was randomised to 10µL of either 3×10^6 $MV_{TNF\alpha}$ (pooled from equal numbers of vesicles from 3 human donors) in the left or right ankle, and vehicle (PBS) alone in the other. Injections were performed with a Hamilton syringe with a 26G needle which was washed with ethanol and then PBS following every injection. Which ankle received which treatment was blinded from its administration until the conclusion of the analysis.

2.22.2 Ankle digest

Forty-eight hours after intra-articular injection, mice were euthanised with a rising concentration of CO_2, and the legs removed and placed in ice-cold RPMI for transport between the *in vivo* facility and the tissue culture laboratory. As much soft tissue was removed from the legs as possible, the femurs were removed, taking care not

to damage the tibia, and the ankle synovium was cut with dissection scissors and opened by mechanical force.

Each leg was placed in a separate Erlenmeyer flask containing 15mL digestion buffer (RPMI + 0.5µg/mL collagenase D [11088866001, Sigma-Aldrich] and 40µg/mL DNAse I [10104159001, Sigma-Aldrich]). Under vigorous agitation with magnetic stirrers, the legs were incubated at 37°C for 30 minutes before collecting the cell suspension through a 70µm cell strainer into a 50mL tube containing 10mL of ice-cold RPMI with 10% v/v FBS (complete RPMI). The legs were covered with 15mL of digestion buffer and incubated again at 37°C for 30 minutes under agitation. Once the second round of cell suspension for each leg had been strained and combined with the first round, the volume was made up to 50mL with ice-cold, complete RPMI and the suspensions were centrifuged at $300\times g$ for 10 minutes at 4°C.

The supernatant was aspirated and the cells were resuspended in 1x Zombie Aqua fixable viability dye (423101, Biolegend) to exclude dead cells, and incubated at 4°C for 20 minutes. 2mL of FACS buffer (PBS + 0.02% w/v BSA) was added to each tube to remove unbound dye from solution, and tubes were centrifuged at $300\times g$ for 10 minutes at 4°C. Cell pellets were processed for flow cytometry, including Fc receptor blocking, and staining for CD45, CD11b, F4/80, CD86, MHCII, CD206, CD90, VCAM-1, and CD55 as per Section 2.7.

2.23 Generating microvesicles from platelets

In confirming that platelets produce microvesicles in response to TNFα stimulation, 500µL of platelet-rich plasma was generated as described in Section 2.2 from 5 healthy donors and stimulated either with 50ng/mL TNFα or vehicle (PBS) for 20 minutes at 37°C. Platelets were removed by centrifuging at $13{,}000\times g$ for 2 minutes at 4°C, supernatant was stained with 50µM BODIPY maleimide, and centrifuged at $20{,}000\times g$ for 30 minutes at 4°C to pellet microvesicles. Pellets were resuspended in 30µL of double sterile-filtered (0.22µm) PBS and enumerated on the ImageStream.

To generate $MV_{TNF\alpha}$ from washed platelets, 2µg/mL of prostacyclin (P6188-1MG Sigma-Aldrich) and 0.02U/mL apyrase were added to platelet-rich plasma and mixed gently for 1 minute, to prevent platelet activation. The plasma was centrifuged at $1{,}000\times g$ for 10 minutes at room temperature to pellet the platelets, the supernatant was discarded, and the pellet was resuspended in MTH buffer (134mM NaCl, 2.9mM KCl, 340µM Na_2HPO_3, 12mM $NaHCO_3$, 20mM HEPES, 1mM $MgCl_2$, 0.1% w/v glucose, 0.35% w/v BSA and 0.02U/mL apyrase) with 2µg/mL of prostacyclin. The platelets were pelleted by centrifuging at $1{,}000\times g$ for 10 minutes at room temperature, the supernatant was aspirated and the pellet was resuspended in MTH buffer. The

platelets were counted using a haemocytometer, their concentration adjusted to 2×10^7/mL and were allowed to rest at room temperature for 30 minutes. Platelets were stimulated with 50ng/mL TNFα for 20 minutes at 37°C, and their microvesicles were isolated (and an aliquot from each donor was labelled and enumerated) as above.

2.24 Cloning anxA1 into a bicistronic expression vector

The expression vector chosen to carry the anxA1 open reading frame (ORF; SC1197-13, OriGene) was the pIRESbsd2 vector. Once the anxA1 ORF is cloned into the XhoI restriction enzyme site, the messenger RNA produced by the vector is bicistronic, containing both the gene of interest, and a blasticidin resistance gene (See Figure 2.3). This ensures that if a cell is expressing the resistance gene, it is also expressing anxA1.

To clone the anxA1 ORF into the XhoI site, it first had to be used as the template in a polymerase chain reaction (PCR) to produce an ORF product with XhoI restriction sites, which would produce complimentary "sticky ends" after digestion with the XhoI enzyme. This was performed by combining 1ng of cDNA template, 0.5µM of forward primer, 0.5µM of reverse primer and 50% v/v of HotStart PCR master mix (K1051, Thermo Fisher) in a total volume of 50µL (made up with molecular biology grade water) per reaction. PCR primers and protocol are shown in Tables 2.5 and 2.6, respectively. Different annealing temperatures were used for different samples, between 50°C and 70°C (in steps of 5°C) but all resulted in amplified ORF. The pIRESbsd2 vector, and the forward and reverse PCR primers were designed and kindly provided by Dr. Graham Craggs (UCB). Amplification was confirmed by loading 5µL of PCR product, 2µL of Green DNA Gel Loading Dye (AG18, DNA Gdansk) and 18µL of molecular biology water into a lane of a 1.8% w/v agarose gel (G501801, Thermo Fisher), with high and low kilobase ladders to confirm size (N3231S & N3232S, New England Biolabs). Gels were imaged using a FluorChem E chemiluminescent imager. The amplicon was purified by running through a GenElute PCR Clean-Up Kit (NA1020, Sigma-Aldrich), following manufacturer's instructions.

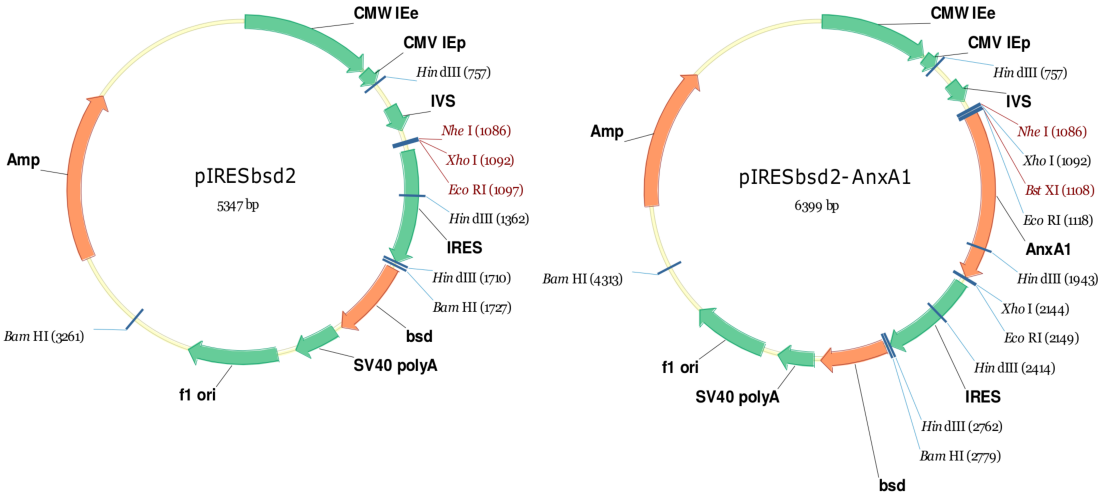

Figure 2.3: Plasmid maps of the pIRESbsd2 expression vector. Annotated plasmid maps of the pIRESbsd2 expression vector before and after ligation of the anxA1 and ORF into the XhoI site.

Table 2.5: PCR Primers

Primer	Sequence
Forward	5'-actg ctcgag ccacc atggcaatggtatcagaattcc-3'
Reverse	5'-actg ctcgag ttagtttcctccacaaagagcc-3'

Table 2.6: PCR Protocol

Step	Temperature (°C)	Duration (sec)
Initial denaturation	98	30
Denaturation	98	5
Annealing	50 - 70	20
Extension	72	20
Final extension	72	120
Hold	4	-

Denaturation, annealing and extension sequence repeated for 30 cycles before proceeding to final extension and hold.

The purified amplicon and pIRESbsd2 vector were separately digested by combining 2.5µg of DNA, 20U of XhoI restriction enzyme (R0146S, New England Biolabs) and 10% v/v of CutSmart buffer (B7204S, New England Biolabs) in a total volume of 50µL (made up with molecular biology grade water). Each reaction was incubated at 37°C for 30 minutes, before adding 20U more XhoI enzyme, and incubating for a further 30 minutes. The digested and undigested vectors were run on an agarose gel (as above) to confirm the absence of supercoiled and nicked DNA bands, and the presence of a single, linear DNA band. The digested amplicon was not run as the difference in size between digested and undigested fragments was too small to resolve. To prevent self-ligation of the plasmid, its ends were dephosphorylated by combining 5µL of digested vector, 25U of Antarctic phosphatase (M0289S, New England Biolabs) and 5µL of Antarctic phosphatase reaction buffer (B0289S, New England Biolabs), and incubating at 37°C for 30 minutes. Both the digested amplicon and vector fragments were purified separately through a GenElute PCR Clean-Up Kit as above.

To ligate the complimentary ends of the anxA1 amplicon and vector, ligation and control reactions were formulated as in Table 2.7 and incubated at room temperature for 5 minutes. Competent *E. coli* (C2987I, New England Biolabs) were thawed on ice, and 2µL of each ligation or control reaction was added to separate vials of bacteria. The bacteria were heat shocked at 42°C for 30 seconds to facilitate uptake of ligated plasmids, and incubated at 4°C for 5 minutes. To each vial, 950µL of SOC outgrowth medium (B9020S, New England Biolabs) was added and mixed vigorously at 37°C for 1 hour. From each vial, 400µL was added to agar plates (containing 50µg/mL carbenicillin C1613-1ML, Sigma-Aldrich), spread with a spreader, allowed to soak in for 10 minutes, and incubated upside down at 37°C overnight.

Table 2.7: Ligation reactions

Sample	Vector (µL)	Amplicon (µL)	Ligase (µL)	Buffer (µL)	Water (µL)
Vector only	1	0	0	10	9
Vector + ligase	1	0	1	10	8
Vector + ligase + amplicon	1	5	1	10	7

Ligase: T4 ligase (M0202T, New England BioLabs);
Buffer: 1x T4 DNA Ligase Reaction Buffer (B0202S, New England BioLabs)

2.25 Picking and identifying correctly ligated clones

After confirming a small number of colonies on the control plates, 24 transformed *E. coli* colonies were picked from the full ligation plate and seeded into individual cultures of 3mL of LB broth with 50µg/mL carbenicillin. Colonies were incubated on a shaker at 37°C overnight. From each culture, 1.8mL was used in a QIAprep Spin Miniprep Kit (27106, Qiagen) to isolate plasmid DNA, following manufacturer's instructions. The remaining volume of cultures was kept. A diagnostic restriction digest with EcoRI enzyme (R3101S, New England Biolabs) was performed for each clone by combining 2µL of plasmid, 20U of EcoRI enzyme and 10% v/v CutSmart buffer in a total volume of 50µL (made up with molecular biology grade water). Each reaction was incubated at 37°C for 30 minutes, before adding 20U more EcoRI enzyme, and incubating for a further 30 minutes. Each plasmid clone was run on an agarose gel as above to confirm diagnostic DNA bands. Two of the retained *E. coli* colonies with EcoRI digest bands diagnostic of anxA1 ORF ligation in the correct orientation, were seeded with an inoculating loop onto agar plates containing 50µg/mL carbenicillin as above, and incubated at 37°C overnight.

A single clone from each plate was picked and seeded into 3mL of LB broth with 50µg/mL carbenicillin and incubated on a shaker at 37°C overnight to form a starter culture. Each 3mL culture was seeded into 3L of LB broth in an Erlenmeyer flask and incubated on a shaker at 37°C overnight to bulk up the bacterial colonies. Each colony was passed through a GenElute HP Endotoxin-Free Plasmid Maxiprep Kit (NA0400, Sigma-Aldrich), following manufacturer's instructions.

Isolated plasmid DNA was concentrated by adding 0.1 volumes of 3M sodium acetate and 0.7 volumes of isopropanol, mixing by inversion, and centrifuging at 15,000×g for 30 minutes at 4°C. The supernatant was aspirated and the pellet was resuspended in 70% v/v ethanol and centrifuged at 15,000×g for 30 minutes at 4°C again. The supernatant was aspirated, the pellet allowed to air dry and resuspended in 200µL of molecular biology grade water. Each DNA preparation was assayed for concentration and purity using a Nanodrop 2000 (Thermo), and adjusted to 1µg/µL. An additional diagnostic restriction digest was performed for each clone by combining 1µg of plasmid, 20U of HindIII enzyme (R3104S, New England Biolabs) and 10% v/v CutSmart buffer in a total volume of 50µL (made up with molecular biology grade water). Each reaction was incubated at 37°C for 30 minutes, before adding 20U more HindIII enzyme, and incubating for a further 30 minutes. Each plasmid clone was run on an agarose gel as above to confirm diagnostic DNA bands. A single clone was used only from this point on.

2.26 Linearising pIRESbsd2-AnxA1 expression vector and transfection

To linearise the pIRESbsd2-AnxA1 expression vector to increase the efficiency of stable transfection, a restriction digest of an AdhI restriction site at position 5495 in the ampicillin resistance gene was performed. This was performed by combining 100µg of plasmid, 10U of AhdI enzyme (R0584S, New England Biolabs) and 10% v/v CutSmart buffer in a total volume of 50µL (made up with molecular biology grade water). Each reaction was incubated at 37°C for 30 minutes, before adding 10U more AhdI enzyme, and incubating for a further 60 minutes. The digested and undigested vectors were run on an agarose gel (as above) to confirm the absence of supercoiled and nicked DNA bands, and the presence of a single, linear DNA band.

The linearised DNA was purified and concentrated by adding 0.1 volumes of 3M sodium acetate and 2 volumes of ethanol, mixing by inversion, and centrifuging at 15,000×g for 30 minutes at 4°C. The supernatant was aspirated and the pellet was resuspended in 70% v/v ethanol and centrifuged at 15,000×g for 30 minutes at 4°C again. The supernatant was aspirated, the pellet allowed to air dry and resuspended in 200µL of molecular biology grade water. Each DNA preparation was assayed for concentration and purity using a Nanodrop 2000, and adjusted to 1µg/µL. The DNA was stored at -20°C until use.

2.27 Transfection of HL60, NB4 and HEK293 cell lines

HEK293 cells were transfected with the linear pIRESbsd2-AnxA1 expression vector by incubating the DNA in ViaFect reagent (E4981, Promega) at 1µg/4µL for 20 minutes at room temperature, and then adding this solution onto HEK293 cells in a 6-well plate at ~70% confluency.

Transfection of HL60 and NB4 cells was attempted with the above method twice (the second time titrating the DNA:ViaFect ratio), and also using Lipofectamine 3000 (L3000008, ThermoFisher) and nucleofection (VACA-1003, Lonza), following manufacturers' instructions.

For all three cell lines, a control well was included which was subjected to the same reagents and/or procedures, but was not given any exogenous DNA. At 48 hours post transfection, all three cell lines were washed once with PBS and cultured in their standard medium, with 10µg/mL blasticidin. Blasticidin medium was removed

and replaced every other day for 5 days (for HEK293 cells) of for 7 days (for HL60 and NB4 cells).

AnxA1 expression was confirmed by immunolabelling cells as described in Section 2.7, and acquiring the samples on a FACSCanto II cytometer.

2.28 Software and statistical analysis

ImageStream data was collected and analysed using the Inspire and IDEAS 6 software, respectively (Amnis). Flow cytometry data was collected and analysed using FACSDiva (BD Biosciences), and FlowJo 10 (FlowJo) and R 3.3.4, respectively. Light scatter phase function simulation was performed using Mie Simulator 1.05. Schematic figures created using Inkscape 0.91. Manuscript prepared in LaTeX (Tex Live 2016 distribution) using TeXstudio 2.10.8.

Statistical and graphical analysis was performed with R 3.3.4. Normality of residuals was evaluated for all models fit. Repeated-measures data was fitted using mixed general linear models (instead of the more traditional repeated measures ANOVA). A major caveat of biological research, where a single donor's cells are split between multiple treatments, is violation of the assumption of independence. In such situations, correlations between residuals were tested for and removed by normalising to a control treatment, or modelled using a mixed model approach.

For *post-hoc* pair-wise comparisons, multiplicity-adjusted p values are shown. Tukey (Kramer) was chosen when all comparisons were of interest in single factor models and Holm-Šidák was chosen when select comparisons were of interest or in factorial models, as indicated in figure legends. All variables used to build linear discriminant models were first standardized by their mean and standard deviation.

2.29 *In vivo* group size calculations

A pilot peritonitis experiment was performed to establish a range of vesicle doses which could elicit a change in macrophage phenotype. A Monte Carlo simulation was performed to determine the minimum number of mice per group needed to achieve the same effect size as seen with the $2x10^7$ MV dose (assuming a coefficient of variance of 20% , as seen in other peritonitis experiments), with 80% power, at an alpha level of 5%. A separate Monte Carlo simulation was performed to determine the minimum number of mice per group needed to detect a 30% decrease in median fluorescence intensity of measured antigens, assuming a 20% coefficient of variation, a power of 80%, and alpha of 5%.

The Monte Carlo simulations were performed by simulating 2 normal distributions, each with 1000 observations, with means and standard deviations corresponding to the estimated variability and effect size considered to be biologically significant. Each distribution was sampled (with replacement) for a range of group sizes, from 3 to 100, and at each iteration, a p value for a t test between each pair of samples was calculated. This process was repeated 10,000 times, and the minimum group size which achieved p values smaller than 0.05 at least 80% of the time were chosen as the required group sizes.

Chapter 3

Results

3.1 Optimisation of microvesicle preparation, storage and analysis

3.1.1 Comparing lower limits of detection between cytometers

To compare the ability of the ImageStream^{x} MKII and an LSRFortessa at resolving small, fluorescent particles, poly-fluorescent latex beads ranging from 1µm to 0.02µm in diameter were acquired on both machines (Figure 3.1). While the LSRFortessa was able to fully discriminate 0.5µm and 1µm beads, the 0.1µm bead population almost completely overlapped with the machine noise in all parameters, and the 0.02µm beads were wholly undetectable. The ImageStream was able to fully resolve all beads larger than 0.1µm, and most of the 0.02µm population based on fluorescence, area and diameter parameters. It is important to note that while area and diameter parameters can be plotted for the beads, they are vastly overestimated for particles under 10µm. Much of the 0.02µm bead population is estimated to be larger than the other bead populations, partly because they are brighter (at least compared to the 0.1µm and 0.5µm populations) and produce a larger fluorescent halo, and partly because there is greater measurement error for small particles, where a single pixel difference equates to a change of 0.3µm^2.

3.1.2 Detecting microvesicles in complex biological fluids

To test if the ImageStream was therefore capable of resolving fluorescent microvesicles, isolated human neutrophils, platelet poor/rich plasma and whole blood (1 in 10) were stained with 50µM BODIPY maleimide and acquired on the ImageStream (Figure 3.2). In all fluid samples, a low scatter, low/medium fluorescent population was detected which, when interrogated, consisted of single, uniformly-rounded objects which could be removed when pelleting at 20,000×g for 20 minutes.

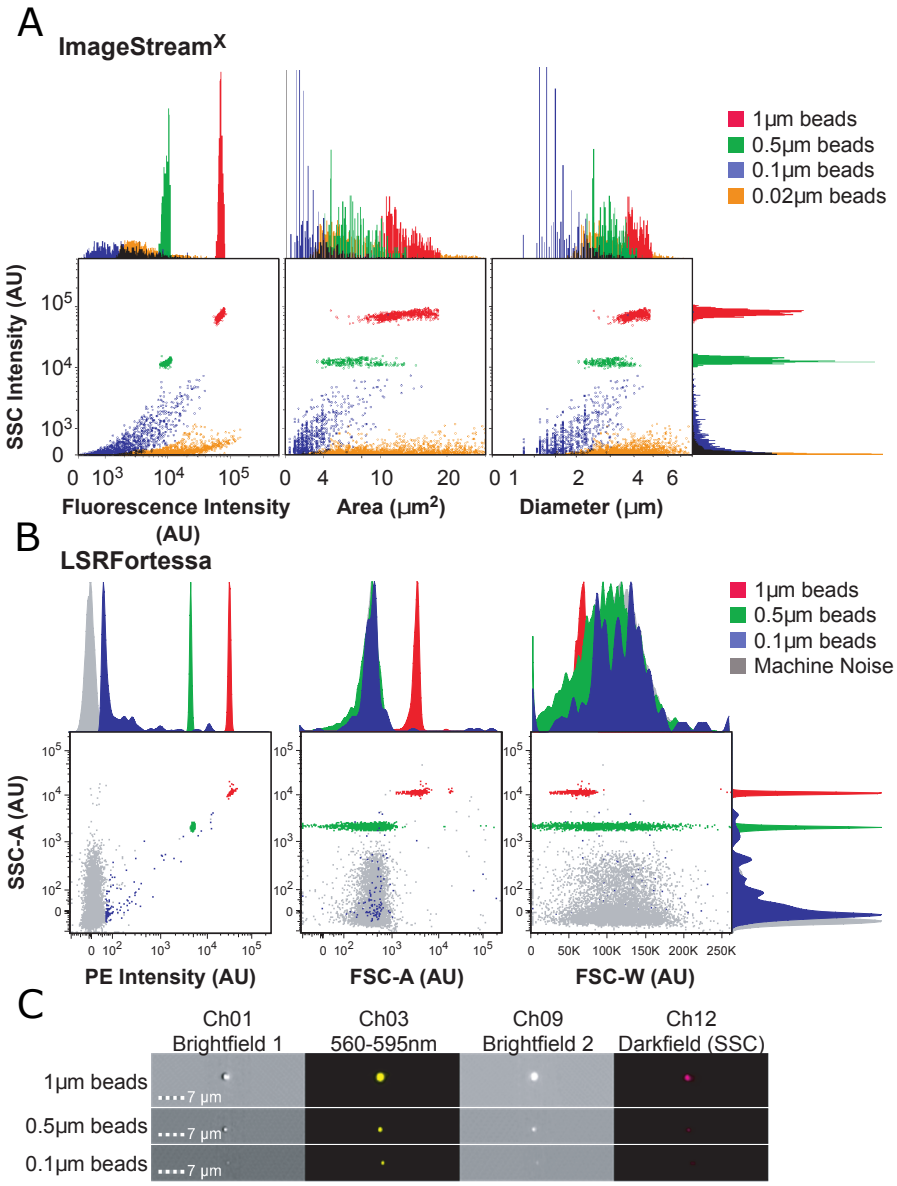

Figure 3.1: Small particle resolution of the ImageStream^X MkII and LSRFortessa. Poly-fluorescent latex beads of 1.0µm, 0.5µm, 0.1µm and 0.02µm were run individually on an ImageStream^X MkII and an LSRFortessa cytometer. Upper panels show dot plots of right angle light/side scatter (SSC) intensity against **A** each bead's brightest channel fluorescence intensity (Channel 2 for the 0.02µm and 0.1µm beads, and channel 3 for the 0.5µm and 1µm beads), area and diameter parameters on the ImageStream, and **B** phycoerythrin (PE) intensity, forward angle light scatter (FSC) area and FSC width on the LSRFortessa (with marginal histograms). **C** Representative ImageStream images of the three largest bead populations showing the two brightfield channels (set here as Ch01 and Ch09), the "PE channel" (Ch03) and the SSC channel (set here as Ch12) where scale bars apply to all images.

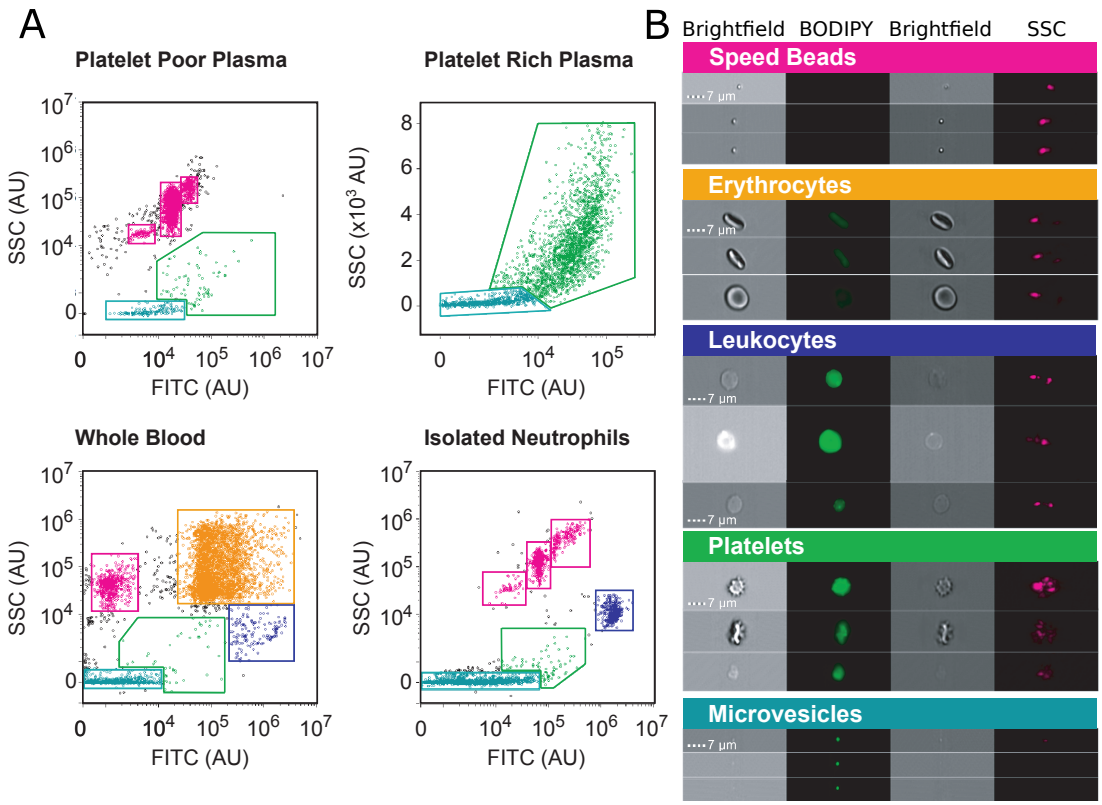

Figure 3.2: Detection of microvesicles in different biological fluids. A Dot plots showing right angle light/side scatter (SSC) against FITC fluorescence for platelet poor plasma, platelet rich plasma, whole blood and isolated neutrophils stained with 50µM BODIPY maleimide. **B** Representative brightfield, BODIPY maleimide and SSC images of events inside dot plot gates.

3.1.3 Comparing fluorescent labels for microvesicle triggering

As a major hurdle in identifying microvesicles is distinguishing them from electronic noise in the cytometer (including the ImageStream), a dye is needed which will label all membrane-bound objects as anxA5 is not a reliable marker for microvesicles[84]. BODIPY maleimide, CFSE and PKH67 are dyes which bind to cysteine residues, intracellular/luminal lysine residues or lipid bilayers, respectively. These dyes were titrated in technical replicates of a single $MV_{TNF\alpha}$ preparation, pooled from 5 donors, to compare relative labelling efficiency (Figure 3.3). When enumerating the detectable microvesicles, CFSE and BODIPY maleimide fully labelled the microvesicles from 4µM and 40µM, respectively, whereas PKH67 did not achieve full labelling.

3.1.4 Freeze-thaw stability of microvesicles and their labels

Microvesicles have previously been shown to be resistant to freeze-thaw cycles, and so can be re-used without aliquotting[87]. To test whether fluorescently labelled

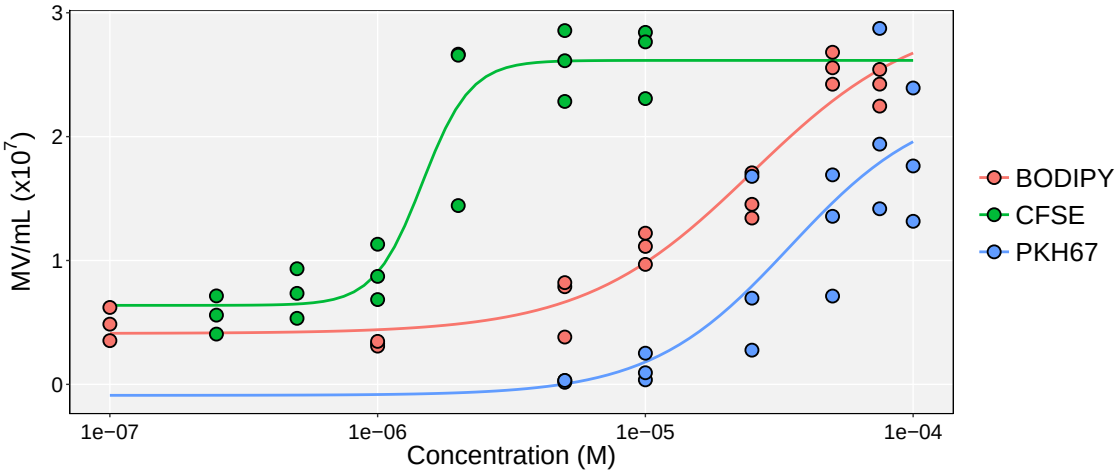

Figure 3.3: Titration of pan-microvesicle labels. A single $MV_{TNF\alpha}$ preparation, pooled between 5 neutrophil donors (2×10^7 cells each), was stained separately with BODIPY maleimide, PKH67 or CFSE in the range 10^{-7}M - 10^{-4}M, and acquired on the ImageStream. Individual technical replicates are shown with model fits by non-linear regression.

microvesicles can be frozen and re-used, a single $MV_{TNF\alpha}$ preparation, pooled from 3 donors, was labelled with 5µM CFSE, 50µM BODIPY maleimide or 50µM PKH67 or left unstained. The stained samples were either run immediately, or freeze-thawed between -80°C and 20°C once, twice or three times (one freeze-thaw cycle per day; Figure 3.4). The unlabelled samples were freeze-thawed 3 times, *then* labelled with each dye separately to control for any loss of vesicles. On enumerating the microvesicles in each sample, there was no difference between the numbers in non-freeze-thawed samples and the samples which underwent 3 cycles and were then labelled. While CFSE was most resistant to loss of fluorescence on freeze-thawing, all three dyes reported fewer positive microvesicles when frozen and re-used.

3.1.5 Comparing microvesicle yields between microfuge tubes

Maximising the yield of microvesicles is important to facilitate efficient experimentation and generate as much data from a single isolation as possible. To optimise microvesicle recovery during the 20,000×g centrifugation step, individual supernatants from TNFα-stimulated neutrophils were labelled with 50µM BODIPY maleimide FL, split between standard and LoBind tubes and pelleted at 20,000×g for 30 minutes at 4°C. Vesicles were resuspended in 30µL of sterile 0.22µm-filtered PBS and counted using an ImageStream(Figure 3.5). The recovery from LoBind tubes was, on average, 1.83 fold higher compared to standard tubes for each sample ($p = 0.054$) although half of samples acquired saw little change or even a small decrease in yield. As this

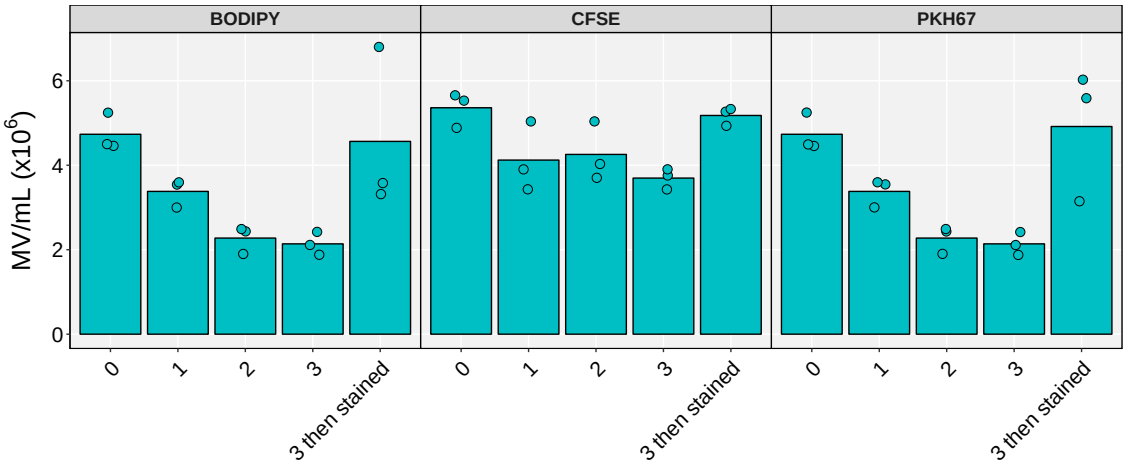

Figure 3.4: Freeze-thaw stability of pan-microvesicle labels. A single $MV_{TNF\alpha}$ preparation, pooled between 3 donors (2×10^7 each), was stained separately with 50µM BODIPY maleimide, 50µM PKH67 or 5µM CFSE and enumerated on the ImageStream after successive freeze-thaw cycles between -80°C and 20°C. The x axis shows the number of freeze-thaw cycles. To control for loss of microvesicles during freeze thaw, one group from each dye was freeze-thawed 3 times prior to staining. Individual technical replicates are shown with bars at group means.

data suggested that yield was either slightly higher or roughly equivalent compared to standard tubes, LoBind tubes were used for all future microvesicle isolations.

3.1.6 Exosomes are not enriched for in the 20,000×g pellet

As their size distribution overlaps with that of microvesicles, exosomes are the most problematic contaminant in microvesicle preparations. While platelets are reasonably easy to identify using the ImageStream, exosomes are indistinguishable from the microvesicle population. To confirm the absence of important numbers of exosomes in the microvesicle preparations, microvesicles were pelleted at 20,000×g for 20 minutes or 100,000×g for 1 hour at 4°C, lysed (along with C28/I2 cells as a positive control), run on a sodium dodecyl sulphate polyacrylamide gel and probed for Tsg101 and β-actin as a house-keeping gene (Figure 3.6). Tsg101 is a protein required for the formation of multivesicular bodies whose only vesicular compartment is exosomes. The protein was present in the C28/I2 and 100,000×g lysates but not the 20,000×g (10 minute exposure).

3.1.7 Microvesicles are stable at -80°C

Experimental use of microvesicles on the day of isolation is not always possible, and so short to mid-term storage is necessary. To evaluate the stability of microvesicles across different temperatures and times, $MV_{TNF\alpha}$ pooled from 3 neutrophil donors

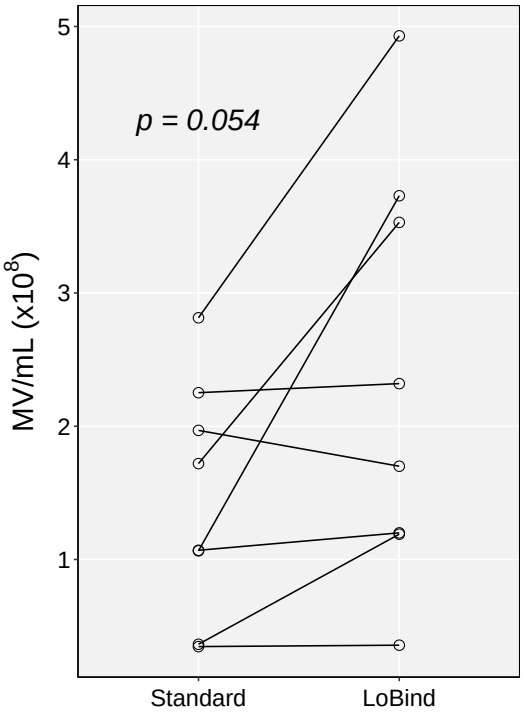

Figure 3.5: Comparison of microvesicle yield recovered after pelleting in standard and LoBind-coated microfuge tubes. 5×10^6 human neutrophils were isolated from whole blood and stimulated for 20 min with 50ng/mL TNFα at 37°C. After removal of cells and small contaminants by centrifugation, vesicles were labelled with 50µM BODIPY maleimide, split equally between standard and LoBind-coated microfuge tubes and pelleted at 20,000×g for 30 min at 4°C. After aspiration of the supernatant, pellets were resuspended in 30µL of sterile-filtered PBS and counted using the ImageStream. Data analysed with paired t test and lines connect data from a single donor.

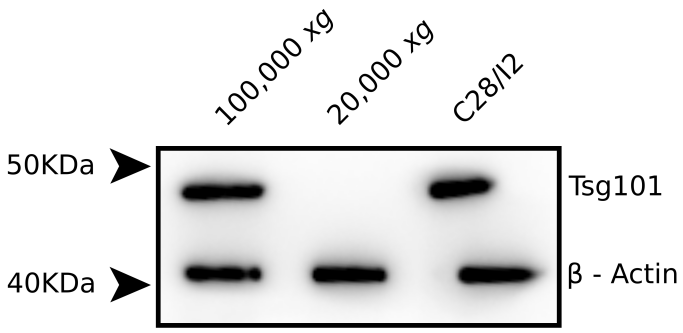

Figure 3.6: Microvesicle preparation is negative for Tsg101. Neutrophil microvesicles were generated with 50ng/mL TNFα and (following removal of cells and platelets/apoptotic bodies), were centrifuged at 20,000×g for 20 minutes or 100,000×g for 1 hour at 4°C (in rotors with k_{adjusted} factors of 692.39 and 406.43, respectively). Microvesicle preparation lysates (30µg of protein) and a control lysate of C28/I2 cells were probed for Tsg101 and β-actin. Representative blot of 3 independent experiments with separate biological replicates.

were incubated at 37°C, room temperature, 4°C, -20°C and -80°C for 1 week, 72 hours, 48 hours, 24 hours or processed immediately (Figure 3.7). Samples were labelled with BODIPY maleimide and enumerated on the ImageStream. Samples incubated at 4°C and above lost around a third of their microvesicles after 24 hours, and none were detected at 1 week. Samples stored at -20°C gradually declined in number with ~50% remaining after 1 week. The only samples to retain their microvesicle numbers were those stored at -80°C.

3.1.8 Neutrophil microvesicles express antigens of their parent cells

To test whether microvesicles can be immunophenotyped in tandem with their parent cells using the ImageStream and whether neutrophil microvesicles express neutrophil antigens, TNFα-stimulated neutrophils were labelled with BODIPY maleimide and fluorescent antibodies against CD66b (a reliable human neutrophil-restricted marker), CD62L and CD11b (Figure 3.8). Neutrophils and microvesicles were gated separately based on their scatter and BODIPY maleimide fluorescence and interrogated for antibody staining. All neutrophils were positive for the three antigens, showing varying degrees of activation (as indicated by CD62L and CD11b expression). Microvesicles were largely positive for all three antigens although were considerably dimmer than the cells.

3.1.9 ImageStream concentrations decline linearly with sample dilution

While evaluating the accuracy of the ImageStream in enumerating microvesicles, it was important to confirm the estimation of concentration was linear with sample dilution. To test this, $MV_{TNF\alpha}$ were generated from 3 donors, labelled with BODIPY maleimide and enumerated on the ImageStream either as they were, or following dilutions of 1 in 2, 1 in 4 and 1 in 8 (Figure 3.9). Microvesicle concentration estimates showed excellent linearity with dilution with Pearson correlation coefficients ≥ 0.992.

3.1.10 Profiling populations of circulating microvesicles

To confirm the ability of the ImageStream to phenotype isolated microvesicle populations, plasma microvesicles were generated from 6 healthy donors, dyed with BODIPY maleimide Texas Red, split between separate staining reactions and immunolabelled separately (i.e. one antibody per reaction) for CD235 (erythrocyte), CD41 (platelet), CD45 (leucocyte), CD146 (endothelial cell), CD14 (monocyte),

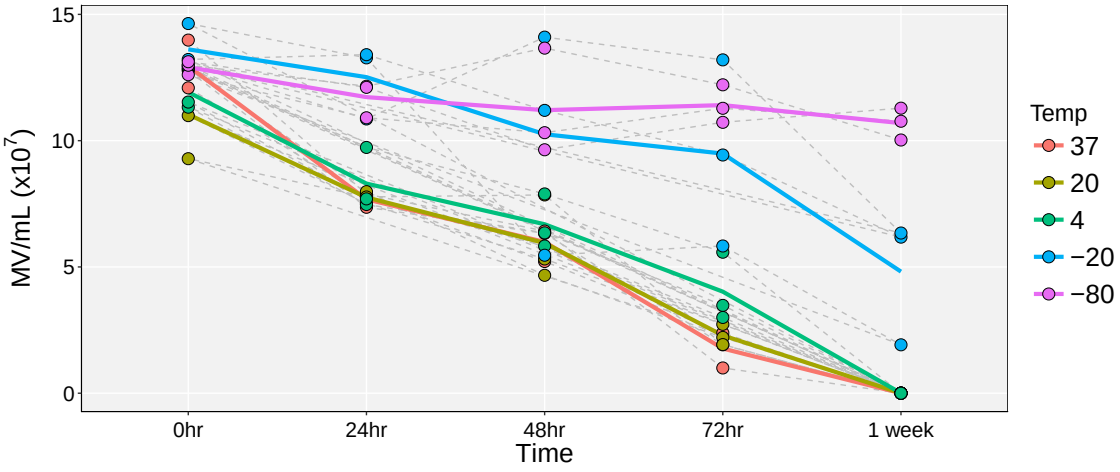

Figure 3.7: The effect of storage temperature on microvesicle stability. $MV_{TNF\alpha}$ were generated from 3×10^7 neutrophils from each of 3 donors, split between 5 groups and stored at a range of temperatures, for different lengths of time up to a week. Stored microvesicles were stained with 50µM BODIPY maleimide (after thawing if necessary) and enumerated on the ImageStream. Individual biological replicates are shown, where solid lines connect group means and dashed lines connect data from each donor.

CD66b (neutrophil) and CD3 (lymphocyte). Microvesicles were acquired on the ImageStream and the number of microvesicles from each population was expressed as a percentage of all BODIPY maleimide$^+$ microvesicles and as their absolute number per mL of plasma (Figure 3.10 and Table 3.1). The most abundant population was erythrocyte-derived (37.5% ± 6.9; mean ± standard deviation), followed by platelet (24.3% ± 3.6), leucocyte (12.0% ± 5.1) and endothelial cell (6.6% ± 2.0), although 11.5% of BODIPY maleimide$^+$ microvesicles were negative for all these antigens. Of the leucocyte populations, monocyte and neutrophil-derived vesicles represented 3.4% ± 2.5 and 3.6 ± 3.1 of the total, respectively, while thymocyte-derived vesicles constituted only 0.9% ± 0.9. A small number of CD45$^+$ vesicles did not express CD14, CD66b or CD3.

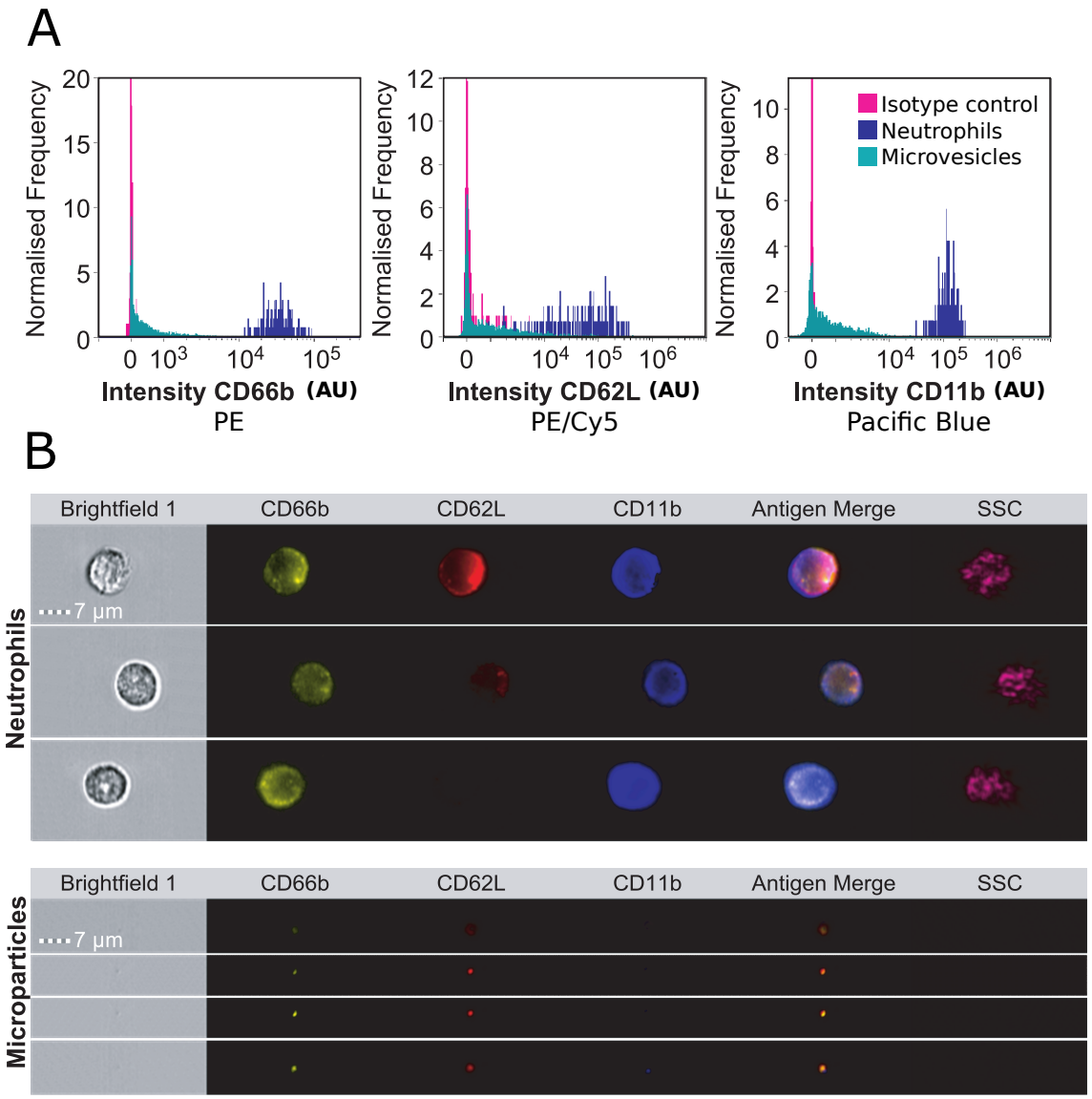

Figure 3.8: Simultaneous phenotyping of neutrophils and their microvesicles. Neutrophils were stimulated with 50ng/mL TNFα for 20 min, stained with 50µM BODIPY maleimide and antibodies against CD66b, CD62L and CD11b, and acquired on the ImageStream. Microvesicles and neutrophils were gated separately. **A** Overlay histograms showing the intensity of antigen staining for neutrophils, microvesicles and isotype controls. **B** Representative brightfield, fluorescence (with merged images) and SSC images for gated neutrophils and microvesicles.

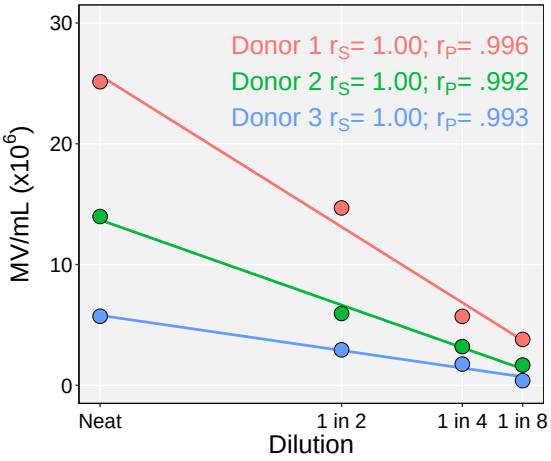

Figure 3.9: Accurate concentration estimates across linear dilution. $MV_{TNF\alpha}$ were generated from three donors, stained with 50µM BODIPY maleimide, diluted up to 1 in 8 with sterile-filtered PBS and enumerated on the ImageStream. Individual samples and linear regression lines shown for each donor. r_S - Spearman correlation coefficient; r_P - Pearson correlation coefficient.

3.1.11 Comparing inflammatory stimuli for inducing microvesicle release

To study the effects of neutrophil microvesicles *in vitro*, model stimuli needed to be characterised for their ability to induce ectocytosis. To this end, a panel of pro-inflammatory stimuli (TNFα, IL-8, LTB_4, zymosan and *E. coli*) were use to treat isolated neutrophils for 20 minutes, and the number of vesicles was quantified. Data were represented as the number of microvesicles per neutrophil, and all treatments induced a comparable $\geq$ 2-fold increase over the vehicle-treated neutrophils (Figure 3.11 A).

3.1.12 TNFα induces rapid and persistent ectocytosis

To assess how the rate of ectocytosis changes upon stimulation, isolated neutrophils labelled with BODIPY maleimide were stimulated with TNFα or vehicle and immediately acquired. Data are shown as objects/second in the microvesicle gate over time for each donor (normalised to vehicle baseline; Figure 3.11 B). TNFα induced a modest increase in rate among all donors (an average increase of 0.57 ± 0.4 microvesicles/cell/second; mean ± standard deviation), but most notably induced a considerable increase in the number of microvesicles in the latent period between treatment and acquisition (from 18.5 ± 6.5 microvesicles/second in vehicle-treated samples to 65.98 ± 28.24 microvesicles/second in TNFα-treated samples at 2 minutes post stimulation; mean ± standard deviation).

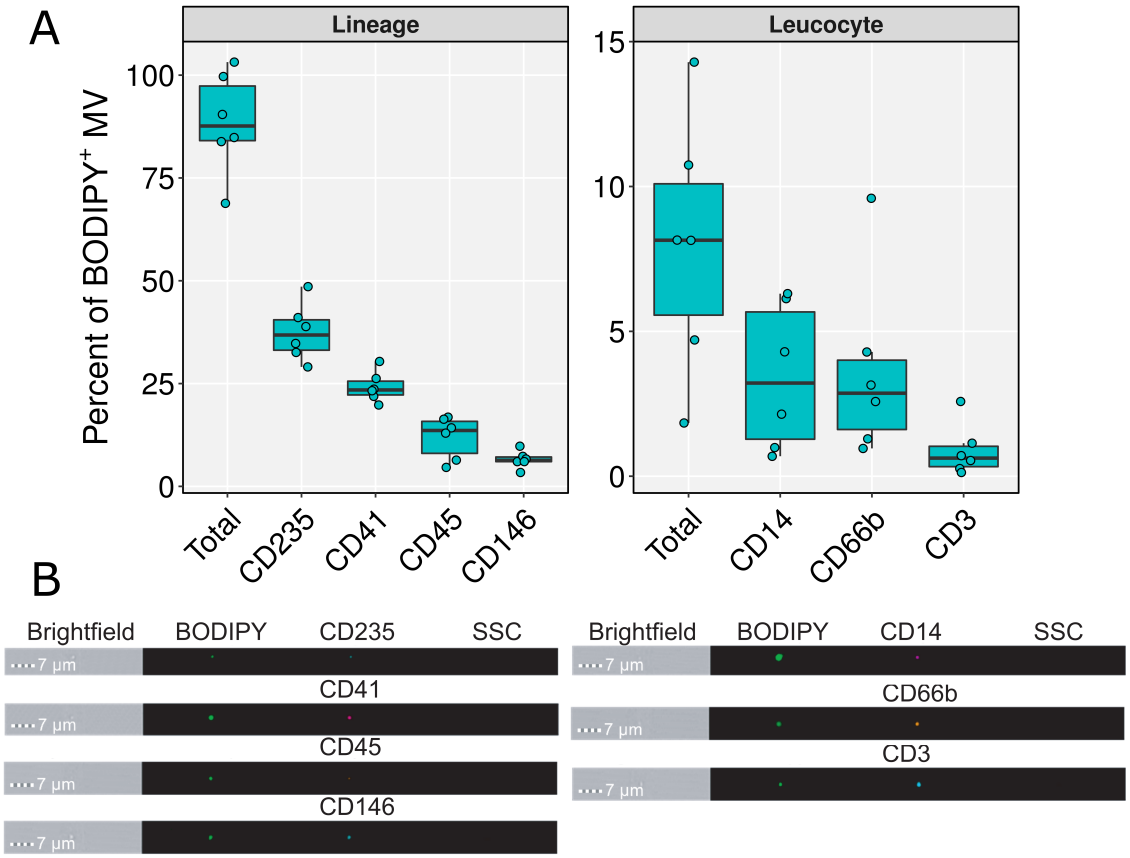

Figure 3.10: Circulating microvesicle populations. Platelet-poor plasma (PPP) was obtained from healthy volunteers, stained with 50µM BODIPY maleimide and antibodies against CD235, CD41, CD45, CD146, CD14, CD66b and CD3, and acquired on the ImageStream. The percentage of BODIPY maleimide$^+$ microvesicles positive for each **A** lineage and **B** leucocyte marker are shown, with representative brightfield, BODIPY maleimide, fluorescence and SSC images.

Table 3.1: Concentrations of microvesicle subsets in human plasma

		Antigen						
	Total	CD235	CD41	CD45	CD146	CD14	CD66b	CD3
Cell type	All	Erythrocyte	Platelet	Leucocyte	Endothelial	Monocyte	Neutrophil	T cell
Mean (x10^6/mL)	2.5	1.06	0.71	0.35	0.18	0.10	0.10	0.02
SD	0.98	0.37	0.32	0.22	0.05	0.10	0.07	0.02

Mean and standard deviation of absolute concentrations of microvesicle lineages per mL of platelet-poor plasma for 6 healthy donors.

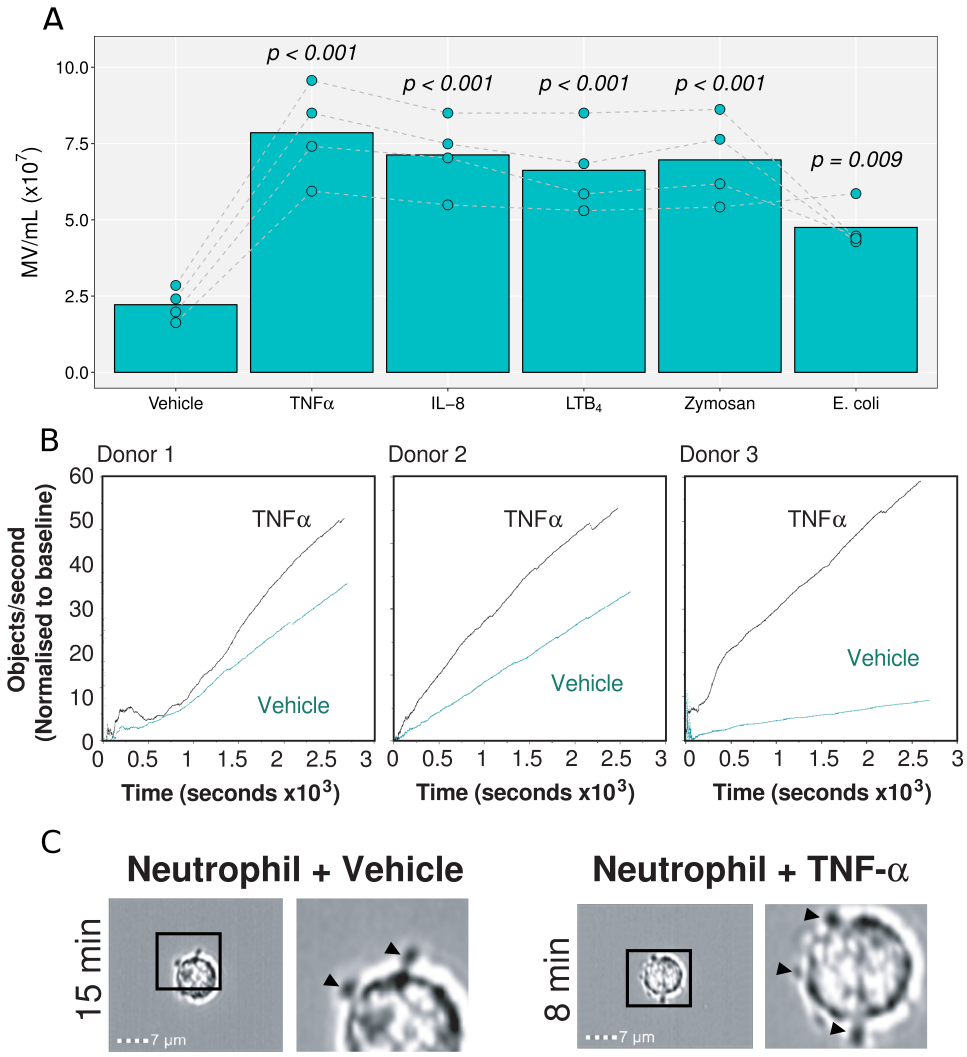

Figure 3.11: Neutrophils release large numbers of microvesicles upon stimulation. **A** $1{\times}10^6$ neutrophils from 4 healthy donors were stimulated with 50ng/mL TNFα, 50ng/mL IL-8, 10nM LTB_4, 1µg/mL zymosan, 10ng/mL *E. Coli* or vehicle alone for 20 min at 37°C. Microvesicles were isolated, stained with 50µM BODIPY maleimide FL and enumerated on the ImageStream. Individual biological replicates (connected by grey lines) are shown with bars at group means. Analysed with a mixed model ANOVA (treating donor as a random factor) with Tukey *post-hoc* test. **B** $2{\times}10^7$ neutrophils from 3 healthy donors were each split between two tubes, stained with 50µM BODIPY maleimide and treated with 50ng/mL TNFα or vehicle alone. Immediately after treatment, each tube was acquired on the Imagestream and the rate of microvesicles passing through the flow cell was tracked as a function of time, with traces shown for each donor (with TNFα traces normalised to vehicle baseline at time 0). **C** Brightfield, images of neutrophils from donor 2. Boxes are magnified x3 in the right-hand images. Arrows indicate outward membrane blebs

3.2 Microvesicles modulate phlogistic macrophage activation

3.2.1 $MV_{TNF\alpha}$ restrict classical activation

To test the hypothesis that neutrophil microvesicles can modulate M1 macrophage polarisation, human monocyte-derived macrophages were treated with increasing concentrations of $MV_{TNF\alpha}$ during LPS and IFNγ-stimulation for 24 hours (Figure 3.12). Microvesicles induced a concentration-dependent decrease in HLA-DR, DP & DQ and CD86 expression, returning levels to those of unstimulated cells at 3×10^6 MV/mL. A concentration-dependent increase in CD206 expression was also observed, returning levels to those of unstimulated macrophages at 1×10^6 MV/mL and continuing to rise at 3×10^6 MV/mL.

3.2.2 Efficacy is microvesicle (and not exosome)-dependent

To confirm that this efficacy was solely attributable to microvesicles and not exosomes, neutrophils were treated with TNFα to induce vesicle release and, after removal of the cells, supernatants were sequentially centrifuged at 20,000$\times g$ and then 100,000$\times g$ to differentially enrich for microvesicles and exosomes, respectively. Macrophages undergoing classical activation were concomitantly treated with the microvesicle pellet, exosome pellet, or the remaining supernatant (Figure 3.13). While treatment of macrophages with the 20,000$\times g$ pellet restricted upregulation of HLA-DR, DP & DQ and CD86 expression during classical activation, and increased CD206 expression, treatment with either the supernatant or 100,000$\times g$ pellet did not.

Nanoparticle tracking analysis of the 20,000$\times g$ pellets showed that these preparations of vesicles had median diameters of between 110nm and 140nm, and while most of the samples contained vesicles under 100nm in size (exosomes), the majority of vesicles were larger than 100nm (Figure 3.14).

As it is has historically been used as a marker of microvesicles, the expression of PtdSer was compared between vesicles in the 20,000$\times g$ and 100,000$\times g$ pellets (Figure 3.15). Exosomes were negative for PtdSer while only ~60% of vesicles in the microvesicle-enriched fraction were positive. Expression of the proresolving protein anxA1, which is known to be exported via microvesicles, was also compared between the fractions. Again while exosomes were negative, ~20% of neutrophil microvesicles were anxA1$^+$.

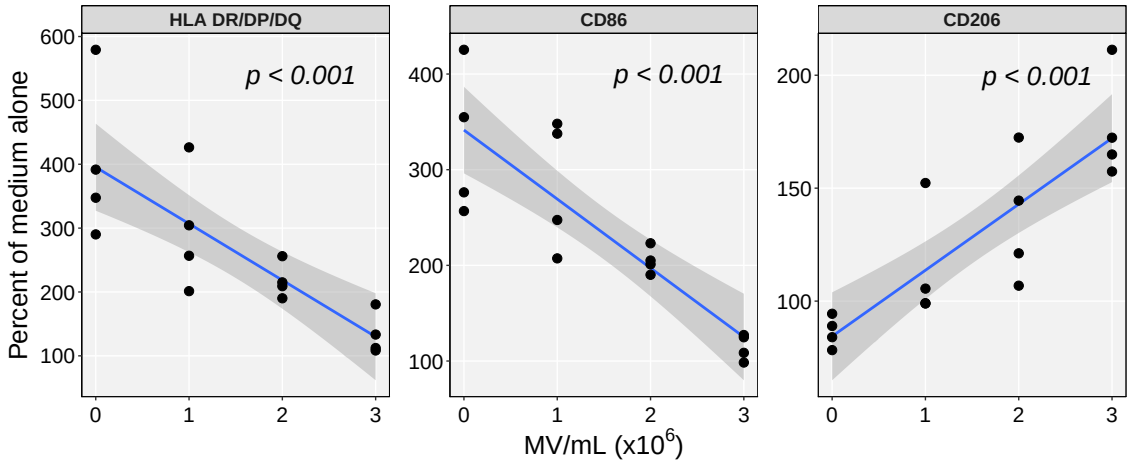

Figure 3.12: Neutrophil microvesicles modulate macrophage polarisation. Human monocyte-derived macrophages from 4 separate donors were classically activated over 24 hours alone, or with increasing concentrations of $MV_{TNF\alpha}$ (pooled from 3 donors, the same preparation for each macrophage donor). Cells were detached, stained for HLA-DR, DP & DQ, CD86 and CD206 expression and analysed by flow cytometry. Data from individual biological replicates are shown as median fluorescence as a percentage of naïve macrophages. Data analysed with separate linear regression for each antigen, where least squares lines and 95% confidence bands are shown.

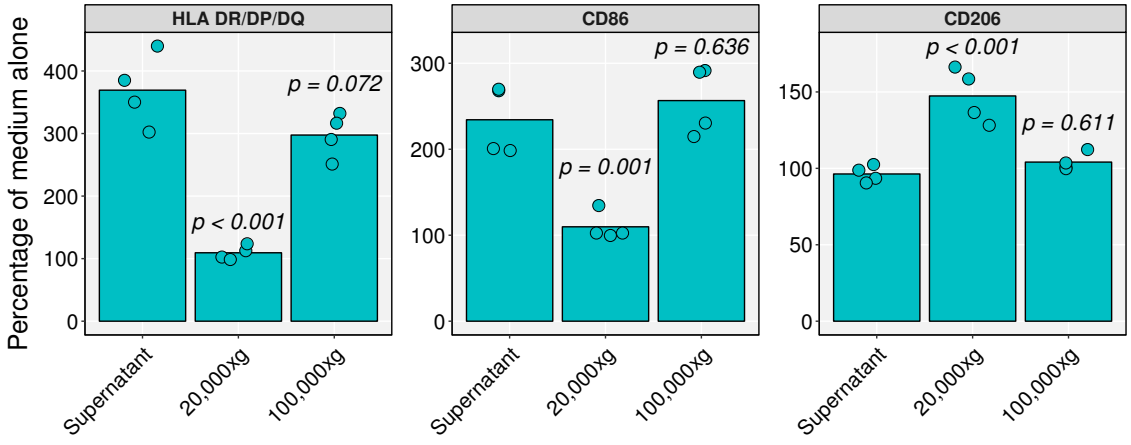

Figure 3.13: Comparison of microvesicle and exosome pellets. From 2×10^7 human neutrophils (each from 3 donors), $MV_{TNF\alpha}$ were produced and differentially isolated from exosomes by sequential centrifugation and $20{,}000\times g$ and $100{,}000\times g$. Both pellets from each neutrophil donor were pooled between donors by resuspending in 100µL of RPMI and, along with the supernatant, were kept. Human monocyte-derived macrophages from 4 separate donors were classically activated for 24 hours, in the presence of the entire $20{,}000\times g$ pellet, $100{,}000\times g$ pellet, or supernatant. Macrophages were detached, stained with antibodies against HLA-DR, DP & DQ, CD86 and CD206, and analysed on a flow cytometer. Data are median fluorescence as a percentage of untreated macrophages, of biological replicates, with bars at group means. Data analysed with separate one-way ANOVA with Tukey *post-hoc* test for each antigen.

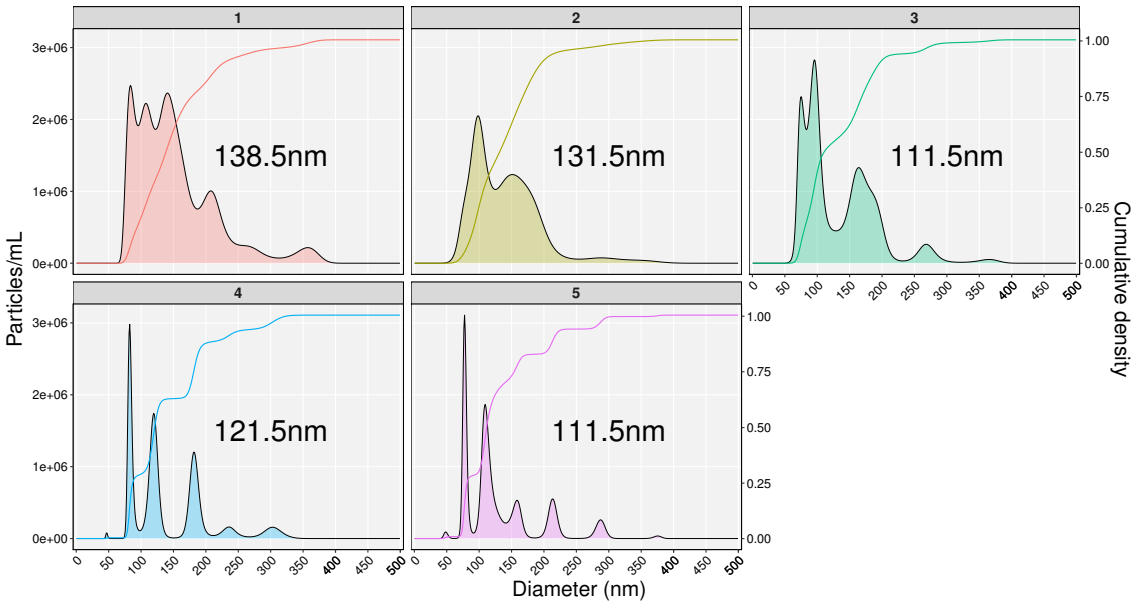

Figure 3.14: Nanoparticle Tracking Analysis of $MV_{TNF\alpha}$. $MV_{TNF\alpha}$ were generated and isolated from 5 human donors (1×10^7 neutrophils each), and pelleted at 20,000×g. Each vesicle pellet was resusended in 500µL of sterile-filtered PBS and acquired under flow, after optimising the focus and capture settings. Concentration of particles at each diameter are shown by the density histogram, and the cumulative density function shows the proportion of particles in each sample below each diameter. Median particle diameters for each sample is shown in the plots.

3.2.3 $MV_{TNF\alpha}$ efficacy is partly PtdSer-dependent

In order to further interrogate the effect of these microvesicles on macrophage phenotype and to determine whether the effects observed were dependent on PtdSer (as for apoptotic bodies[151]), monocyte-derived macrophages were treated with combinations of LPS and IFNγ, standard $MV_{TNF\alpha}$ (3×10^6/mL) and those pre-coated with anxA5 as per Section 2.9 (and IL-4 as a positive M2 control) for 24 hours (Figure 3.16). The expression of HLA-DR, DP & DQ, CD86 and CD206 was compared as above, and supernatants were also assessed for IL-12p70, TGFβ, IL-10 and IL-1β expression. $MV_{TNF\alpha}$ had no effect on the expression of HLA-DR, DP & DQ, CD86, CD206, IL-12p70, IL-10 or IL-1β, but did cause ~20-fold increase in TGFβ release. LPS and IFNγ-treatment induced ~2.5-fold increase in HLA-DR, DP & DQ and CD86 expression, a small but non-significant decrease in CD206 expression, 3.3-fold increase in IL-12p70, a 3.75-fold increase in IL-1β, a small but non-significant increase in IL-10, and no change in TGFβ levels. $MV_{TNF\alpha}$-treatment in the presence of LPS and IFNγ decreased HLA-DR, DP & DQ, CD86 and IL-12p70, IL-10 and IL-1β expression compared to LPS and IFNγ alone while inducing an increase in CD206. The effects of microvesicles on all phenotypic markers were lost when pre-coated with anxA5, except IL-12p70 which was partially restored in the coated microvesicle treatment,

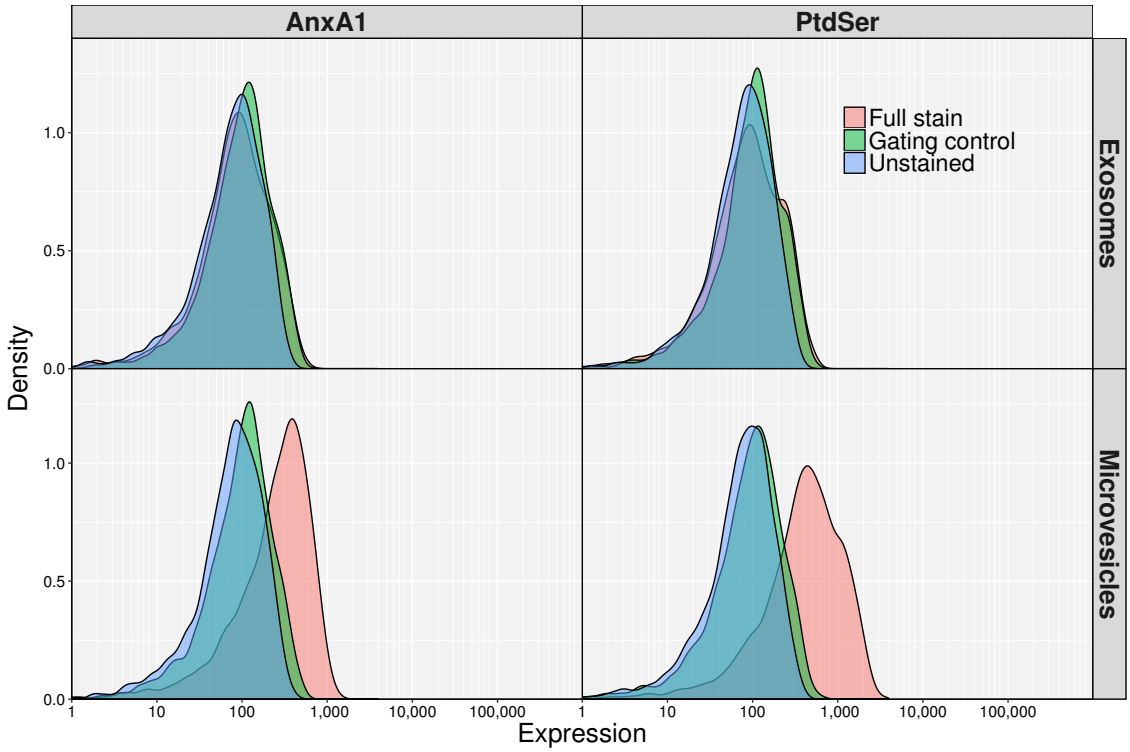

Figure 3.15: PtdSer and anxA1 expression in neutrophil vesicles. From 2×10^7 human neutrophils (each from 3 donors, labelled with 2.5µM BODIPY maleimide Texas red), $MV_{TNF\alpha}$ were produced and differentially isolated from exosomes by sequential centrifugation and 20,000×g and 100,000×g. Both pellets were resuspended in 100µL of 1x anxA5-binding buffer (or Ca^{2+}-free buffer to control for non-specific anxA5-binding), labelled with anxA5-FITC or antibodies against anxA1 (or a secondary antibody only), and acquired on the ImageStream. "Gating control" refers to secondary antibody-only or Ca^{2+}-free conditions for anxA1 and PtdSer-labelling, respectively. Kernel density plots of 10,000 microvesicles are shown for each condition.

and TGFβ which was independent of PtdSer. To confirm that the microvesicles were not, in fact, the source of the TGFβ, the same number of vesicles from the same preparation was lysed using 0.02% v/v triton X-100 by gentle pipetting, centrifuged at 13,000×g for 2 minutes to remove membrane fragments, and the concentration of TGFβ measured by cytometric bead array. There was no detectable TGFβ in the preparation (data not shown).

3.2.4 $MV_{TNF\alpha}$ do not modulate alternative activation

As microvesicles in isolation did not seem to induce an alternative activation phenotype, their effect on IL-4-mediated polarisation was tested by titrating IL-4 on monocyte-derived macrophages in the presence of 3×10^6/mL $MV_{TNF\alpha}$ or vehicle alone for 24 hours (Figure 3.17). There was a concentration-dependent decrease in HLA-DR, DP & DQ and CD86 expression and increase in CD206 expression with IL-4 which was unaffected by microvesicle addition.

3.2.5 Internalisation of microvesicles depends on PtdSer and MerTK

The phagocytosis of apoptotic moieties by macrophages is mediated in large part by the receptor-tyrosine kinase MerTK, which is a member of the tyro-3/Axl/MerTK family of receptors[174,240]. To determine whether blocking the interaction between PtdSer and MerTK abrogated the uptake and subsequent efficacy of microvesicles on macrophage phenotype, a vesicle internalisation assay was optimised. To compare their suitability, BODIPY maleimide, CFSE and PKH67 dyes were used to label microvesicles which were loaded onto macrophage cultures for 90 minutes. The percentage of positive cells, the fluorescence intensity and detectable microvesicles per cell for each dye was compared using the ImageStream (Figure 3.18). PKH67-labelled vesicles were detected in more macrophages than CFSE and BODIPY maleimide-labelled vesicles (the latter of which was detected in $< 10\%$).

When masked, intracellular PKH67-labelled vesicles were $>$ 3-fold brighter than their CFSE and BODIPY maleimide counterparts (which were equivalent). The median number of microvesicles detected per cell was higher for PKH67-labelled samples (7 ± 1.5; median $\pm$ range) followed by CFSE (6 ± 1) and BODIPY maleimide (2 ± 1.5). While PKH67 outperformed the other two dyes, it was noticed that a considerable amount of lysis occurred when staining with this dye (possibly due to its ethanol solvent), and that it contributes a number of fluorescent particles, even in the absence of microvesicles. For this reason, CFSE was chosen as the most appropriate label for internalisation assays.

To test the hypothesis that microvesicle internalisation by macrophages is PtdSer-dependent, monocyte-derived macrophages were treated with 5×10^6/mL standard $MV_{TNF\alpha}$ or those pre-coated with 50µg/mL anxA5 (both labelled with CFSE), for

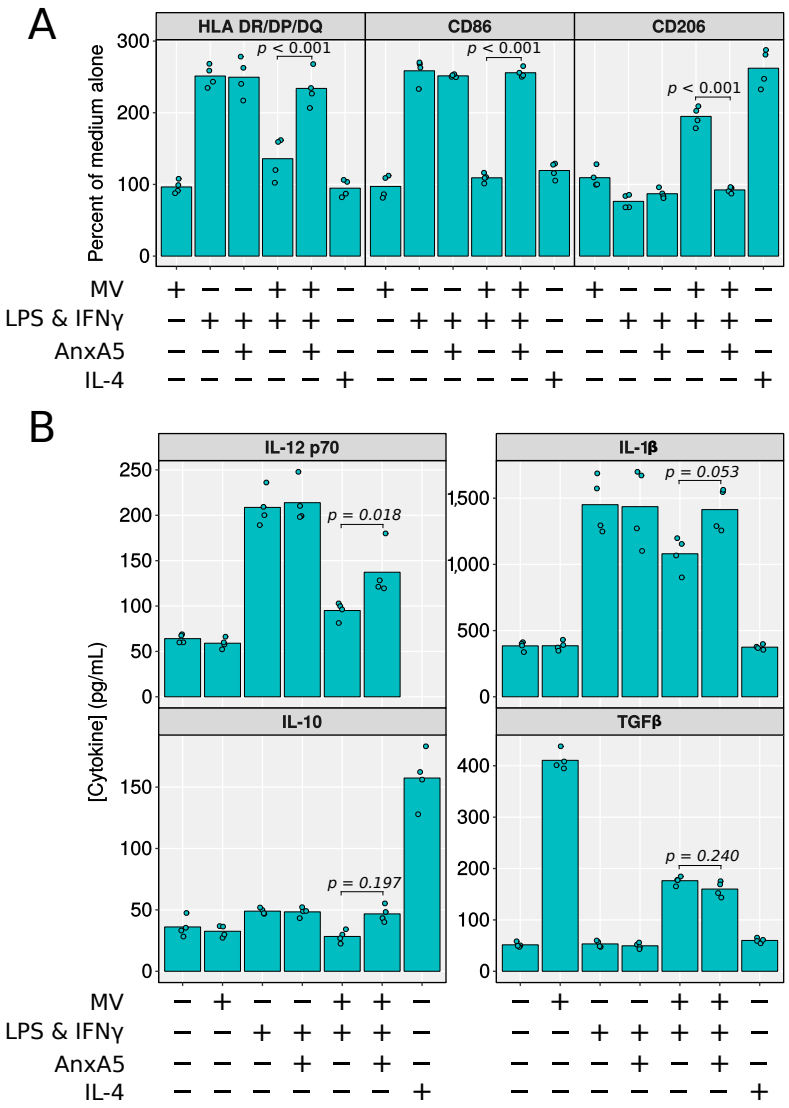

Figure 3.16: Macrophage polarisation is partially modulated via phosphatidylserine. Human monocyte-derived macrophages were treated with combinations of 3×10^6/mL $MV_{TNF\alpha}$ (pooled from 3 donors, with or without anxA5 blocking) and 10ng/mL IFNγ & 10ng/mL LPS or vehicle for 24 hours. Naïve macrophages were used as negative controls and those treated only with IL-4 acted as positive controls for alternative activation. **A** Cells were detached, stained for HLA-DR, DP & DQ, CD86 and CD206 expression and analysed by flow cytometry. **B** Supernatants were collected and levels of IL-12p70, TGFβ-1 and IL-1β were quantified using a Cytometric Bead Array. Data are median fluorescence as a percentage of untreated cells for surface proteins and absolute concentration for cytokines. Individual biological replicates are shown with bars at group means. IL-12 p70 could not be detected following IL-4 stimulation. Data analysed with separate one-way ANOVA with Tukey *post-hoc* tests for each antigen.

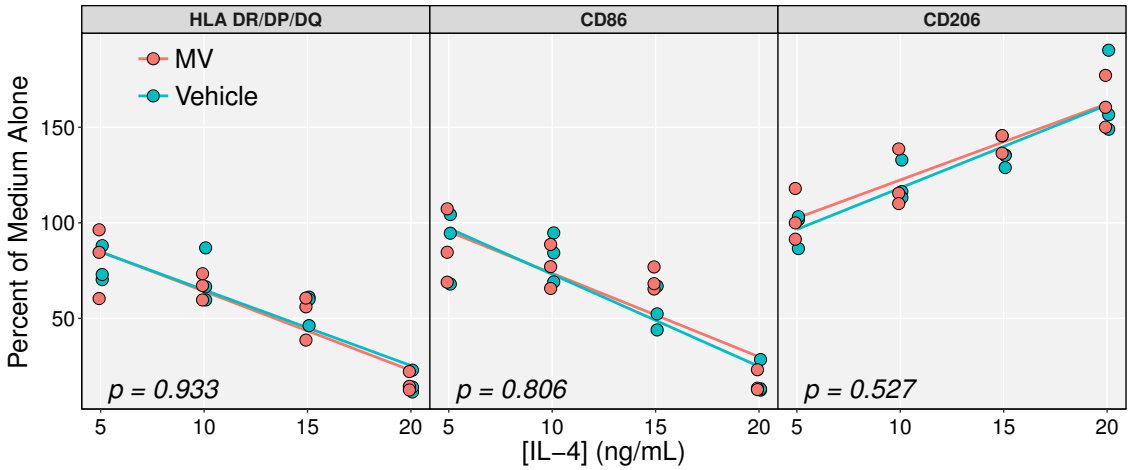

Figure 3.17: Neutrophil microvesicles do not promote M2 macrophage polarisation. Human monocyte-derived macrophages were alternatively activated with between 5ng/mL and 20ng/mL IL-4, with or without 3×10^6/mL $MV_{TNF\alpha}$ (pooled between 3 donors) for 24 hours. Cells were detached, stained with antibodies against HLA-DR, DP & DQ, CD86 and CD206, and analysed using flow cytometry. Data from individual biological replicates are shown as median fluorescence as a percentage of untreated cells. Data analysed with separate ANCOVA for each antigen, where least squares lines are shown.

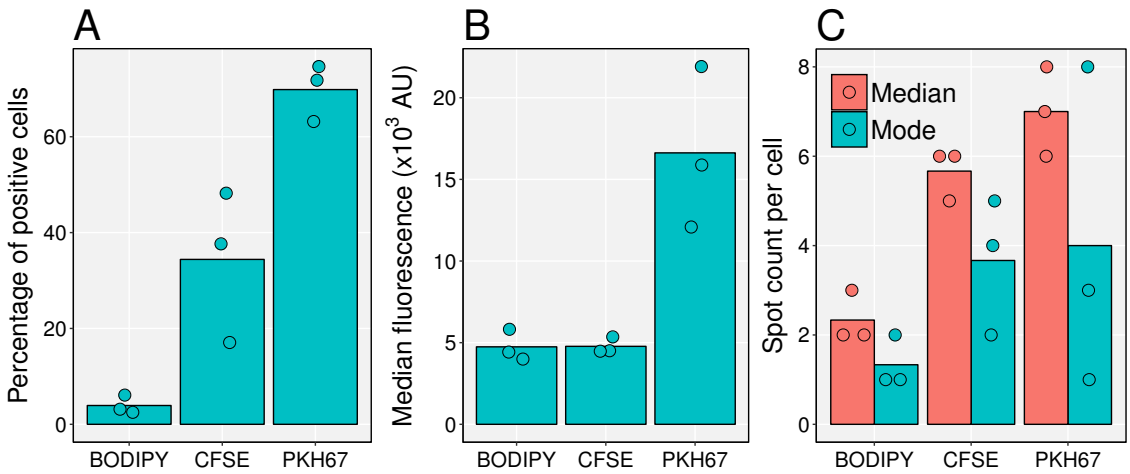

Figure 3.18: Comparison of different labels for microvesicle internalisation. $MV_{TNF\alpha}$ pooled from 3 donors were stained with 5µM CFSE, 50µM BODIPY maleimide or 50µM PKH67, washed by pelleting, counted, and resuspended at 5×10^6/mL in sterile-filtered PBS. Human monocyte-derived macrophage supernatant was aspirated and replaced with 1mL of $MV_{TNF\alpha}$ suspension (9×10^5 macrophages per well of 12-well plates; MV:cell ratio of 5.6:1) for 90 minutes. Cells were washed, detached, fixed and acquired on the ImageStream. **A** Data showing the % of positive cells, **B** the median fluorescence intensity of masked-fluorescence and **C** the median and modal microvesicles per cell for each dye. Data are technical replicates with bars at group means.

5, 30, 60 and 90 minutes at 37°C (Figure 3.19). The percentage of macrophages positive for microvesicles was significantly reduced from 30 minutes in samples treated with anxA5-coated vesicles. To test whether this effect was related to MerTK, the experiment was repeated, but instead of blocking PtdSer, macrophages were treated with a small molecule inhibitor of MerTK auto-phosphorylation, UNC-569, or vehicle. Blockade of MerTK auto-phosphorylation significantly reduced microvesicle uptake from 60 minutes compared to vehicle.

3.2.6 PtdSer-dependent effects are mediated through MerTK

As blockade of the PtdSer-MerTK interaction was shown to be responsible for microvesicle uptake, it was hypothesised that this may also be the mechanism by which microvesicles condition macrophage phenotype. To test this, macrophages were classically activated in the presence of 3×10^6/mL $MV_{TNF\alpha}$ or vehicle, with 10nM UNC-569 or vehicle in a 2x2 factorial design (Figure 3.20). Protection against classical upregulation of HLA-DR, DP & DQ, CD86 and IL-10 by $MV_{TNF\alpha}$ was lost in cells treated UNC-569, as was the upregulation of CD206. There was a similar, though not significant, loss of protection against classical upregulation of IL-12 p70 and IL-1β with UNC-569 . Conversely, TGFβ secretion was independent of UNC-569 treatment (an experiment which was conducted both during classical activation and in naïve macrophages, due to increased secretion in the latter).

3.2.7 Efficacy of microvesicles generated by activated endothelium

Interactions between neutrophils and macrophages *in vivo* occur post transmigration through the endothelium. It was therefore desirable to compare whether microvesicles generated in response to trans-endothelial migration exerted similar control of macrophage phenotype compared to those generated in suspension with TNFα. This is especially important as microvesicles generated by TNFα in suspension have been shown to have a different proteome to those generated on endothelial monolayers[82].

In order to generate microvesicles released in response to trans-endothelial migration from neutrophils, an *in vitro* transmigration system had to be established and optimised. As serum contains large numbers of exosomes and microvesicles, and complement induces microvesicle release, serum-free transmigration was attempted, either on its own or with IL-8 under the transwell to provide a chemotactic gradient

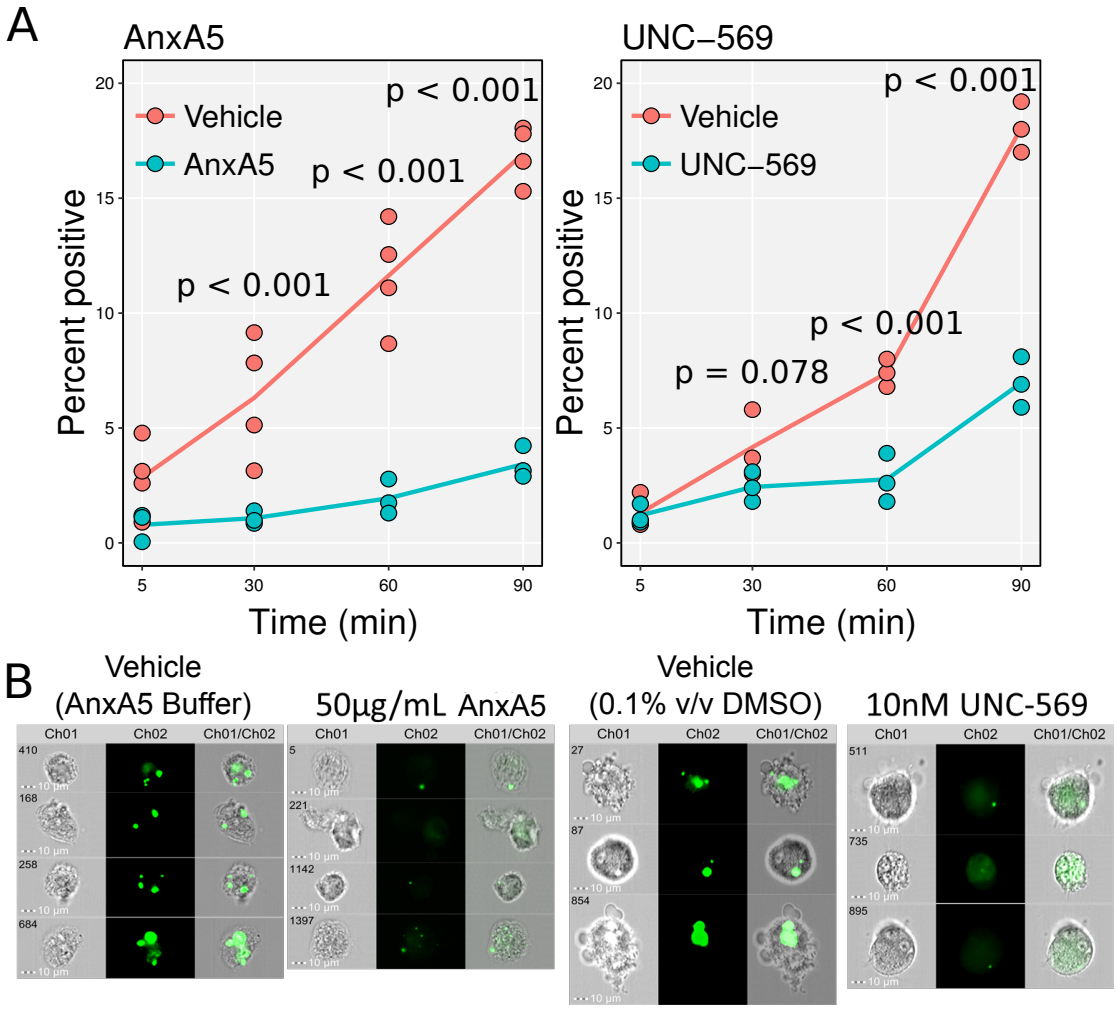

Figure 3.19: Microvesicle internalisation is phosphatidylserine and MerTK-dependent. $MV_{TNF\alpha}$ microvesicles (pooled from 6 donors) were stained with 5µM CFSE, washed by pelleting, counted, and resuspended at 5×10^6/mL in sterile-filtered PBS. Human monocyte-derived macrophage supernatant was aspirated and replaced with 1mL of $MV_{TNF\alpha}$ suspension (9×10^5 macrophages per well of 12-well plates; MV:cell ratio of 5.6:1). **A** Macrophages were treated with anxA5-blocked $MV_{TNF\alpha}$ or vehicle, and 10nM UNC-569 or vehicle. Cells were washed, detached and fixed at 5, 30, 60 and 90 minutes post microvesicle addition and acquired on the ImageStream to quantify microvesicle internalisation. AnxA5 and UNC-569 blockades were performed as two separate experiments, each with 4 biological replicates (lines connecting group means). Data analysed with two-way ANOVA and Šidak *post-hoc* tests comparing treatments at each time point. **B** Representative brightfield (Ch01), CFSE (Ch02) and overlay images for macrophages gated as $CFSE^+$.

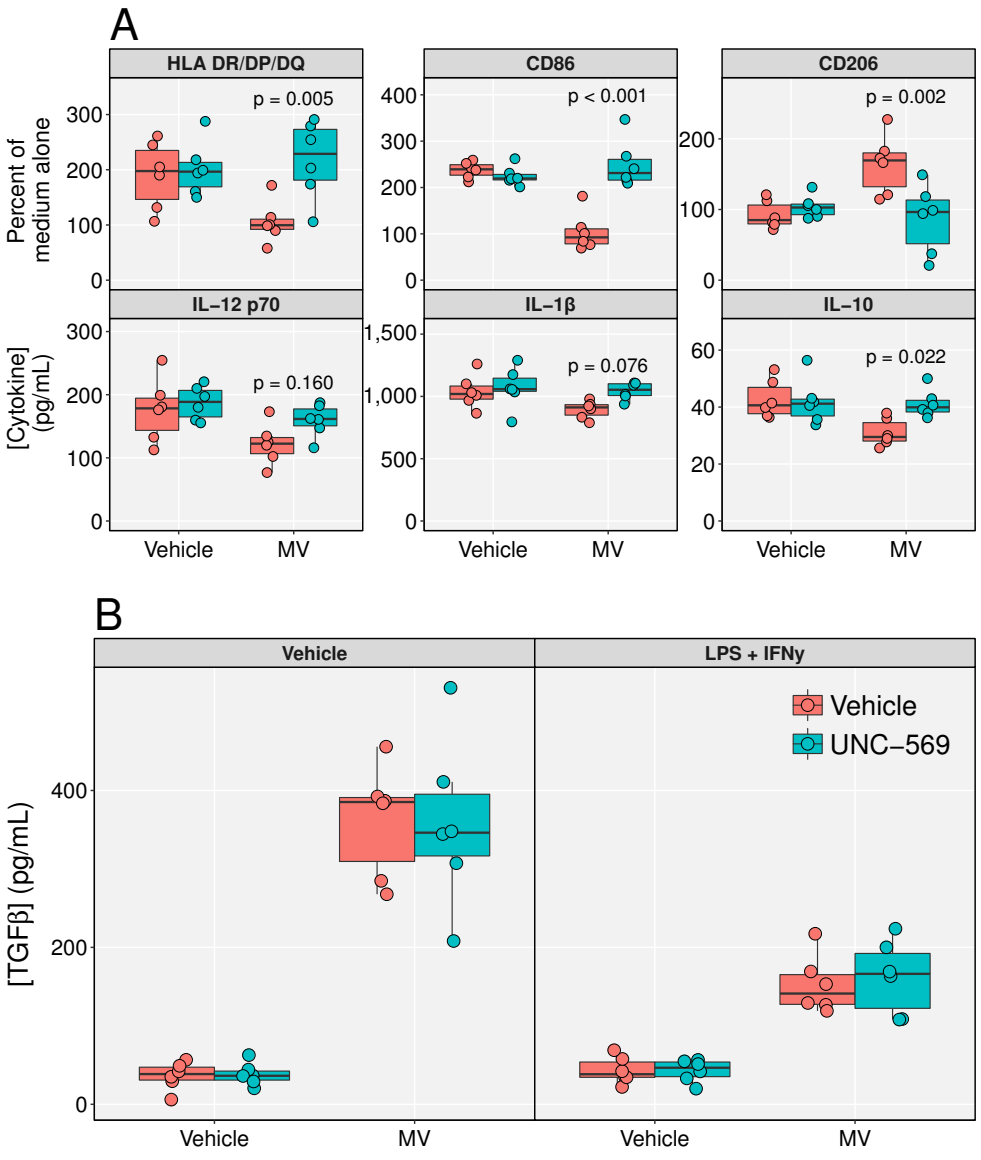

Figure 3.20: Phosphatidylserine-dependent efficacy is mediated by MerTK. Human monocyte-derived macrophages were classically activated in the presence of 3×10^6/mL $MV_{TNF\alpha}$ (pooled between 3 donors) or vehicle, and with 10nM UNC-569 (a small molecule inhibitor of MerTK) or vehicle for 24 hours. Supernatants were collected and levels of **A** IL-12p70, IL-1β, IL-10 and **B** TGFβ-1 were quantified using a Cytometric Bead Array. Cells were detached, stained for HLA-DR, DP & DQ, CD86 and CD206 expression and analysed by flow cytometry. Data are median fluorescence as a percentage of untreated cells for surface proteins and absolute concentration for cytokines. Individual biological replicates are shown. Data analysed with separate two-way (three-way for TGFβ-1) ANOVA with Šidák *post-hoc* tests for each antigen.

(Figure 3.21). The yield of transmigrated cells after 90 minutes was poor under both conditions but was ~2-fold greater in the presence of IL-8. To test whether serum could improve the yield of transmigrated cells, the experiment was repeated in the presence of 10% v/v extracellular vesicle-depleted FBS. Although there was no change in the percentage of cells between serum-free and 10% FBS in the absence of IL-8, the presence of serum allowed the neutrophils to chemotax with considerably more efficiency towards the IL-8 (~2.5-fold more than IL-8 alone). When comparing the total number of microvesicles under the transwell post transmigration, there was a significant effect of IL-8 treatment on the number of microvesicles, but the presence of serum had a limited and non-significant effect.

Immunophenotyping the microvesicles below the transwell at 90 minutes in the serum and IL-8-treated wells showed that 78% ± 9.3 were CD66b$^+$, 19% ± 3.4 were CD146$^+$ and 3% negative for both (n = 3, mean ± standard deviation). Above the transwell the microvesicles were 89% ± 4.9 CD66b$^+$, 10.2% ± 2.1 CD146$^+$ and 0.8% negative for both. The proportion of neutrophil-derived microvesicles under the transwell treated with IL-8 in the absence of serum was only 67% ± 7.8, where CD146$^+$ microvesicles made up 31%.

Although a mixed population of neutrophil and endothelial cell vesicles, microvesicles collected from above (MV_{Pre}) and below (MV_{Post}) the transwell after 90 minutes of transmigration were compared to $MV_{TNF\alpha}$ for their ability to affect macrophage phenotype (Figure 3.22). Macrophages were treated with LPS and IFNγ as before, alone or in the presence of 3×10^6/mL $MV_{TNF\alpha}$, MV_{Pre} or MV_{Post} for 24 hours. All three microvesicle populations reduced HLA-DR, DP & DQ and CD86 and increased CD206 expression to a similar degree with no significant differences between the three.

3.2.8 Arthritis-relevant stimuli induce vesicle release

To test whether more arthritis-relevant stimuli induced microvesicle release, and whether these microvesicles were enriched in the pro-resolving mediator anxA1 (as has been previously reported[36]), isolated neutrophils were treated with RPMI alone, TNFα (as a positive control), 1 in 10 rheumatoid arthritis patient or osteoarthritis patient synovial fluid (made microvesicle-free by centrifuging at 20,000$\times g$ as per Section 1.3) for 20 minutes, or transmigrated in the presence of 10% v/v vesicle-free serum (generated as per Section 2.4.2) towards IL-8 for 90 minutes. Microvesicles were isolated, immunolabelled for anxA1 and acquired on the ImageStream (Figure 3.23). All stimuli induced the release of similar numbers of microvesicles per neutrophil and higher percentage of anxA1$^+$ microvesicles compared to control. TNFα and transmigration-induced microvesicles were similarly enriched in anxA1 (16% ± 2.8

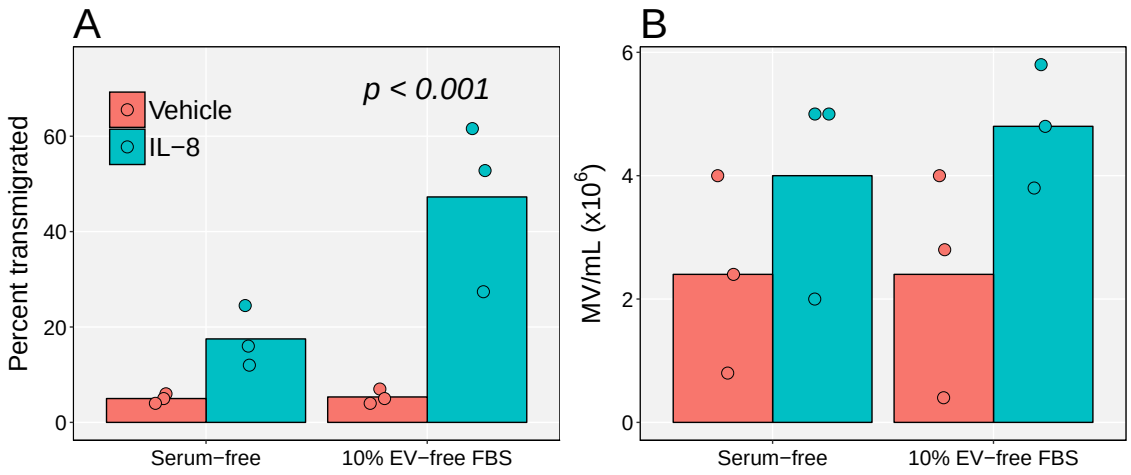

Figure 3.21: Optimisation of *in vitro* neutrophil transmigration. Isolated human neutrophils were seeded onto HUVEC-coated 3µm-pore, 6-well transwells at 3×10^6/well, after 4 hours of HUVEC stimulation with 50ng/mL TNFα. Neutrophils were allowed to transmigrate for 90 minutes at 37°C with or without 10 % v/v extracellular vesicle-depleted FBS (in PBS), and with or without 50ng/mL IL-8 stimulation. Neutrophils and total microvesicles were enumerated. **A** the percentage of neutrophils that transmigrated and **B** the concentration of total microvesicles under the transwell after transmigration. Individual biological replicates are shown with bars at group means. Data analysed with separate two-way ANOVA and Šidak *post-hoc* tests for each dependent variable.

and 17.5% ± 5.1, respectively; mean ± standard deviation), while rheumatoid and osteoarthritis synovial fluid-induced microvesicles were the most positive (26% ± 2.8 and 30% ± 5.2, respectively).

3.2.9 Induction of TGFβ release by $MV_{TNF\alpha}$ is anxA1-dependent

While most of the phenotypic effects of $MV_{TNF\alpha}$ studied appeared PtdSer and MerTK-dependent, the mechanism for the induction of TGFβ was still not described. As activated neutrophil microvesicles were enriched in the pro-resolution mediator anxA1 and that this has been shown to contribute to vesicle-induced TGFβ release from chondrocytes[3], the role this protein may have in this mechanism was tested. Human monocyte-derived macrophages were treated with 3×10^6/mL $MV_{TNF\alpha}$, MV_{RA} or MV_{OA} in the presence of a neutralising anti-anxA1 antibody or a mIgG1 control for 24 hours (Figure 3.24). Quantification of TGFβ concentration in the supernatants showed potent TGFβ release above control in all microvesicle-treated samples treated with the isotype control, but ~1.71-fold reduction in samples treated with the anti-anxA1 antibody.

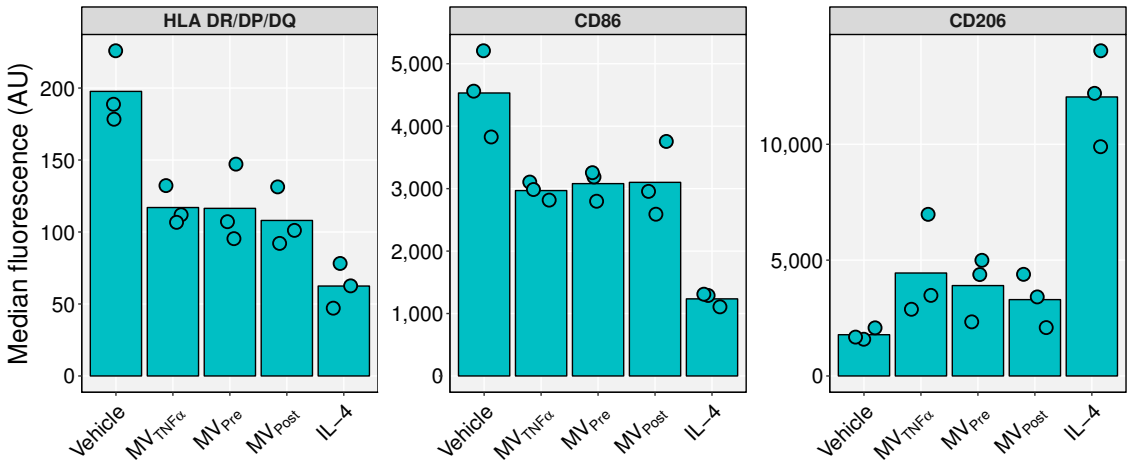

Figure 3.22: Transmigration-induced microvesicles have similar efficacy to $MV_{TNF\alpha}$. Human monocyte-derived macrophages were classically activated alone or in combination with $3{\times}10^6$/mL $MV_{TNF\alpha}$, MV_{Post} or MV_{Pre} (each pooled between 3 donors) for 24 hours. Alternatively activated macrophages were used as a positive control. Cells were washed, detached, stained for HLA-DR, DP & DQ, CD86 and CD206 expression and analysed using flow cytometry. Data are median fluorescence intensity of individual biological replicates with a bars at group means. Data analysed with separate one-way ANOVA and Tukey *post-hoc* tests for each antigen.

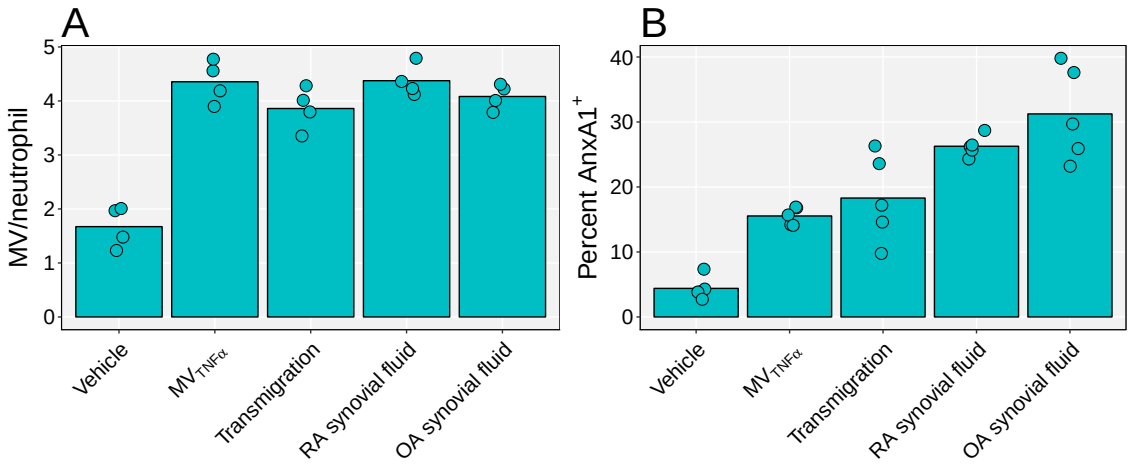

Figure 3.23: Activated neutrophils release large numbers of anxA1$^+$ microvesicles. $2{\times}10^6$ human neutrophils were isolated and stimulated with 50ng/mL TNFα, by transmigration through an activated HUVEC monolayer, or pooled microvesicle-free synovial fluid diluted 1 in 10 from 3 rheumatoid arthritis or 3 osteoarthritis patients, for 20 minutes at 37°C. Samples were stained with BODIPY maleimide and an antibody against anxA1 and analysed on the ImageStream. **A** The number of microvesicles per neutrophil and **B** the % of microvesicles positive for anxA1 are shown for each biological replicate with bars at group means. Data analysed with separate one-way ANOVA with Tukey *post-hoc* tests for each dependent variable.

3.2.10 Classically-activated macrophages express higher levels of FPR2

Expression of the pro-resolving, cognate receptor for anxA1, FPR2, was confirmed and compared across macrophage phenotypes (Figure 3.25). Classically-activated macrophages expressed higher levels of FPR2 than alternatively-activated of naïve macrophages, both in total (in fixed and permeabilised cells) and at the plasma membrane. While all three phenotypes were comparable in the percentage of cells positive for FPR2 in total, twice as many classically-activated macrophages were positive at the plasma membrane, with levels matching their total expression.

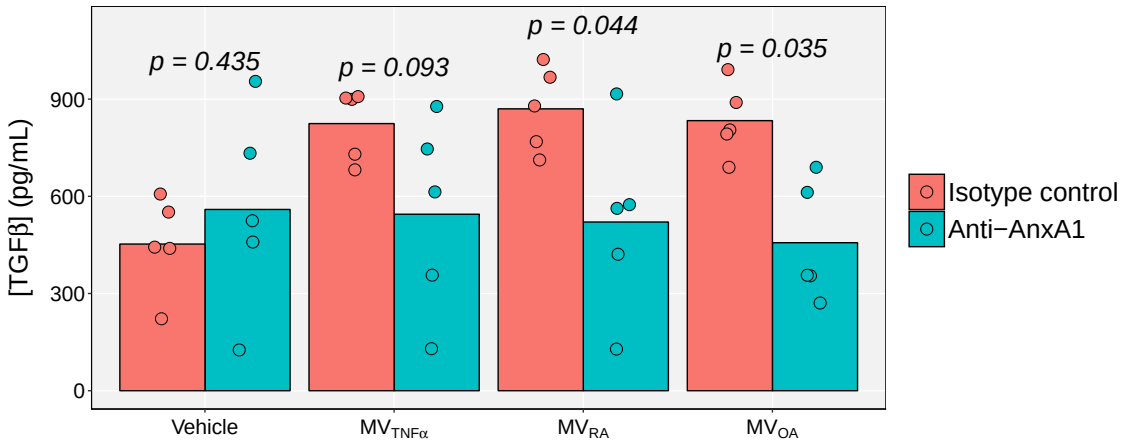

Figure 3.24: Neutrophil microvesicle-induced TGFβ release is anxA1-dependent. Human monocyte-derived macrophages were treated with vehicle, $MV_{TNF\alpha}$, MV_{RA} or MV_{OA} (at $3{\times}10^6$/mL each) in the presence of 10µg/mL neutralising-anxA1 antibody, or 10µg/mL of an isotype-matched control antibody, for 24 hours. Supernatants were collected and analysed for TGFβ quantification by Cytometric Bead Array. Individual biological replicates are shown with bars at group means. Data analysed with two-way ANOVA and Šidak *post-hoc* tests.

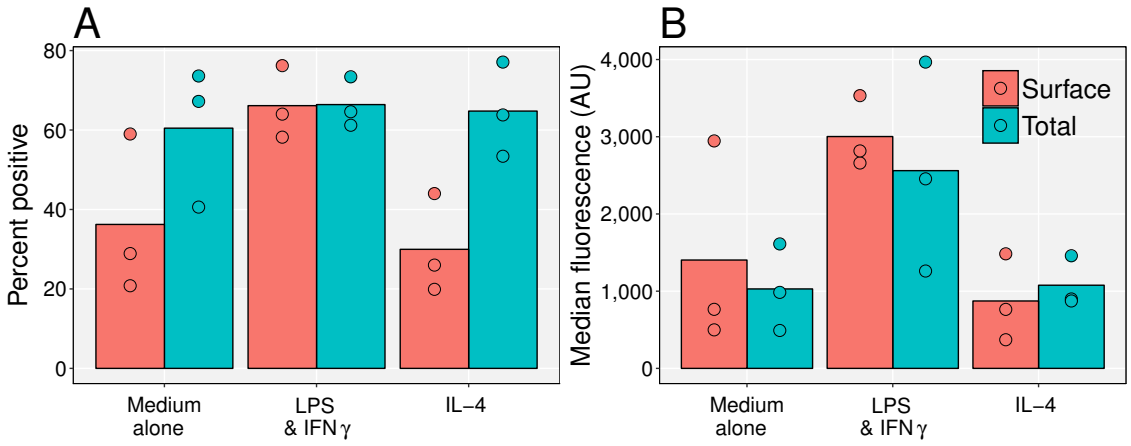

Figure 3.25: Total and surface expression of FPR2 across macrophage phenotypes. Human monocyte-derived macrophages were classically activated, alternatively activated or left naïve for 24 hours, detached, and stained with an antibody against FPR2 either with or without prior fixation and permeabilisation. Cells were analysed by flow cytometry and data are **A** percentage of cells positive for FPR2 and **B** median fluorescence for each donor, with bars at group means.

3.3 Interactions between macrophages, and chondrocytes and fibroblasts

While the data thus far demonstrate phenotypic control of macrophage activation by $MV_{TNF\alpha}$, it was important to determine whether this translates into a functional effect. The ability to modulate chondrocyte and fibroblast function by macrophages was chosen as an arthritis-specific functional readout, as these are two ways in which macrophages may drive inflammation and joint destruction[236].

3.3.1 Interaction with chondrocytes

To explore the role macrophage phenotype may play in the deposition of sulphated glycosaminoglycans by chondrocytes, the C28/I2 3D micromass culture system was employed. This system, developed and validated in detail by Greco *et al.*[241], involves seeding a high density, 3D colony of C28/I2 cells and inducing chondrocytogenesis with serum-starvation and insulin, from which point the cultures begin to deposit cartilage-associated glycosaminoglycans. To validate this system for the present project, micromasses were first treated with 10ng/mL TGFβ or vehicle alone and the amount of glycans deposited after 24 hours was quantified with alcian blue and normalised to DNA content, to control for variable numbers of cells per micromass (Figure 3.26). Micromasses treated with TGFβ deposited ~1.8-fold more glycans than vehicle-treated.

Macrophages within the rheumatic synovium are known to contribute to cartilage degradation[242]. To test whether soluble mediators released from different macrophage phenotypes could differentially control cartilage deposition/degradation, micromasses were treated for 24 hours with the conditioned medium of macrophages treated with complete medium alone, IFNγ, IL-4, rheumatoid or osteoarthritis synovial fluid diluted 1 in 100 (made microvesicle-free by centrifuging at 20,000×g as per Section 1.3; Figure 3.27). To control for the direct effects of these stimuli on the chondrocytes, micromasses were also treated with identical "conditioned" medium from cell-free cultures. IFNγ, IL-4 and rheumatoid synovial fluid on their own did not alter glycan deposition/degradation, whereas osteoarthritis synovial fluid reduced these levels ($p = 0.059$). Although there was a trend for a decrease in glycan levels in micromasses cultured with medium, IFNγ and rheumatoid synovial fluid-treated macrophage-conditioned medium, these differences were not significant. The only conditioned-medium to increase glycan levels above that of the mediator alone was from IL-4-treated macrophages.

To determine whether conditioned-medium from microvesicle-treated macrophages could affect glycosaminoglycan deposition by chondrocytes, and whether this was dependent on anxA1, macrophages were treated with complete medium alone, $MV_{TNF\alpha}$, MV_{RA} or MV_{OA} for 24 hours in the presence of an anxA1-neutralising antibody or mIgG1 (Figure 3.28). Conditioned-medium from all microvesicle-treated macrophage cultures increased the amount of glycans present by ~2-fold, an effect lost in the presence of the anti-anxA1 antibody.

A similar experiment was performed to test the hypothesis that this cartilage-protection conferred by the microvesicles to the macrophages was a result of anxA1-induced TGFβ release (Figure 3.29). Macrophages were treated with complete medium or with $MV_{TNF\alpha}$, in the presence of the neutralising anxA1 antibody or the mIgG1 control for 24 hours. These supernatants were incubated with beads coated with an anti-TGFβ antibody, or control beads for 2 hours in order to adsorb soluble TGFβ. After depletion of TGFβ and microvesicles by centrifugation, micromasses were treated with the supernatants for a further 24 hours. In the absence of microvesicles, there was no effect of the anti-anxA1 antibody, and a small but non-significant decrease in glycan deposition with TGFβ-depletion. In samples treated with $MV_{TNF\alpha}$, there was a significant increase in glycans compared to vehicle in the control group; an effect completely lost upon blockade of anxA1 ($p = 0.049$) or depletion of TGFβ ($p = 0.006$).

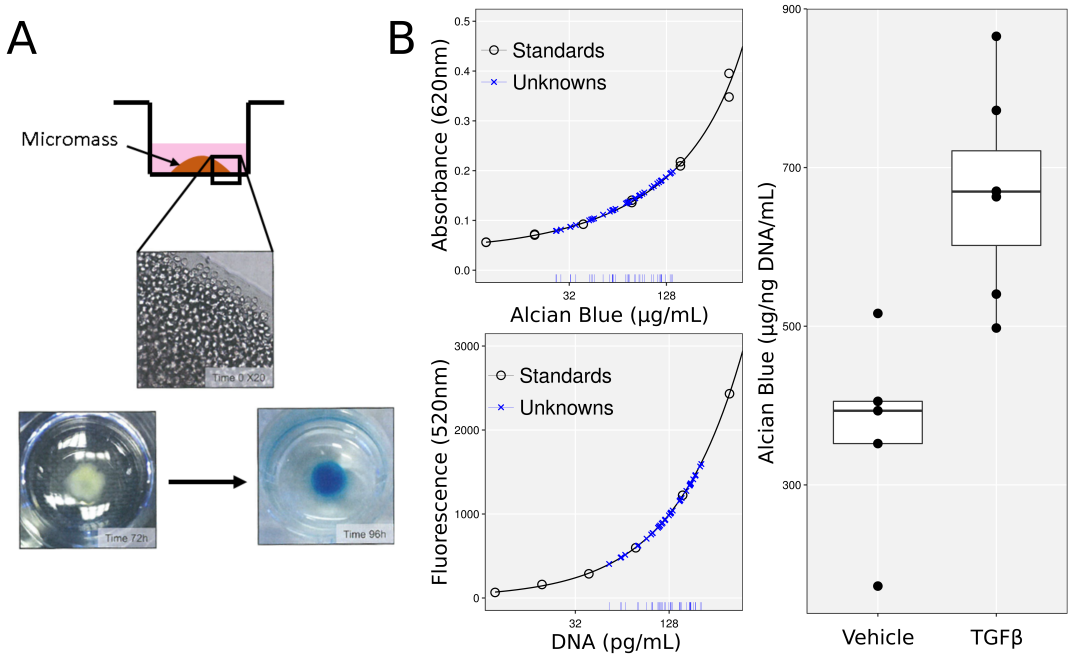

Figure 3.26: The C28\I2 chondrocyte model of cartilage deposition. A Graphical scheme of the C28/I2 chondrocyte micromass culture system. Photographs show the edge of the micromass at day 0 (x20) and the micromass pre and post alcian blue staining (at 72 and 96 hours, respectively). **B** Micromasses were treated with vehicle or 10ng/mL TGFβ for 24 hours before quantification of glycosaminoglycans (by alcian blue staining and extraction) relative to DNA content/mL. DNA and alcian blue standard curves with standards and interpolated unknowns are shown, as well as the final normalisation of technical replicates treated with vehicle (n = 5) and TGFβ (n = 6).

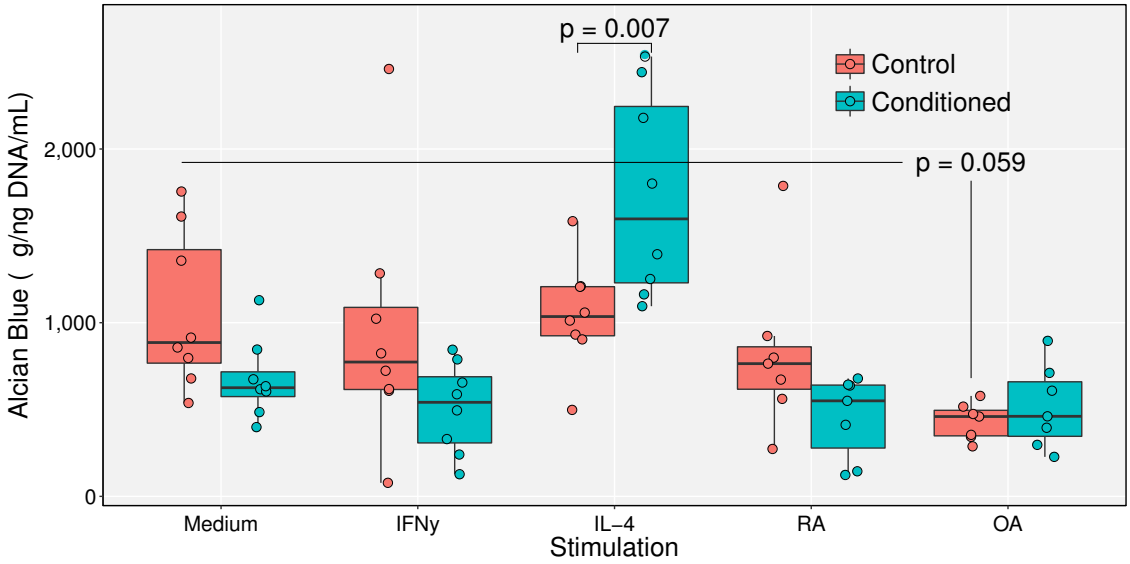

Figure 3.27: Polarised macrophage-conditioned media modulates cartilage deposition. Human monocyte-derived macrophages or wells containing no cells were treated with medium alone, 50ng/mL IFNγ, 50ng/mL IL-4, rheumatoid arthritis synovial fluid or osteoarthritis synovial fluid (both pooled from 3 donors, diluted 1 in 100 and microvesicle-free) for 24 hours. Supernatants were collected, made cell and microvesicle-free and used to treat C28/I2 chondrocyte micromasses for a further 24 hours. Glycosaminoglycan quantification relative to DNA content are shown for each biological replicate (n = 7/8). Data analysed with two-way ANOVA with Holm-Šidák *post-hoc* tests.

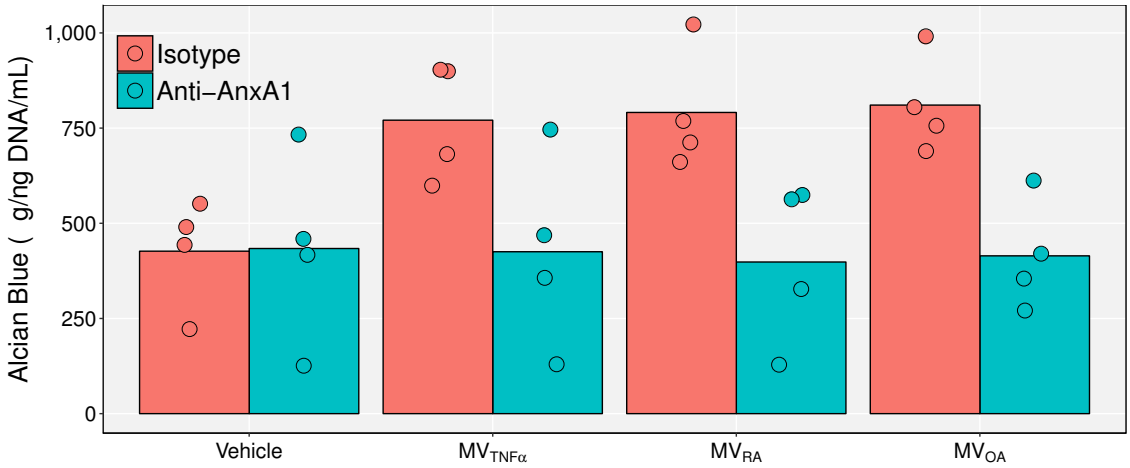

Figure 3.28: AnxA1^{+} microvesicles stimulate release of chondrogenerative factor(s). Human monocyte-derived macrophages were treated with vehicle, or 3×10^{6}/mL $MV_{TNF\alpha}$, MV_{RA} or MV_{OA} in the presence of 10µg/mL neutralising-anxA1 antibody or 10µg/mL isotype-matched control antibody for 24 hours. Supernatants were collected, made cell and microvesicle-free and used to treat C28/I2 chondrocyte micromasses for a further 24 hours. Glycosaminoglycan quantification relative to DNA content are shown for each biological replicate. Data analysed with two-way ANOVA with Šidák *post-hoc* tests.

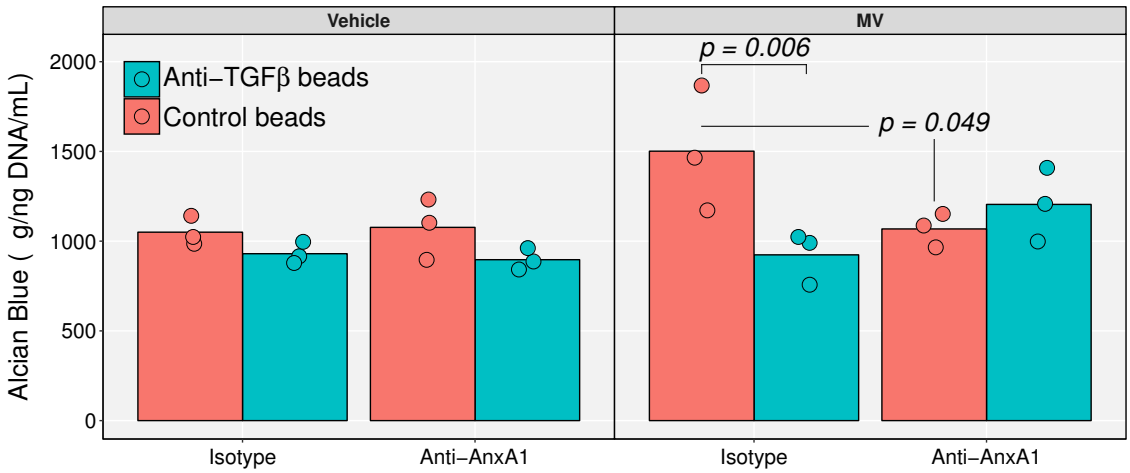

Figure 3.29: TGFβ is the chondrogenerative factor induced by anxA1$^+$ microvesicles. Human monocyte-derived macrophages were treated with vehicle, or $3{\times}10^6$/mL $MV_{TNF\alpha}$ in the presence of 10µg/mL neutralising-anxA1 antibody or 10µg/mL isotype-matched control antibody for 24 hours. Supernatants were collected, made cell-free and incubated with beads coated with an anti-TGFβ-1 antibody (to capture soluble TGFβ-1), or an isotype-matched control for 2 hours. Supernatants were centrifuged to remove beads and microvesicles, and used to treat C28/I2 chondrocyte micromasses for a further 24 hours. Glycosaminoglycan quantification relative to DNA content are shown for each biological replicate. Data analysed with three-way ANOVA with Holm-Šidák *post-hoc* tests.

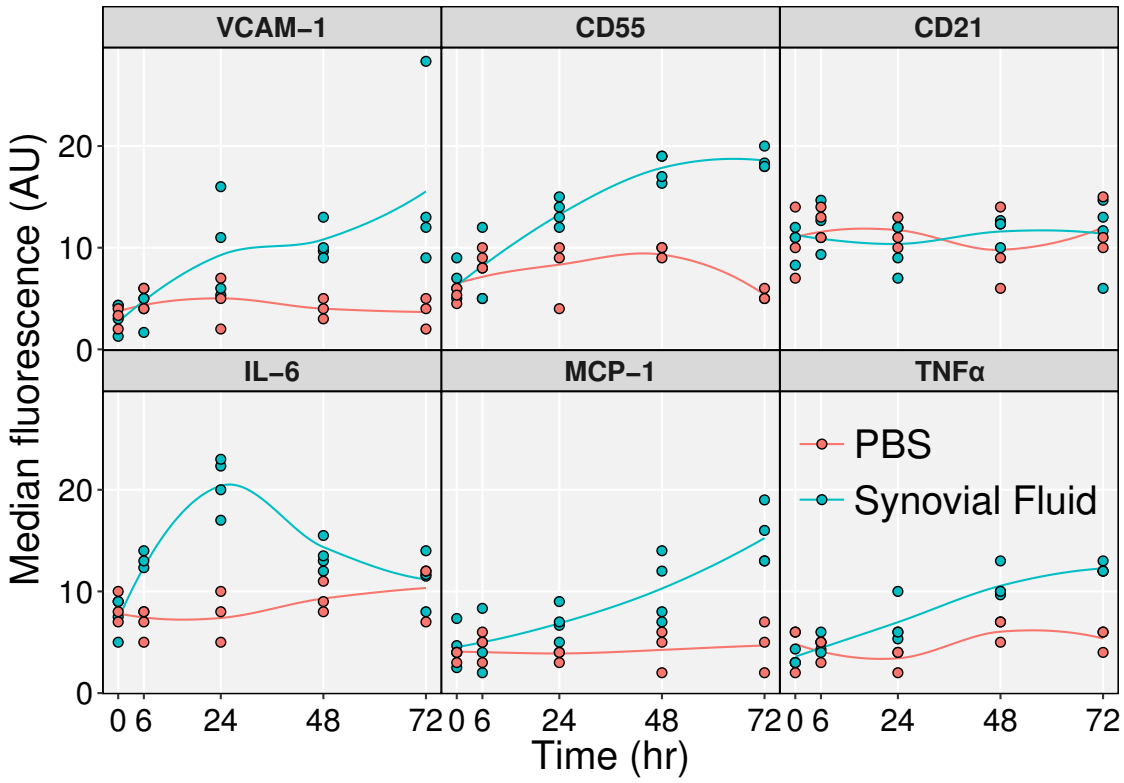

Figure 3.30: Establishing an inflammatory phenotype in synovial fibroblasts. Primary synovial fibroblasts from patients with osteoarthritis were seeded onto glass coverslips and allowed to attach overnight. Fibroblasts were then stimulated with synovial fluid pooled from 3 other rheumatoid arthritis patients for varying lengths of time. Six hours prior to fixation, fibroblasts were treated with golgi block, before fixation with 1% v/v formaldehyde, permeabilisation with triton-X 100 and antibody staining for immunofluorescence (one antigen per coverslip). Individual biological replicates shown, with LOESS fits to each group (span = 1).

3.3.2 Interaction with fibroblasts

Macrophages and synovial fibroblasts interact within the synovium to condition each other's phenotypes. To study this interaction *in vitro*, a panel of phenotypic markers had to be defined which could discriminate an inflammatory phenotype in synovial fibroblasts. Primary synovial fibroblasts were stimulated with synovial fluid from rheumatoid arthritis patients for varying lengths of time and the expression of a range of antigens reported to respond to inflammatory stimuli[243] was quantified by fluorescence microscopy (Figure 3.30). While an increase in expression could be detected in VCAM-1, CD55, IL-6, MCP-1 and TNFα after 24 hours in synovial fluid, CD21 remained unchanged. These responsive markers were therefore used as indicators of fibroblast phenotype in future experiments.

To model the close proximity of synovial macrophages and fibroblasts *in vitro*, a

co-culture system was devised where macrophages are cultured and polarised on transwell inserts, and placed on top of coverslips of fibroblasts to initiate co-culture. In determining whether, in this artificial system, monocyte-derived macrophage phenotype can condition fibroblast phenotype, classical, alternative, and naïve macrophages were co-cultured with fibroblasts for 24 hours. After quantifying the expression of fibroblast phenotypic markers by fluorescence microscopy, it was observed that VCAM-1, CD55, IL-6 and TNFα were all increased in fibroblasts cultured with classically activated macrophages compared to those cultured with naïve and alternatively activated macrophages (whose expression level was comparable; Figure 3.31 A). MCP-1 expression was highest in fibroblasts cultured with alternatively-activated macrophages, followed by those cultured with classically-activated macrophages, and finally those with naïve macrophages.

To compare overall similarity of these three fibroblast populations across the antigens studied, and to compare which antigens best discriminated between them, data were used to construct a linear discriminant model (Figure 3.31 B & C). The first discriminant factor accounted for 84.5% of the variability between groups, primarily separating groups by their MCP-1 expression, which correlated positively with it. The second discriminant factor accounted for 15.5% of the variability between groups and primarily separates fibroblasts cultured with alternatively-activated macrophages from the other two populations, by their expression of VCAM-1, CD55, IL-6 and TNFα which all correlated negatively with it.

In order to test whether treating macrophages with $MV_{TNF\alpha}$ during classical activation affected their modulation of fibroblast phenotype, macrophages were given $MV_{TNF\alpha}$ or vehicle during classical activation, or to naïve cells, before co-culture with fibroblasts for 24 hours. For all antigens studied, co-culture with classically activated macrophages (devoid of $MV_{TNF\alpha}$ treatment) increased their expression as previously demonstrated (Figure 3.32 A). This upregulation was not induced by co-culture with macrophages given $MV_{TNF\alpha}$ during their activation, where expression levels for all antigens was comparable to when fibroblasts were cultured with naïve macrophages treated with $MV_{TNF\alpha}$.

To compare overall similarity of these four fibroblast populations across the antigens studied, and to compare which antigens best discriminated between them, data were used to construct a linear discriminant model (Figure 3.32 B & C). The first discriminant factor accounted for 99.2% of the variability between groups, primarily separating fibroblasts cultured with classically activated macrophages by all antigens, which correlated positively with it. The second discriminant factor only accounted for 0.8% of the variability between groups, primarily separating fibroblasts cultured with completely naïve macrophages, from the other three populations by their TNFα

and IL-6 expression.

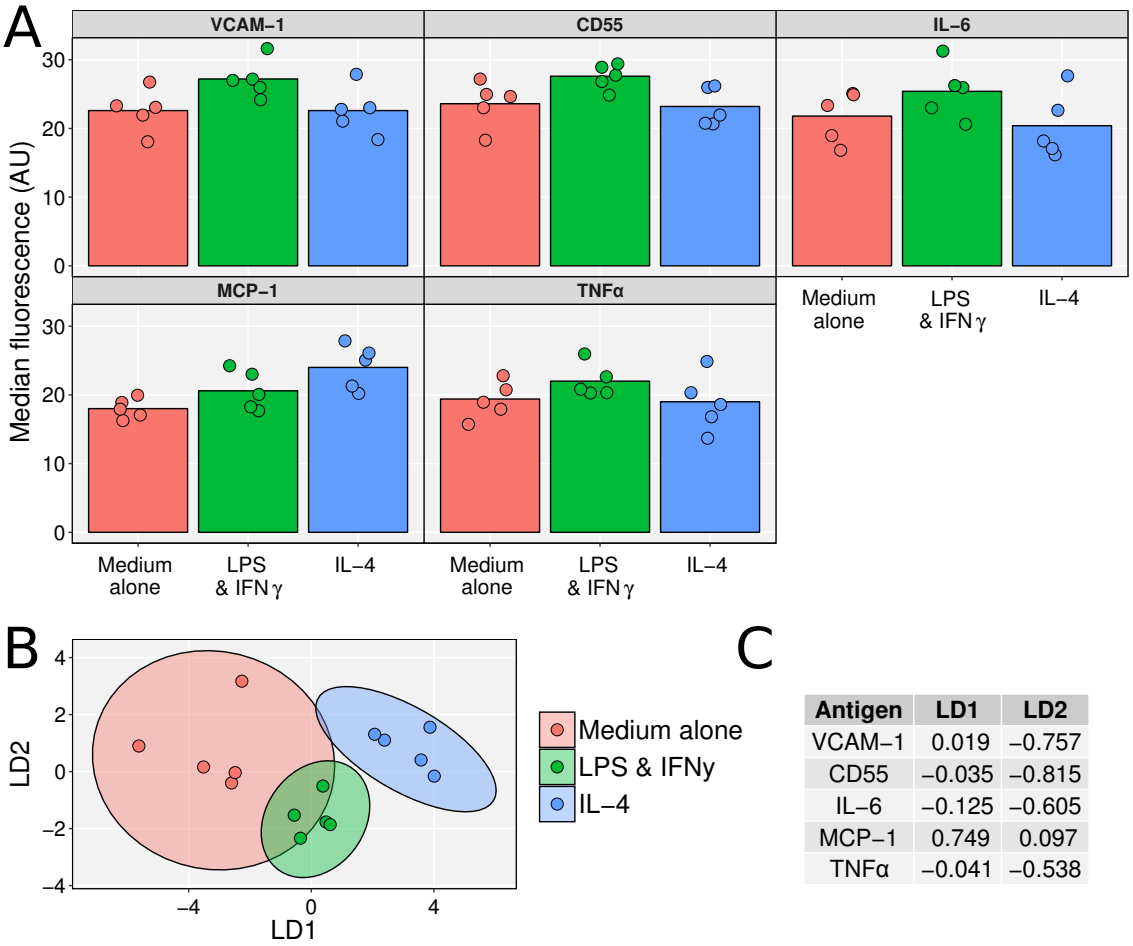

Antigen	LD1	LD2
VCAM–1	0.019	−0.757
CD55	−0.035	−0.815
IL–6	−0.125	−0.605
MCP–1	0.749	0.097
TNFα	−0.041	−0.538

Figure 3.31: Macrophage phenotype controls fibroblast phenotype in co-culture. Human monocyte-derived macrophages differentiated in 6-well transwell inserts were classically activated, alternatively activated, or left naïve for 24 hours. Macrophage transwell inserts were then washed and placed on top of primary synovial fibroblasts from osteoarthritis patients cultured on glass coverslips, and co-cultured for a further 24 hours. Six hours prior to fixation, fibroblasts were treated with golgi block, before fixation with 1% v/v formaldehyde, permeabilisation with triton X-100 and antibody staining for immunofluorescence (one antigen per coverslip). Individual biological replicates shown (one macrophage donor to one fibroblast donor) with **A** bars at group means for individual antigens, and **B** result of linear discriminant analysis with 95% confidence ellipses for each group. **C** Standardized factor loadings for both discriminant factors are tabulated.

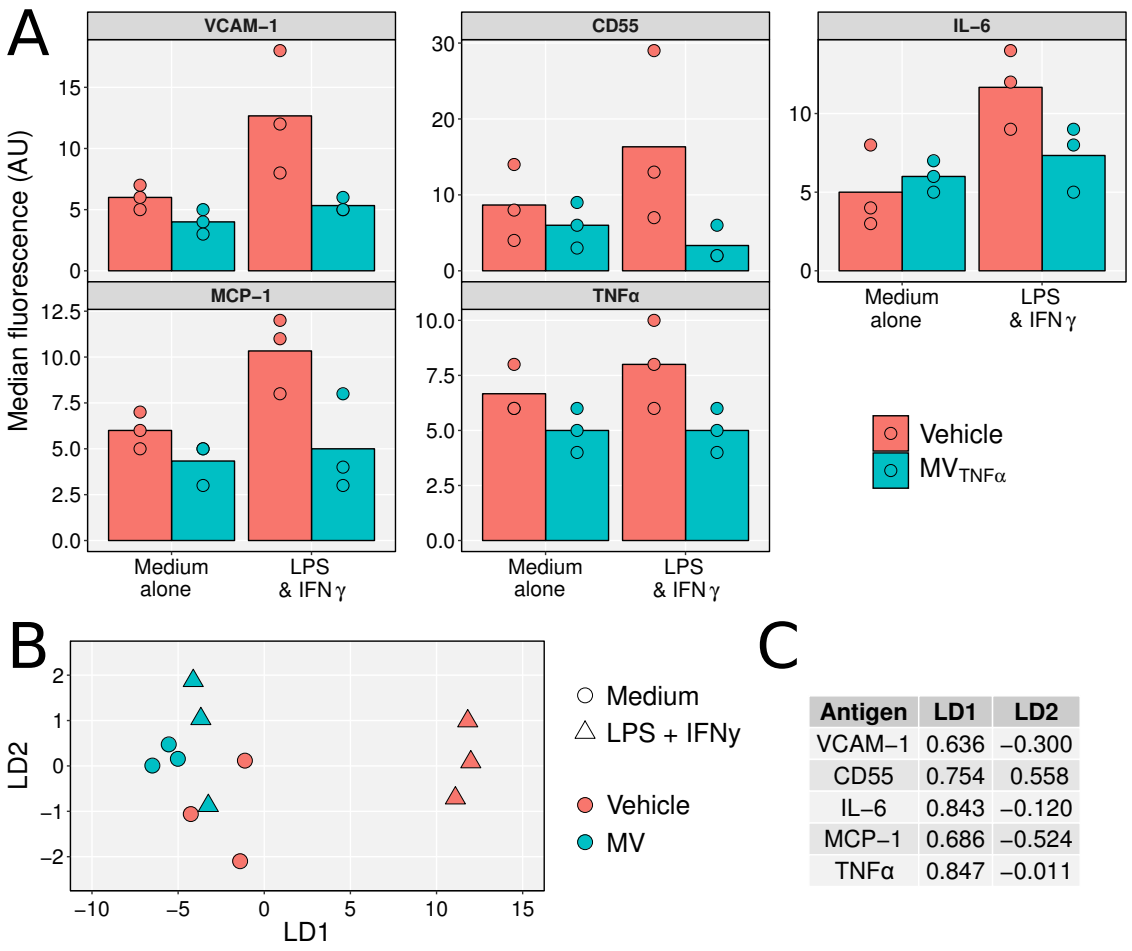

Antigen	LD1	LD2
VCAM−1	0.636	−0.300
CD55	0.754	0.558
IL−6	0.843	−0.120
MCP−1	0.686	−0.524
TNFα	0.847	−0.011

Figure 3.32: MV$_{TNFα}$ modulate macrophage control of fibroblast phenotype. Human monocyte-derived macrophages differentiated in 6-well transwell inserts were classically activated or left naïve for 24 hours in the presence of 3×10^6 MV$_{TNFα}$ (pooled between 3 donors) or vehicle. Macrophage transwell inserts were then washed and placed on top of primary synovial fibroblasts from osteoarthritis patients cultured on glass coverslips, and co-cultured for a further 24 hours. Six hours prior to fixation, fibroblasts were treated with golgi block, before fixation with 1% v/v formaldehyde, permeabilisation with triton X-100 and antibody staining for immunofluorescence (one antigen per coverslip). Individual biological replicates shown (one macrophage donor to one fibroblast donor) with **A** bars at group means for individual antigens, and **B** result of linear discriminant analysis with 95% confidence ellipses for each group. **C** Standardized factor loadings for both discriminant factors are tabulated.

3.4 Microvesicles modulate macrophage phenotype *in vivo*

3.4.1 Zymosan-induced peritonitis

While $MV_{TNF\alpha}$-mediated control of macrophage phenotype *in vitro* could be demonstrated, it was important to confirm whether the same phenomenon could be observed in a living system. Zymosan-induced peritonitis was chosen as an initial model to test vesicles *in vivo* as it is a simple model of sterile acute inflammation with a defined compartment within which treatments can be administered and cells (particularly macrophages) can be extracted[244]. Following intraperitoneal injection with 1mg zymosan (a glucan polysaccharide component of fungal cell walls), tissue resident peritoneal macrophages initiate an innate immune response, culminating in the recruitment of neutrophils and monocytes to the cavity[245]. The peak of monocyte-derived macrophage presence in the peritoneum is at 48 hours, at which point the peritoneum can be lavaged and the macrophages immunophenotyped[244].

To maximise the likelihood of observing efficacy of microvesicles in this model, mice were randomised to a range of doses of human $MV_{TNF\alpha}$ (or vehicle) injected intraperitoneally 24 hours post zymosan, before lavage 24 hours later (Figure 3.33). The cells were stained for F4/80, MHCII, CD86 and CD206 and acquired on a flow cytometer. Singlet, $F4/80^+$ cells' MHCII and CD86 expression decreased with $MV_{TNF\alpha}$ dose, whereas CD206 increased with dose, although the absolute changes in median fluorescence were relatively small. No adverse effects of injecting the mice with human material was observed.

To repeat the model but with replicate treatments, the same model was performed except that mice were randomised to receive intraperitoneal injection of either vehicle, or 2×10^7 $MV_{TNF\alpha}$ (the maximum number of vesicles which could realistically be generated for the experiment, which still showed efficacy in Figure 3.33). As shown in Figure 3.34, in support of the previous peritonitis data and the *in vitro* data generated thus far, macrophages isolated from mice injected with $MV_{TNF\alpha}$ expressed lower MHCII and CD86, and higher CD206. The cell-free lavage fluid was sent to Labospace for cytokine profiling by luminex. While there were no differences in KC (CXCL1), IL-1β or TNFα expression (the latter of which was mostly below the limit of detection), mice injected with $MV_{TNF\alpha}$ expressed lower levels of MCP-1 ($p = 0.009$) and increased expression of TGFβ ($p = 0.006$). The was a non-significant decrease in IL-6 expression in mice injected with $MV_{TNF\alpha}$ ($p = 0.109$).

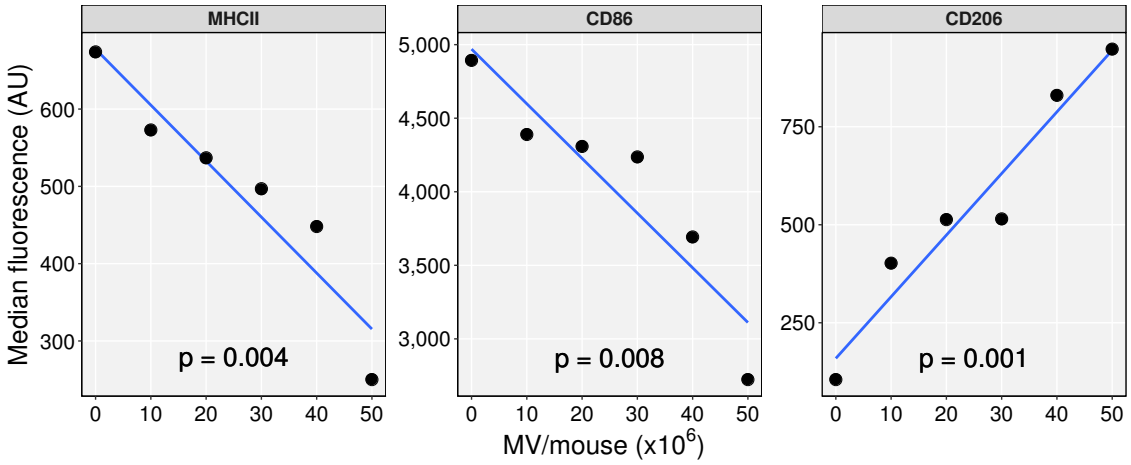

Figure 3.33: *In vivo* titration of $MV_{TNF\alpha}$ on macrophage phenotype. Six, 10 week-old C57BL/6 mice were injected with 500µL of 2mg/mL zymosan intraperitoneally. After 24 hours, mice were randomised to a range of doses of human $MV_{TNF\alpha}$ (pooled between 6 donors) injected intraperitoneally in 500µL. A further 24 hours later, mice were culled and a peritoneal lavage performed with 2mM EDTA. Cells were stained with antibodies against F4/80, MHCII, CD86 and CD206, and analysed by flow cytometry. Data are median fluorescence of each antigen of $F4/80^+$ cells, for each mouse. Data analysed with linear regression for each antigen, where least square lines are shown. Both treatment and analysis were blinded.

3.4.2 K/BxN arthritis

While the data from both peritonitis models supported the data generated *in vitro*, the absolute effect sizes of vesicle treatment were small, possibly due to the large surface area and volume of the peritoneal cavity relative to the number of vesicles administered (whose production is rate limiting). Therefore, to examine the effects of $MV_{TNF\alpha}$ in a smaller compartment relative to their number, and in a model which is more relevant to arthritis, the K/BxN model of acute arthritis was chosen.

Mice injected with K/BxN serum on days 0 and 2, develop an acute, neutrophil-driven model of systemic and symmetrical arthritis. As the model is symmetrical, intra-articular injection of an experimental agent can be given into one joint, and its control treatment administered to the contralateral joint. To maximise the number of cells recovered, the ankle synovia were chosen as these undergo the greatest swelling and cell infiltration during the model. 24 hours after the second K/BxN serum injection, mice were randomised to receive intra-articular injection of 3×10^6 $MV_{TNF\alpha}$ in one of their ankles, and vehicle in the other. After a further 24 hours, all soft tissue was removed from the ankle, the synovium was digested and the cells immunophenotyped for flow cytometry (Figure 3.35). In support of data presented thus far, singlet $CD45^+$, $CD11b^+$, $F4/80^+$ macrophages isolated from ankles which received $MV_{TNF\alpha}$ expressed lower (but not significantly) MHCII ($p = 0.006$) and

CD86 ($p = 0.117$), and higher CD206 ($p = 0.001$) compared to their contralateral controls. Antibodies raised against CD90, CD55 and VCAM-1 were also included in the panel to immunophenotype synovial fibroblasts ($CD45^-$, $CD11b^-$, $CD90^+$), but not enough could be acquired from individual joints.

3.5 $MV_{TNF\alpha}$ from RA patients are protective

3.5.1 RA patient neutrophils release anxA1$^+$ microvesicles

Microvesicles with protective properties could represent a novel form of autologous therapy. If such vesicles can be generated from a patient's cells, isolated, and administered, they may achieve efficacy with minimal side effects (being of the patient's own tissue) and represent the ultimate personalised therapy. To consider this as an application for $MV_{TNF\alpha}$ in the treatment of rheumatoid arthritis, it was first important to address the question of whether blood neutrophils from rheumatoid arthritis patients produce microvesicles in response to TNFα, and if so, whether these $MV_{TNF\alpha}$ are protective.

To address the first question, blood neutrophils were isolated from 5 rheumatoid arthritis patients and stimulated with 50ng/mL TNFα or vehicle for 20 minutes at 37°C. Microvesicles were isolated, labelled with BODIPY maleimide and a primary-secondary antibody combination to label anxA1, and acquired on the ImageStream (Figure 3.36). TNFα induced a 2.42-fold mean increase in vesicle release over vehicle ($p = 0.044$) and a 1.67-fold mean increase in anxA1 expression ($p = 0.049$). While the fold change in vesicle release was comparable to data observed in healthy controls (Figure 3.11), the fold increase in anxA1 expression was smaller, owing to the higher expression of anxA1 at baseline.

The number of microvesicles isolated per starting neutrophil was plotted and compared between healthy controls and rheumatoid arthritis patients (Figure 3.37). Overall, the number of vesicles recovered per cell increased with the starting number of neutrophils. While the relationship appears shallower for preparations from rheumatoid arthritis patients, it was difficult to isolate large enough numbers of neutrophils to make a like-for-like comparison, and there are too few data to conclude.

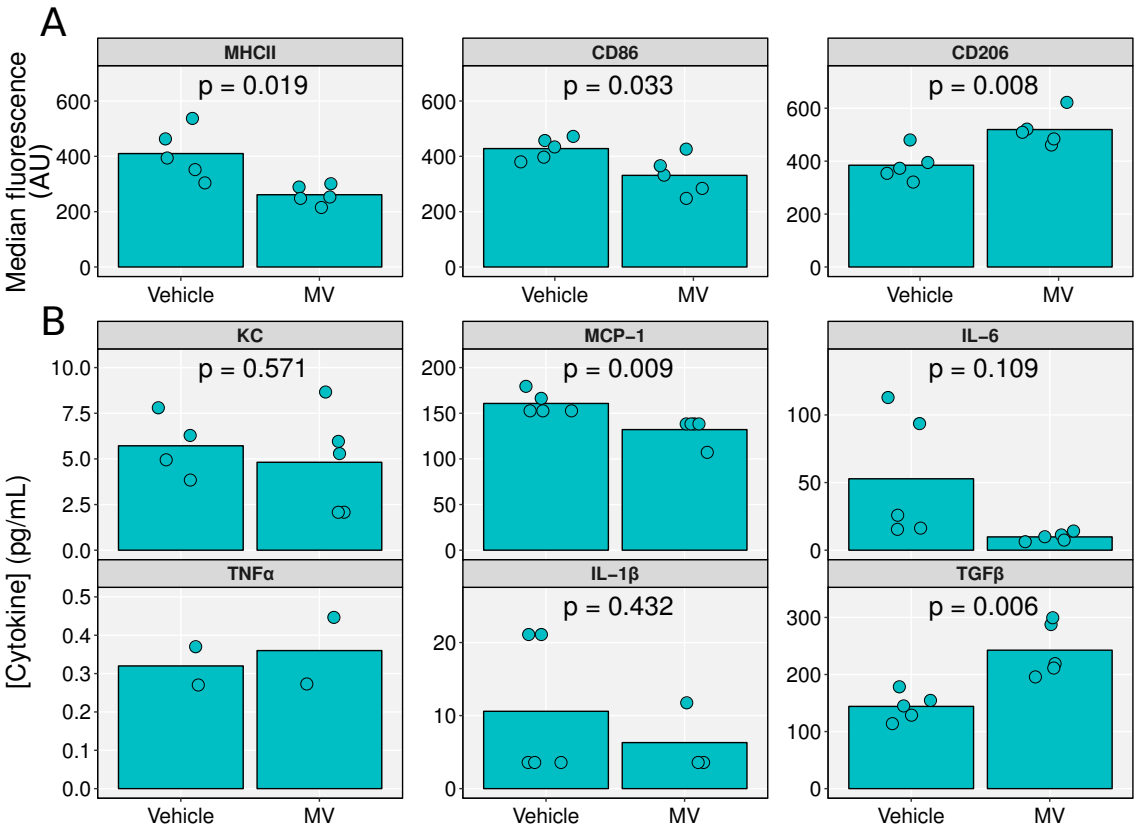

Figure 3.34: Confirmatory, two group peritonitis. Ten week-old C57BL/6 mice were injected with 500µL of 2mg/mL zymosan intraperitoneally. After 24 hours, mice were randomised to intraperitoneal injection of 2×10^7 human $MV_{TNF\alpha}$ (pooled between 6 donors) or vehicle alone (both 500µL). A further 24 hours later, mice were culled and a peritoneal lavage performed with 2mM EDTA. **A** Cells were stained with antibodies against F4/80, MHCII, CD86 and CD206, and analysed by flow cytometry. **B** Cell-free lavage fluid was sent to Labospace for Luminex cytokine profiling. Data are median fluorescence of each surface antigen of singlet $F4/80^+$ cells, or absolute concentration of cytokine, for each mouse. Data analysed with separate two-tailed t tests for each antigen, with bars at group means. Both treatment and analysis were blinded.

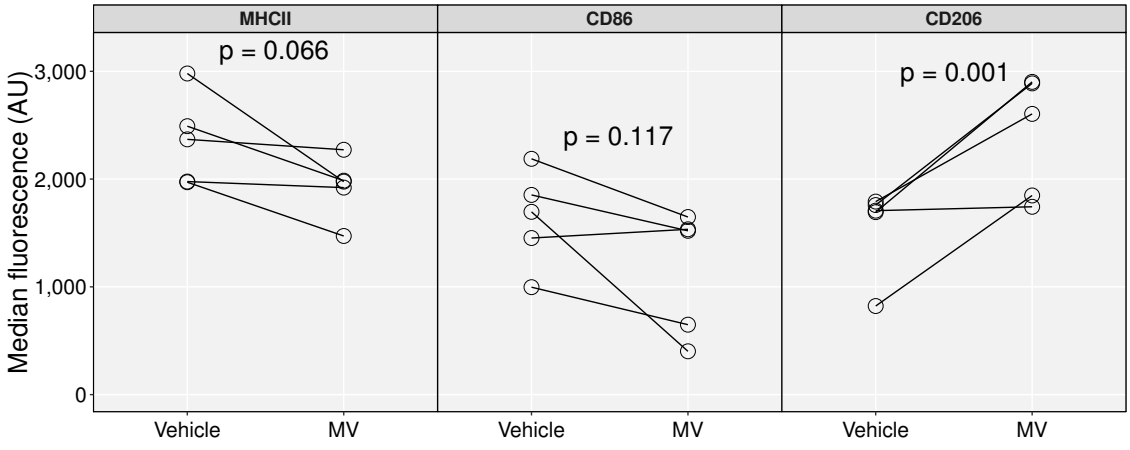

Figure 3.35: Intra-articular efficacy of $MV_{TNF\alpha}$ in K/BxN arthritis. Four, 8 week-old C57BL/6 mice were injected with 200µL of K/BxN serum, diluted 1 in 2 with PBS, intraperitoneally on days 0 and 2. After 24 hours, mice were given intra-articular (ankle) injections of 3×10^6 human $MV_{TNF\alpha}$ (pooled between 3 donors) in one ankle, and an equal volume of PBS in the contralateral ankle (which ankle received each treatment was randomised for each mouse). After 48 hours, mice were culled, ankles were made skin and muscle-free, and digested with 0.5µg/mL collagenase D and 40 µg/mL DNAse I for 1 hour at 37°C. Cell suspensions were stained with Zombie Aqua, and antibodies against CD45, CD11b, F4/80, MHCII, CD86 and CD206, and analysed by flow cytometry. Data are median fluorescence of each antigen on $CD45^+$, $CD11b^+$, $F4/80^+$ macrophages for each mouse. Lines connect ankles within each mouse. Data analysed with paired, two-tailed t tests for each antigen.

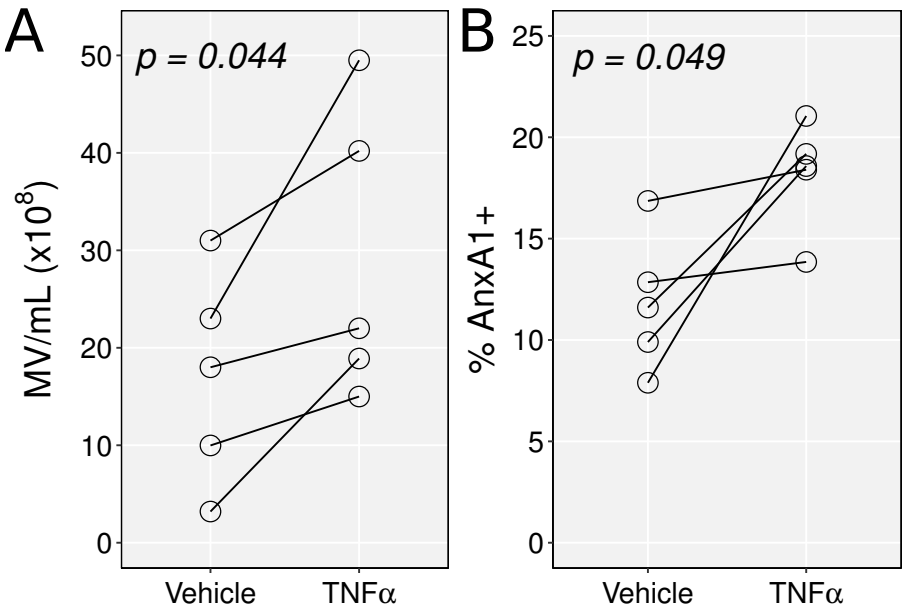

Figure 3.36: Blood neutrophils from RA patients produce anxA1$^+$ MV$_{\mathbf{TNF\alpha}}$. As many neutrophils as possible were isolated from the blood of 5 rheumatoid arthritis patients and split between two tubes for each. One tube was treated with 50ng/mL TNFα and the other with equal volume of vehicle, for 20 minutes at 37°C. Neutrophils were removed by centrifugation, samples were labelled with 50µM BODIPY maleimide and an anti-anxA1 antibody, and centrifuged at 20,000×g for 30 minutes at 4°C to pellet microvesicles. Pellets were resuspended in 30µL of PBS and enumerated on the ImageStream. Data are expressed as **A** the concentration of BODIPY maleimide$^+$ microvesicles and **B** the percentage of microvesicles positive for anxA1, with lines connecting each donor. Data were analysed with separate paired, two-tailed t tests.

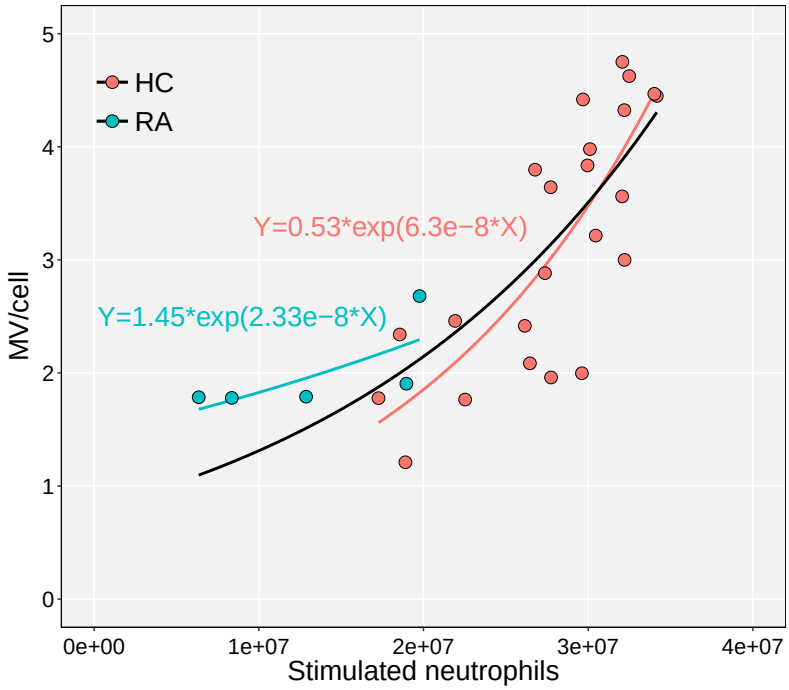

Figure 3.37: Relationship between starting neutrophil number, and vesicle yield. Blood neutrophils from healthy controls (HC) or rheumatoid arthritis patients (RA) were stimulated with 50ng/mL TNFα for 20 minutes at 37°C. Cells were removed, the supernatant was labelled with 50µM BODIPY maleimide and microvesicles pelleted at 20,000×g for 30 minutes at 4°C and enumerated on the ImageStream. Data are the number of vesicles recovered per cell against starting number of naïve neutrophils for each donor. Non-linear regression lines are fit within and between groups.

3.5.2 Plasma microvesicles in healthy donor and RA patients

Due to the higher level of baseline anxA1 expression observed on $MV_{TNF\alpha}$ from rheumatoid arthritis patients compared to healthy controls, circulating microvesicles from both populations were immunophenotyped to quantify anxA1 expression on microvesicles from neutrophils, monocytes, and platelets (as a negative control; Figure 3.38). In this small sample, the levels of circulating neutrophil, monocyte and platelet microvesicles was comparable between healthy controls and rheumatoid arthritis patients. The percentage of total $anxA1^+$ microvesicles was 11.3% higher in rheumatoid arthritis patients than in healthy controls, although when stratifying anxA1 expression by cell type, no differences were observed between the groups.

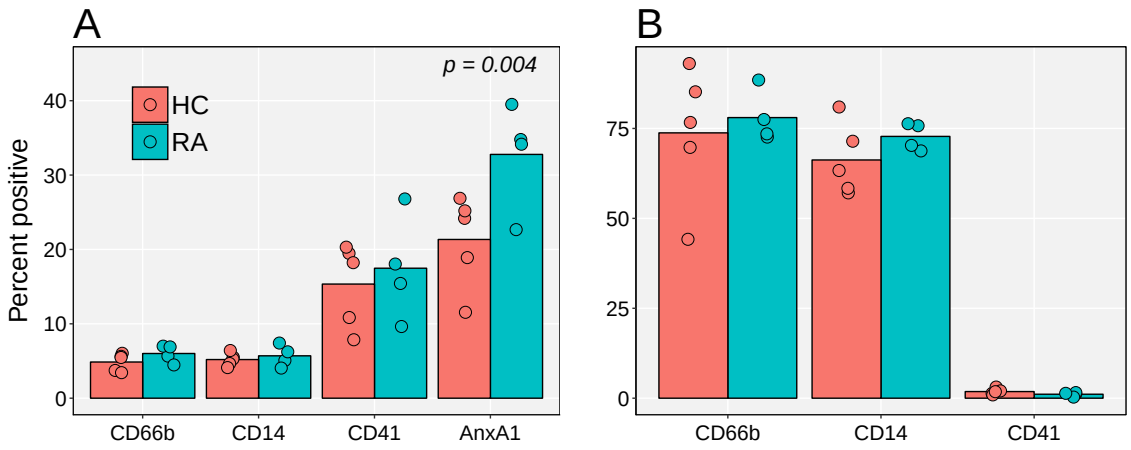

Figure 3.38: Phenotype of healthy and RA plasma microvesicles. 500µL of platelet-free plasma from healthy donors and rheumatoid arthritis patients were stained with 50µM BODIPY maleimide and split between 3 tubes. Each tube was stained with antibodies against anxA1, then either with antibodies against CD66b, CD14 or CD41, and acquired on the ImageStream. Data are the percentage of BODIPY maleimide$^+$ vesicles which were **A** positive for each lineage antigen, or **B** double positive for each lineage antigen and anxA1 for each donor, with bars at group means.

3.5.3 RA and healthy neutrophil $MV_{TNF\alpha}$ have similar efficacy

To test whether $MV_{TNF\alpha}$ generated from rheumatoid arthritis patient neutrophils had similar efficacy to those from healthy controls, monocyte-derived macrophages (generated from rheumatoid arthritis patient monocytes) were classically activated in the presence of 3×10^6/mL $MV_{TNF\alpha}$ (pooled from 3 donors) from healthy controls or rheumatoid arthritis patients, or vehicle alone (Figure 3.39). Supernatants were processed for Cytometric Bead Array, and cells were immunophenotyped by flow cytometry. $MV_{TNF\alpha}$ from healthy controls and rheumatoid arthritis patients had similar effects on macrophage phenotype across all antigens assayed. Linear discriminant analysis showed that macrophages treated with either $MV_{TNF\alpha}$ preparation separated from vehicle-treated macrophages by all antigens, most strongly HLA-DR, DP & DQ, CD86 and TGFβ, along the first discriminant factor (which accounted for 88.2% of the variability between groups). Macrophages treated with the two $MV_{TNF\alpha}$ populations had very similar expression profiles, separating along the second discriminant factor (which accounted for 11.8% of the variability between groups) by IL-12 p70, IL-10, and TGFβ. IL-12 p70 and IL-10 were more highly expressed in macrophages treated with rheumatoid arthritis $MV_{TNF\alpha}$, whereas TGFβ (the antigen which varied the greatest between them) was more highly expressed by macrophages treated with healthy control $MV_{TNF\alpha}$.

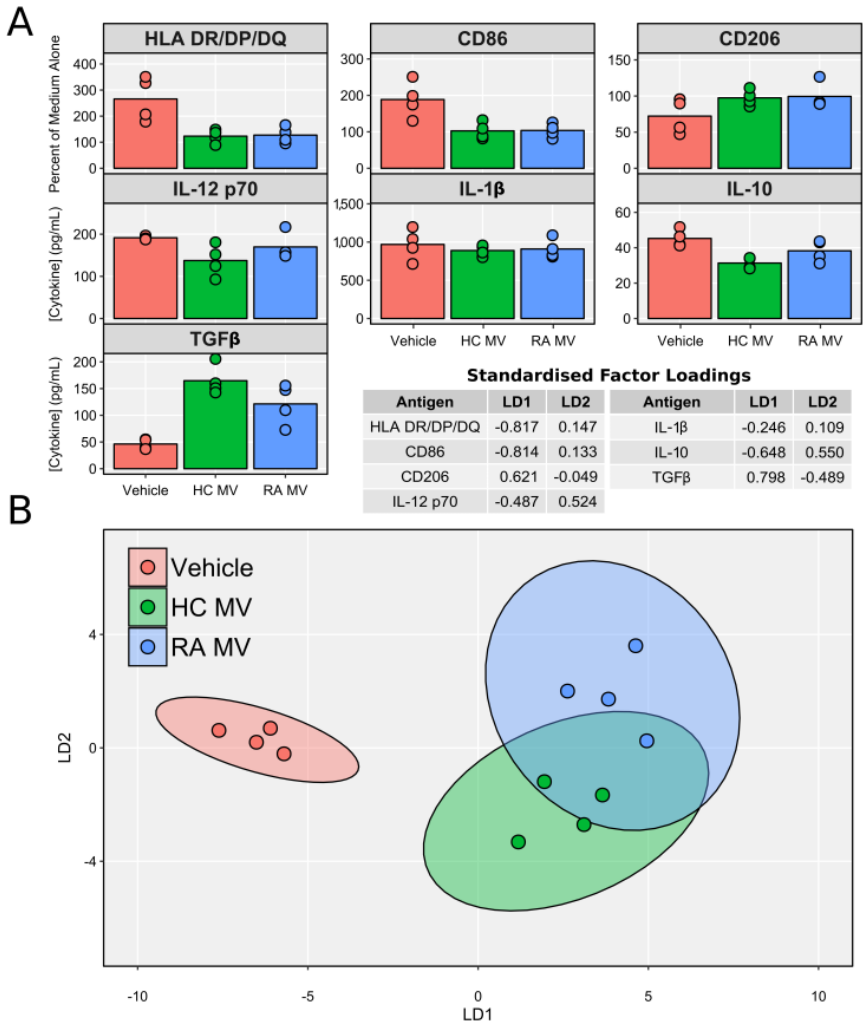

Figure 3.39: $MV_{TNF\alpha}$ from healthy and RA blood neutrophils have similar efficacy. Monocyte-derived macrophages were classically activated for 24 hours alone or in combination with 3×10^6/mL $MV_{TNF\alpha}$ from healthy controls (HC) or rheumatoid arthritis patients (RA; each pooled between 3 donors). Supernatants were collected and the concentration of IL-12 p70, IL-1β, IL-10 and TGFβ was measured by a Cytometric Bead Array. Cells were detached and stained with antibodies against HLA-DR, DP & DQ, CD86 and CD206, and analysed by flow cytometry. **A** Data are median fluorescence as a percentage of untreated cells for surface antigens, and absolute concentration of cytokines for each donor, with bars at group means for each antigen. **B** Results of linear discriminant analysis with 95% confidence ellipses for each group. Standardised factor loadings for both discriminant factors are tabulated.

3.5.4 Platelets release pro-inflammatory $MV_{TNF\alpha}$

The rheumatoid synovium contains large numbers of microvesicles, the majority of which are pro-inflammatory[246]. For an autologous, vesicle-based therapy to be viable, it must be shown that exogenously-administered microvesicles are able to achieve efficacy, even in the presence of a large number of endogenous vesicles with potentially opposing effects. The ratio of exogenous to endogenous vesicles required to achieve efficacy can also aid in determining effective doses.

To address this, platelet microvesicles were first used as a model, pro-inflammatory microvesicle population. To compare microvesicles generated by platelets and neutrophils generated by the same stimulus, it was desirable to generate vesicles from platelets using TNFα. To test whether platelets released microvesicles in response to TNFα (not a typical platelet agonist) platelet-rich plasma was stimulated with 50ng/mL TNFα or vehicle alone for 20 minutes at 37°C and the number of microvesicles quantified using the ImageStream (Figure 3.40). TNFα induced a mean 3.6-fold increase in the number of microvesicles over vehicle ($p = 0.066$), demonstrating that platelets release $MV_{TNF\alpha}$, although a single donor produced fewer vesicles post TNFα stimulation.

To determine the effects platelet $MV_{TNF\alpha}$ have on macrophage phenotype, macrophages were treated with 1×10^6, 2×10^6, 3×10^6 platelet $MV_{TNF\alpha}$/mL or vehicle alone for 24 hours (Figure 3.41). Supernatants were processed for Cytometric Bead Array, and cells immunophenotyped by flow cytometry. There was a weak but positive relationship between the number of platelet $MV_{TNF\alpha}$ and macrophage expression of HLA-DR, DP & DQ (p <0.001) and CD86 ($p = 0.008$) but no change in CD206, IL-12 p70, IL-1β, IL-10 or TGFβ. Although the p value of the slope for IL-12 p70 was <0.05, the effect was not biologically significant.

3.5.5 The effects of platelet $MV_{TNF\alpha}$ can be outcompeted

To confirm whether neutrophil $MV_{TNF\alpha}$ from rheumatoid arthritis patients can outcompete the effects platelet $MV_{TNF\alpha}$ have on macrophage HLA-DR, DP & DQ and CD86 expression, macrophages were treated with a fixed concentration of platelet $MV_{TNF\alpha}$ (3×10^6/mL) alone, or with increasing ratios of neutrophil $MV_{TNF\alpha}$ (Figure 3.42). Neutrophil $MV_{TNF\alpha}$ were able to abrogate platelet $MV_{TNF\alpha}$-mediated increases in HLA-DR, DR & DQ and CD86, and increase release of TGFβ. Neutrophil $MV_{TNF\alpha}$ completely reversed the effects of platelet $MV_{TNF\alpha}$ from a ratio of 5:1.

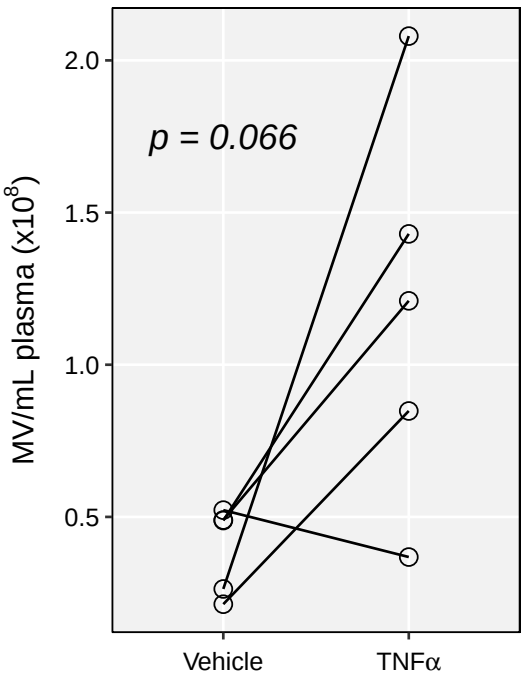

Figure 3.40: Platelets produce microvesicles in response to TNFα. Platelet-rich plasma was generated from 5 donors and split into two tubes. One tube was treated with 50ng/mL TNFα and the other with equal volume of vehicle, for 20 minutes at 37°C. Platelets were depleted by centrifuging at 13,000×g for 2 minutes at 4°C, samples were labelled with 50µM BODIPY maleimide and centrifuged at 20,000×g for 30 minutes at 4°C to pellet microvesicles. Pellets were resuspended in 30µL of PBS and enumerated on the ImageStream. Data are expressed as the number of microvesicles per mL of starting plasma, with lines connecting each donor. Data analysed with a paired, two-tailed t test.

3.5.6 Total RA synovial fluid microvesicles are pro-inflammatory

Once the principle had been demonstrated that neutrophil $MV_{TNF\alpha}$ can outcompete the effects of a model inflammatory microvesicle population, the same was repeated but using the total population of microvesicles isolated from the synovial fluid of patients with rheumatoid arthritis. Macrophages treated with increasing concentrations of total synovial fluid microvesicles demonstrated a similar increase in HLA-DR, DP & DQ and CD86 as seen with the platelet $MV_{TNF\alpha}$ (Figure 3.43). There were small but variable increases in IL-12 p70, IL-1β, and TGFβ with increased vesicle treatment, but no change in CD206 or IL-10.

3.5.7 The effects of synovial fluid microvesicles can be outcompeted

In a similar experiment as was performed with platelet $MV_{TNF\alpha}$, to confirm whether rheumatoid arthritis patient neutrophil $MV_{TNF\alpha}$ can outcompete the effects synovial fluid microvesicles have on macrophage HLA-DR, DP & DQ and CD86 expression, macrophages were treated with a fixed concentration of synovial fluid microvesicles (3×10^6/mL) alone, or with increasing ratios of neutrophil $MV_{TNF\alpha}$ (Figure 3.44). Neutrophil $MV_{TNF\alpha}$ were able to abrogate synovial microvesicle-mediated increases in HLA-DR, DR & DQ and CD86, and increase release of TGFβ. A higher ratio of

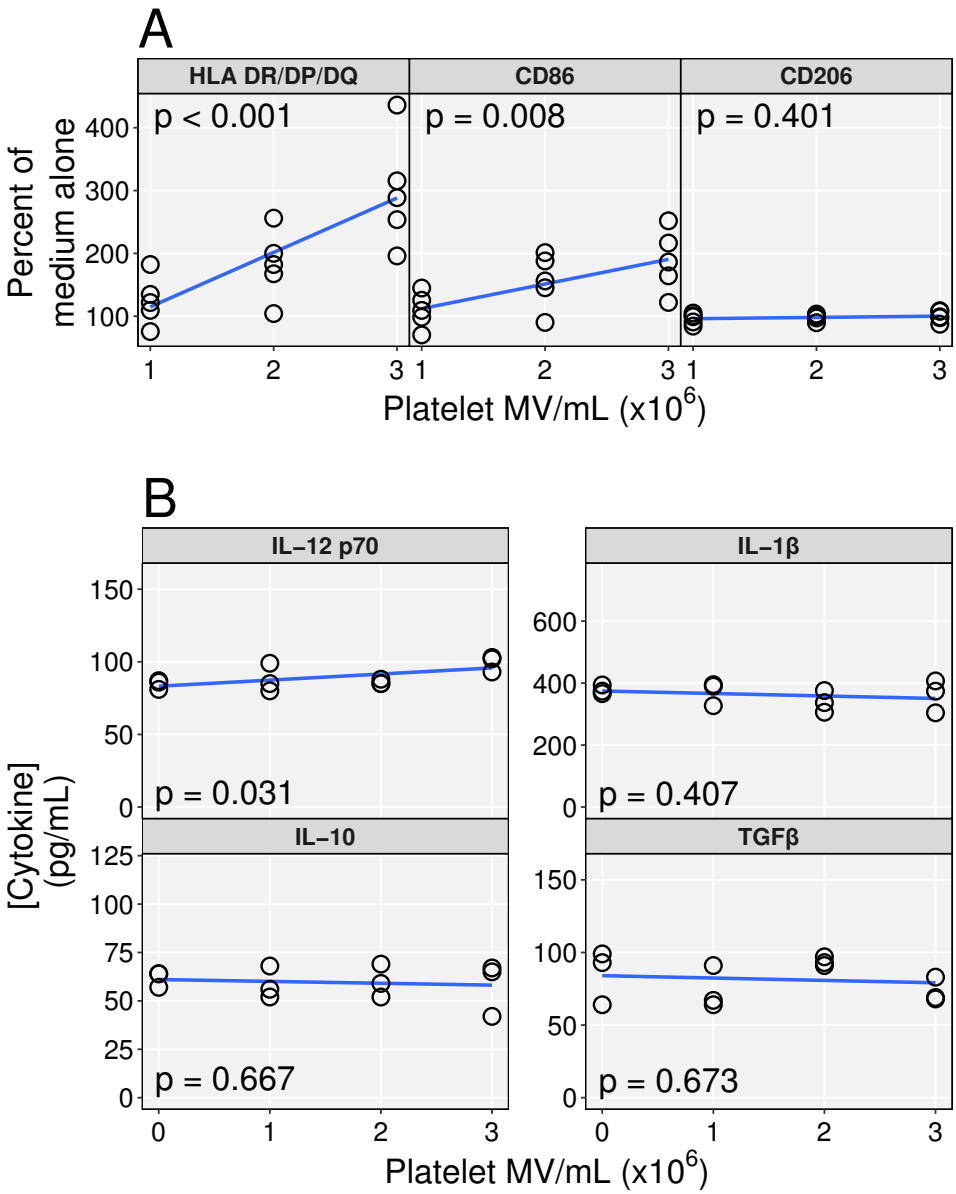

Figure 3.41: Platelet $MV_{TNF\alpha}$ are pro-inflammatory for macrophages. $MV_{TNF\alpha}$ were generated from washed platelets from 5mL of platelet-rich plasma each from 3 donors and pooled together. Monocyte-derived macrophages were treated with medium alone, or increasing concentrations of platelet $MV_{TNF\alpha}$ for 24 hours at 37°C. Supernatants were analysed by a Cytometric Bead Array for IL-12 p70, IL-1β, IL-10 and TGFβ, and cells were detached and stained for HLA-DR, DP & DQ, CD86 and CD206 expression and analysed by flow cytometry. Data are expressed as median fluorescence as a percentage of untreated cells for surface antigens, or absolute concentration of cytokines for each donor. Data analysed with linear regression for each antigen, with least square lines.

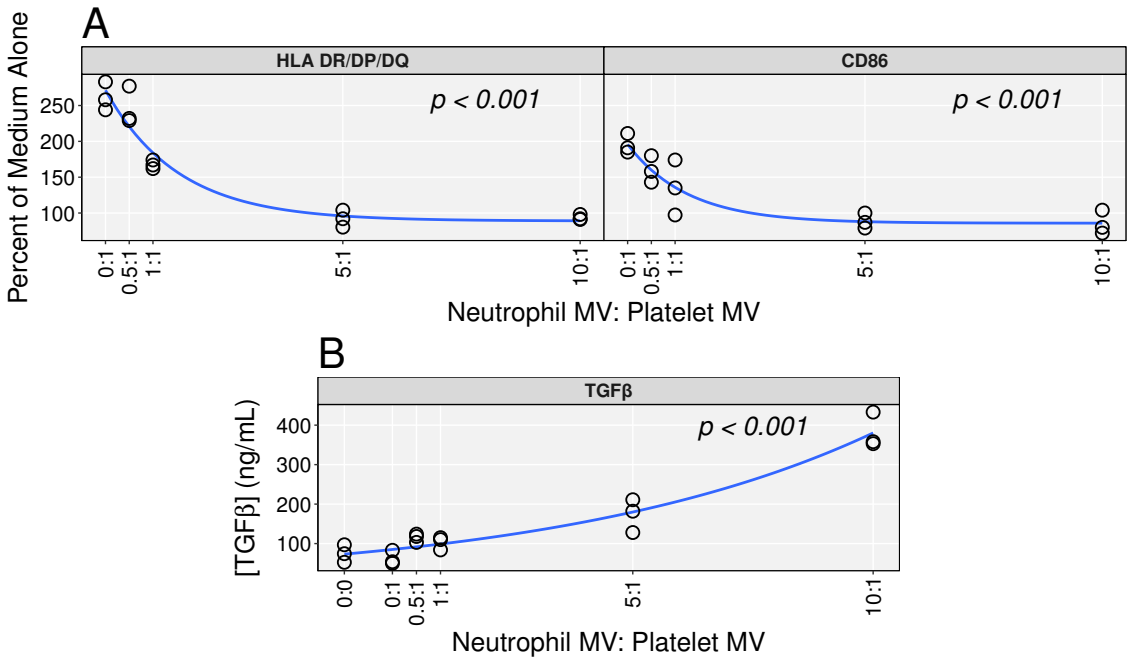

Figure 3.42: Neutrophil and platelet $MV_{TNF\alpha}$ have opposing efficacy. Human monocyte-derived macrophages were treated for 24 hours at 37°C with medium alone, or 3×10^6 platelet $MV_{TNF\alpha}$/mL alone, or in combination with increasing ratios of neutrophil $MV_{TNF\alpha}$. Supernatants were collected and TGFβ concentration was measured with a Cytometric Bead Array, and cells were detached and stained with antibodies against HLA-DR, DP & DQ and CD86. Data are median fluorescence as a percentage of untreated cells for surface antigens, and absolute concentration of TGFβ for each donor. Data analysed with non-linear regression,where least squares lines are shown in blue and p values compare the full fits shown to intercept-only fits.

neutrophil $MV_{TNF\alpha}$ to synovial fluid microvesicles was required to completely reverse the effects of synovial microvesicles, than for platelet $MV_{TNF\alpha}$.

3.6 Generating a cell line to produce anxA1$^+$ microvesicles

While using autologous vesicle preparations is attractive as a novel form of therapy, it does present the issues of volume of production, and of preparation quality control. An alternative which deals with these issues is the prospect of engineering a cell line to produce vesicles with desirable properties, and produce large-scale vesicle batches which can be quality control checked prior to administration. As a simple proof of principle, and based on the observed relationship between vesicular anxA1 and macrophage TGFβ expression, it was determined that a cell line(s) would be generated to produce anxA1$^+$ microvesicles. Once generated, the effects of wild type

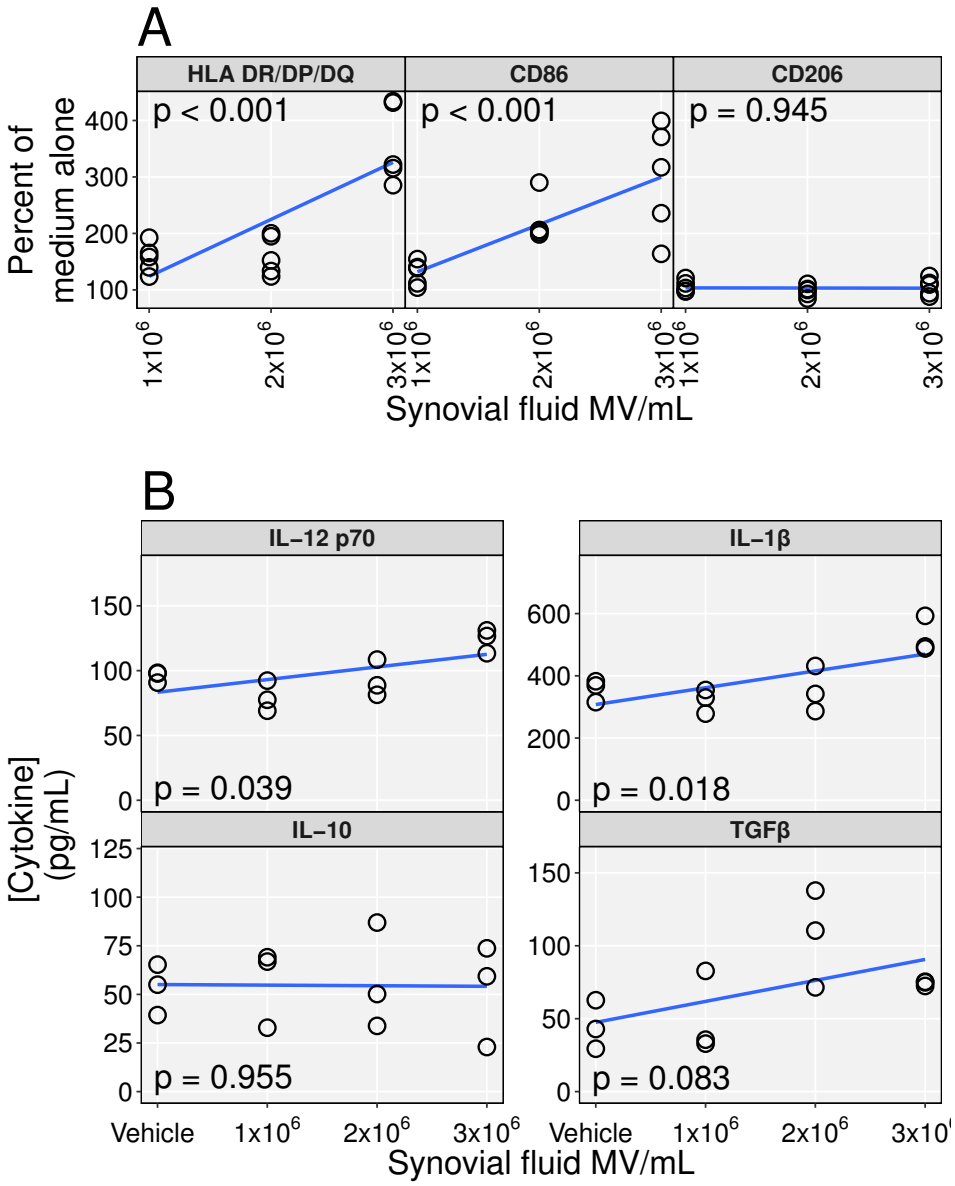

Figure 3.43: Total RA synovial fluid microvesicles are pro-inflammatory. Synovial fluid from 3 rheumatoid arthritis patients was digested with 20U/mL hyaluronidase for 30 minutes at 37°C, depleted of cells, and centrifuged at 20,000×g to pellet microvesicles. Monocyte-derived macrophages were treated with medium alone, or increasing concentrations of synovial fluid microvesicles for 24 hours at 37°C. Supernatants were analysed by a Cytometric Bead Array for IL-12 p70, IL-1β, IL-10 and TGFβ, and cells were detached and stained for HLA-DR, DP & DQ, CD86 and CD206 expression and analysed by flow cytometry. Data are expressed as median fluorescence as a percentage of untreated cells for surface antigens, or absolute concentration of cytokines for each donor. Data analysed with linear regression for each antigen, with least square lines.

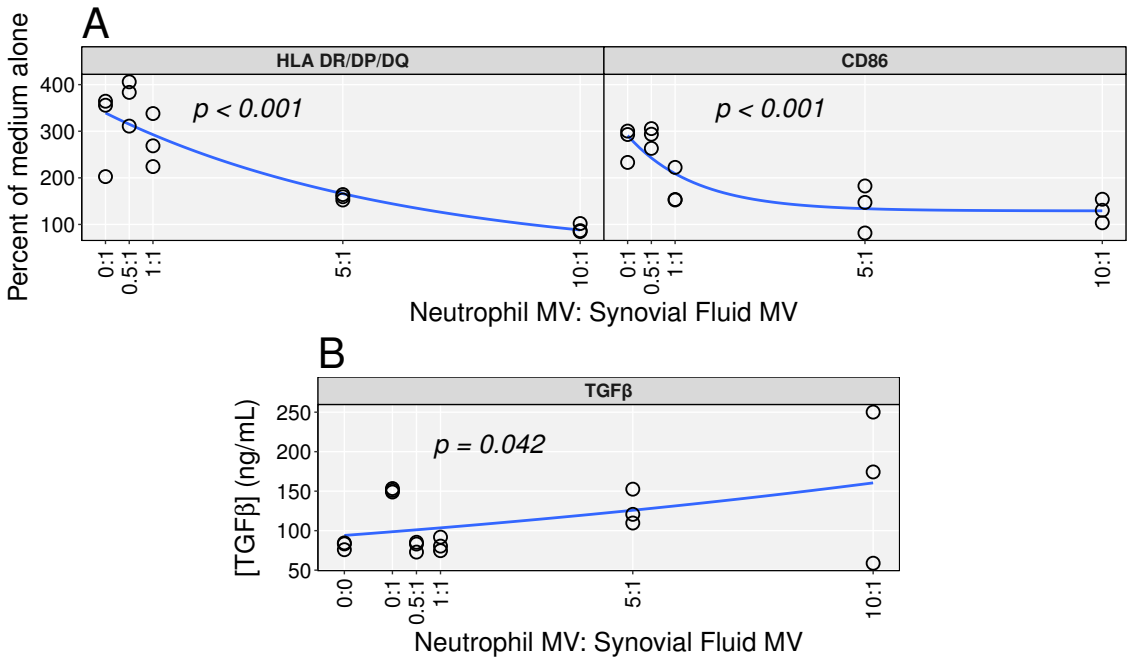

Figure 3.44: Neutrophil and synovial fluid microvesicles have opposing efficacy. Human monocyte-derived macrophages were treated for 24 hours at 37°C with medium alone, or 3×10^6 synovial fluid microvesicles/mL (pooled between 3 rheumatoid arthritis patients) alone, or in combination with increasing ratios of neutrophil $MV_{TNF\alpha}$. Supernatants were collected and TGFβ concentration was measured with a Cytometric Bead Array, and cells were detached and stained with antibodies against HLA-DR, DP & DQ and CD86. Data are median fluorescence as a percentage of untreated cells for surface antigens, and absolute concentration of TGFβ for each donor. Data analysed with non-linear regression, where least squares lines are shown in blue and p values compare the full fits shown to intercept-only fits.

vs. $anxA1^+$ microvesicles could be directly compared.

HL60 and NB4 cells were chosen as they are promyelocytic cell lines which can be differentiated into monocyte and neutrophil-like cells experimentally[237,247]. The HEK293 cell line was also included as it is more amenable to transfection than HL60 and NB4 cells (which have not been widely transfected successfully).

3.6.1 Optimising conditions for antibiotic selection

The vector selected to transfect the cell lines contained a blasticidin resistance gene, blasticidin-S deaminase (bsd), and once transfected, cells expressing the bsd gene (and therefore anxA1) would be selected for by culturing in blasticidin. To determine a minimum concentration of blasticidin required to kill all cells after culture for 5-10 days, an assay was constructed to allow repeated sampling of cell viability over time. Alamar blue is a non-cytotoxic, membrane-permeable substrate which is reduced by

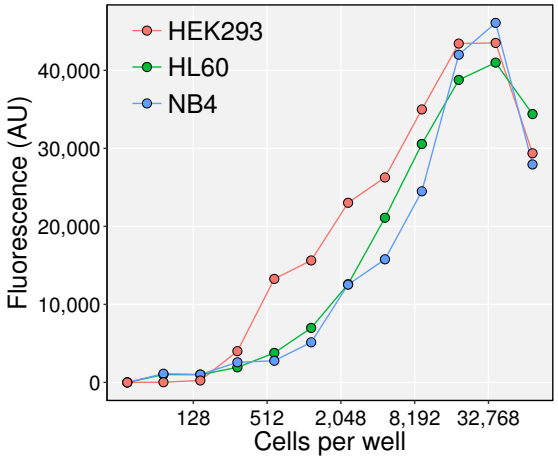

Figure 3.45: Titration of cell number for alamar blue viability assay. The number of HL60, NB4 and HEK293 cells per well was serially-diluted 1 in 2 in a 96-well plate and stained for 1 hour with 10% v/v alamar blue. Fluorescence at 590nm was measured upon excitation at 560nm using a fluorescence plate reader. Data are blank-subtracted fluorescence intensity of an individual reading per cell number, per cell line.

viable cells into a product which fluoresces red upon excitation with a yellow-green laser. Labelling cells with alamar blue allows repeated viability measurements from tissue culture samples without the need to perform a trypan blue exclusion count for every sample.

To optimise the number of cells per well to achieve the greatest fluorescence signal, HEK293, HL60 and NB4 cells were labelled with alamar blue, serially diluted across a 96-well plate, and read using a fluorescence plate reader (Figure 3.45). While HEK293 cells generally required fewer cells per well to achieve a higher fluorescence reading, all three cell lines produced the greatest fluorescence reading at 3.75×10^4 cells/well, with fluorescence values dropping upon further increase of cell number.

To determine the optimal concentration and length of blasticidin incubation, the three cell lines were cultured in 5, 10, 15 or 20µg/mL blasticidin, or vehicle for 13 days. Every other day, the untreated cells of each line were counted using a haemocytometer, and 3×10^4 (just below the saturation of the alamar blue signal) of these cells and an equal volume of the cells in culture with blasticidin were labelled with alamar blue and their fluorescence read on a plate reader (Figure 3.46). This facilitated the quantification of viable cells, relative to the number in the vehicle-treated wells. Blasticidin treatment induced cell death in all three cell lines, in a concentration-dependent manner. HEK293 cells were most sensitive to blasticidin, followed by NB4 and then HL60 cells which were least sensitive. 5 days of selection for HEK293 cells, and 7 days for NB4 and HL60 cells in 10µg/mL blasticidin were chosen as appropriate selection conditions post transfection.

After ligation of the anxA1 ORF into the pIRESbsd2 vector and transformation of *E. coli* with the putative pIRESbsd2-AnxA1 construct, it was important to select bacterial clones which contained plasmids containing anxA1 ORF, and in the correct orientation. Plasmids were isolated for each clone by miniprep, digested with EcoRI and separated by size using agarose gel electrophoresis (Figure 3.47). Clones A, H, I, O, R, S, U, V, W and X displayed bands at 5368bp and 1031bp, diagnostic of the

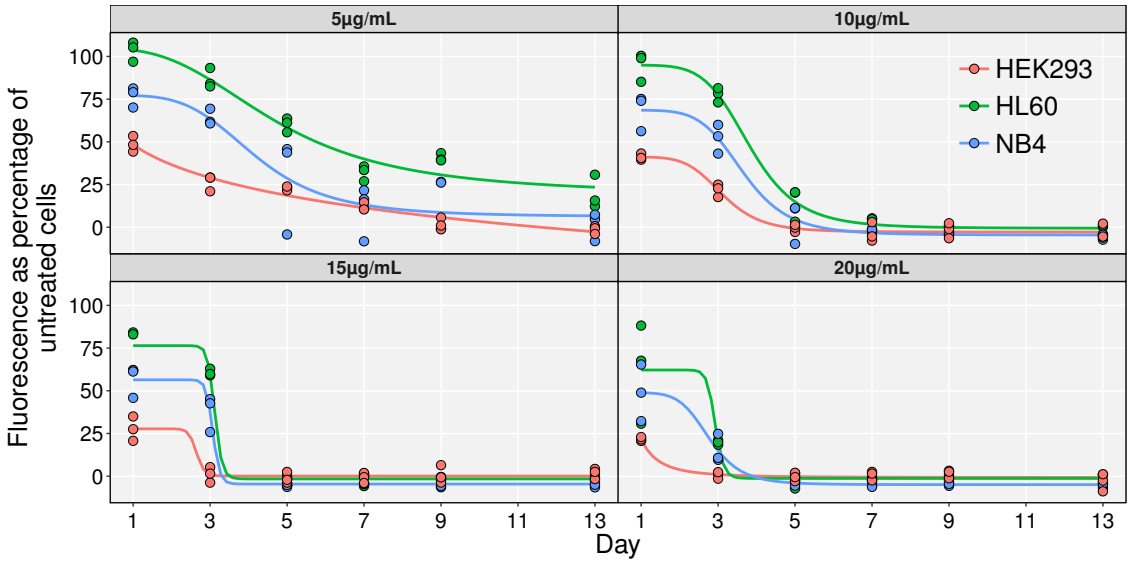

Figure 3.46: Blasticidin titration on cell viability. HL60, NB4 and HEK293 cells were seeded at 2×10^5 cells in 1mL in 12-well plates in their complete media containing increasing concentrations of blasticidin antibiotic as shown in panel headings (or were untreated). Every other day, the untreated cells were counted using a haemocytometer, and 3×10^4 cells were transferred to a 96-well plate. The same volume of cells was transferred to the plate from every other condition, and all wells were stained with 10% v/v alamar blue for 1 hour and their fluorescence read at 590nm upon excitation at 560nm. The fluorescence intensity as a percentage of untreated cells is shown for each technical replicate, with non-linear regression curves plotted for each group.

pIRESbsd2-AnxA1 vector (with AnxA1 in the correct orientation).

Bacterial clones W and X were selected for outgrowth and maxiprep isolation of enough plasmid for purification and transfection. As an additional round of confirmation, plasmids isolated by miniprep were digested with HindIII and separated by size using agarose gel electrophoresis (Figure 3.48). Both clones displayed bands at 4394bp, 1186bp, 471bp and 348bp, diagnostic of the pIRESbsd2-AnxA1 vector (with AnxA1 in the correct orientation).

After transfection, NB4 and HL60 cells did not survive antibiotic selection, whereas HEK293 cells did. After repeating the transfection multiple times with the NB4 and HL60 cells, and achieving no antibiotic resistance each time, only the HEK293 cells were used from here on. To confirm their expression of anxA1, HEK293 cells were fixed, permeabilised, and immunophenotyped for anxA1 expression by flow cytometry (Figure 3.49). Despite being antibiotic resistant, only 14.7% of cells were positive for anxA1.

To generate lines of cells which was 100% positive for anxA1, this polyclonal population of cells was serially diluted and seeded at ~1 cell per well of several 96-well plates, in order to grow up clonal colonies. Once expanded enough, each colony was

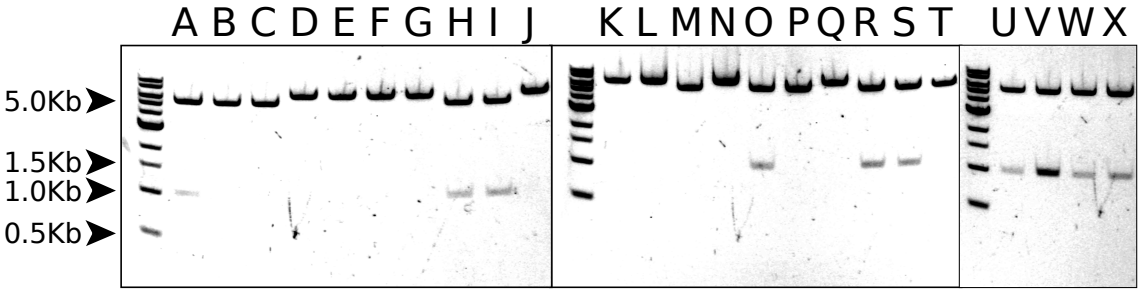

Figure 3.47: Diagnostic EcoRI restriction digest. Individual colonies of E. coli transformed with the pIRESbsd2 vector were picked, expanded and put through a miniprep to isolate the plasmid DNA. Plasmid from each clone was digested with EcoRI and run on agarose gels with DNA ladders to confirm insertion of the anxA1 gene in the correct orientation.

sampled, fixed, permeabilised and immunophenotyped for anxA1 expression by flow cytometry (Figure 3.50). Clones 3, 11, 14, 23 and 32 were almost all completely positive for anxA1 and so were expanded in order to generate microvesicles from them.

To confirm the presence of anxA1 on the microvesicles of each HEK-AnxA1 clone, each clone was washed twice with PBS, and treated with serum-free RPMI containing 1µM ionomycin (I3909, Sigma-Aldrich) for 30 minutes at 37°C. Untransfected HEK293 cells were also stimulated to generate biological-negative vesicles, and $MV_{TNF\alpha}$ were generated from a single donor's primary neutrophils to act as a positive control. Microvesicles were labelled with BODIPY maleimide and immunophenotyped for anxA1 expression using the ImageStream (Figure 3.51). Despite almost all HEK-AnxA1 cells expressing anxA1, on average, only 3.4% of vesicles from each clone expressed detectable levels of the protein on their surface.

Monocyte-derived macrophages treated with microvesicles isolated from HEK-AnxA1 cells stimulated with 1µM ionomycin as above, did not secrete higher levels of TGFβ than those treated with microvesicles generated in the same way from untransfected HEK293 cells (Figure 3.52). The levels of TGFβ in the supernatant was also independent of anxA1 blockade under these conditions. $MV_{TNF\alpha}$ from primary human neutrophils were included as a positive control, which induced TGFβ production in the presence of the isotype-matched control antibody only, supporting previous results.

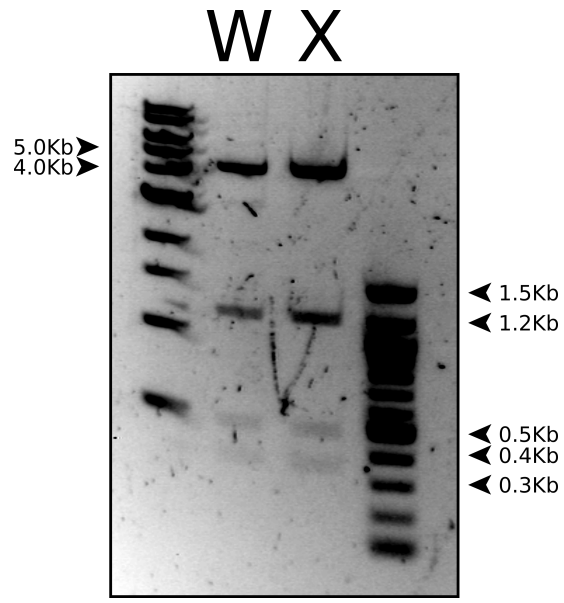

Figure 3.48: Diagnostic HindIII restriction digest. Plasmid DNA from clones W and X, isolated by miniprep, were digested with HindIII and run on an agarose gel with DNA ladders to confirm with an additional restriction digest that the anxA1 gene was inserted into the pIRESbsd2 vector in the correct orientation.

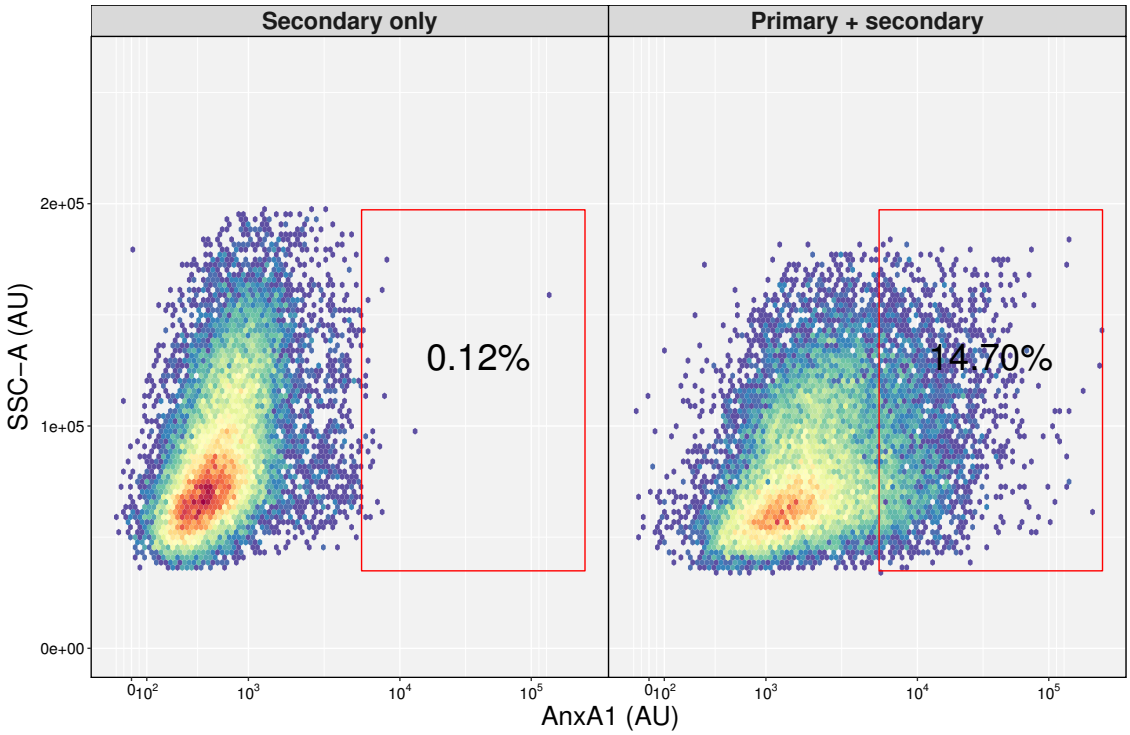

Figure 3.49: Screening transfected HEK293 colony for anxA1 expression. HEK293 cells after transfection and blasticidin selection were fixed, permeabilised and immunolabelled for total anxA1 expression, and acquired on a Canto II cytometer. Hexagon bin plots shaded by density of gated singlet cells labelled with primary and secondary antibodies, or just the secondary as a gating control.

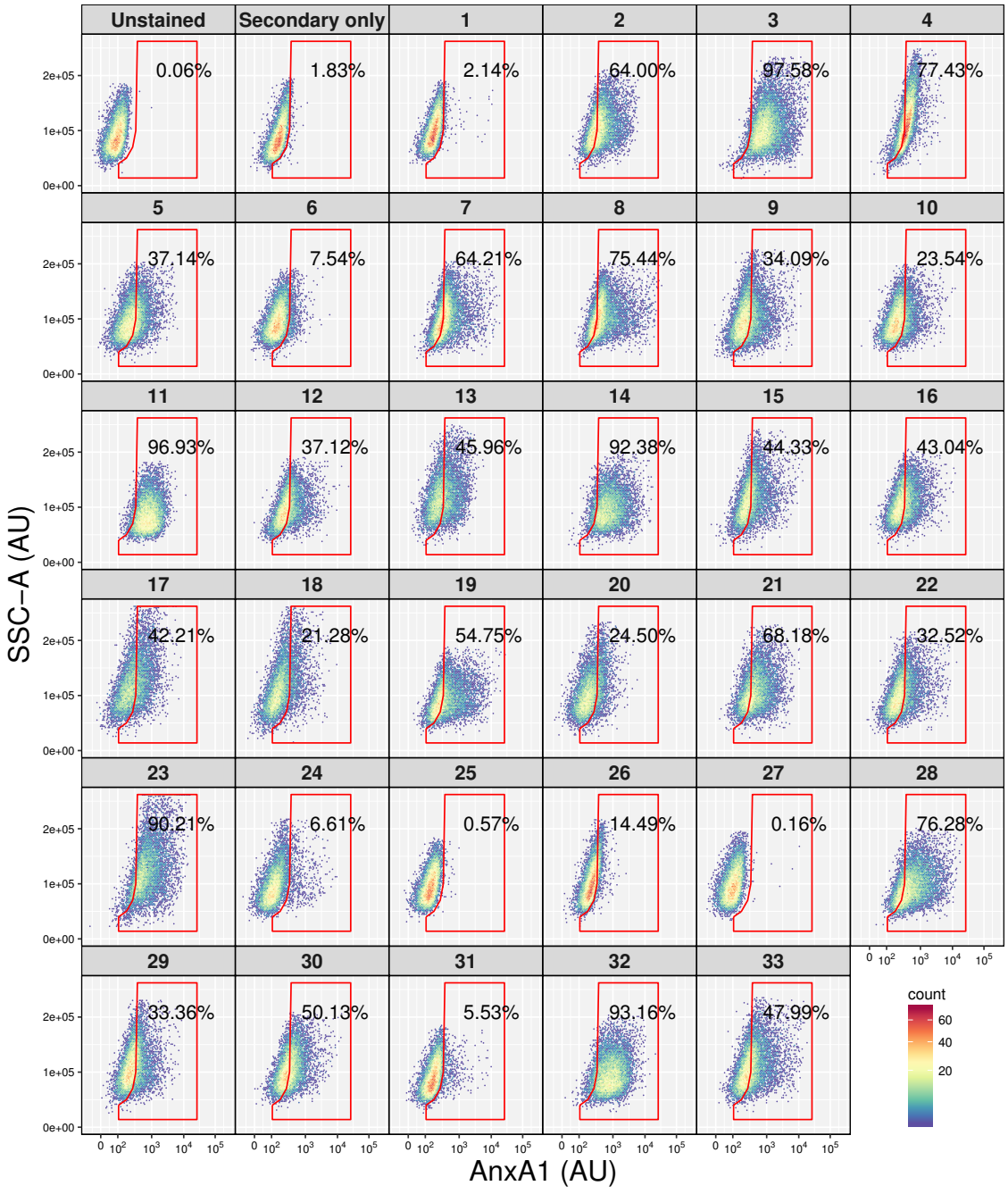

Figure 3.50: Screening HEK293 colonies for anxA1 expression. Transfected HEK293 cell colonies were stained for total anxA1 expression and acquired on a Canto II cytometer. Hexagon bin plots shaded by density of gated singlet cells for each clone, secondary antibody-only and unstained cells are shown, with polygon gate drawn against the secondary-only population.

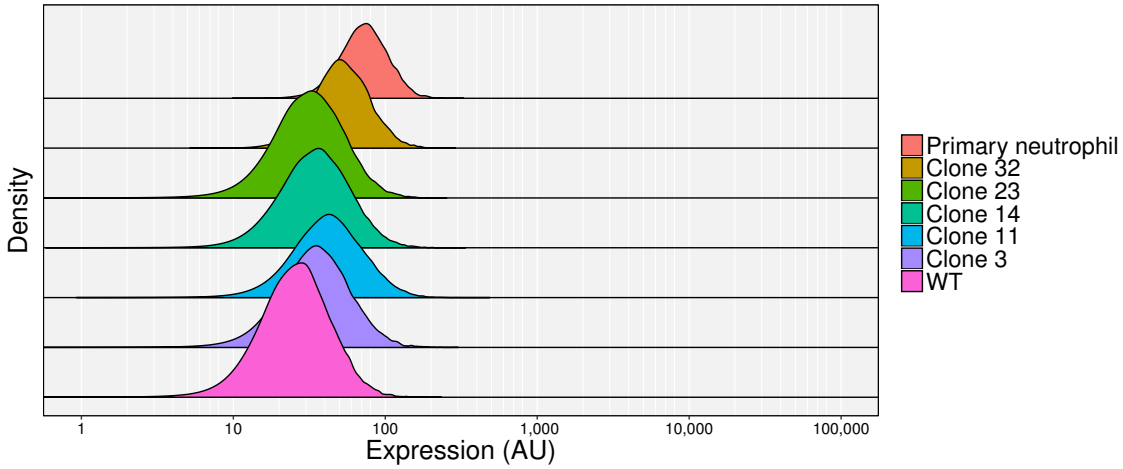

Figure 3.51: Low expression of anxA1 on HEK-AnxA1 microvesicles. HEK-AnxA1 clones and wild type (WT) HEK293 cells were stimulated with 1µM ionomycin for 30 min at 37°C in serum-free medium before isolation of their microvesicles. Microvesicles were labelled with BODIPY maleimide and immunophenotyped for anxA1 expression using the ImageStream. $MV_{TNF\alpha}$ from a single, primary neutrophil donor were included as a positive control. Kernel density plots are shown of 10,000 microvesicles per condition.

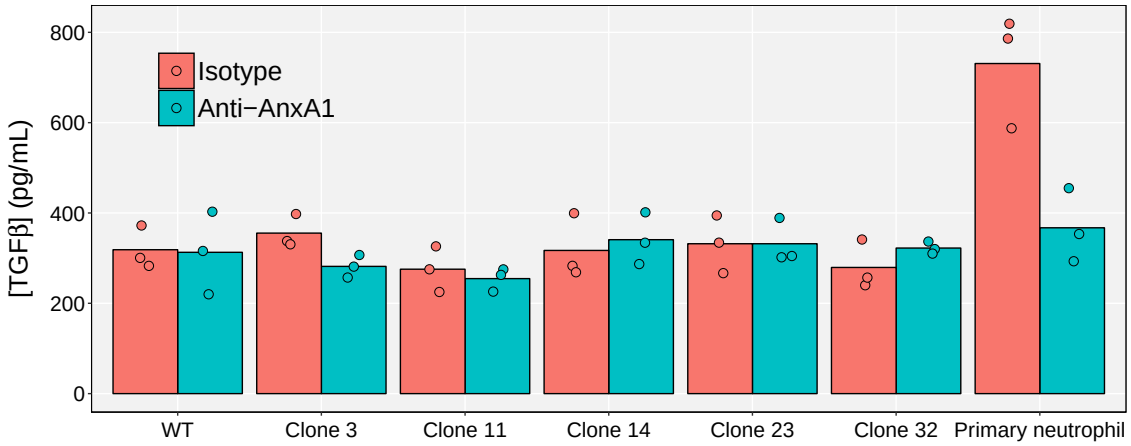

Figure 3.52: HEK-AnxA1 clones do not induce macrophage TGFβ production. Human monocyte-derived macrophages were treated with 3×10^6/mL ionomycin-induced microvesicles from HEK293 cells (WT) or HEK-AnxA1 clones, or the same concentration of $MV_{TNF\alpha}$ from a single primary neutrophil donor. Stimulations from each source of vesicles were performed in the presence of 10µg/mL neutralising anti-anxA1 antibody, or 10µg/mL of an isotype-matched control antibody for 24 hours. Supernatants were collected and analysed for TGFβ quantification by Cytometric Bead Array. Individual biological replicates are shown with bars at group means.

Chapter 4

Discussion

4.1 Microvesicle analysis is robust

Flow cytometry remains one of the most widely used methods of analysing microvesicles due to its high throughput and mutliparameter output. When comparing the modern LSRFortessa cytometer to the ImageStream^{x} MKII, the latter was able to resolve fluorescent particles as small as 20nm in diameter where the former was unable to detect 100nm particles. As the Imagestream bases its detection and analysis on the collection of light by its CCDs, it seems surprising that its limit of detection is not $\geq$ 400nm, the shortest wavelength of light at which most light microscopy techniques are limited. This limitation is in fact in effect; the instrument cannot detect brightfield signals of particles smaller than this threshold, but instead relies on the fluorescent haloing of a labelled particle to make it appear larger than it actually is. The advantage of this is that it allows particles <100nm in diameter to be detected and analysed provided they are appropriately labelled, allowing detection of microvesicles and *possibly* exosomes (although this application has not been tested). This platform provides four advantages over traditional cytometry: firstly its limit of detection for fluorescent particles is considerably lower, secondly (and related to the first) with appropriate labelling these particles can completely separate from the noise population (which is less considerable), thirdly the concentration of any population is given without the need for additional beads, and finally each event can be visually interrogated to ensure correct gating and exclusion of doublets (which are very rare given the instrument's flow rate of 40nL/sec). These benefits have allowed the simple identification and enumeration of microvesicles in different biological fluids. The major drawback of this instrument compared to the LSRFortessa, is smaller dynamic range of fluorescence detection which impacts its ability to separate vesicle populations by antigen expression. Nevertheless, microvesicles from plasma and isolated neutrophils can be phenotyped with optimisation of antibody labelling.

In comparing the relative efficiency of CFSE, BODIPY maleimide and PKH in labelling a concentrated preparation of microvesicles, CFSE achieved full labelling at a 10-fold lower concentration than BODIPY maleimide. PKH did not achieve full labelling because across all concentrations used, the ethanol solvent lysed a

proportion of the vesicles after the 5 minute incubation. Additionally, even in the absence of microvesicles, PKH contained a number of fluorescent particles which overlapped with the microvesicle gate. These are likely to be micelles given the lipophilic nature of this class of dyes[248]. While both CFSE and BODIPY maleimide were deemed appropriate as pan-microvesicle dyes, BODIPY maleimide was considerably cheaper, even at the higher concentration needed, and so was used for most assays. As microvesicles can be freeze-thawed multiple times with no injurious effect on structure or function, it would be useful to store fluorescently labelled microvesicles to reuse at a later date. Although CFSE was the most resistant label to freeze-thaw, all three dyes used lost fluorescence and therefore underestimated microvesicle number, prohibiting the long term storage of fluorescent microvesicles.

Centrifugation at 20,000×g is widely accepted as too low a force to pellet significant numbers of exosomes in several hours, let alone 20 minutes. The absence of important numbers of exosomes was demonstrated by the lack of Tsg101 expression in a 20,000×g pellet, where considerable expression was detected in a 100,000×g pellet. While generating a pure population of any vesicle is as yet impossible, this suggests that this protocol generates vesicle preparations highly enriched in microvesicles.

While their resilience to freeze-thaw allows storage of microvesicles, it was important to know how stable they were for prolonged periods of time and at which temperatures. Storage at temperatures greater than -20°C are not appropriate, resulting in rapid vesicle loss, and while stable for 48 hours at -20°C preparations stored longer than this need to be stored at -80°C. Although the exact mechanisms by which microvesicles expire in storage are not known, a large proportion of them are reported to contain mitochondria and can generate superoxide[82,249]. The presence of ROS may damage the membrane, even in those stored at -20°C, where subsequent thawing causes membrane rupture.

While neutrophil-derived microvesicles can be immunophenotyped without the need to remove their maternal neutrophils, the neutrophils themselves act as an antigenic sink, reducing the fluorescent intensity of the microvesicles in the absence of a saturating concentration of antibody. For this reason microvesicles were always subsequently phenotyped in isolation (where stronger separation from isotype controls was observed).

The fluidics system of the ImageStream differs from most standard cytometers in that the sample is aspirated and syringe-driven into the flow cell by motors. A consequence of this is that the volume of sample acquired is accurately estimated to the nearest 10nL. The number of events in a population detected within this volume is used to estimate the concentration of those objects in the sample. The instrument showed linearity of estimates of microvesicle concentration with sequential

sample dilution, demonstrating the reliability of this method to estimate microvesicle concentration. It is important to note, however, that sample acquisition must take more than ~2 seconds, or the instrument is unable to measure the volume injected, and therefore concentration cannot be estimated.

The profile of circulating erythrocyte, platelet and leucocyte microvesicle populations in healthy human plasma largely correlates with the abundance of each cell type, as may be expected. The level of endothelial cell-derived microvesicles was surprisingly low, although may demonstrate a relative absence of ectocytosis of these cells in the resting state. The abundance follows erythrocyte > platelet > leukocyte > endothelial cell. Monocyte and neutrophil-derived microvesicle levels also do not represent the difference in circulating numbers of these cells, where far higher neutrophil-derived microvesicles may have been expected. For the leukocyte subsets, the abundance follows neutrophil ~ monocyte > lymphocyte.

It is important to note that ~10% of the total microvesicles remain unidentified. The reason for this may lie in fringe populations of microvesicles, as well as variability and error in labelling/acquisition. Until more powerful methods are developed, full identification of the remainder of "unknown" microvesicles is likely to remain asymptotic. An additional caveat to this experiment is that it was not possible to conduct all immunolabelling in a single reaction but instead was split into 3 separate reactions. Regardless, this data demonstrates the ability of this platform to type a patient's vesicle profile, and could therefore facilitate their use as biomarkers.

4.2 Inflammatory stimuli induce ectocytosis in neutrophils

While constitutively occurring, ectocytosis is a regulated process and efficacy of microvesicles is conceptually dependent on both their contents and density within a tissue compartment. For this reason, and for the purpose of producing sufficient numbers of vesicles for experimentation, different model stimuli were applied to human neutrophils to quantify the number of vesicles they release. Increased ectocytosis in neutrophils was induced by all inflammatory stimuli tested, sugesting the universal nature of this process in response to activating stimuli. The observation that "unstimulated" neutrophils released ~2×10^7 microvesicles/mL after 20 minutes would seem to indicate constitutive microvesicle release from resting cells. While this is likely (although *in vivo* all cells are always receiving stimulation in one form or another), the procedure of isolating cells (neutrophils in particular) from whole blood does cause partial activation.

Interestingly, the number of microvesicles released in response to various stimuli did not vary as much as expected. While this could be ascribed as a coincidence, this was observed repeatedly with different classes of stimuli and may suggest a limitation in the number of microvesicles released, equilibrium between release and re-uptake, or more likely be related to the initial release and trivial change in rate of release described below.

Although important, the increase in the rate of microvesicle release upon TNFα stimulation is not sufficient to explain the rise in total microvesicle number at 20 minutes. Surprisingly, there is a large initial burst of microvesicle release within 2 minutes of stimulation (before the ImageStream was able to start enumerating them). This would suggest that a number of primed sites for ectocytosis exist in the resting cell which bud off rapidly. One limitation of this experiment is that the rate of microvesicles/second flowing through the flow cell is both a function of the number of neutrophils *and* the flow rate, and so is not a direct measure of microvesicle release from the cells. However, given that neutrophils were suspended at 1×10^6/mL and therefore flowing at 40 cells/40nL/second, it can be estimated that TNFα caused a mean increase in rate from 0.59 to 1.16 microvesicles/second/cell. This, however, does not take into consideration the loss of neutrophils to waste as the sample was run.

While this experiment demonstrated a continual increase in the rate of ectocytosis, 20 minutes was chosen as an optimal length for subsequent neutrophil stimulation to provide as many microvesicles as possible while avoiding the initiation of NETosis. An experiment performed in collaboration with Dr. Elisa Corsiero (William Harvey Research Institute) showed that NETs were abundant after 60 minutes of stimulation with TNFα (these data are not shown in the thesis as I did not produce them, but are published in reference 3).

4.3 $MV_{TNF\alpha}$ inhibit classical activation of macrophages

$MV_{TNF\alpha}$ microvesicles inhibited classical activation in monocyte-derived macrophages, completely restoring the expression of HLA-DR, DP & DQ and CD86 to control levels at 3×10^6/mL. On their own, microvesicles did not seem to affect macrophage phenotype, suggesting that they inhibit classical activation rather than imparting alternative activation (supported by their lack of effect on IL-4-mediated polarisation). The exception to this is in the presence of LPS and IFNγ where they actually increased CD206 expression (an effect seen in neither treatment alone). 3×10^6 microvesicles/mL was chosen for all future treatments (except where specified),

although both the concentration and the ratio of microvesicles:macrophage seem important for the magnitude of their effects, where in a 24-well format, the ratio is ~3:1.

Due to differences in isolation protocol and insufficient sensitivity of analysis techniques, which population of vesicles is responsible for a reported efficacy is often ambiguous. While more sophisticated methods of enriching for a populations of exosomes are becoming more widespread (such as size exclusion chromatography[250]), the differential centrifugation of the activated neutrophil supernatant allowed for the relative enrichment of microvesicles and exosomes. The data indicate clearly that the regulation of classical macrophage activation imparted by the $MV_{TNF\alpha}$ preparations was attributable to the microvesicle-enriched fraction, and was not imparted by the exosome-enriched fraction. While theoretically the lack of efficacy from the 100,000×g pellet could merely be due to a smaller number of exosomes released during the 20 minute timescale, it nevertheless shows that for the $MV_{TNF\alpha}$ preparations used in this project, exosomes were not responsible for the effects seen. As subsequent data demonstrates that the effects on macrophage phenotype were PtdSer and anxA1-dependent (and exosomes do not express either), it seems unlikely that exosomes contribute to this phenomenon. Even if exosomes contribute to the conditioning of an aspect of macrophage phenotype not studied, the release of microvesicles in response to a stimulus is a much more rapid process[251] and may exert more immediate control.

The dis-inhibition of HLA-DR, DP & DQ, CD86 and CD206 upregulation by coating and making PtdSer unavailable for binding with anxA5, suggests these effects are similar to those imparted by apoptotic bodies which also present PtdSer. A similar effect is seen with IL-1β, although the initial decrease with $MV_{TNF\alpha}$ treatment is less striking and not significant. A much larger decrease in IL-12p70 was induced by $MV_{TNF\alpha}$, but which was only partially restored by blocking PtdSer, suggesting other factors may also mediate this effect. Perhaps the most striking effect of these microvesicles was their induction of TGFβ release regardless of other stimulation. In the presence of LPS and IFNγ this effect was diminished, but was independent of PtdSer blockade, suggesting that these microvesicles modulate macrophage phenotype by at least two separate pathways: one which is PtdSer-dependent, and one which is PtdSer-independent and culminates in the release of TGFβ. A caveat of this experiment is that an $MV_{TNF\alpha}$ + anxA5 in the absence of LPS and IFNγ was not included. Overall, these data are supported by work from the Schifferli lab demonstrating that control of macrophage activation and dendritic cell maturation is mediated, in part, by PtdSer exposed by neutrophil microvesicles[37,150,252].

These observations suggest a similarity between neutrophil microvesicles and

apoptotic bodies in the conditioning of macrophage phenotype. The tethering and phagocytosis of apoptotic bodies by macrophages depends on the interaction between PtdSer and a plethora of PtdSer receptors, including TAM receptors such as MerTK[253]. Uptake of apoptotic bodies and cells promotes a pro-resolving, wound-healing phenotype in macrophages which secretes TGFβ[254]. However, while it is tempting to make the assumption that neutrophil microvesicles and apoptotic bodies are acting in an identical manner on macrophages, apopotic bodies induce the secretion of IL-10 and even small amounts of IL-12 p70, whereas microvesicles reduced expression of both[255]. While they may share an uptake mechanism and perhaps some signalling pathways, the reduction of both IL-10 and IL-12 p70 by microvesicles suggest they achieve a net reduction in NFκB activation. It seems unlikely therefore that PtdSer is the only or even the primary signal in both cases and that the downstream effects depend on other mediators contained within the vesicles. This seems especially so as it was anxA1 and not PtdSer which was responsible for TGFβ release in response to neutrophil microvesicles.

The effects on cell phenotype that are mediated directly by PtdSer can be distinguished from those related to other mediators by treating macrophages with empty, PtdSer-exposing lipsomes. In fact, this has been performed both *in vitro* and in a model of myocardial infarct[256]. In this study, PtdSer was shown to be directly responsible for decreasing CD86 and increasing CD206 expression in the presence of LPS, but that it also strongly induces IL-10 secretion, and that it did not induce TGFβ release *in vitro* (although it did once administered *in vivo*). Taking these reported findings and the observations herein together, would suggest that PtdSer is both important for tethering, uptake, and signalling, but that the other components are also at work. For example, the reduction in IL-10 production despite PtdSer strongly inducing its secretion is interesting.

It is important to consider whether induction of TGFβ from macrophages is beneficial in the context of the rheumatic joint. In addition to being anti-inflammatory/pro-resolving, TGFβ is pro-fibrotic, and has been shown to drive pathological fibrosis in several disease settings[257–259]. Nevertheless, arthritides are diseases of destruction and catabolism, and supplementation has been shown to provide joint protection in models of osteoarthritis[260].

In light of the contribution of PtdSer to the pharmacodynamic effects of these microvesicles, the question was raised whether this is purely a signalling event, or whether it relies on the internalisation of the microvesicle to elicit the effect, due to PtdSer's role as an "eat me" signal. When comparing microvesicle labels, although PKH appeared the best detected and brightest fluorescent dye, it caused microvesicle lysis, making it difficult to tell whether membrane fragments or intact vesicles were

inside the cells. Additionally, this increased brightness may be attributable to the fluorescent particles present in this label. As such, CFSE was chosen as the most appropriate internalisation label instead.

The internalisation assay demonstrated that microvesicles are indeed quickly taken up, and that the process is dependent on both PtdSer on the microvesicle and its cognate receptor Mer expressed on the macrophages. As of yet, the question of whether internalisation or merely juxtacrine contact are required for the PtdSer-dependent effects on phenotype is not known, but future work where microvesicles are allowed to bind, but not enter the macrophages may answer this. This may also be addressed by selectively blocking the PI3 kinase and STAT1-mediated pathways from the receptor. This is relevant, as while PtdSer is important for internalisation, other components of the vesicles may be exerting control over phenotype, such as miRNA species. It also is not clear whether the primary uptake mechanism is endocytosis or phagocytosis-dependent. This could be addressed in future by using specific inhibitors of each process, although existing publications argue for both cases[119,120].

The presentation of apoptotic moeities, prominantly apoptotic neutrophils, at a site of acute inflammation is considered a critical checkpoint for resolution[155]. The expression of PtdSer receptors by macrophages facilitates both the removal of dead and dying cells (to prevent the release of DAMP during secondary necrosis) and the transition from a pro-inflammatory to an pro-resolving phenotype[255]. That MerTK, the best studied member of the TAM receptor family, is responsible for the PtdSer-mediated effects of $MV_{TNF\alpha}$ is suggestive that in some ways, neutrophil microvesicles mimic apoptotic bodies. In the context of acute inflammation, this process may serve to balance macrophage activation in a way that primes them for the resolution phase. The other TAM receptor family members, Tyro3 and Axl also bind PtdSer via Gas6 and Protein S, but as inhibition of MerTK signalling was sufficient to fully attenuate vesicle efficacy, these were not examined.

There are, however, two issues with this mechanism. The first is that not all neutrophil microvesicles express PtdSer, which begs the questions: are only the $PtdSer^+$ vesicles able to restrict activation in this way; and what, if any, effect do $PtdSer^-$ impart? The second issue is that most cell types have been reported to release a subset of $PtdSer^+$ microvesicles, and yet largely induce a pro-inflammatory phenotype in macrophages[261,262]. The only other cell type reported to release vesicles which restrict classical macrophage activation are those derived from mesenchymal stem cells[263].

MerTK was responsive to vesicle-presented PtdSer, despite the absence of exogenously added Gas6 or Protein S, the adaptors required for signalling to occur. While

one or both of these adaptors may be present in the culture medium (bovine Gas6 and Protein S share 81% and 82% sequence homology, respectively with the human proteins [BLAST accession numbers NP_000811.1, XP_005214103.1, NP_000304.2 & NP_776863.1]), it seems more likely that they are secreted in an autocrine fashion by the macrophages in culture themselves, as Gas6 in particular has been shown to be secreted from macrophages[174].

The proteome of microvesicles released from neutrophils stimulated in suspension with TNFα is different from those exposed to an activated endothelium[82]. Microvesicles produced in suspension induced a less inflammatory gene expression profile in naïve endothelium, while those *activated* by endothelium induced an inflammatory gene signature. While not fully explored, this may represent a dichotomy in functionality of neutrophil microvesicles produced pre and post extravasation, where intravascular vesicle release may serve to recruit additional waves of leucocytes, while their release in the inflammatory site promotes resolution. There was therefore rationale for comparing the effect of vesicles released from neutrophils before and after transmigration.

The transmigration of isolated neutrophils across HUVEC-coated transwells is a useful *in vitro* system to study extravasation and the phenotypic changes it induces. If only studying the number of cells which transmigrate, low yields of transmigration are still sufficient to see changes in response to different stimuli. The purpose of this system in the present study however, was to generate large numbers of microvesicles in response to transmigration and for this reason, microvesicles generated in the presence of serum (made extracellular vesicle-free and confirmed using the ImageStream) and a gradient of IL-8 were used for future study. IL-8 on its own induced a modest increase in neutrophil transmigration, but acted in synergy with serum (which on its own had no effect). Although this increase in transmigrated neutrophils did not raise the total yield of microvesicles below the transwell (paradoxically), it did raise the proportion of vesicles of neutrophil origin.

Perhaps unexpectedly, microvesicles collected from this system, both above and below the transwell, imparted similar effects on macrophage phenotype as $MV_{TNF\alpha}$. This might suggest that endothelial microvesicles share the pro-resolving properties of their neutrophil counterparts (for which there is evidence[264]), or simply that their presence was inconsequential and overcome by the neutrophil majority (as pro-inflammatory roles of endothelial microvesicles are also documented[34]).

When comparing the number of microvesicles per neutrophil (below the transwell) at collection, again the numbers were similar to those generated with TNFα or with synovial fluid from rheumatoid and osteoarthritis patients. As reported previously, microvesicles generated in response to these model stimuli were enriched in anxA1

where diluted synovial fluid induced the highest expression (although it is possible that the fluid itself contains soluble anxA1 which bound to the microvesicle PtdSer).

The induction of TGFβ by microvesicles generated from TNFα and synovial fluid (and likely any inflammatory stimulus) is at least partially dependent on anxA1 expressed on the microvesicle surface, despite only ≤20% of $MV_{TNF\alpha}$ expressing it on their surface. While this is not a response typically associated with the anxA1-ALX/FPR2 axis, it may be related to a general shift in the macrophages' phenotype towards M2a/c, which produce TGFβ and are classically induced with IL-4 or IL-10 (or glucocorticoids), respectively. AnxA1 also positively regulates TGFβ-signalling in breast cancer cells and may play a similar role in macrophages[265]. A similar effect has been reported in the induction of TGFβ release from chondrocytes induced by neutrophil $MV_{TNF\alpha}$[3], and $anxA1^+$ microvesicles derived from the gut epithelial cells have been shown to resolve tissue damage in the gut via activation of FPR2[2].

While FPR2, the cognate receptor for anxA1, was expressed in classical, alternative and naïve macrophages, its upregulation in classically activated macrophages may represent a negative feedback mechanism to regulate a pro-inflammatory phenotype. Interestingly, the percentage of $FPR2^+$ macrophages was comparable between phenotypes in permeabilised cells, suggesting that FPR2 may be stored in the cells and translocate to the plasma membrane in classical macrophages. *De novo* synthesis must also occur, as even in permeabilised cells, the relative expression values were higher than in alternative and naïve cells.

4.4 Microvesicle-treated macrophages are chondroprotective

The increase in glycosaminoglycan deposition by C28/I2 chondrocyte micromasses in response to TGFβ (known to be chondroprotective[266]) demonstrated the sensitivity of the model to anabolic stimuli. The lack of catabolic activity of IFNγ and IL-4 shows they have no direct effects on the chondrocytes themselves. Osteoarthritis synovial fluid was highly catabolic, likely due to the presence of metalloproteinases and cytokines, such as IL-1β. Surprisingly, rheumatoid arthritis synovial fluid showed only a trivial and non-significant reduction in matrix although this may reflect osteoarthritis as being the more overtly degradative disease[267]. IFNγ and rheumatoid synovial fluid-treated macrophage-conditioned medium was modestly catabolic, likely due to the induction of proteinases and/or IL-1β. Even medium from resting "M0" macrophages appeared catabolic, despite these cells appearing similar to M2 cells in culture. The anabolic effects of M2 macrophages may be related to decreased release of proteinases and/or an increase in TGFβ.

$MV_{TNF\alpha}$, MV_{RA} and MV_{OA} caused macrophages to release an anabolic mediator(s) into their medium, an effect which was wholly dependent on microvesicle-anxA1 and produced similar results to IL-4 treatment. As microvesicle delivery of anxA1 had already been shown to induce TGFβ release, it was only a small step to demonstrate in a single experiment that this is the primary mediator induced by the microvesicles to confer chondroprotection. This set of experiments demonstrates a long-lasting effect of $MV_{TNF\alpha}$, which are able to educate the macrophages.

4.5 Microvesicles affect the macrophage-fibroblast interaction

Synovial fibroblasts participate in disease progression during rheumatoid arthritis[268]. While during homeostasis, fibroblasts provide structure to the intimal lining of the synovium and facilitate movement of cells in and out of the synovial space, following onset of rheumatoid arthritis, they respond to the inflammatory synovium and adopt an activated phenotype. Once activated, synovial fibroblasts secrete proteinases, such as MMP1, MMP3, MMP13, cathepsins and aggrecanases, which degrade the extracellular matrix and cartilage surface[269–271].

Activated synovial fibroblasts contribute to the inflammatory milieu by releasing cytokines and growth factors, such as MCP-1[269], VEGF[272], IL-6[273] and GM-CSF[274], supporting leucocyte recruitment, delaying neutrophil apoptosis and propagating pannus hyperplasia. As the synovial lining is comprised of fibroblasts and macrophages, whether microvesicle stimulation could promulgate an anti-inflammatory phenotype from macrophages to fibroblasts was examined.

Responding to arthritic synovial fluid as a model stimulus, the increased expression of VCAM-1, CD55, IL-6, MCP-1 and TNFα was indicative of an inflammatory phenotype in primary synovial fibroblasts, although CD21 expression didn't increase as reported[243]. Incubation of otherwise naïve fibroblasts with classically activated macrophages resulted in a pro-inflammatory change in fibroblast phenotype. While the change in each individual antigen was not as pronounced as in response to synovial fluid, the combined change in antigen expression was sufficient to discriminate these fibroblasts from those cultured with alternatively-activated or naïve macrophages. Interestingly, alternatively-activated macrophages induced even higher MCP-1 production from fibroblasts which appears counter-intuitive. A major caveat of this co-culture system is that while the fibroblasts are derived from the inflamed synovia of rheumatoid arthritis patients, the macrophages are not.

The ability of $MV_{TNF\alpha}$ to abrogate the pro-inflammatory effect classically activated macrophages have on fibroblast phenotype is most likely due to the fact that

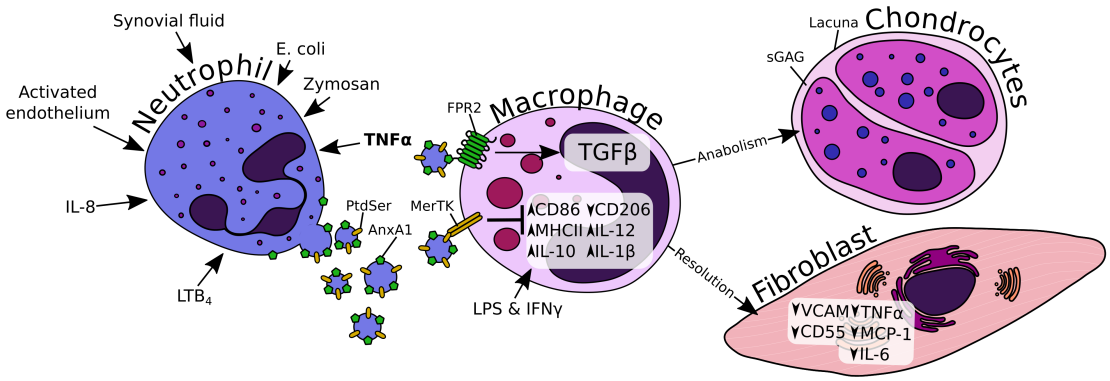

Figure 4.1: Graphical summary of the working hypothesis. Stimulation of neutrophils by pro-inflammatory mediators induces the release of microvesicles, a proportion of which expose phosphatidylserine (PtdSer) and annexin A1 (AnxA1). Vesicle-bound anxA1 induces the production of transforming growth factor β (TGFβ) which stimulates the production of sulphated glycosaminoglycans (sGAG) by chondrocytes. The interaction between PtdSer and MerTK restricts macrophage response to pro-inflammatory stimuli, and prevents the pro-inflammatory activation of synovial fibroblasts.

the microvesicles prevent the classical activation in the first place. Nevertheless, the data suggest that in an inflamed synovium, microvesicle-induced resistance to classical activation has consequences for the influence macrophages exert on other cell types.

The working hypothesis based on the data collected thus far is therefore that within the synovium of rheumatoid arthritis patients, recruitment and activation of neutrophils induces the release of microvesicles. These microvesicles, by interacting with synovial macrophages, can deliver pro-resolving signals via engagement of the MerTK receptor by exposed PtdSer, and regulate the pro-inflammatory polarisation of these macrophages. Engagement of ALX/FPR2 by anxA1 and the subsequent release of TGFβ could also modulate macrophage phenotype but may also directly counter cartilage degradation (summarised in Figure 4.1). While these mechanisms, if present, are clearly not sufficient to induce resolution, they may prolong cartilage integrity. It must be noted that the approach taken in the project has not been unbiased in selection of antigens to compare macrophage phenotype. As such, it is possible and quite likely that many other antigens are modulated by $MV_{TNF\alpha}$ that were not probed for, and which may be dependent or independent of the PtdSer and anxA1 mechanisms identified thus far. An unbiased approach, such as a microarray or RNA sequencing of $MV_{TNF\alpha}$-conditioned macrophages, would provide a broader view.

4.6 Biological functions of $MV_{TNF\alpha}$ are relevant *in vivo*

The recapitulation of the efficacy seen in human macrophages *in vitro* in mice, demonstrates that the efficacy observed is a real biological phenomenon. The modulation of MHCII, CD86 and CD206 seen in mice completely reproduced the trends seen in human cells. What is more interesting is that these effects are observed despite the xenogeneic nature of the vesicle adoptive transfer, where human neutrophil vesicles are administered to mice. This *modus operandi* was chosen as it is difficult to generate large numbers of microvesicles from mouse neutrophils, and has been demonstrated to be effective with no immunogenic response[3]. The increase in TGFβ in the cavity in response to $MV_{TNF\alpha}$ was particularly supportive of the previous data, although it must be remembered that in this crude *in vivo* model, microvesicles interact with more cell types than just macrophages, and that an array of different cell types contribute to the overall cytokine profile of the lavage fluid.

It must be noted that despite the recapitulation of antigen expression changes in the peritonitis model, the absolute changes in relative expression were much smaller than observed *in vitro*. This is likely partially due to the complex nature of an *in vivo* compartment, containing many competing signals and generating a larger amount of noise above which the signal must rise, but also because the ratio of microvesicles to macrophages would be considerably smaller than in the *in vitro* setting. Indeed, the peritoneal cavity of a mouse has a large surface area, and even after the injection of 5×10^7 $MV_{TNF\alpha}$, the change in macrophage phenotype observed was small, despite being statistically significant.

To address this second issue, and to test this effect in a more arthritis-relevant setting, a smaller inflammatory compartment was chosen: the synovial space in the ankles of mice undergoing K/BxN arthritis. In this model, a smaller number of vesicles could be injected per compartment, but still achieve a higher concentration of vesicles in the biological space. Again the phenotype of the macrophages in this setting responded to $MV_{TNF\alpha}$ treatment as supported by all the previous *in vitro* and *in vivo* data. Not only this, but the magnitude of change in antigen expression was greater than in the peritonitis model (though still not as large as *in vitro*). While this experiment also aimed to phenotype synovial fibroblasts using the phenotypic markers thus far shown to indicate an inflammatory phenotype, not enough cells could be identified from such a small source of tissue.

The importance of the findings thus far is that microvesicles may represent a manipulatable mechanism to target the inflammatory diseases, such as arthritides, including the prospect of using them as autologous therapeutic vectors as previously

demonstrated in mice[158,275]. This form of therapy could rely on the generation of certain populations of microvesicles from the patient and reintroducing them "as are" or following biochemical manipulation, to form a truly personalised medicine.

4.7 RA $MV_{TNF\alpha}$ as an autologous biologic therapy

While blood neutrophils from rheumatoid arthritis patients produced anxA1$^+$ microvesicles in response to TNFα, the relative increase in number was smaller than generally observed in healthy donors. Additionally, while the expression of anxA1 was comparable between healthy donor and rheumatoid arthritis patient $MV_{TNF\alpha}$, the expression of anxA1 on constitutively released microvesicles was higher from these patients than observed in healthy controls. This is perhaps surprising in that no major differences are reported between circulating neutrophils of healthy and rheumatoid arthritis donors[276,277], although the sample size is small and patient blood had to be transported before neutrophil isolation could begin. There were also no differences in the proportion of anxA1$^+$ *neutrophil* microvesicles in the plasma of rheumatoid arthritis patients and healthy controls. This data is surprising, because *overall* there is an increase in the proportion of anxA1$^+$ microvesicles, these differences are not represented across monocyte or neutrophil vesicles, typically the two main populations to express anxA1.

It would be interesting to compare blood neutrophils from these patients with their synovial neutrophils, which have been shown to be greatly activated[276], but the logistics of isolating enough neutrophils from the available volume of synovial fluid was prohibitive in this study.

There is a clear relationship between the number of neutrophils stimulated with TNFα and the number of microvesicles which could be recovered per cell. This relationship could suggest that the interaction with other neutrophils increases their release of microvesicles or, perhaps more likely, that the number of microvesicles lost during isolation remains largely constant and independent of starting number. The purpose of comparing this relationship between healthy control and rheumatoid arthritis patient neutrophils, was to compare whether they have equivalent potential for ectocytosis. As the volume of blood that could be drawn from rheumatoid arthritis patients was lower, enough neutrophils could not be isolated to compare across the range of starting neutrophils collected from healthy controls, although the relationship is similar in the lower end of neutrophil numbers.

Despite slight differences in the number of microvesicles produced and their increased basal level of anxA1 expression, $MV_{TNF\alpha}$ from rheumatoid arthritis patients

demonstrated remarkably similar efficacy on macrophage phenotype as those derived from healthy control neutrophils. The main difference observed between the populations was in their induction of TGFβ production, despite comparable proportions of each expressing the protein. This suggested that, at least in a pharmacodynamic sense, microvesicles generated *ex vivo* from the neutrophils of rheumatoid arthritis patients have the potential to restrict classical macrophage activation.

The issue had been considered that use of autologous microvesicles as a therapy would involved the administration of protective vesicles, into a milieu highly dense with heterologous vesicles. As such, a model system was created to explore whether $MV_{TNF\alpha}$ from rheumatoid arthritis patients could outcompete the effects of pro-inflammatory populations of vesicles. This was performed by using both platelet-derived vesicles (as an isolated population) and total synovial fluid microvesicles (as a heterologous, disease-model population).

It was desirable to generate vesicles from platelets using the same stimulation as neutrophils to examine whether any differences observed between the microvesicles was purely cell type-dependent. Despite not widely considered a canonical platelet agonist, platelets do express TNF receptors 1 and 2, are activated by TNFα[278], and as the data demonstrate, release large numbers of microvesicles in response to it.

Platelet microvesicles appeared to mildly induce a pro-inflammatory phenotype in macrophages, although their lack of cytokine modulation may be due to a lack of any TLR signal. Although much of the efficacy observed in neutrophil $MV_{TNF\alpha}$ is attributable to PtdSer, a subset of platelet microvesicles (and those from other cell types) also express PtdSer[83]. This suggests that induction of the STAT1 signalling pathway through MerTK is insufficient on its own to restrict macrophage activation, and that internalisation of the microvesicles to deliver their luminal cargo via PtdSer may be more important.

A similar, but more pronounced, effect on macrophage activation is observed in response to total synovial fluid microvesicles. The small increases observed in IL-12 p70 and IL-1β release may have been related to residual TLR ligands from the synovial fluid used to isolate the vesicles, although the changes seen cannot be considered biologically relevant.

Neutrophil $MV_{TNF\alpha}$ from rheumatoid arthritis patients were able to outcompete the pro-inflammatory effects of those derived from platelets. This demonstrates that populations of vesicles with seemingly opposing actions, are in competition to bind to, and exert their efficacy on their target cells. When the ratio of neutrophil:platelet vesicles was 1:1, platelet efficacy was reduced to ~50% , suggesting that both populations of vesicles may be competing for the same binding sites, or that macrophages have a limited capacity to internalise these structures.

Neutrophil $MV_{TNF\alpha}$ were also able to compete with the total synovial fluid vesicles, although a 1:1 ratio was not sufficient to reduce the efficacy of synovial vesicles to 50%. In fact, a much larger ratio of neutrophil:synovial microvesicles was required to nullify the effects of the latter, possibly suggestive of an overall more inflammatory profile compared to platelet microvesicles.

4.8 HEK-AnxA1 cells

Despite the use of a bicistronic expression vector to transfect anxA1 and bsd genes into HEK293 cells, after antibiotic selection (which completely killed the control-transfected cells), only 14.7% of cells were positive. Serial dilution of the polyclonal population identified 5 colonies which were almost completely positive for the anxA1.

Vesicles released from these colonies in response to the Ca^{2+} ionophore, ionomycin, were only 3.7% positive for anxA1 despite virtually all the cells being positive. This may be related to low anxA1 copy numbers per cell post transfection or that HEK cells lack the cellular machinery to externalise anxA1 onto outer membrane leaflets. Neutrophils themselves express high levels of anxA1 which is split between two compartments: the granules (mainly gelatinase), and the cytosol[279]. Upon cell activation and Ca^{2+} flux, the granule pool of anxA1 is rapidly translocated to the cell surface[167], and it is thought that this is the pool of anxA1 which is subsequently incorporated onto the outer microvesicle membrane leaflet[36]. HEK cells do not contain such granules and may therefore lack the machinery to efficiently externalise anxA1, despite storing a cytosolic pool. It may therefore not be that surprising to observe such low expression on the surface their vesicles, but may potentially be luminal instead.

Perhaps to be expected after observing such low anxA1 levels on their surface, HEK-AnxA1 microvesicles did not induce TGFβ release from macrophages. This is in stark contrast to microvesicles from primary neutrophils, whose induction of TGFβ was entirely dependent on their anxA1 exposure. While this may be due to the low frequency of $anxA1^{+}$ vesicles released by HEK-AnxA1 cells, even vesicles from primary neutrophils are only ~20% positive for anxA1, and so an absence of any effect is quite surprising. The result could also depend on the antigen density of anxA1 on each vesicle, which may be much higher in primary neutrophils. An alternative explanation is that anxA1 is serving to target microvesicles to the plasma membrane of macrophages, rather than directly signalling through FPR2, and that they achieve their efficacy by another component, perhaps luminal, which is present in neutrophil microvesicles, but not those from HEK293 cells. These results suggest that while cells can be engineered to secrete vesicles expressing proteins of interest,

the process is non-trivial, depends on the level of expression, the protein being naturally secreted via vesicles, and a more intimate understanding of how the protein is responsible for the desired efficacy. A more pragmatic approach may be to identify endogenous populations of vesicles with beneficial components, and attempt to harness or even manipulate them for therapeutic gain. It is also possible that a cell line more amenable to become a "neutrophil-like" cell upon specific stimulation (such as HL60 or NB4 cells) might be more suitable than HEK293 cells.

4.9 Perspective and future work

This project has reproduced initial findings by others, demonstrating that microvesicles released from neutrophils are able to restrict the classical activation of macrophages, although do not themselves promote alternative activation. In a manner similar to the control apoptotic bodies exert control over macrophage phenotype, microvesicles from neutrophils mediate most of the effects studied by presenting PtdSer to macrophage-expressed MerTK. In this way, neutrophils, which are becoming recognised as orchestrators of resolution in their own right, may prime cells within an inflamed environment for the initiation of resolution.

That the PtdSer-independent induction of TGFβ by $MV_{TNF\alpha}$ has been shown to depend on anxA1 demonstrates a previously un-reported function of this glucocorticoid-induced mediator of resolution. The temporally-appropriate secretion of TGFβ at sites of inflammation is important for the restoration of the homeostatic tissue architecture during the resolution phase.

As rheumatoid arthritis is a disease of loss of tolerance, it is unlikely that the use of microvesicles will offer a curative therapy. However, the regulation of macrophage phenotypes *in vitro* and *in vivo*, and the modulation of the way macrophages condition cartilage matrix deposition by chondrocytes and fibroblast phenotype, suggest that neutrophil microvesicles could regulate the inflammation and tissue damage in the rheumatic joint. They may, therefore, produce potentially long lasting effects within the joint compartment. Indeed, data on the direct effects of these vesicles on chondrocyte survival and cartilage integrity in arthritic mice[3] suggest that while they may not induce resolution, they can reverse cartilage destruction, something no therapy currently does. The data presented here suggest the potential for neutrophil microvesicles to provide this protection via cell-mediated, as well as a direct, interactions.

While this project has only touched the surface of exploring the appropriateness of neutrophil microvesicles as a therapy, there is far more work to be done to explore both the mechanism of control, and whether disease benefit can be observed in *in*

vivo models. For example, the question of whether vesicle internalisation (and by endocytosis or phagocytosis) is required for the PtdSer-mediated effects is unclear, and difficult to separate. One way in which this may be addressed is by selectively inhibiting the PI3 kinase and STAT1 pathways downstream of MerTK, individually, and establishing if the efficacy is perturbed when one or both pathways is blocked. While clear effects on phenotype could be observed in the K/BxN model of arthritis, this study has not been able to evaluate whether this translates into a reduction in disease score. This is an important pre-clinical experiment to perform for these vesicles to be considered a credible treatment, but presents challenges, particularly around dosing. The number of vesicles per dose, frequency of dosing and the route of administration will need careful planning and experimentation. Vesicles injected intravenously are readily lost to the spleen, liver and intestinal tract[280], and so vesicles administered by this route may need to be injected in larger numbers, or otherwise targeted to the joints. Alternatively, intra-articular injection largely avoids this problem, but repeated administration via this route is likely to cause damage, and is unjustifiable in both mice and humans.

Whether autologous or cell line-produced vesicles represent the greatest chance of success depends largely on whether cell lines can be easily engineered to produce vesicles possessing beneficial properties. While physiological populations of vesicles, such as those from neutrophils and mesenchymal stem cells, may already possess these properties physiologically, they represent problems of volume and quality control. Nevertheless, this study has provided basic evidence of the potential of vesicles as therapies in inflammatory conditions, that future work can build upon.

Bibliography

1. Headland, S. E., Jones, H. R., D'Sa, A. S. V., Perretti, M. & Norling, L. V. Cutting-Edge Analysis of Extracellular Microparticles using ImageStreamX Imaging Flow Cytometry. en. *Sci. Rep.* **4.** ISSN: 2045-2322. doi:10.1038/srep05237 (June 2014).
2. Leoni, G. *et al.* Annexin A1–containing extracellular vesicles and polymeric nanoparticles promote epithelial wound repair. *J. Clin. Invest.* ISSN: 0021-9738. doi:10.1172/JCI76693 (Feb. 2015).
3. Headland, S. E. *et al.* Neutrophil-derived microvesicles enter cartilage and protect the joint in inflammatory arthritis. *Sci. Transl. Med.* **7,** 315ra190–315ra190. ISSN: 1946-6234 (Nov. 2015).
4. Jones, H. R., Robb, C. T., Perretti, M. & Rossi, A. G. The role of neutrophils in inflammation resolution. *Semin. Immunol.* **28,** 137–145. ISSN: 10445323 (Apr. 2016).
5. Norling, L. L. V. L. *et al.* Proresolving and cartilage-protective actions of resolvin D1 in inflammatory arthritis. *JCI Insight* **1,** 2707–2710. ISSN: 2379-3708 (Apr. 2016).
6. Chargaff, E. & West, R. The biological significance of the thromboplastic protein of blood. *J. Biol. Chem.* **166,** 189–97. ISSN: 0021-9258 (Nov. 1946).
7. Wolf, P. The Nature and Significance of Platelet Products in Human Plasma. *Br. J. Haematol.* **13,** 269–288. ISSN: 0007-1048 (May 1967).
8. Palay, S. L. & Palade, G. E. The fine structure of neurons. *J. Biophys. Biochem. Cytol.* **1,** 69–88. ISSN: 0095-9901 (Jan. 1955).
9. Estable, C., Acosta-ferreira, W. & Sotelo, j. r. An electron microscope study of the regenerating nerve fibers. *Z. Zellforsch. Mikrosk. Anat.* **46,** 387–99. ISSN: 0340-0336 (Jan. 1957).
10. Zettergvist, H. *The ultrastructural organization of the columnar absorbing cells of the mouse jejunum: an electron microscopic study including some experiments regarding the problem of fixation and an investigation of vitamin A deficiency* (1956).
11. Palade, G. E. Studies on the endoplasmic reticulum. II. Simple dispositions in cells in situ. *J. Biophys. Biochem. Cytol.* **1,** 567–82. ISSN: 0095-9901 (Nov. 1955).

12. Sotelo, J. R. & Porter, K. R. An electron microscope study of the rat ovum. *J. Biophys. Biochem. Cytol.* **5,** 327–42. ISSN: 0095-9901 (Mar. 1959).

13. Feller, W. F. & Chopra, H. C. A small virus-like particle observed in human breast cancer by means of electron microscopy. *J. Natl. Cancer Inst.* **40,** 1359–73. ISSN: 0027-8874 (June 1968).

14. Benz, E. W. & Moses, H. L. Small, Virus-Like Particles Detected in Bovine Sera by Electron Microscopy. *J. Natl. Cancer Inst.* **52,** 1931–4. ISSN: 0027-8874 (June 1974).

15. Dalton, A. J. Microvesicles and vesicles of multivesicular bodies versus "virus-like" particles. *J. Natl. Cancer Inst.* **54,** 1137–48. ISSN: 0027-8874 (May 1975).

16. ODOR, D. L. Electron microscopic studies on ovarian oocytes and unfertilized tubal ova in the rat. *J. Biophys. Biochem. Cytol.* **7,** 567–74. ISSN: 0095-9901 (June 1960).

17. Wischnitzer, S. An electron microscope study of cytoplasmic organelle transformations in developing mouse oocytes. *Wilhelm Roux. Arch. Entwickl. Mech. Org.* **166,** 150–172. ISSN: 0949-944X (June 1970).

18. Hascall, G. K. Ultrastructure of the chondrocytes and extracellular matrix of the Swarm rat chondrosarcoma. *Anat. Rec.* **198,** 135–146. ISSN: 0003-276X (Oct. 1980).

19. Trams, E. G., Lauter, C. J., Salem, N. & Heine, U. Exfoliation of membrane ecto-enzymes in the form of micro-vesicles. *Biochim. Biophys. Acta* **645,** 63–70. ISSN: 0006-3002 (July 1981).

20. Ronquist, G. & Brody, I. The prostasome: its secretion and function in man. *Biochim. Biophys. Acta* **822,** 203–18. ISSN: 0006-3002 (Sept. 1985).

21. Johnstone, R. M., Bianchini, A. & Teng, K. Reticulocyte maturation and exosome release: transferrin receptor containing exosomes shows multiple plasma membrane functions. *Blood* **74,** 1844–51. ISSN: 0006-4971 (Oct. 1989).

22. Johnstone, R. M. & Ahn, J. A common mechanism may be involved in the selective loss of plasma membrane functions during reticulocyte maturation. *Biomed. Biochim. Acta* **49,** S70–5. ISSN: 0232-766X (Jan. 1990).

23. Johnstone, R. M., Mathew, A., Mason, A. B. & Teng, K. Exosome formation during maturation of mammalian and avian reticulocytes: evidence that exosome release is a major route for externalization of obsolete membrane proteins. *J. Cell. Physiol.* **147,** 27–36. ISSN: 0021-9541 (Apr. 1991).

24. Stein, J. M. & Luzio, J. P. Ectocytosis caused by sublytic autologous complement attack on human neutrophils. The sorting of endogenous plasma-membrane proteins and lipids into shed vesicles. *Biochem. J.* **274 (Pt 2,** 381–6. ISSN: 0264-6021 (Mar. 1991).

25. Scott, R. E. Undifferentiated and differentiated L6 myoblast plasma membranes. I: Comparison of the morphology of plasma membrane vesiculation and the factors influencing the vesiculation process. *Cell Differ.* **7,** 325–34. ISSN: 0045-6039 (Dec. 1978).

26. Nomura, S. *et al.* Microparticle generation during in vitro platelet activation by anti-CD9 murine monoclonal antibodies. *Thromb. Res.* **62,** 429–39. ISSN: 0049-3848 (June 1991).

27. Scott, R. E. & Maercklein, P. B. Plasma membrane vesiculation in 3T3 and SV3T3 cells. II. Factors affecting the process of vesiculation. *J. Cell Sci.* **35,** 245–52. ISSN: 0021-9533 (Feb. 1979).

28. Kerr, J. F. R. A histochemical study of hypertrophy and ischaemic injury of rat liver with special reference to changes in lysosomes. *J. Pathol. Bacteriol.* **90,** 419–435. ISSN: 0368-3494 (Oct. 1965).

29. Kerr, J. F. R., Wyllie, A. H. & Currie, A. R. Apoptosis: A Basic Biological Phenomenon with Wideranging Implications in Tissue Kinetics. *Br. J. Cancer* **26,** 239–257. ISSN: 0007-0920 (Aug. 1972).

30. Bennett, M. R., Gibson, D. F., Schwartz, S. M. & Tait, J. F. Binding and phagocytosis of apoptotic vascular smooth muscle cells is mediated in part by exposure of phosphatidylserine. *Circ. Res.* **77,** 1136–42. ISSN: 0009-7330 (Dec. 1995).

31. Chang, C. P., Zhao, J., Wiedmer, T. & Sims, P. J. Contribution of platelet microparticle formation and granule secretion to the transmembrane migration of phosphatidylserine. *J. Biol. Chem.* **268,** 7171–8. ISSN: 0021-9258 (Apr. 1993).

32. MacKenzie, A. *et al.* Rapid secretion of interleukin-1beta by microvesicle shedding. *Immunity* **15,** 825–35. ISSN: 1074-7613 (Nov. 2001).

33. Lee, R., Williams, J. C. & Mackman, N. P2X7 regulation of macrophage tissue factor activity and microparticle generation. *J. Thromb. Haemost.* **10,** 1965–7. ISSN: 1538-7836 (Sept. 2012).

34. Curtis, A. M. *et al.* p38 mitogen-activated protein kinase targets the production of proinflammatory endothelial microparticles. *J. Thromb. Haemost.* **7,** 701–9. ISSN: 1538-7836 (Apr. 2009).

35. Barry, O. P., Pratico, D., Lawson, J. A. & FitzGerald, G. A. Transcellular activation of platelets and endothelial cells by bioactive lipids in platelet microparticles. en. *J. Clin. Invest.* **99,** 2118–27. ISSN: 0021-9738 (May 1997).

36. Dalli, J. *et al.* Annexin 1 mediates the rapid anti-inflammatory effects of neutrophil-derived microparticles. *Blood* **112,** 2512–9. ISSN: 1528-0020 (Sept. 2008).

37. Gasser, O. & Schifferli, J. A. Activated polymorphonuclear neutrophils disseminate anti-inflammatory microparticles by ectocytosis. *Blood* **104,** 2543–8. ISSN: 0006-4971 (Oct. 2004).

38. Martin, P. J., Treves, S., Schifferli, J. A., Eken, C. & Sadallah, S. *Ectosomes of polymorphonuclear neutrophils activate multiple signaling pathways in macrophages* 2012. doi:10.1016/j.imbio.2012.05.021.

39. Van der Pol, E., Böing, A. N., Harrison, P., Sturk, A. & Nieuwland, R. Classification, functions, and clinical relevance of extracellular vesicles. *Pharmacol. Rev.* **64,** 676–705. ISSN: 1521-0081 (July 2012).

40. Kulp, A. & Kuehn, M. J. Biological functions and biogenesis of secreted bacterial outer membrane vesicles. *Annu. Rev. Microbiol.* **64,** 163–84. ISSN: 1545-3251 (Jan. 2010).

41. Morel, O., Jesel, L., Freyssinet, J.-M. & Toti, F. Cellular mechanisms underlying the formation of circulating microparticles. *Arterioscler. Thromb. Vasc. Biol.* **31,** 15–26. ISSN: 1524-4636 (Jan. 2011).

42. Wilson, H. L., Francis, S. E., Dower, S. K. & Crossman, D. C. Secretion of intracellular IL-1 receptor antagonist (type 1) is dependent on P2X7 receptor activation. *J. Immunol.* **173,** 1202–8. ISSN: 0022-1767 (July 2004).

43. Heijnen, H. F., Schiel, A. E., Fijnheer, R., Geuze, H. J. & Sixma, J. J. Activated platelets release two types of membrane vesicles: microvesicles by surface shedding and exosomes derived from exocytosis of multivesicular bodies and alpha-granules. *Blood* **94,** 3791–9. ISSN: 0006-4971 (Dec. 1999).

44. Obregon, C., Rothen-Rutishauser, B., Gitahi, S. K., Gehr, P. & Nicod, L. P. Exovesicles from Human Activated Dendritic Cells Fuse with Resting Dendritic Cells, Allowing Them to Present Alloantigens. *Am. J. Pathol.* **169,** 2127–2136. ISSN: 00029440 (Dec. 2006).

45. Heemskerk, J. W., Vuist, W. M., Feijge, M. A., Reutelingsperger, C. P. & Lindhout, T. Collagen but not fibrinogen surfaces induce bleb formation, exposure of phosphatidylserine, and procoagulant activity of adherent platelets: evidence for regulation by protein tyrosine kinase-dependent Ca2+ responses. *Blood* **90,** 2615–25. ISSN: 0006-4971 (Oct. 1997).

46. Pasquet, J. M., Dachary-Prigent, J. & Nurden, A. T. Microvesicle release is associated with extensive protein tyrosine dephosphorylation in platelets stimulated by A23187 or a mixture of thrombin and collagen. *Biochem. J.* **333 (Pt 3,** 591–9. ISSN: 0264-6021 (Aug. 1998).

47. Hakoshima, T., Shimizu, T. & Maesaki, R. Structural basis of the Rho GTPase signaling. *J. Biochem.* **134,** 327–31. ISSN: 0021-924X (Sept. 2003).

48. Tybulewicz, V. L. J. & Henderson, R. B. Rho family GTPases and their regulators in lymphocytes. *Nat. Rev. Immunol.* **9,** 630–44. ISSN: 1474-1741 (Sept. 2009).

49. Traut, T. W. Physiological concentrations of purines and pyrimidines. *Mol. Cell. Biochem.* **140,** 1–22. ISSN: 0300-8177 (1994).

50. Trahey, M. & McCormick, F. A cytoplasmic protein stimulates normal N-ras p21 GTPase, but does not affect oncogenic mutants. *Science* **238,** 542–5. ISSN: 0036-8075 (Oct. 1987).

51. Vogel, U. S. *et al.* Cloning of bovine GAP and its interaction with oncogenic ras p21. *Nature* **335,** 90–93. ISSN: 0028-0836 (Sept. 1988).

52. Trahey, M. *et al.* Molecular cloning of two types of GAP complementary DNA from human placenta. *Science* **242,** 1697–700. ISSN: 0036-8075 (Dec. 1988).

53. Sapet, C. *et al.* Thrombin-induced endothelial microparticle generation: identification of a novel pathway involving ROCK-II activation by caspase-2. en. *Blood* **108,** 1868–76. ISSN: 0006-4971 (Sept. 2006).

54. Ishizaki, T. *et al.* The small GTP-binding protein Rho binds to and activates a 160 kDa Ser/Thr protein kinase homologous to myotonic dystrophy kinase. *EMBO J.* **15,** 1885–93. ISSN: 0261-4189 (Apr. 1996).

55. Matsui, T. *et al.* Rho-associated kinase, a novel serine/threonine kinase, as a putative target for small GTP binding protein Rho. *EMBO J.* **15,** 2208–16. ISSN: 0261-4189 (May 1996).

56. Leung, T., Chen, X. Q., Manser, E. & Lim, L. The p160 RhoA-binding kinase ROK alpha is a member of a kinase family and is involved in the reorganization of the cytoskeleton. *Mol. Cell. Biol.* **16,** 5313–27. ISSN: 0270-7306 (Oct. 1996).

57. Coleman, M. L. *et al.* Membrane blebbing during apoptosis results from caspase-mediated activation of ROCK I. *Nat. Cell Biol.* **3,** 339–345. ISSN: 14657392 (Apr. 2001).

58. Hugel, B., Martínez, M. C., Kunzelmann, C. & Freyssinet, J.-M. Membrane Microparticles: Two Sides of the Coin. *Physiology* **20** (2005).

59. Martinez, M. C., Tual-Chalot, S., Leonetti, D. & Andriantsitohaina, R. Microparticles: targets and tools in cardiovascular disease. *Trends Pharmacol. Sci.* **32,** 659–665. ISSN: 1873-3735 (Nov. 2011).

60. Betapudi, V. *et al.* Anti-β2GPI antibodies stimulate endothelial cell microparticle release via a nonmuscle myosin II motor protein-dependent pathway. *Blood* **122.** ISSN: 1528-0020. doi:10.1182/blood-2013-03-490318 (Aug. 2013).

61. Vardouli, L., Moustakas, A. & Stournaras, C. LIM-kinase 2 and cofilin phosphorylation mediate actin cytoskeleton reorganization induced by transforming growth factor-beta. *J. Biol. Chem.* **280,** 11448–57. ISSN: 0021-9258 (Mar. 2005).

62. Galkin, V. E. *et al.* Remodeling of actin filaments by ADF/cofilin proteins. *Proc. Natl. Acad. Sci.* **108,** 20568–20572. ISSN: 0027-8424 (Dec. 2011).

63. Weernink, P. A. O. Stimulation of Phosphatidylinositol-4-phosphate 5-Kinase by Rho-Kinase. *J. Biol. Chem.* **275,** 10168–10174. ISSN: 00219258 (Mar. 2000).

64. Shcherbina, A. & Remold-O'Donnell, E. Role of caspase in a subset of human platelet activation responses. *Blood* **93,** 4222–31. ISSN: 0006-4971 (June 1999).

65. Dachary-Prigent, J., Pasquet, J. M., Freyssinet, J. M. & Nurden, A. T. Calcium involvement in aminophospholipid exposure and microparticle formation during platelet activation: a study using Ca2+-ATPase inhibitors. *Biochemistry* **34,** 11625–34. ISSN: 0006-2960 (Sept. 1995).

66. Khorchid, A. & Ikura, M. How calpain is activated by calcium. *Nat. Struct. Biol.* **9,** 239–241. ISSN: 10728368 (Apr. 2002).

67. Yano, Y. *et al.* The effects of calpeptin (a calpain specific inhibitor) on agonist induced microparticle formation from the platelet plasma membrane. *Thromb. Res.* **71,** 385–96. ISSN: 0049-3848 (Sept. 1993).

68. Schoenwaelder, S. M. & Burridge, K. Evidence for a Calpeptin-sensitive Protein-tyrosine Phosphatase Upstream of the Small GTPase Rho: A NOVEL ROLE FOR THE CALPAIN INHIBITOR CALPEPTIN IN THE INHIBITION OF PROTEIN-TYROSINE PHOSPHATASES. *J. Biol. Chem.* **274,** 14359–14367. ISSN: 0021-9258 (May 1999).

69. Van Meer, G., Voelker, D. R. & Feigenson, G. W. Membrane lipids: where they are and how they behave. *Nat. Rev. Mol. Cell Biol.* **9,** 112–24. ISSN: 1471-0080 (Feb. 2008).

70. Rothman, J. & Lenard, J. Membrane asymmetry. *Science (80-.).* **195** (1977).

71. Buton, X., Morrot, G., Fellmann, P. & Seigneuret, M. Ultrafast glycerophospholipid-selective transbilayer motion mediated by a protein in the endoplasmic reticulum membrane. *J. Biol. Chem.* **271,** 6651–7. ISSN: 0021-9258 (Mar. 1996).

72. Bell, R. M., Ballas, L. M. & Coleman, R. A. Lipid topogenesis. *J. Lipid Res.* **22,** 391–403. ISSN: 0022-2275 (Mar. 1981).

73. Heemskerk, J. W. M., Bevers, E. M. & Lindhout, T. Platelet activation and blood coagulation. *Thromb. Haemost.* **88,** 186–93. ISSN: 0340-6245 (Aug. 2002).

74. Bodin, S. & Welch, M. D. Plasma membrane organization is essential for balancing competing pseudopod- and uropod-promoting signals during neutrophil polarization and migration. *Mol. Biol. Cell* **16,** 5773–83. ISSN: 1059-1524 (Dec. 2005).

75. Tang, X., Halleck, M. S., Schlegel, R. A. & Williamson, P. A subfamily of P-type ATPases with aminophospholipid transporting activity. *Science* **272,** 1495–7. ISSN: 0036-8075 (June 1996).

76. Devaux, P. F., Herrmann, A., Ohlwein, N. & Kozlov, M. M. How lipid flippases can modulate membrane structure. *Biochim. Biophys. Acta - Biomembr.* **1778,** 1591–1600. ISSN: 00052736 (2008).

77. Serra, M. V., Kamp, D. & Haest, C. W. Pathways for flip-flop of mono- and di-anionic phospholipids in the erythrocyte membrane. *Biochim. Biophys. Acta* **1282,** 263–73. ISSN: 0006-3002 (July 1996).

78. Yang, H. *et al.* TMEM16F forms a Ca2+-activated cation channel required for lipid scrambling in platelets during blood coagulation. *Cell* **151,** 111–22. ISSN: 1097-4172 (Sept. 2012).

79. Suzuki, J. & Nagata, S. *Phospholipid scrambling by TMEM16F* Dec. 2011. doi:10.1038/nature09583.

80. Suzuki, J., Umeda, M., Sims, P. J. & Nagata, S. Calcium-dependent phospholipid scrambling by TMEM16F. *Nature* **468,** 834–8. ISSN: 1476-4687 (Dec. 2010).

81. Van Kruchten, R. *et al.* Both TMEM16F-dependent and TMEM16F-independent pathways contribute to phosphatidylserine exposure in platelet apoptosis and platelet activation. *Blood* **121,** 1850–1857. ISSN: 00064971 (2013).

82. Dalli, J. *et al.* Heterogeneity in neutrophil microparticles reveals distinct proteome and functional properties. *Mol. Cell. Proteomics* **12,** 2205–19. ISSN: 1535-9484 (Aug. 2013).

83. Arraud, N., Gounou, C., Linares, R. & Brisson, A. R. A Simple Flow Cytometry Method Improves the Detection of Phosphatidylserine-Exposing Extracellular Vesicles. *J. Thromb. Haemost.* ISSN: 1538-7836. doi:10.1111/jth.12767 (Oct. 2014).

84. Connor, D. E., Exner, T., Ma, D. D. F. & Joseph, J. E. The majority of circulating platelet-derived microparticles fail to bind annexin V, lack phospholipid-dependent procoagulant activity and demonstrate greater expression of glycoprotein Ib. *Thromb. Haemost.* **103,** 1044–52. ISSN: 0340-6245 (May 2010).

85. Mettlen, M., Pucadyil, T., Ramachandran, R. & Schmid, S. L. Dissecting dynamin's role in clathrin-mediated endocytosis. *Biochem. Soc. Trans.* **37,** 1022–6. ISSN: 1470-8752 (Oct. 2009).

86. Southcombe, J., Tannetta, D., Redman, C. & Sargent, I. The immunomodulatory role of syncytiotrophoblast microvesicles. *PLoS One* **6,** e20245. ISSN: 1932-6203 (Jan. 2011).

87. Gasser, O. *et al.* Characterisation and properties of ectosomes released by human polymorphonuclear neutrophils. *Exp. Cell Res.* **285,** 243–57. ISSN: 0014-4827 (May 2003).

88. Chandler, W. L. Microparticle counts in platelet-rich and platelet-free plasma, effect of centrifugation and sample-processing protocols. *Blood Coagul. Fibrinolysis* **24,** 125–32. ISSN: 1473-5733 (Mar. 2013).

89. Danzer, K. M. *et al.* Exosomal cell-to-cell transmission of alpha synuclein oligomers. *Mol. Neurodegener.* **7,** 42. ISSN: 1750-1326 (Jan. 2012).

90. Johnstone, R. M., Adam, M., Hammond, J. R., Orr, L. & Turbide, C. Vesicle formation during reticulocyte maturation. Association of plasma membrane activities with released vesicles (exosomes). *J. Biol. Chem.* **262,** 9412–20. ISSN: 0021-9258 (July 1987).

91. Filipe, V., Hawe, A. & Jiskoot, W. Critical evaluation of Nanoparticle Tracking Analysis (NTA) by NanoSight for the measurement of nanoparticles and protein aggregates. *Pharm. Res.* **27,** 796–810. ISSN: 1573-904X (May 2010).

92. Soo, C. Y. *et al.* Nanoparticle tracking analysis monitors microvesicle and exosome secretion from immune cells. *Immunology* **136,** 192–7. ISSN: 1365-2567 (June 2012).

93. Van der Pol, E. *et al.* Particle size distribution of exosomes and microvesicles determined by transmission electron microscopy, flow cytometry, nanoparticle tracking analysis, and resistive pulse sensing. *J. Thromb. Haemost.* **12,** 1182–1192. ISSN: 15387933 (May 2014).

94. Lebowitz, J., Lewis, M. S. & Schuck, P. Modern analytical ultracentrifugation in protein science: a tutorial review. *Protein Sci.* **11,** 2067–79. ISSN: 0961-8368 (Sept. 2002).

95. Cvjetkovic, A., Lötvall, J. & Lässer, C. The influence of rotor type and centrifugation time on the yield and purity of extracellular vesicles. *J. Extracell. vesicles* **3.** doi:10.3402/jev.v3.23111 (2014).

96. Stratton, D. *et al.* Label-free real-time acoustic sensing of microvesicle release from prostate cancer (PC3) cells using a Quartz Crystal Microbalance. *Biochem. Biophys. Res. Commun.* ISSN: 1090-2104. doi:10.1016/j.bbrc.2014.09.132 (Oct. 2014).

97. Yamada, T., Inoshima, Y., Matsuda, T. & Ishiguro, N. Comparison of methods for isolating exosomes from bovine milk. *J. Vet. Med. Sci.* **74,** 1523–5. ISSN: 1347-7439 (Nov. 2012).

98. Van Deun, J. *et al.* The impact of disparate isolation methods for extracellular vesicles on downstream RNA profiling. *J. Extracell. Vesicles* **3,** 24858. ISSN: 2001-3078 (Jan. 2014).

99. Zarovni, N. *et al.* Integrated isolation and quantitative analysis of exosome shuttled proteins and nucleic acids using immunocapture approaches. *Methods* **87,** 46–58. ISSN: 10462023 (2015).

100. Yuana, Y., Levels, J., Grootemaat, A., Sturk, A. & Nieuwland, R. *Co-isolation of extracellular vesicles and high-density lipoproteins using density gradient ultracentrifugation* en. July 2014.

101. Raposo, G. *et al.* B lymphocytes secrete antigen-presenting vesicles. *J. Exp. Med.* **183,** 1161–72. ISSN: 0022-1007 (Mar. 1996).

102. Conde-Vancells, J. *et al.* Characterization and comprehensive proteome profiling of exosomes secreted by hepatocytes. *J. Proteome Res.* **7,** 5157–66. ISSN: 1535-3893 (Dec. 2008).

103. Issman, L., Brenner, B., Talmon, Y. & Aharon, A. Cryogenic transmission electron microscopy nanostructural study of shed microparticles. *PLoS One* **8,** e83680. ISSN: 1932-6203 (Jan. 2013).

104. Van der Pol, E., van Gemert, M. J. C., Sturk, A., Nieuwland, R. & van Leeuwen, T. G. Single vs. swarm detection of microparticles and exosomes by flow cytometry. *J. Thromb. Haemost.* **10,** 919–30. ISSN: 1538-7836 (May 2012).

105. Jones, S. H., King, M. D. & Ward, A. D. Determining the unique refractive index properties of solid polystyrene aerosol using broadband Mie scattering from optically trapped beads. *Phys. Chem. Chem. Phys.* **15,** 20735–41. ISSN: 1463-9084 (2013).

106. Gardiner, C. *et al.* Measurement of refractive index by nanoparticle tracking analysis reveals heterogeneity in extracellular vesicles. *J. Extracell. vesicles* **3,** 25361. ISSN: 2001-3078 (Nov. 2014).

107. Nebe-von-Caron, G. Standardization in microbial cytometry. *Cytometry. A* **75,** 86–9. ISSN: 1552-4930 (Feb. 2009).

108. Maas, S. L. N. *et al.* Possibilities and limitations of current technologies for quantification of biological extracellular vesicles and synthetic mimics. *J. Control. Release* **200,** 87–96. ISSN: 18734995 (Feb. 2015).

109. Hulst, H. C. v. d. (C. *Light scattering by small particles* 470. ISBN: 0486642283 (Dover Publications, 1981).

110. Chandler, W. L., Yeung, W. & Tait, J. F. A new microparticle size calibration standard for use in measuring smaller microparticles using a new flow cytometer. *J. Thromb. Haemost.* **9,** 1216–24. ISSN: 1538-7836 (June 2011).

111. Lacroix, R., Robert, S., Poncelet, P. & Dignat-George, F. Overcoming limitations of microparticle measurement by flow cytometry. *Semin. Thromb. Hemost.* **36,** 807–18. ISSN: 1098-9064 (Nov. 2010).

112. Schmaier, A. A. *et al.* Occlusive thrombi arise in mammals but not birds in response to arterial injury : evolutionary insight into human cardiovascular disease Occlusive thrombi arise in mammals but not birds in response to arterial injury : evolutionary insight into human card. *Blood* **118,** 3661–3669 (2012).

113. Sowerby, S. J., Broom, M. F. & Petersen, G. B. Dynamically resizable nanometre-scale apertures for molecular sensing. *Sensors Actuators B Chem.* **123,** 325–330. ISSN: 09254005 (2007).

114. Reverdatto, S., Burz, D. S. & Shekhtman, A. Peptide aptamers: development and applications. *Curr. Top. Med. Chem.* **15,** 1082–101. ISSN: 1873-4294 (2015).

115. Garzetti, L. *et al. Activated macrophages release microvesicles containing polarized M1 or M2 mRNAs* Dec. 2013. doi:10.1189/jlb.0913485. (2015).

116. D'Souza-Schorey, C. & Chavrier, P. ARF proteins: roles in membrane traffic and beyond. *Nat. Rev. Mol. Cell Biol.* **7,** 347–58. ISSN: 1471-0072 (May 2006).

117. Donaldson, J. G. Multiple roles for Arf6: sorting, structuring, and signaling at the plasma membrane. *J. Biol. Chem.* **278,** 41573–6. ISSN: 0021-9258 (Oct. 2003).

118. Liang, Y. *et al.* Complex N-linked glycans serve as a determinant for exosome/microvesicle cargo recruitment. *J. Biol. Chem.* **289,** 32526–37. ISSN: 1083-351X (Nov. 2014).

119. Faille, D. *et al.* Endocytosis and intracellular processing of platelet microparticles by brain endothelial cells. *J. Cell. Mol. Med.* **16,** 1731–8. ISSN: 1582-4934 (Aug. 2012).

120. Montecalvo, A. *et al.* Mechanism of transfer of functional microRNAs between mouse dendritic cells via exosomes. en. *Blood* **119,** 756–66. ISSN: 1528-0020 (Jan. 2012).

121. Bohdanowicz, M. & Grinstein, S. Role of phospholipids in endocytosis, phagocytosis, and macropinocytosis. *Physiol. Rev.* **93,** 69–106. ISSN: 1522-1210 (Jan. 2013).

122. Burger, K. N. Greasing membrane fusion and fission machineries. *Traffic* **1,** 605–13. ISSN: 1398-9219 (Aug. 2000).

123. Ridder, K. *et al.* Extracellular Vesicle-Mediated Transfer of Genetic Information between the Hematopoietic System and the Brain in Response to Inflammation. *PLoS Biol.* **12,** e1001874. ISSN: 1545-7885 (June 2014).

124. Castaman, G., Yu-Feng, L., Battistin, E. & Rodeghiero, F. Characterization of a novel bleeding disorder with isolated prolonged bleeding time and deficiency of platelet microvesicle generation. *Br. J. Haematol.* **96,** 458–63. ISSN: 0007-1048 (Mar. 1997).

125. Dustin, M. L. The immunological synapse. *Cancer Immunol. Res.* **2,** 1023–33. ISSN: 2326-6074 (Nov. 2014).

126. Rughetti, A. *et al.* Microvesicle cargo of tumor-associated MUC1 to dendritic cells allows cross-presentation and specific carbohydrate processing. en. *Cancer Immunol. Res.* **2,** 177–86. ISSN: 2326-6074 (Feb. 2014).

127. Qazi, K. R., Gehrmann, U., Domange Jordo, E., Karlsson, M. C. I. & Gabrielsson, S. Antigen-loaded exosomes alone induce Th1-type memory through a B cell-dependent mechanism. *Blood* **113,** 2673–2683. ISSN: 0006-4971 (Jan. 2009).

128. Théry, C., Ostrowski, M. & Segura, E. Membrane vesicles as conveyors of immune responses. *Nat. Rev. Immunol.* **9,** 581–93. ISSN: 1474-1741 (Aug. 2009).

129. Wieckowski, E. U. *et al.* Tumor-derived microvesicles promote regulatory T cell expansion and induce apoptosis in tumor-reactive activated CD8+ T lymphocytes. *J. Immunol.* **183,** 3720–30. ISSN: 1550-6606 (Sept. 2009).

130. Waring, P. & Mullbacher, A. Cell death induced by the Fas/Fas ligand pathway and its role in pathology. *Immunol. Cell Biol.* **77,** 312–317. ISSN: 0818-9641 (Aug. 1999).

131. Choudhuri, K., Llodra, J., Kam, L., Stokes, D. & Dustin, M. Antigen-induced release and retroviral subversion of TCR-enriched microvesicles at the CD4+ T cell immunological synapse. *J. Immunol.* **188,** 58.5 (May 2012).

132. Wurdinger, T. *et al.* Extracellular vesicles and their convergence with viral pathways. *Adv. Virol.* **2012,** 767694. ISSN: 1687-8647 (Jan. 2012).

133. Frleta, D. *et al.* HIV-1 infection-induced apoptotic microparticles inhibit human DCs via CD44. *J. Clin. Invest.* **122,** 4685–97. ISSN: 1558-8238 (Dec. 2012).

134. Netea, M. G. *et al.* IL-1beta processing in host defense: beyond the inflammasomes. *PLoS Pathog.* **6,** e1000661. ISSN: 1553-7374 (Feb. 2010).

135. Srinivasula, S. M. *et al.* The PYRIN-CARD protein ASC is an activating adaptor for caspase-1. *J. Biol. Chem.* **277,** 21119–22. ISSN: 0021-9258 (June 2002).

136. Auron, P. E. *et al.* Nucleotide sequence of human monocyte interleukin 1 precursor cDNA. *Proc. Natl. Acad. Sci. U. S. A.* **81,** 7907–11. ISSN: 0027-8424 (Dec. 1984).

137. Larsen, Z. M. *Non-classical secreted proteins* 2013. (2015).

138. Andrei, C. *et al.* The secretory route of the leaderless protein interleukin 1beta involves exocytosis of endolysosome-related vesicles. *Mol. Biol. Cell* **10,** 1463–75. ISSN: 1059-1524 (May 1999).

139. Eder, C. Mechanisms of interleukin-1beta release. *Immunobiology* **214,** 543–53. ISSN: 1878-3279 (Jan. 2009).

140. Croce, M. *et al.* 305 Detection of circulating galectin-1 in the microvesicle fraction of serum from breast cancer patients. English. *Eur. J. Cancer Suppl.* **8,** 79. ISSN: 13596349 (June 2010).

141. Ansa-Addo, E. A. *et al.* Human plasma membrane-derived vesicles halt proliferation and induce differentiation of THP-1 acute monocytic leukemia cells. en. *J. Immunol.* **185,** 5236–46. ISSN: 1550-6606 (Nov. 2010).

142. Lopez-Castejon, G. & Brough, D. Understanding the mechanism of IL-1β secretion. *Cytokine Growth Factor Rev.* **22,** 189–195. ISSN: 13596101 (2011).

143. Dinarello, C. A. Immunological and inflammatory functions of the interleukin-1 family. *Annu. Rev. Immunol.* **27,** 519–50. ISSN: 0732-0582 (Jan. 2009).

144. Pugin, J., Ulevitch, R. J. & Tobias, P. S. Tumor necrosis factor-alpha and interleukin-1 beta mediate human endothelial cell activation in blood at low endotoxin concentrations. *J. Inflamm.* **45,** 49–55. ISSN: 1078-7852 (Jan. 1995).

145. Mantovani, A., Cassatella, M. A., Costantini, C. & Jaillon, S. Neutrophils in the activation and regulation of innate and adaptive immunity. *Nat. Rev. Immunol.* **11,** 519–31. ISSN: 1474-1741 (Aug. 2011).

146. Hyun, Y.-M. *et al.* Uropod elongation is a common final step in leukocyte extravasation through inflamed vessels. *J. Exp. Med.* **209,** 1349–62. ISSN: 1540-9538 (July 2012).

147. Del Conde, I., Shrimpton, C. N., Thiagarajan, P. & López, J. A. Tissue-factor-bearing microvesicles arise from lipid rafts and fuse with activated platelets to initiate coagulation. *Blood* **106,** 1604–11. ISSN: 0006-4971 (Sept. 2005).

148. Mack, M. *et al.* Transfer of the chemokine receptor CCR5 between cells by membrane-derived microparticles: a mechanism for cellular human immunodeficiency virus 1 infection. *Nat. Med.* **6,** 769–75. ISSN: 1078-8956 (July 2000).

149. Timár, C. I. *et al.* Antibacterial effect of microvesicles released from human neutrophilic granulocytes. *Blood* **121,** 510–8. ISSN: 1528-0020 (Jan. 2013).

150. Eken, C. *et al.* Polymorphonuclear neutrophil-derived ectosomes interfere with the maturation of monocyte-derived dendritic cells. *J. Immunol.* **180,** 817–24. ISSN: 0022-1767 (Jan. 2008).

151. Dalli, J. & Serhan, C. N. Specific lipid mediator signatures of human phagocytes: microparticles stimulate macrophage efferocytosis and pro-resolving mediators. *Blood* **120,** e60–72. ISSN: 1528-0020 (Oct. 2012).

152. Morgan, G. T. *First Principles of Surgery; being an outline of inflammation and its effects* (S. Highley, MacLachlan & Stewart, London & Edinburgh, 1838).

153. Serhan, C. N. & Savill, J. Resolution of inflammation: the beginning programs the end. *Nat. Immunol.* **6,** 1191–7. ISSN: 1529-2908 (Dec. 2005).

154. Levy, B. D., Clish, C. B., Schmidt, B., Gronert, K. & Serhan, C. N. Lipid mediator class switching during acute inflammation: signals in resolution. *Nat. Immunol.* **2,** 612–9. ISSN: 1529-2908 (July 2001).

155. Buckley, C. D., Gilroy, D. W. & Serhan, C. N. Proresolving lipid mediators and mechanisms in the resolution of acute inflammation. *Immunity* **40,** 315–27. ISSN: 1097-4180 (Mar. 2014).

156. Serhan, C. N. *et al.* Maresins: novel macrophage mediators with potent antiinflammatory and proresolving actions. *J. Exp. Med.* **206,** 15–23. ISSN: 1540-9538 (Jan. 2009).

157. Spite, M. *et al.* Resolvin D2 is a potent regulator of leukocytes and controls microbial sepsis. *Nature* **461,** 1287–91. ISSN: 1476-4687 (Oct. 2009).

158. Norling, L. V. *et al.* Cutting edge: Humanized nano-proresolving medicines mimic inflammation-resolution and enhance wound healing. en. *J. Immunol.* **186,** 5543–7. ISSN: 1550-6606 (May 2011).

159. El Kebir, D., Gjorstrup, P. & Filep, J. G. Resolvin E1 promotes phagocytosis-induced neutrophil apoptosis and accelerates resolution of pulmonary inflammation. *Proc. Natl. Acad. Sci. U. S. A.* **109,** 14983–8. ISSN: 1091-6490 (Sept. 2012).

160. McCauley, L. K., Dalli, J., Koh, A. J., Chiang, N. & Serhan, C. N. Cutting Edge: Parathyroid Hormone Facilitates Macrophage Efferocytosis in Bone Marrow via Proresolving Mediators Resolvin D1 and Resolvin D2. *J. Immunol.* ISSN: 0022-1767. doi:10.4049/jimmunol.1301945 (June 2014).

161. Colotta, F., Re, F., Polentarutti, N., Sozzani, S. & Mantovani, A. Modulation of granulocyte survival and programmed cell death by cytokines and bacterial products. *Blood* **80,** 2012–20. ISSN: 0006-4971 (Oct. 1992).

162. Liles, W. C., Kiener, P. A., Ledbetter, J. A., Aruffo, A. & Klebanoff, S. J. Differential expression of Fas (CD95) and Fas ligand on normal human phagocytes: implications for the regulation of apoptosis in neutrophils. *J. Exp. Med.* **184** (1996).

163. El Kebir, D. & Filep, J. G. Modulation of Neutrophil Apoptosis and the Resolution of Inflammation through β2 Integrins. English. *Front. Immunol.* **4,** 60. ISSN: 1664-3224 (Jan. 2013).

164. Filardy, A. A. *et al.* Proinflammatory Clearance of Apoptotic Neutrophils Induces an IL-12lowIL-10high Regulatory Phenotype in Macrophages. *J. Immunol.* **185,** 2044–2050. ISSN: 0022-1767 (Aug. 2010).

165. Lu, J. *et al.* Discrete functions of M2a and M2c macrophage subsets determine their relative efficacy in treating chronic kidney disease. *Kidney Int.* **84,** 745–55. ISSN: 1523-1755 (Oct. 2013).

166. Leibovich, S. J. *et al.* Synergistic up-regulation of vascular endothelial growth factor expression in murine macrophages by adenosine A(2A) receptor agonists and endotoxin. *Am. J. Pathol.* **160,** 2231–44. ISSN: 0002-9440 (June 2002).

167. Perretti, M. *et al.* Mobilizing lipocortin 1 in adherent human leukocytes downregulates their transmigration. *Nat. Med.* **2,** 1259–62. ISSN: 1078-8956 (Nov. 1996).

168. Perretti, M. *et al.* Annexin I is stored within gelatinase granules of human neutrophil and mobilized on the cell surface upon adhesion but not phagocytosis. *Cell Biol. Int.* **24,** 163–74. ISSN: 1065-6995 (Jan. 2000).

169. Traverso, V., Morris, J. F., Flower, R. J. & Buckingham, J. Lipocortin 1 (annexin 1) in patches associated with the membrane of a lung adenocarcinoma cell line and in the cell cytoplasm. *J. Cell Sci.* **111 (Pt 1,** 1405–18. ISSN: 0021-9533 (May 1998).

170. Solito, E., Nuti, S. & Parente, L. Dexamethasone-induced translocation of lipocortin (annexin) 1 to the cell membrane of U-937 cells. *Br. J. Pharmacol.* **112,** 347–8. ISSN: 0007-1188 (June 1994).

171. Babiychuk, E. B., Monastyrskaya, K. & Draeger, A. Fluorescent annexin A1 reveals dynamics of ceramide platforms in living cells. *Traffic* **9,** 1757–75. ISSN: 1600-0854 (Sept. 2008).

172. Scannell, M. & Maderna, P. Lipoxins and annexin-1: resolution of inflammation and regulation of phagocytosis of apoptotic cells. *ScientificWorldJournal.* **6,** 1555–73. ISSN: 1537-744X (Jan. 2006).

173. Rothlin, C. V. *et al.* TAM Receptors Are Pleiotropic Inhibitors of the Innate Immune Response. *Cell* **131,** 1124–36. ISSN: 00928674 (Dec. 2007).

174. Zizzo, G., Hilliard, B. A., Monestier, M. & Cohen, P. L. Efficient Clearance of Early Apoptotic Cells by Human Macrophages Requires M2c Polarization and MerTK Induction. *J. Immunol.* **189,** 3508–3520. ISSN: 0022-1767 (Oct. 2012).

175. Linger, R. M. A., Keating, A. K., Earp, H. S. & Graham, D. K. *TAM Receptor Tyrosine Kinases: Biologic Functions, Signaling, and Potential Therapeutic Targeting in Human Cancer* 2008. doi:10.1016/S0065-230X(08)00002-X. arXiv: 0402594v3 [arXiv:cond-mat].

176. Neubauer, A. *et al.* Expression of axl, a transforming receptor tyrosine kinase, in normal and malignant hematopoiesis. *Blood* **84,** 1931–41. ISSN: 0006-4971 (Sept. 1994).

177. Hall, M. O., Agnew, B. J., Abrams, T. A. & Burgess, B. L. The phagocytosis of OS is mediated by the PI3-kinase linked tyrosine kinase receptor, Mer, and is stimulated by GAS6. *Adv. Exp. Med. Biol.* **533,** 331–6. ISSN: 0065-2598 (2003).

178. Wan, E. *et al.* Enhanced efferocytosis of apoptotic cardiomyocytes through myeloid-epithelial-reproductive tyrosine kinase links acute inflammation resolution to cardiac repair after infarction. *Circ. Res.* **113,** 1004–1012. ISSN: 00097330 (Sept. 2013).

179. Lee, Y. J. *et al.* Preventing cleavage of Mer promotes efferocytosis and suppresses acute lung injury in bleomycin treated mice. *Toxicol. Appl. Pharmacol.* **263,** 61–72. ISSN: 0041008X (Aug. 2012).

180. Cohen, Z., Gonzales, R. F., Davis-Gorman, G. F., Copeland, J. G. & McDonagh, P. F. Thrombin activity and platelet microparticle formation are increased in type 2 diabetic platelets: a potential correlation with caspase activation. *Thromb. Res.* **107,** 217–21. ISSN: 0049-3848 (Sept. 2002).

181. Lu, Q. & Lemke, G. Homeostatic Regulation of the Immune System by Receptor Tyrosine Kinase of the Tyro 3 Family. *Science (80-.).* **293,** 306–311. ISSN: 00368075 (July 2001).

182. Lu, Q. *et al.* Tyro-3 family receptors are essential regulators of mammalian spermatogenesis. *Nature* **398,** 723–728. ISSN: 0028-0836 (Apr. 1999).

183. Randolph, G. J. Emigration of monocyte-derived cells to lymph nodes during resolution of inflammation and its failure in atherosclerosis. *Curr. Opin. Lipidol.* **19,** 462–8. ISSN: 0957-9672 (Oct. 2008).

184. Jantsch, J., Binger, K. J., Müller, D. N. & Titze, J. Macrophages in homeostatic immune function. *Front. Physiol.* **5,** 146. ISSN: 1664-042X (Jan. 2014).

185. Davies, L. C., Jenkins, S. J., Allen, J. E. & Taylor, P. R. Tissue-resident macrophages. en. *Nat. Immunol.* **14,** 986–95. ISSN: 1529-2916 (Oct. 2013).

186. Chorro, L. *et al.* Langerhans cell (LC) proliferation mediates neonatal development, homeostasis, and inflammation-associated expansion of the epidermal LC network. *J. Exp. Med.* **206,** 3089–3100. ISSN: 0022-1007 (Dec. 2009).

187. Schulz, C. *et al.* A Lineage of Myeloid Cells Independent of Myb and Hematopoietic Stem Cells. *Science (80-.).* **336,** 86–90. ISSN: 0036-8075 (Apr. 2012).

188. Epelman, S., Lavine, K. J. & Randolph, G. J. Origin and Functions of Tissue Macrophages. English. *Immunity* **41,** 21–35. ISSN: 10747613 (July 2014).

189. Ginhoux, F. *et al.* Langerhans cells arise from monocytes in vivo. *Nat. Immunol.* **7,** 265–73. ISSN: 1529-2908 (Mar. 2006).

190. Shi, C. & Pamer, E. G. Monocyte recruitment during infection and inflammation. *Nat. Rev. Immunol.* **11,** 762–74. ISSN: 1474-1741 (Nov. 2011).

191. Ziegler-Heitbrock, L. *et al.* Nomenclature of monocytes and dendritic cells in blood. *Blood* **116,** e74–80. ISSN: 1528-0020 (Oct. 2010).

192. Passlick, B., Flieger, D. & Ziegler-Heitbrock, H. W. Identification and characterization of a novel monocyte subpopulation in human peripheral blood. *Blood* **74,** 2527–34. ISSN: 0006-4971 (Nov. 1989).

193. Hristov, M. & Heine, G. H. Monocyte subsets in atherosclerosis. *Hamostaseologie* **35.** ISSN: 0720-9355. doi:10.5482/HAMO-14-08-0030 (Nov. 2014).

194. Savill, J. Apoptosis in resolution of inflammation. *J. Leukoc. Biol.* **61,** 375–80. ISSN: 0741-5400 (Apr. 1997).

195. Misharin, A. V. *et al.* Nonclassical Ly6C- Monocytes Drive the Development of Inflammatory Arthritis in Mice. *Cell Rep.* **9,** 591–604. ISSN: 22111247 (Oct. 2014).

196. Wong, K. L. *et al.* Gene expression profiling reveals the defining features of the classical, intermediate, and nonclassical human monocyte subsets. *Blood* **118,** e16–31. ISSN: 1528-0020 (Aug. 2011).

197. Metchnikoff, É. *Immunity in Infective Diseases* (Cambridge University Press, Cambridge, 1905).

198. MACKANESS, G. B. THE IMMUNOLOGICAL BASIS OF ACQUIRED CELLULAR RESISTANCE. *J. Exp. Med.* **120,** 105–20. ISSN: 0022-1007 (July 1964).

199. Dalton, D. K. *et al.* Multiple defects of immune cell function in mice with disrupted interferon-gamma genes. *Science* **259,** 1739–42. ISSN: 0036-8075 (Mar. 1993).

200. BoseDasgupta, S. & Pieters, J. Inflammatory Stimuli Reprogram Macrophage Phagocytosis to Macropinocytosis for the Rapid Elimination of Pathogens. *PLoS Pathog.* **10** (ed Ehrt, S.) e1003879. ISSN: 1553-7374 (Jan. 2014).

201. Stein, M., Keshav, S., Harris, N. & Gordon, S. Interleukin 4 potently enhances murine macrophage mannose receptor activity: a marker of alternative immunologic macrophage activation. *J. Exp. Med.* **176,** 287–92. ISSN: 0022-1007 (July 1992).

202. Anthony, R. M. *et al.* Memory T(H)2 cells induce alternatively activated macrophages to mediate protection against nematode parasites. *Nat. Med.* **12,** 955–60. ISSN: 1078-8956 (Aug. 2006).

203. Bhatia, S. *et al.* Rapid host defense against Aspergillus fumigatus involves alveolar macrophages with a predominance of alternatively activated phenotype. *PLoS One* **6,** e15943. ISSN: 1932-6203 (Jan. 2011).

204. Biswas, S. K. & Mantovani, A. Macrophage plasticity and interaction with lymphocyte subsets: cancer as a paradigm. en. *Nat. Immunol.* **11,** 889–96. ISSN: 1529-2916 (Oct. 2010).

205. Becker, S. & Daniel, E. G. Antagonistic and additive effects of IL-4 and interferon-gamma on human monocytes and macrophages: effects on Fc receptors, HLA-D antigens, and superoxide production. *Cell. Immunol.* **129,** 351–62. ISSN: 0008-8749 (Sept. 1990).

206. Martinez, F. O. Macrophage activation and polarization. en. *Front. Biosci.* **13,** 453. ISSN: 10939946 (Jan. 2008).

207. Zhang, Y. *et al.* Immune Complex/Ig Negatively Regulate TLR4-Triggered Inflammatory Response in Macrophages through Fc RIIb-Dependent PGE2 Production. en. *J. Immunol.* **182,** 554–562. ISSN: 0022-1767 (Dec. 2008).

208. Vogelpoel, L. T. C. *et al.* Fc gamma receptor-TLR cross-talk elicits pro-inflammatory cytokine production by human M2 macrophages. *Nat. Commun.* **5,** 5444. ISSN: 2041-1723 (Jan. 2014).

209. Martinez, F. O. & Gordon, S. The M1 and M2 paradigm of macrophage activation: time for reassessment. *F1000Prime Rep* **6** (Mar. 2014).

210. Haskó, G. & Cronstein, B. Regulation of Inflammation by Adenosine. *Front. Immunol.* **4,** 85. ISSN: 1664-3224 (2013).

211. Gleissner, C. A., Shaked, I., Little, K. M. & Ley, K. CXC chemokine ligand 4 induces a unique transcriptome in monocyte-derived macrophages. *J. Immunol.* **184,** 4810–8. ISSN: 1550-6606 (May 2010).

212. Hadadi, E., Kiss-Toth, E., Wilson, H. L. & Wong, S. C. Functional Characterisation of Monocyte Derived Macrophage Phenotypes for their Role in Atherosclerosis. *Heart* **100 Suppl,** A117. ISSN: 1468-201X (June 2014).

213. Boyle, J. J. Heme and haemoglobin direct macrophage Mhem phenotype and counter foam cell formation in areas of intraplaque haemorrhage. *Curr. Opin. Lipidol.* **23,** 453–61. ISSN: 1473-6535 (Oct. 2012).

214. Carmona-Rivera, C. *et al.* Neutrophil extracellular traps are a source of citrullinated autoantigens and stimulate inflammatory responses in rheumatoid arthritis (P4061). *J. Immunol.* **190,** 127.2 (May 2013).

215. Kallberg, H. *et al.* Gene-gene and gene-environment interactions involving HLA-DRB1, PTPN22, and smoking in two subsets of rheumatoid arthritis. *Am. J. Hum. Genet.* **80,** 867–75. ISSN: 0002-9297 (May 2007).

216. Schellekens, G. A., de Jong, B. A., van den Hoogen, F. H., van de Putte, L. B. & van Venrooij, W. J. Citrulline is an essential constituent of antigenic determinants recognized by rheumatoid arthritis-specific autoantibodies. *J. Clin. Invest.* **101,** 273–81. ISSN: 0021-9738 (Jan. 1998).

217. Szekanecz, Z. *et al.* Anti-citrullinated protein antibodies in rheumatoid arthritis: as good as it gets? *Clin. Rev. Allergy Immunol.* **34,** 26–31. ISSN: 1559-0267 (Feb. 2008).

218. Itoh, K. *et al.* Clonal expansion is a characteristic feature of the B-cell repertoire of patients with rheumatoid arthritis. *Arthritis Res* **2,** 50–58. ISSN: 1465-9905 (2000).

219. Lundy, S. K., Sarkar, S., Tesmer, L. A. & Fox, D. A. Cells of the synovium in rheumatoid arthritis. T lymphocytes. *Arthritis Res. Ther.* **9,** 202. ISSN: 1478-6362 (Jan. 2007).

220. Fossati, G., Bucknall, R. C. & Edwards, S. W. Insoluble and soluble immune complexes activate neutrophils by distinct activation mechanisms: changes in functional responses induced by priming with cytokines. *Ann. Rheum. Dis.* **61,** 13–9. ISSN: 0003-4967 (Jan. 2002).

221. Wang, C.-H. *et al.* Expression of CD147 (EMMPRIN) on neutrophils in rheumatoid arthritis enhances chemotaxis, matrix metalloproteinase production and invasiveness of synoviocytes. *J. Cell. Mol. Med.* **15,** 850–60. ISSN: 1582-4934 (Apr. 2011).

222. Cross, A., Bucknall, R. C., Cassatella, M. A., Edwards, S. W. & Moots, R. J. Synovial fluid neutrophils transcribe and express class II major histocompatibility complex molecules in rheumatoid arthritis. *Arthritis Rheum.* **48,** 2796–806. ISSN: 0004-3591 (Oct. 2003).

223. Wright, H. L., Moots, R. J. & Edwards, S. W. The multifactorial role of neutrophils in rheumatoid arthritis. *Nat. Rev. Rheumatol.* **10,** 593–601. ISSN: 1759-4804 (June 2014).

224. Raza, K. *et al.* Synovial fluid leukocyte apoptosis is inhibited in patients with very early rheumatoid arthritis. *Arthritis Res. Ther.* **8,** R120. ISSN: 1478-6362 (Jan. 2006).

225. Wong, S. H. *et al.* Lactoferrin is a survival factor for neutrophils in rheumatoid synovial fluid. *Rheumatology (Oxford).* **48,** 39–44. ISSN: 1462-0332 (Jan. 2009).

226. Brinkmann, V. *et al.* Neutrophil extracellular traps kill bacteria. *Science* **303,** 1532–5. ISSN: 1095-9203 (Mar. 2004).

227. Fehr, K. *et al.* [Chronic polyarthritis: role of polymorphonuclear leukocytes in the destruction of pannus-free articular cartilage]. *Bull. Schweiz. Akad. Med. Wiss.* **35,** 317–27. ISSN: 0036-7494 (Sept. 1979).

228. Mori, G., D'Amelio, P., Faccio, R. & Brunetti, G. The Interplay between the bone and the immune system. *Clin. Dev. Immunol.* **2013,** 720504. ISSN: 1740-2530 (Jan. 2013).

229. López-Armada, M. J. *et al.* Cytokines, tumor necrosis factor-alpha and interleukin-1beta, differentially regulate apoptosis in osteoarthritis cultured human chondrocytes. *Osteoarthritis Cartilage* **14,** 660–9. ISSN: 1063-4584 (July 2006).

230. Chomarat, P., Rissoan, M. C., Pin, J. J., Banchereau, J. & Miossec, P. Contribution of IL-1, CD14, and CD13 in the increased IL-6 production induced by in vitro monocyte-synoviocyte interactions. *J. Immunol.* **155,** 3645–52. ISSN: 0022-1767 (Oct. 1995).

231. Kinne, R. W., Stuhlmüller, B. & Burmester, G.-R. Cells of the synovium in rheumatoid arthritis. Macrophages. *Arthritis Res. Ther.* **9,** 224. ISSN: 1478-6362 (Jan. 2007).

232. Danks, L., Sabokbar, A., Gundle, R. & Athanasou, N. A. Synovial macrophage-osteoclast differentiation in inflammatory arthritis. *Ann. Rheum. Dis.* **61,** 916–21. ISSN: 0003-4967 (Oct. 2002).

233. Kirchner, S., Holler, E., Haffner, S., Andreesen, R. & Eissner, G. Effect of different tumor necrosis factor (TNF) reactive agents on reverse signaling of membrane integrated TNF in monocytes. *Cytokine* **28,** 67–74. ISSN: 1043-4666 (Oct. 2004).

234. Wenink, M. H. *et al.* Abatacept modulates proinflammatory macrophage responses upon cytokine-activated T cell and Toll-like receptor ligand stimulation. *Ann. Rheum. Dis.* **71,** 80–3. ISSN: 1468-2060 (Jan. 2012).

235. Feldmann, M. & Maini, R. N. Anti-TNF therapy, from rationale to standard of care: what lessons has it taught us? *J. Immunol.* **185,** 791–4. ISSN: 1550-6606 (July 2010).

236. Ma, Y. & Pope, R. M. The role of macrophages in rheumatoid arthritis. *Curr. Pharm. Des.* **11,** 569–80. ISSN: 1381-6128 (2005).

237. Birnie, G. D. The HL60 cell line: a model system for studying human myeloid cell differentiation. *Br. J. Cancer. Suppl.* **9,** 41–5. ISSN: 0306-9443 (Dec. 1988).

238. Idres, N., Benoit, G., Flexor, M. A., Lanotte, M. & Chabot, G. G. Granulocytic Differentiation of Human NB4 Promyelocytic Leukemia Cells Induced by All-trans Retinoic Acid Metabolites. *Cancer Res.* **61,** 700–705 (Jan. 2001).

239. Christensen, A. D., Haase, C., Cook, A. D. & Hamilton, J. A. *K/BxN serum-transfer arthritis as a model for human inflammatory arthritis* June 2016. doi:10.3389/fimmu.2016.00213.

240. Scott, R. S. *et al.* Phagocytosis and clearance of apoptotic cells is mediated by MER. *Nature* **411,** 207–211. ISSN: 0028-0836 (May 2001).

241. Greco, K. V. *et al.* High density micromass cultures of a human chondrocyte cell line: a reliable assay system to reveal the modulatory functions of pharmacological agents. *Biochem. Pharmacol.* **82,** 1919–29. ISSN: 1873-2968 (Dec. 2011).

242. Li, J., Hsu, H.-C. & Mountz, J. D. Managing macrophages in rheumatoid arthritis by reform or removal. *Curr. Rheumatol. Rep.* **14,** 445–54. ISSN: 1534-6307 (Oct. 2012).

243. EDWARDS, J. C. W., LEIGH, R. D. & CAMBRIDGE, G. Expression of molecules involved in B lymphocyte survival and differentiation by synovial fibroblasts. *Clin. Exp. Immunol.* **108,** 407–414. ISSN: 0009-9104 (June 1997).

244. Cash, J. L., White, G. E. & Greaves, D. R. in *Methods Enzymol.* 379–396 (2009). doi:10.1016/S0076-6879(09)05417-2.

245. Rao, T. S., Currie, J. L., Shaffer, A. F. & Isakson, P. C. In vivo characterization of zymosan-induced mouse peritoneal inflammation. *J. Pharmacol. Exp. Ther.* **269,** 917–25. ISSN: 0022-3565 (June 1994).

246. Malda, J., Boere, J., van de Lest, C., van Weeren, P. & Wauben, M. Extracellular vesicles - new tool for joint repair and regeneration - IN PRESS. *Nat. Rev. Rheumatol.* **12,** 243–249. ISSN: 1759-4790 (Jan. 2016).

247. Lanotte, M. *et al.* NB4, a maturation inducible cell line with t(15;17) marker isolated from a human acute promyelocytic leukemia (M3). *Blood* **77** (1991).

248. Wallace, P. K. *et al.* Tracking antigen-driven responses by flow cytometry: Monitoring proliferation by dye dilution. *Cytom. Part A* **73A,** 1019–1034. ISSN: 15524922 (Nov. 2008).

249. Boudreau, L. H. *et al.* Platelets release mitochondria serving as substrate for bactericidal group IIA-secreted phospholipase A2 to promote inflammation. *Blood* **124,** 2173–83. ISSN: 1528-0020 (Oct. 2014).

250. Böing, A. N. *et al.* Single-step isolation of extracellular vesicles by size-exclusion chromatography. *J. Extracell. vesicles* **3.** ISSN: 2001-3078. doi:10.3402/jev.v3.23430 (Jan. 2014).

251. Raposo, G. & Stoorvogel, W. Extracellular vesicles: exosomes, microvesicles, and friends. *J. Cell Biol.* **200,** 373–83. ISSN: 1540-8140 (Feb. 2013).

252. Eken, C. *et al.* Ectosomes released by polymorphonuclear neutrophils induce a MerTK-dependent anti-inflammatory pathway in macrophages. *J. Biol. Chem.* **285,** 39914–39921. ISSN: 0021-9258 (2010).

253. Freeman, S. A. & Grinstein, S. Phagocytosis: receptors, signal integration, and the cytoskeleton. *Immunol. Rev.* **262,** 193–215. ISSN: 01052896 (Nov. 2014).

254. Huynh, M.-L. N., Fadok, V. A. & Henson, P. M. Phosphatidylserine-dependent ingestion of apoptotic cells promotes TGF-beta1 secretion and the resolution of inflammation. *J. Clin. Invest.* **109,** 41–50. ISSN: 0021-9738 (Jan. 2002).

255. Ferracini, M., Rios, F. J. O. F., Pecenin, M. & Jancar, S. Clearance of apoptotic cells by macrophages induces regulatory phenotype and involves stimulation of cd36 and platelet-activating factor receptor. en. *Mediators Inflamm.* **2013,** 1–8. ISSN: 0962-9351 (Dec. 2013).

256. Harel-Adar, T. *et al.* Modulation of cardiac macrophages by phosphatidylserine-presenting liposomes improves infarct repair. *Proc. Natl. Acad. Sci. U. S. A.* **108,** 1827–32. ISSN: 1091-6490 (Feb. 2011).

257. Sanderson, N. *et al.* Hepatic expression of mature transforming growth factor beta 1 in transgenic mice results in multiple tissue lesions. *Proc. Natl. Acad. Sci. U. S. A.* **92,** 2572–6. ISSN: 0027-8424 (Mar. 1995).

258. Kopp, J. B. *et al.* Transgenic mice with increased plasma levels of TGF-beta 1 develop progressive renal disease. *Lab. Invest.* **74,** 991–1003. ISSN: 0023-6837 (June 1996).

259. Epstein, F. H., Border, W. A. & Noble, N. A. Transforming Growth Factor Beta in Tissue Fibrosis. *N. Engl. J. Med.* **331,** 1286–1292. ISSN: 0028-4793 (Nov. 1994).

260. Blaney Davidson, E. N., Vitters, E. L., van den Berg, W. B. & van der Kraan, P. M. TGF beta-induced cartilage repair is maintained but fibrosis is blocked in the presence of Smad7. *Arthritis Res. Ther.* **8,** R65. ISSN: 1478-6362 (2006).

261. Moon, H.-G. *et al.* Lung epithelial cell-derived extracellular vesicles activate macrophage-mediated inflammatory responses via ROCK1 pathway. *Cell Death Dis.* **6,** e2016. ISSN: 2041-4889 (Dec. 2015).

262. Lee, H., Zhang, D., Zhu, Z., Dela Cruz, C. S. & Jin, Y. Epithelial cell-derived microvesicles activate macrophages and promote inflammation via microvesicle-containing microRNAs. *Sci. Rep.* **6,** 35250. ISSN: 2045-2322 (Dec. 2016).

263. Lo Sicco, C. *et al.* Mesenchymal Stem Cell-Derived Extracellular Vesicles as Mediators of Anti-Inflammatory Effects: Endorsement of Macrophage Polarization. *Stem Cells Transl. Med.* **6,** 1018–1028. ISSN: 21576564 (Mar. 2017).

264. Njock, M.-S. *et al.* Endothelial cells suppress monocyte activation through secretion of extracellular vesicles containing anti-inflammatory microRNAs. *Blood.* ISSN: 1528-0020. doi:10.1182/blood-2014-11-611046 (Apr. 2015).

265. De Graauw, M. *et al.* Annexin A1 regulates TGF-beta signaling and promotes metastasis formation of basal-like breast cancer cells. *Proc. Natl. Acad. Sci. U. S. A.* **107,** 6340–5. ISSN: 1091-6490 (Apr. 2010).

266. Finnson, K. W., Chi, Y., Bou-Gharios, G., Leask, A. & Philip, A. TGF-b signaling in cartilage homeostasis and osteoarthritis. *Front. Biosci. (Schol. Ed).* **4,** 251–68. ISSN: 1945-0524 (Jan. 2012).

267. Ross, C. A comparison of osteoarthritis and rheumatoid arthritis: diagnosis and treatment. *Nurse Pract.* **22,** 20, 23–4, 27–8 passim, quiz 39–41. ISSN: 0361-1817 (Sept. 1997).

268. Bottini, N. & Firestein, G. S. Duality of fibroblast-like synoviocytes in RA: passive responders and imprinted aggressors. *Nat. Rev. Rheumatol.* **9,** 24–33. ISSN: 1759-4790 (Nov. 2012).

269. Kumkumian, G. K. *et al.* Platelet-derived growth factor and IL-1 interactions in rheumatoid arthritis. Regulation of synoviocyte proliferation, prostaglandin production, and collagenase transcription. *J. Immunol.* **143,** 833–7. ISSN: 0022-1767 (Aug. 1989).

270. Lotz, M. & Guerne, P. A. Interleukin-6 induces the synthesis of tissue inhibitor of metalloproteinases-1/erythroid potentiating activity (TIMP-1/EPA). *J. Biol. Chem.* **266,** 2017–20. ISSN: 0021-9258 (Feb. 1991).

271. Lee, D. M. *et al.* Cadherin-11 in Synovial Lining Formation and Pathology in Arthritis. *Science (80-.).* **315,** 1006–1010. ISSN: 0036-8075 (Feb. 2007).

272. Palmer, C. D., Mutch, B. E., Page, T. H., Horwood, N. J. & Foxwell, B. M. Bmx regulates LPS-induced IL-6 and VEGF production via mRNA stability in rheumatoid synovial fibroblasts. *Biochem. Biophys. Res. Commun.* **370,** 599–602. ISSN: 0006291X (June 2008).

273. Guerne, P. A., Zuraw, B. L., Vaughan, J. H., Carson, D. A. & Lotz, M. Synovium as a source of interleukin 6 in vitro. Contribution to local and systemic manifestations of arthritis. *J. Clin. Invest.* **83,** 585–592. ISSN: 0021-9738 (Feb. 1989).

274. Parsonage, G. *et al.* Prolonged, granulocyte-macrophage colony-stimulating factor-dependent, neutrophil survival following rheumatoid synovial fibroblast activation by IL-17 and TNFalpha. *Arthritis Res. Ther.* **10,** R47. ISSN: 1478-6362 (2008).

275. Dalli, J. *et al.* Microparticle alpha-2-macroglobulin enhances pro-resolving responses and promotes survival in sepsis. *EMBO Mol. Med.* **6,** 27–42. ISSN: 1757-4684 (Jan. 2014).

276. De Clerck, L. S., De Gendt, C. M., Bridts, C. H., Van Osselaer, N. & Stevens, W. J. Expression of neutrophil activation markers and neutrophil adhesion to chondrocytes in rheumatoid arthritis patients: relationship with disease activity. *Res. Immunol.* **146,** 81–7. ISSN: 0923-2494 (Feb. 1995).

277. Dominical, V. M. *et al.* Neutrophils of Rheumatoid Arthritis Patients on Anti-TNF-α Therapy and in Disease Remission Present Reduced Adhesive Functions in Association with Decreased Circulating Neutrophil-Attractant Chemokine Levels. *Scand. J. Immunol.* **73,** 309–318. ISSN: 03009475 (Apr. 2011).

278. Pignatelli, P. *et al.* Tumor necrosis factor- as trigger of platelet activation in patients with heart failure. *Blood* **106,** 1992–1994. ISSN: 0006-4971 (Sept. 2005).

279. Vong, L. *et al.* Annexin 1 cleavage in activated neutrophils: a pivotal role for proteinase 3. *J. Biol. Chem.* **282,** 29998–30004. ISSN: 0021-9258 (Oct. 2007).

280. Wiklander, O. P. B. *et al.* Extracellular vesicle in vivo biodistribution is determined by cell source, route of administration and targeting. *J. Extracell. vesicles* **4,** 26316 (2015).